UNIVERSITY OF
KWAZULU-NATAL
INYUVESI
YAKWAZULU-NATALI

Complexes and Clusters of Group 9-11 Metal Dithiophosphonates: Synthesis, Reactivity, Luminescence Properties and Structural Investigations

by

Michael Nivendran Pillay

2016

Dissertation submitted in fulfilment of the academic requirements for the degree of Doctor of Philosophy

School of Chemistry & Physics, College of Agriculture, Engineering and Science, University of KwaZulu-Natal, Durban

As the candidate's supervisor I have approved this dissertation for submission.

_____ _____

Prof. W. E. van Zyl Date

Abstract

This study describes the synthesis of novel bifunctional dithiophosphonate ligands with an emphasis on the solid state structure of selected isolated complexes. A variety of transition metals are utilised to underline the diverse coordination modes of the newly developed ligands.

Preliminary evaluation of diol and tetrol precursors for the preparation of bis- and tetrakis(dithiophosphonates) was carried out. The reaction of these ligands with iodine yielded products of the type [{-$CH_2OP(S)(Fc)S$-}$_2$] (**1**), [$(S_2P\text{-}Fc)_2$(*trans*-1,2-O,O'-C_6H_{10})] (**2**) and [C{$CH_2OP(S)(Fc)S$}$_4$] (**3**), which were novel heterocyclic compounds with disulfide -S-S- bridges. The electrochemical properties of **1**-**3** were investigated and the ferrocenyl moieties were found to be electronically different from ferrocene. A newly developed dithiophosphonate, $(NH_4)_2$[{$(S_2P\text{-}1,4\text{-}C_6H_4OEt)_2$(trans-1,2-O,O'-$C_6H_{10}$)}] (**L4**), derived from a saturated cyclic diol, afforded a dianionic bis(bidentate) ligand. The coordination capabilities of the ligand are notable, and had the capacity to stabilise Cu(I), Ag(I), Au(I), Au(III) and Ni(II) metal centres. Complexation to Cu(I) and Ag(I) afforded tetranuclear metal frameworks of the general type $[M_4L_2]$ (M = Cu(I) **4** and Ag(I) **5**). Cluster **5** contains a tetrahedron of Ag(I) atoms stabilised by Ag···Ag interactions and represents the first Ag(I) dithiophosphonate cluster reported. Complexation of **L4** to Au(I) afforded a coordination-driven self-assembled structure of the type $[Au_2\{(S_2P\text{-}4\text{-}C_6H_4OEt)_2$(*trans*-1,2-O,O'-$C_6H_{10}$)}]$_3$, **6**. Complex **6** is a hexanuclear metallatriangle which contained three discrete dinuclear units, with two distinct intramolecular Au···Au interactions observed at *ca* 3.0 and 3.3 Å, which assists in the complex stabilisation. The oxidative addition reaction of bromine across the Au(I) centres present in **6**, resulted in the formation of a Au(III) homovalent dinuclear complex, of the type $[Au_2(Br)_4\{(S_2P\text{-}1,4\text{-}C_6H_4OEt)_2$(*trans*-1,2-O,O'-C6H10)}], **7**. Furthermore the reaction of **L4** with $NiCl_2{\cdot}6H_2O$ yielded a dinuclear complex of the type [Ni{$(S_2P\text{-}4\text{-}C_6H_4OEt)_2$(*trans*-1,2-O,O'-$C_6H_{10}$)}]$_2$, **8**. Cofacial dinuclear Ni(II) units in **8** showed an unexpected interaction with CH_2Cl_2, which caused differential crystal growth in the same confined environment and resulted in the isolation of morphologically different crystals.

The first series of luminescent Cu(I) dithiophosphonate clusters of the type Cu_4L_4 is reported. Importantly, the new synthetic methodology circumvents the use of a Cu(I) precursor and the

synthesis was carried out in aqueous medium with a Cu(II) salt precursor. The ligand has a dual function and acts as a sacrificial reducing agent, which oxidises to form a disulfide. The redox reaction yielded clusters, of the general type $[Cu\{(S_2P(R)(OR')\}]_4$ (**9**-**15**), in good yield and their luminescent characteristics were investigated. The sulfur atoms coordinate in both μ_1 and μ_2 bridging modes which facilitated interaction between a tetrahedral arrangement of Cu(I) atoms.

A bifunctional ligand which combines dithiophosphonates and pyridyl functionalities on a common backbone was found to be an effective ligand for the formation of unique metal complexes. The ligand $[S_2P(4\text{-}C_6H_4OEt)\{OCH_2CH_2\text{-}2\text{-}C_5H_4N]$ (**L11**) is zwitterionic (formal negative charge on S and formal positive charge on N atoms) in the solid state as confirmed by single crystal X-ray crystallography. The reactivity of **L11** to Co(II) and Cd(II) salts afforded coordination polymers $[Co\{S_2P(4\text{-}C_6H_4OEt)(\ OCHCH_2\text{-}2\text{-}C_5H_5N)\}]_2$ (**16**) and $[Cd\{S_2P(4\text{-}C_6H_4OEt)(\ OCHCH_2\text{-}2\text{-}C_5H_5N)\}]_2$ (**21**), respectively. Complex **16** represents a rare example of a Co(II) dithiophosphonate and significantly both complexes display the elusive *cis* configuration of the ligand substituents. Based on NMR results, complexes $[Ni\{S_2P(4\text{-}C_6H_4OEt)(\ OCHCH_2\text{-}2\text{-}C_5H_5N)\}]_2$ (**17**) and $[Pd\{S_2P(4\text{-}C_6H_4OEt)(\ OCHCH_2\text{-}2\text{-}C_5H_5N)\}]_2$ (**19**) displayed fluxional behaviour in solution, with the former also isolated in the solid-state with two different crystal morphologies observed. Coordination of the pyridyl moiety in **17** resulted in the formation of a dinuclear Ni(II) complex (**17b**). The molecular structure of **19** revealed a discrete square planar complex. Reaction of **L11** with [AuCl(tht)] (tht = tetrahydrothiophene) (molar ratio 1:1) yielded a novel dinuclear Au(I) complex, of the type $[Au\{S_2P(4\text{-}C_6H_4OEt)\}\{(OCH_2CH_2\text{-}2\text{-}C_5H_4N\})]_2$, **20**. Complex **20** displayed intramolecular Au···Au interactions of *ca*. 3.105 Å and no intermolecular Au···Au interactions. Hydrogen bonding due to the pyridyl moiety induced directional packing of the molecular units in the crystal lattice.

Declarations

Declaration 1: Plagiarism

I, Michael Nivendran Pillay, declare that:

1. The research reported in this thesis, except where otherwise indicated, is my original research.
2. This thesis has not been submitted for any degree or examination at any other university.
3. This thesis does not contain other persons' data, pictures, graphs or other information, unless specifically acknowledged as being sourced from other persons.
4. This thesis does not contain other persons' writing, unless specifically acknowledged as being sourced from other researchers. Where other written sources have been quoted, then:
    a. Their words have been re-written but the general information attributed to them has been referenced
    b. Where their exact words have been used, then their writing has been placed in italics and inside quotation marks, and referenced.
5. This thesis does not contain text, graphics or tables copied and pasted from the Internet, unless specifically acknowledged, and the source being detailed in the thesis and in the References sections.

Signed

_____

Michael Nivendran Pillay

Declaration 2: Publications

DETAILS OF CONTRIBUTION TO PUBLICATIONS that form part and/or include research presented in this thesis. I am also a co-author on 2 other papers where I helped with the X-ray crystallography but that work do not form part of this thesis.

Publication 1 (published)

Michael N. Pillay, Werner E. van Zyl, Fluoro**-, Fluoroalkyl-, and Heterofluorogold Complexes.** *Comments Inorg. Chem.* **2013**, *33*, 122-160.

Contributions: Compiled all the literature and relevant materials, and helped with the writing of the manuscript.

Publication 2 (published)

Michael N. Pillay, Hendriette van der Walt, Richard J. Staples, Werner E. van Zyl. **C/O/P/S cycles derived from oxidative intramolecular disulfide (–S–S–) coupling of ferrocenyl dithiophosphonates**. *J. Organomet. Chem.* **2015,** *794*, 33.

Contributions: I carried out the synthesis and characterisation of the compounds. Prepared and modified the draft through to publication. Dr. Staples provided X ray crystallographic analysis.

Publication 3 (published)

Michael N. Pillay, Bernard Omondi, Richard J. Staples, Werner van Zyl. **A hexanuclear gold(I) metallatriangle derived from a chiral dithiophosphate: synthesis, structure, luminescence and oxidative bromination reactivity**. *CrystEngComm* **2013,** *15* (22), 4417.

Contributions: I carried out the synthesis and characterisation of the compounds. Prepared and modified the draft through to publication. Drs Staples and Omondi provided X ray crystallographic analysis.

Signed: _____

Declaration 3: Conference proceedings

1. Michael N. Pillay, Richard J. Staples, Bernard Omondi, Werner E. van Zyl. Gold dithiophosphonate complexes derived from chiral diols. (Poster presented at 16th South African Chemical Institute (SACI) – INORG2013. Inorganic Chemistry Conference, Durban, South Africa, 2013)
2. Michael N. Pillay, Richard J. Staples, Werner E. van Zyl. Nickel(II) dithiophosphonate complex with unique solvation properties. (Poster presented at 41st International Conference on Coordination Chemistry (ICCC41), Singapore, 2014.)

Declaration 4: Crystallographic contributions

Table FI: Declaration of Crystallographic contributions.

Crystal	Location	Collection and Refinement
3	MSU	Staples
4	UKZN	Pillay
5	MSU	Staples
6	NDHU	Liao and Pillay
7	UKZN	Pillay
8	MSU	Staples and Omondi
8·CH_2Cl_2	MSU	Staples
11	NDHU	Liao
14	NDHU	Liao
L11z	UKZN	Pillay
16	UKZN	Pillay
17	UKZN	Pillay
18	UKZN	Pillay
19	UKZN	Pillay
20	MSU	Staples
21	UKZN	Pillay

- **MSU** = Michigan State University (USA); **NDHU** = National Dong Hwa University (Taiwan); **UKZN** = University of KwaZulu-Natal Westville (South Africa).
- **Staples** = Dr Richard J. Staples; **Liao** = Jian-Hong Liao; **Pillay** = Michael N. Pillay (author of this thesis); **Omondi** = Bernard O. Omondi

To my family

“In a dark place we find ourselves…a little more knowledge lights our way.”

Yoda

Acknowledgements

- My family, for their patience and support.
- Prof Werner E. van Zyl, especially for his positive outlook which instilled confidence in my research, and ultimately this dissertation.
- Prof C. W. Liu, for accommodating me during a research visit for 4 months and the many fruitful discussions which have had an influence on aspects in this study.
- Dr. R. J. Staples, for data collection and refinement of the crystal structures presented in this study.
- Jian-Hong, Yan-Lu Lin, for providing the first steps in my journey to become crystallographer. They truly have shown that science is a universal language.
- The Taiwanese group: Alex, Bean, Ping, Ria and Wilson. They were amazing hosts to a newcomer.
- The technical and academic staff at UKZN, School of Chemistry and Physics, Westville Campus.
- My friends Drushan, Harinarayana, Lynette, Kaalin, Kadwa, Kavashan, Kershen, Kyle, Samashen, Shirveen, Vashen, Veresha and Zidaan who made an invaluable contribution.
- University of KwaZulu-Natal.
- National Dong Hwa University.
- The National Research Foundation/Department of Science and Technology (NRF/DST) for financial support through an Innovative Grant.
- Rand Refinery for a generous gift of gold salt

List of Ligands

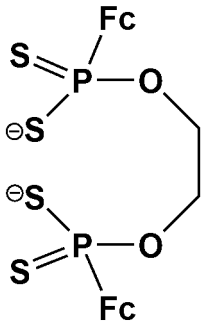

L1

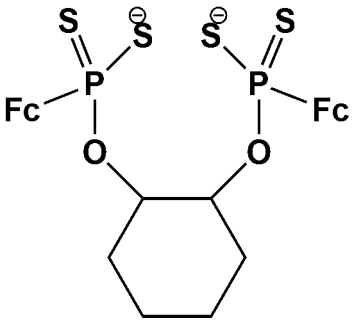

L2

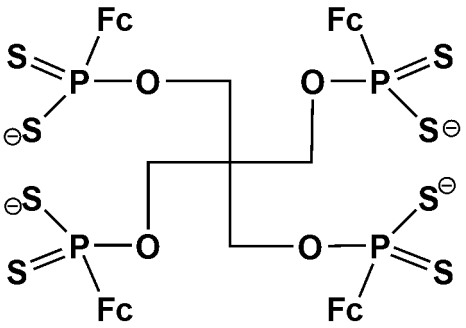

L3

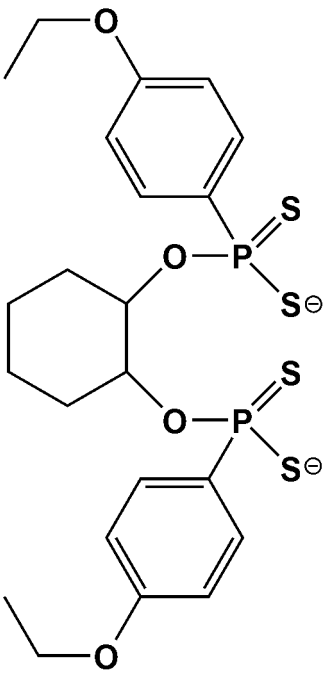

L4

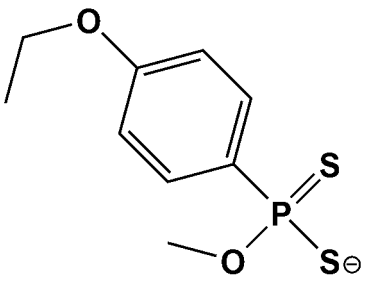

L5

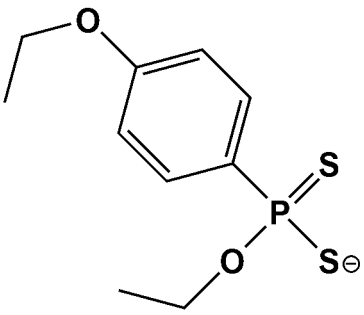

L6

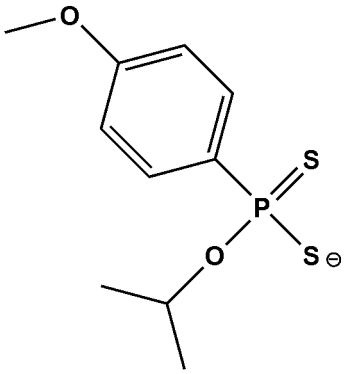

L7

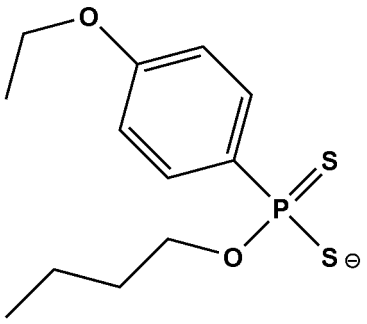

L8

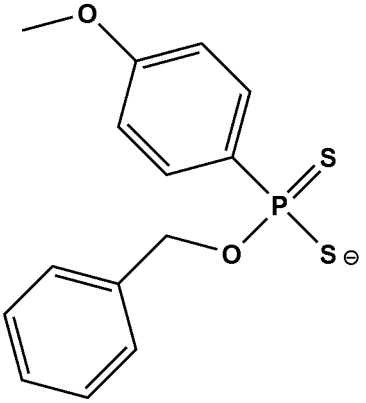

L9

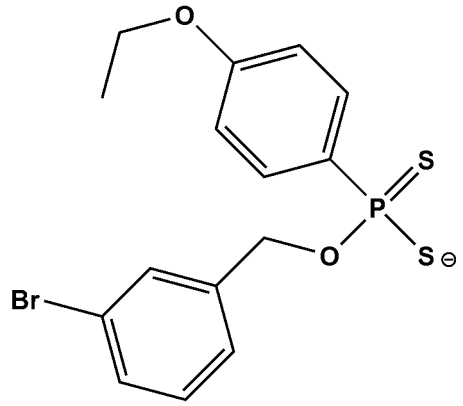

L10

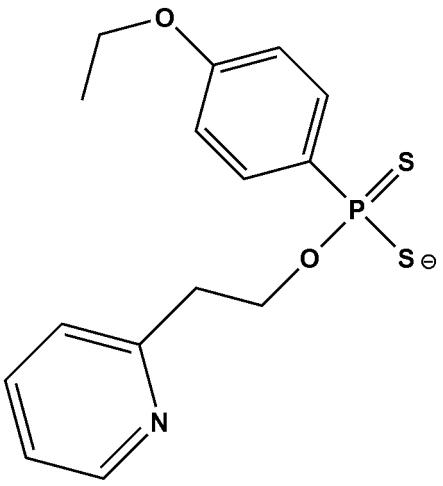

L 11

List of Complexes

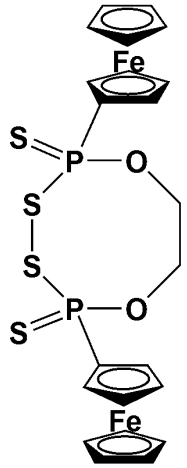

1

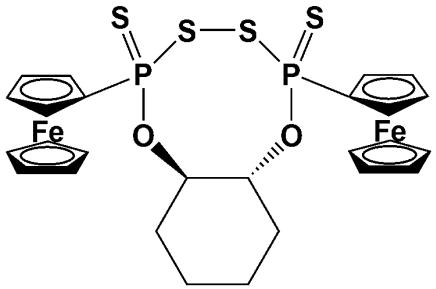

2

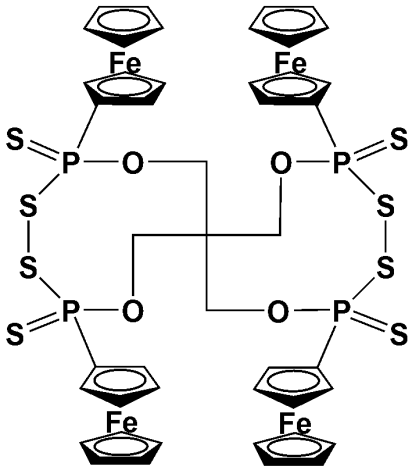

3

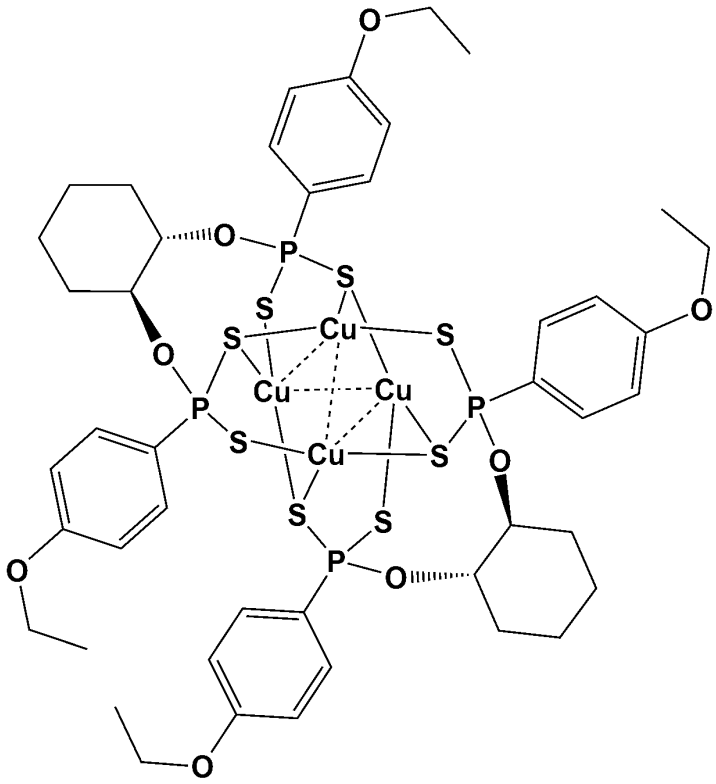

4

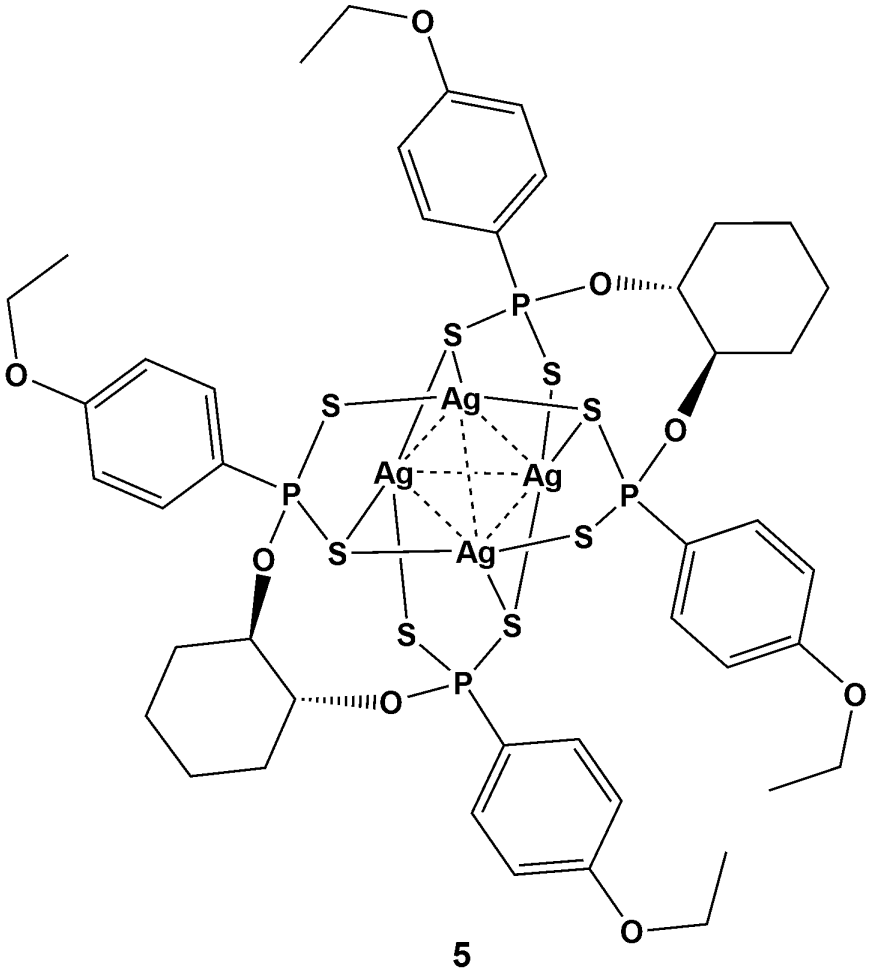
O
P
O
S
S
S
Ag
S
Ag
Ag
P
O
S
Ag
S
O
S
S
P
O
O
O

5

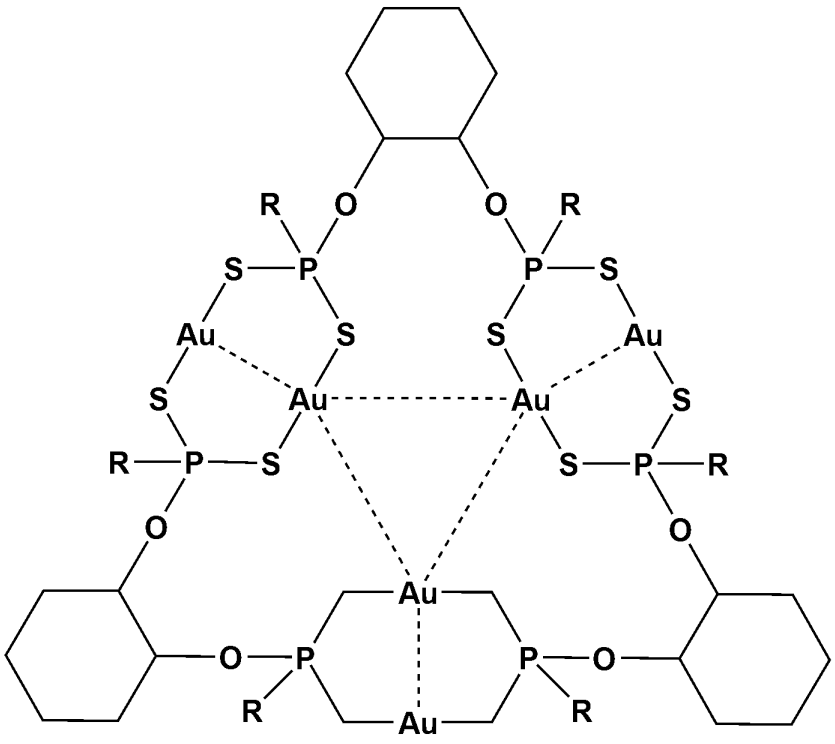
R
O
O
R
P
P
S
S
Au
S
S
Au
Au
Au
S
S
R
P
S
S
P
R
O
O
Au
O
P
P
O
R
Au
R

6

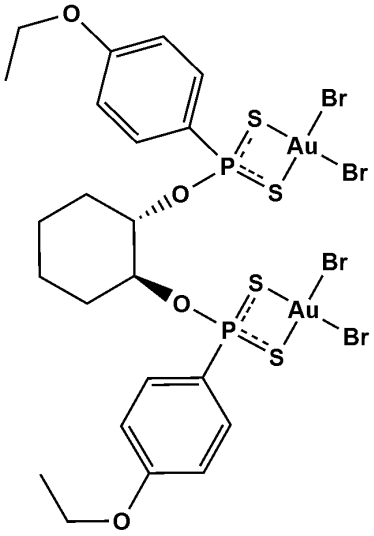
O
S
Br
Au
P
O
S
Br
O
S
Br
Au
P
O
S
Br
O

7

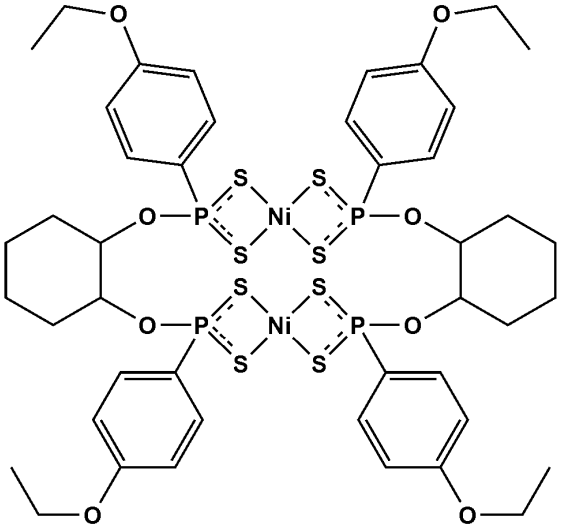
O
O
O
P
S
S
Ni
S
S
P
O
O
S
S
O
P
S
S
Ni
S
S
P
O
O
O

8

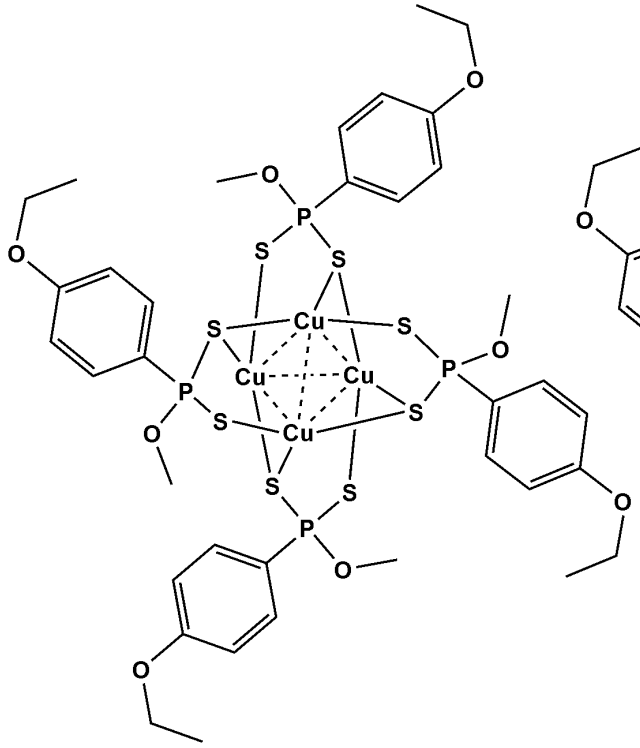
O
O
O
P
S
S
S
Cu
S
Cu
Cu
P
O
O
S
Cu
S
S
P
O
O
S
S
P
O
O

9

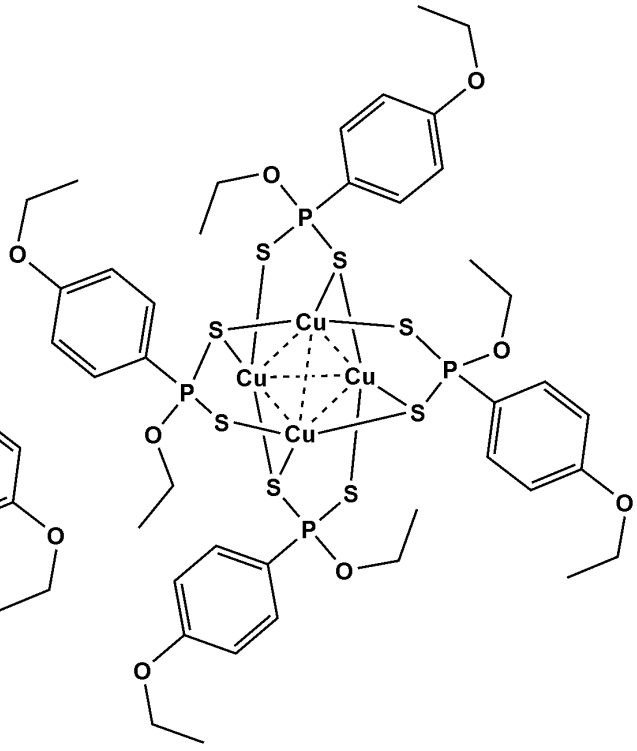
O
O
O
P
S
S
S
Cu
S
Cu
Cu
P
O
O
S
Cu
S
S
P
O
O
S
S
P
O
O

10

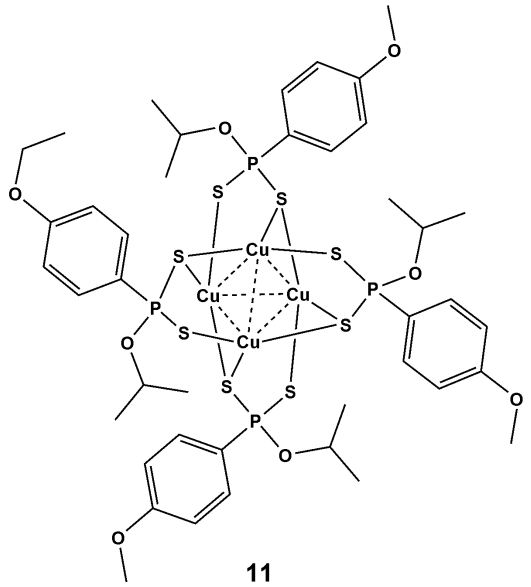

11

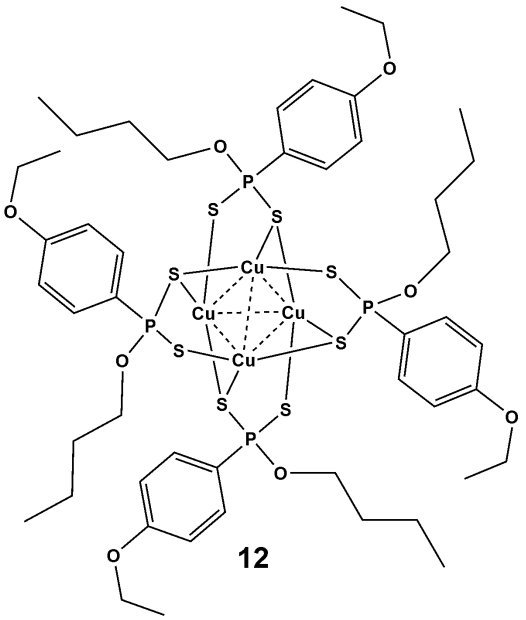

12

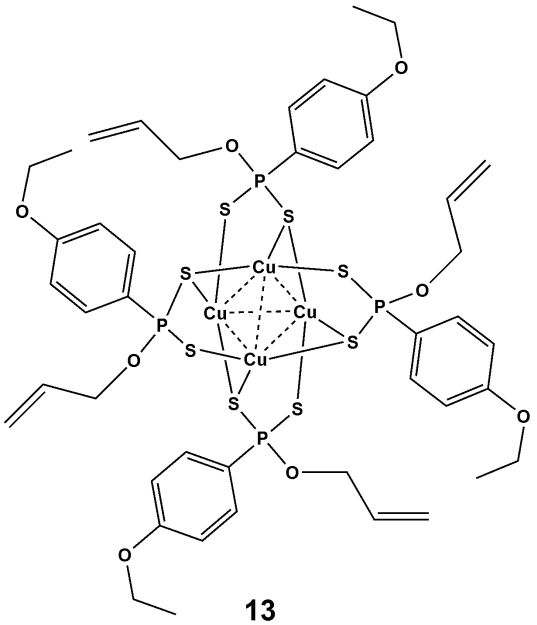

13

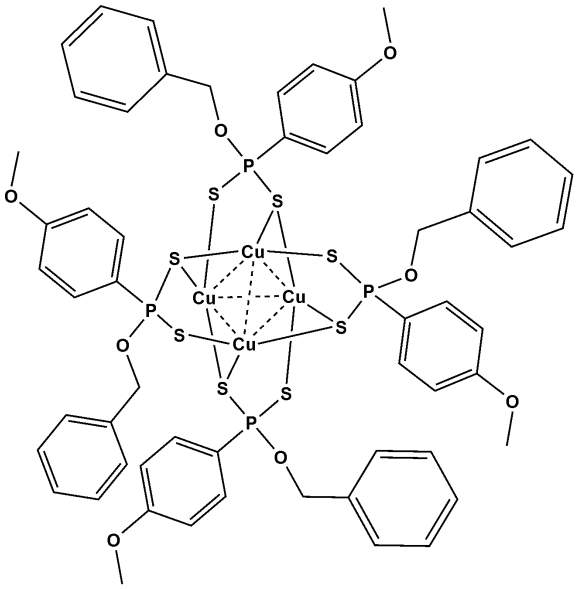

14

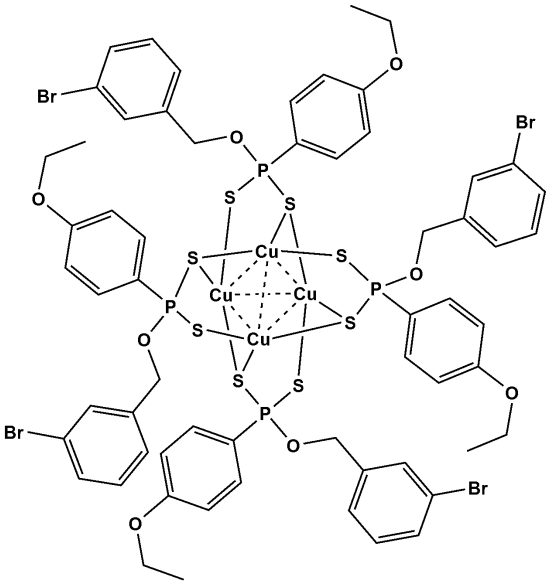

15

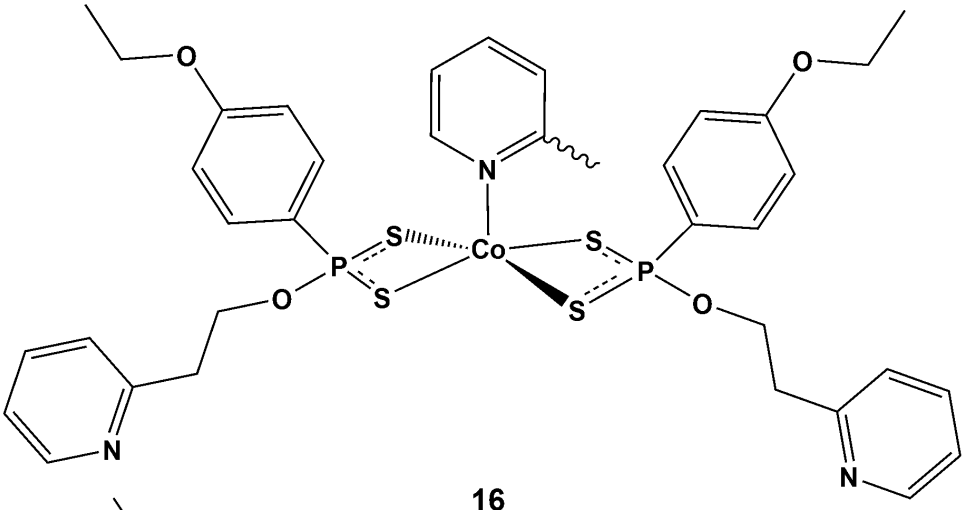
O
O
N
S
P
Co
S
S
P
S
O
O
N
N

16

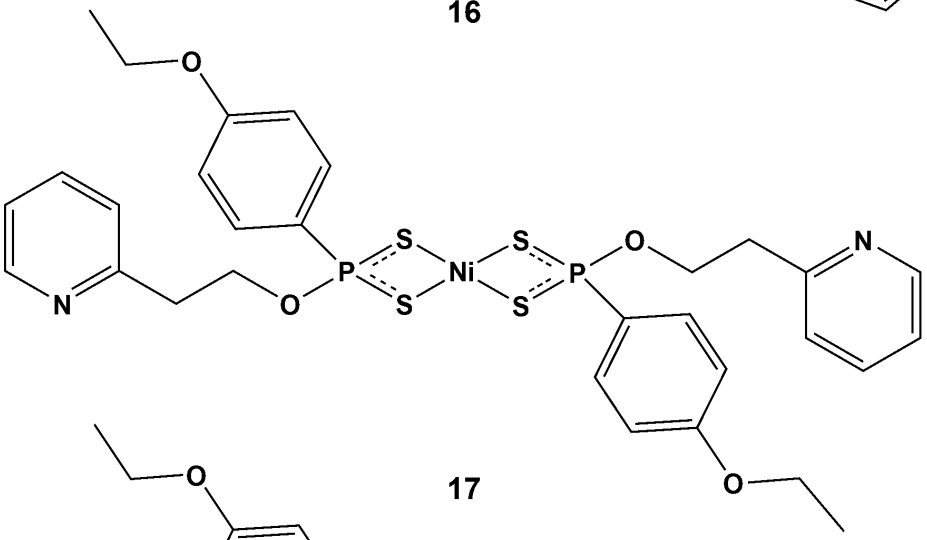
O
S
S
P
Ni
S
S
P
O
N
N
O
O

17

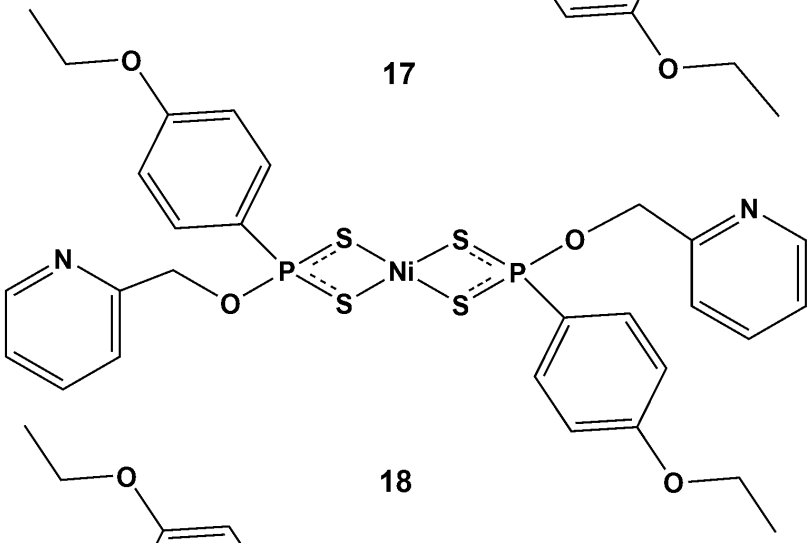
O
S
S
P
Ni
S
S
P
O
N
N
O
O

18

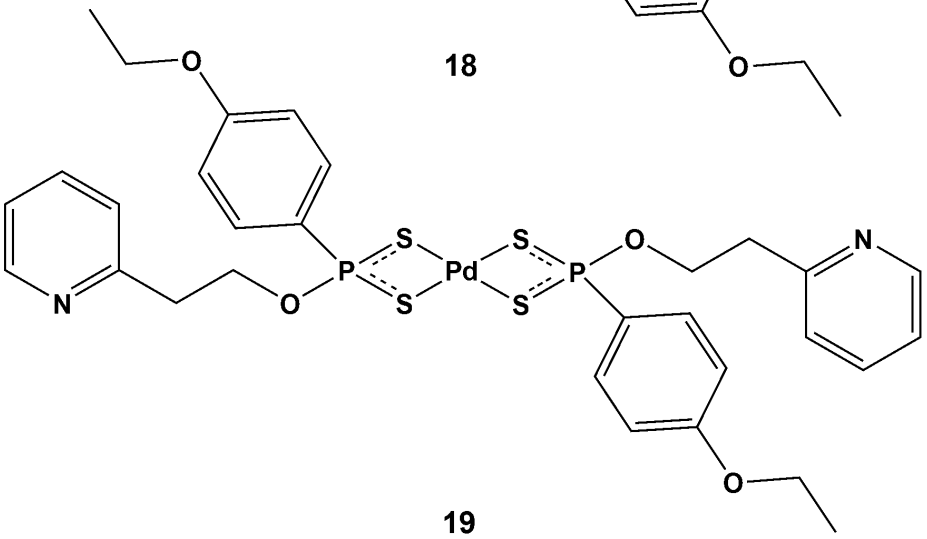
O
S
S
P
Pd
S
S
P
O
N
N
O
O

19

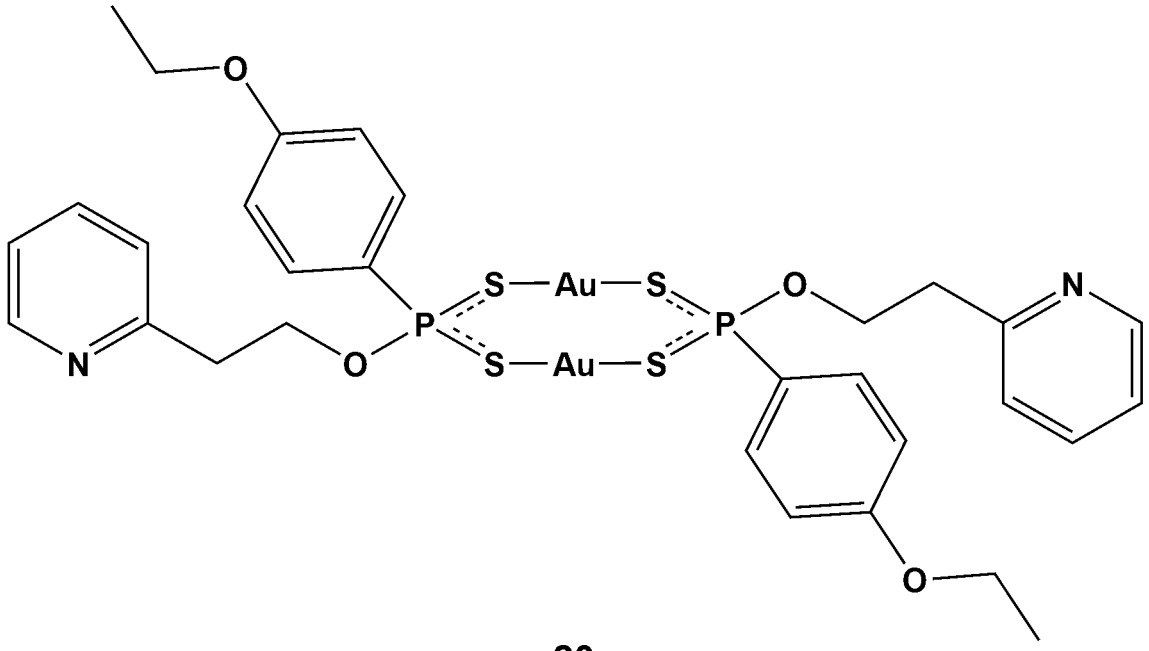

20

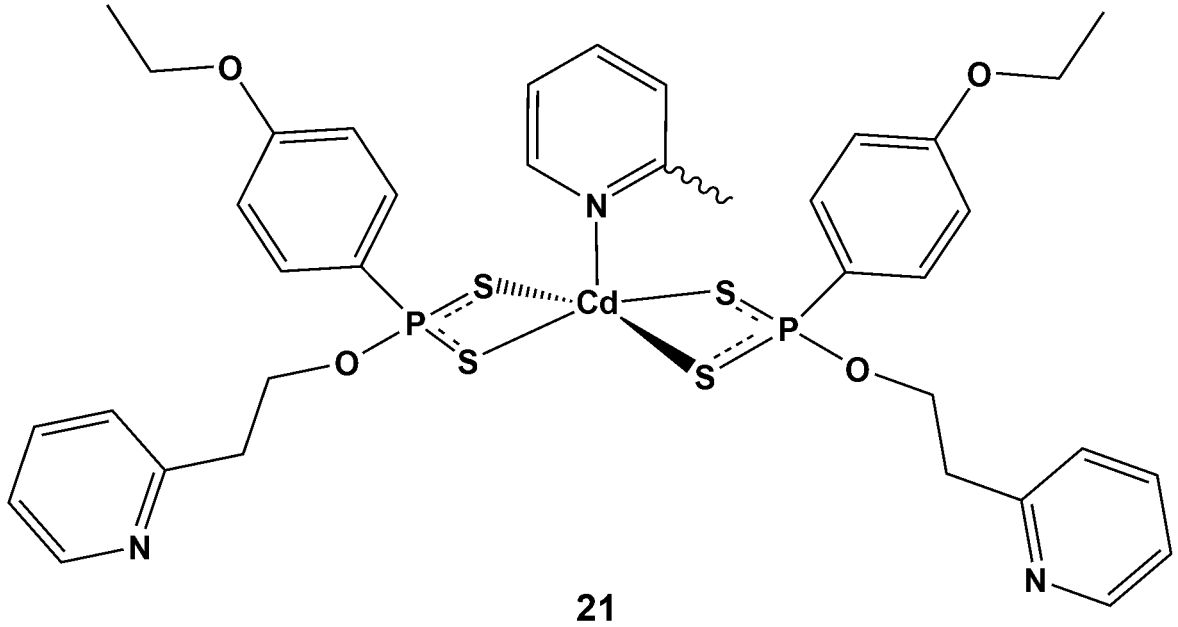

21

List of Figures

List of Schemes

List of Tables

List of Abbreviations

LR Lawesson's Reagent

An Anisole

Cp Cyclopentadienyl

Fc Ferrocene

THF Tetrahydrofuran

MeOH Methanol

EtOH Ethanol

DCM Dichloromethane

NMR Nuclear Magnetic resonance

- **ppm** parts per million
- **s** singlet
- **d** doublet
- **t** triplet
- **q** quartet
- **p** quintet
- **dd** doublet of doublets

MS Mass spectroscop**y**

ca. Circa

e.s.d. Estimated standard deviation

MLCT Metal to Ligand Charge Transfer

LMCT Ligand to Metal Charge Transfer

Table of Contents

Chapter 1
Introduction

Organophosphorus compounds have fascinated researchers for decades due to their presence in both malicious (nerve gas) and vital (DNA and RNA) systems. Ultimately the most fundamental component of any living organism on earth contains a 4-coordinate phosphorus(V) linker, the topic of this study, which connects amino acids in a sequence that has tremendous impact.

As early as 1854, the synthesis of tetraethylpyrophosphate (TEPP) as an alternative to the current botanical insecticide of the time, initiated an exponential growth in organophosphorus compounds. This could be related to their application as pesticides, which increased the efficiency of food production. However, evidence of their potent physiological effects, and the eminent outbreak of war could have also played a role in the development of these compounds. The P(III) derivatives were found to be effective insecticides, however, the highly oxophillic P(III) centre was prone to rapid hydrolysis and subsequent oxidation to P(V). The ability of these compounds to inhibit nerve transmission (cholinergic) was reported by Lange and Krueger.[1] They specifically noted the choking sensation and blurred vision that occurs from the inhalation of dimethyl and diethyl phosphorofluoridates. A german team of chemists led by Schrader, then embarked on an expansive study of organophosphorus pesticides and synthesized a plethora of these compounds, including notorious chemical warfare agents (CWA): tabun, soman and sarin.[2] With the outbreak of World War II, a rapid increase in the variation of these compounds as well as their production methods, resulted in an arsenal of these materials. The mechanism of action of these compounds has been well established and assigned to the disruption of the acetylcholinesterase (AChE) enzyme.[3] The devastating terrorist attack in a Tokyo subway in 1995, illustrated the potency of these agents to cause death and have detrimental prolonged effects on survivors. [4]

Even though its origins can be traced to malicious intentions, these phosphorus compounds have an undeniable impact on current society. In this study the focus was on the dithio analogues, particular dithiophosphonates. Dithiophosphonates have been applied to a variety of industrial applications, which include metal ore extraction/flotation reagents[5]

(mining industry); petroleum additive for lubrication in combustion engines[6] (automobile industry); and as insecticides[7] (agricultural industry).

The following sections aim to provide an overview of this ligand class and its coordination patterns to metal centres pertinent to this thesis. The thesis focuses on the modification of these ligand types in the formation of novel coordination-driven assemblies.

1.1 Dithiophosphonates: a phosphor-1, 1-dithiolate with a difference

The phosphor-1,1,-dithiolate class of compounds can be broadly defined as dithiophosphates, dithiophosphinates, and the hybrid dithiophosphonates (Figure 1.1). The asymmetric nature of the dithiophosphonates allows for the formation of isomers, not accessible to symmetric **A** and **B** (in delocalized form). The dithiophosphates and dithiophosphinates were well established much earlier as compared to the other two groups, presumably due to the relative ease of ligand preparation, and their complexes with main group and transition metals have been reviewed.[8,9]

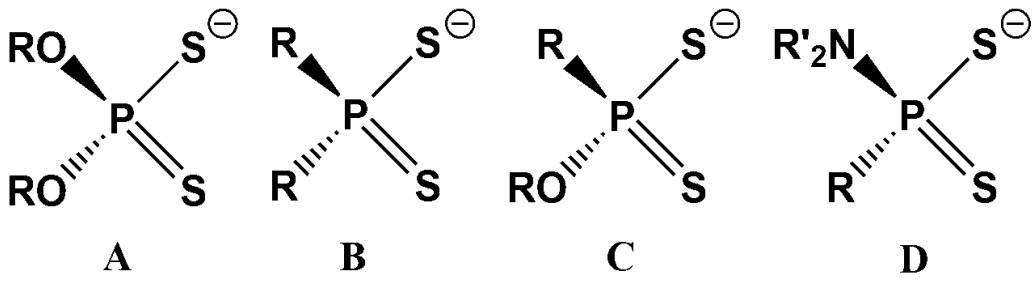

Figure 1.1. Phosphor-1, 1-dithiolates comprise ligands derived from dithiophosphoric (**A**), dithiophosphinic (**B**), the hybrid dithiophosphonic (**C**) and amido-dithiophosphonic (**D**) anions.

The development of dithiophosphonates took significantly longer and the number of complexes containing the ligand are still in the minority when compared to its counterparts. A significant breakthrough occurred when it was shown that 2,4-diaryl-1,3-dithiaphosphetane disulfide dimers react with two stoichiometric equivalents of alcohol to form corresponding dithiophosphonic acids.[10] The first derivative was prepared in 1952 by Fay and Lankelma, from the reaction of cyclohexene with phosphorus pentasulfide, which was produced in a

moderate yield and purity.[11] In 1962 an improvement in the yield and purity was reported, it involved the reaction between $PhPCl_2$ (l) and H_2S (g) to form $[PhP(\mu\text{-}S)S]_2$ (s) at temperatures above 210° C.[12,13] But the conditions for the production of the dimer were hazardous, due to the formation of stoichiometric amounts of HCl released at elevated temperatures. These conditions, coupled with its growing popularity as a sulfur transfer reagent warranted the need for an improved syntheses. In 1978, Lawesson and co-workers reported a greatly improved method for the preparation of a related dimer and laid the foundation for preparation of a plethora of derivatives.[14-16] Lawesson reported that the reaction of electron rich aromatics with P_4S_{10} resulted in phosphetane cyclic dimers (Lawesson's reagent, LR), shown in Scheme 1.1. The use of Lawesson's reagent in organic chemistry for the conversion of various oxygen substituted derivatives to their related thio-analogues has been reviewed in 1985[17] and 2012.[18]

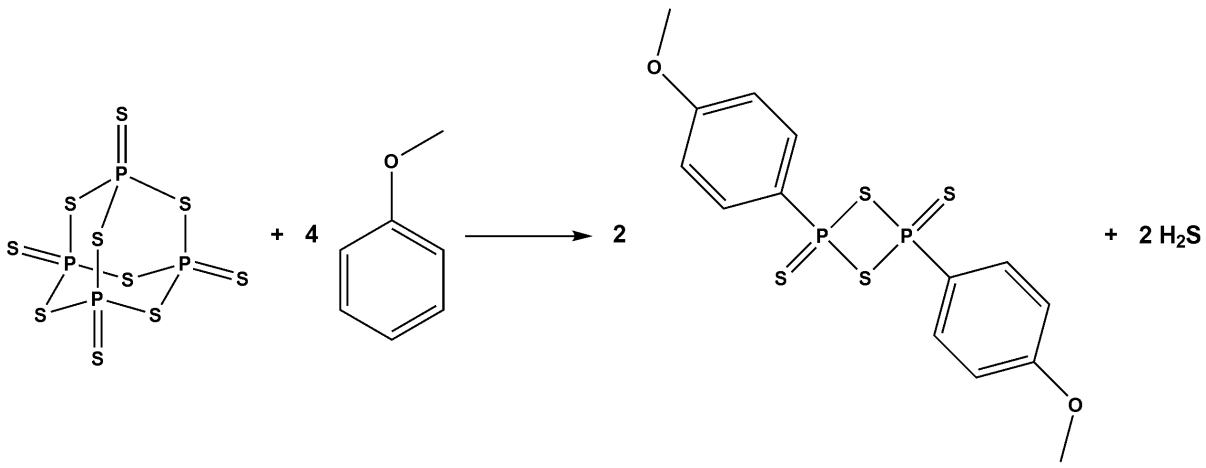

Scheme 1.1. Synthesis of phosphetane dimers (LR) from electron rich aromatic compounds.

With this new strategy, a significant number of novel dimers were prepared, two of which are the ferrocenyl analogue[19] (**C**) and selenium analogue[20] (**D**). These dimers were prepared by Woollins et al. and **C** has become a popular reagent for the syntheses of dithiophosphonate ligands bearing the electroactive ferrocenyl moiety.

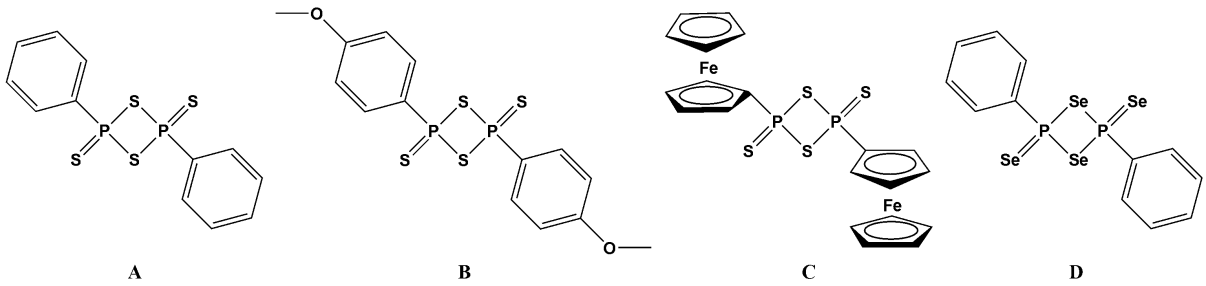

Figure 1.2. Phosphetane cyclic dimers: The original dimer prepared by Fay and Lankelma (**A**); Lawesson's Reagent (LR) (**B**); organometallic derivative (**C**) and the commercially available selenium analogue (**D**) (Woollins' Reagent).

The mechanism for the application of LR as a sulfur transfer reagent has been proposed by several authors,[21-23] and recent computational studies have given further insight into the mechanism.[24] Although not directly a study on the alcoholysis of LR, some insight can be drawn on the formation of dithiophosphonates. All reports attribute the initial step to the reversible dissociation of the dimer into a 3-coordinate phosphorus(V) reactive species (PhPSS).[14-16] The electrophilic phosphorus centre is then highly susceptible to nucleophilic attack from the oxygen atom, resulting in the formation of the dithiophosphonic acid. In this way a variety of dithiophosphonic acids can be prepared in a facile manner, which allows ligand properties (sterics and electronics) to be tuned based on the type of alcohol employed, Scheme 1.2. Alcohols which have a melting point at 70 °C or below can be used to produce ligands *via* a "green" approach, i.e. solvent free. The relative acidity of the proton allows for deprotonation with a base, resulting in the formation of monoanionic salts.

Scheme 1.2. Synthesis of dithiophosphonate ammonium salts form phosphetane cyclic dimers.

1.2 Coordination versatility of S-P-S fragment

The research potential of the S-P-S moiety has long been exploited, due to its inherent ability to accommodate a diverse group of coordination modes.[25] This variation can be attributed to the multiple resonance structures of the monoanionic ligand. The hyper-valency of both the phosphorus and sulfur atoms, play a key role in this regard.[26] This is due to their ability to accommodate greater electron density in their valence shells, which become available upon coordination. A comparison of the resonance forms with the corresponding coordination is given in Figure 1.3. It describes an increasing delocalisation of the P-S π-bond across the S-P-S chelate.

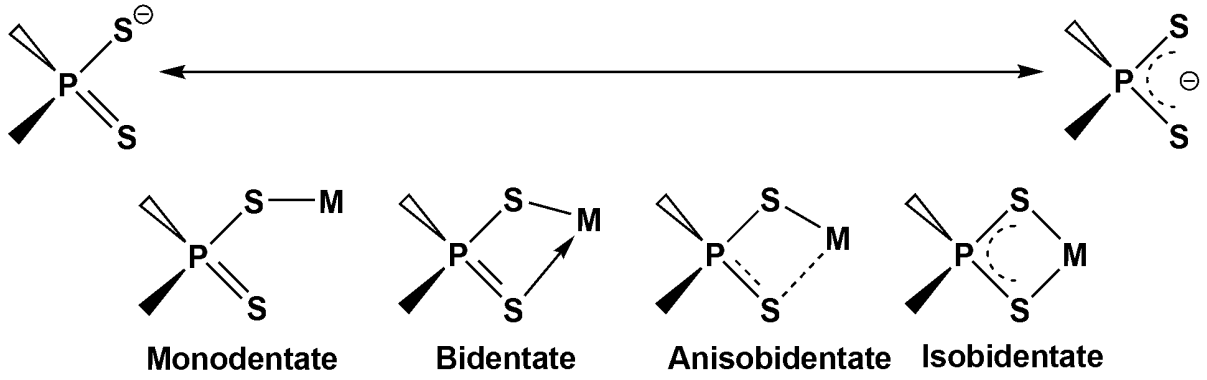

Figure 1.3. Resonance structures of phosphor-1,1-dithiolato ligands, *mono*dentate with a non-coordinating P=S bond; bidentate dative coordination; *aniso*bidentate increasing the sulfur interaction; *iso*bidentate with equal sulfur interactions.

Therefore, when considering mononuclear systems the inherent ability of the sulfur atoms to act both independently or in conjunction is as a result of the variation in the position of the electron density across the S-P-S fragment. This allows the dithiophosphonate ligand to support essentially all main group and transition metals. The flexibility in the coordination becomes more apparent in the ability of the ligand to stabilise multiple metallic systems, shown in Figure 1.4.

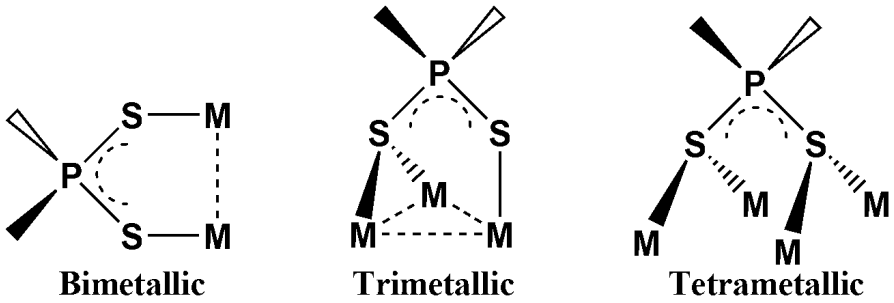

Figure 1.4. Multi-nuclear coordination patterns observed for dithiophosphonates.

In non-chelating systems the sulfur atoms have the ability to accommodate both μ_1 and μ_2 binding modes. This allows the sulfur atoms to accommodate multi-metallic configurations and various coordination geometries. The bimetallic bi-connective coordination mode is synonymous with linear 2-coordinate Au(I) dithiophosphonates and has been described as an effective framework for the study of aurophilic interactions.[27] The trimetallic tri-connective mode, which contains both μ_1- and μ_2-S atoms, has only been recently demonstrated for dithiophosphonates in tetranuclear Cu(I) clusters, and are responsible for the stabilisation of a tetrahedron of copper atoms.[28] The tetranuclear coordination is yet to be seen for the dithiophosphonates but has been observed for related dithiophosphates in cubic octanuclear copper clusters.[29]

The coordination capabilites of the S-P-S fragment is undeniable, and this study will aim to present novel metal configurations which have not been reported for the dithiophosphonate ligand. In an effort to highlight the novelty of this study, an analysis of the Cambridge Crystallographic Data Centre (CCDC) was done in relation to the metal complexes reported here. Table 1.1 gives a summary of this analysis and indicates the number of reported single crystal X-ray structures as a function of the metal centre, oxidation state and nuclearity. Apart from the mononuclear Ni(II) complexes, all other metal complexes can be regarded as reasonably uncommon. Of note is the complete absence of a Co(II) complex, and a single report of a tetranuclear Cu(I) derivative. Furthermore, Ag(I) complexes are rare and only one mononuclear is represented. The Au(I) complexes are limited to dinuclear examples. In total this study contributes 15 novel structures, several of which display new metal topologies, herewith unknown for the dithiophosphonate ligand.

Table 1.1. Complexes of dithiophosphonate structures deposited in CCDC.

Metal(oxidation state)	Nuclearity	Structures
Co(II)	-	-
Co(III)	1	1
Ni(II)	1	49
Cu(I)	1	2
Cu(I)	4	1
Pd(II)	1	6
Pd(II)	2	1
Ag(I)	1	3
Cd(II)	1	5
Cd(II)	2	4
Au(I)	1	1
Au(I)	2	7

*The data in the table is limited to complexes containing dithiophosphonates of the type [S(S)PROR']. Search was conducted on Conquest 1.18 with CCDC version5.37.

1.3 Dithiophosphonate metal complexes

The resulting coordination geometry from metal complexation to a ligand is dictated by a combination of factors including the nature of the ligand and metal centre. The inherent flexibility of the dithiophosphonate ligand to coordinate in several different modes, makes it an invaluable ligand in coordination studies. The following sections describe coordination patterns of dithiophosphonates found in the literature with a focus on metals applied in this study. The metals are arranged based on atomic number.

1.3.1 Cobalt dithiophosphonates

A structural analyses of a Co(II) complex stabilised solely by dithiophosphonates remains elusive. However, dinuclear Co(II) complexes derived from a podand ligand containing bis(dithiophosphonate) has been described, without crystallographic evidence.[30] Only recently has it been shown that for the related dithiophos*phinates*, that stabilisation of a Co(II) centre requires the use of an additional ligand.[31] In that study pyridine was employed which yielded both penta-coordinate and hexa-coordinate Co(II) complexes, which demonstrated square pyramidal and octahedral geometry, respectively. Co(III) complexes have been reported with the cobalt centre in an octahedral environment.[32] In the current study, a novel approach to the stabilisation of a Co(II) centre has yielded the first Co(II) dithiophosphonate to be structurally characterised.

1.3.2 Nickel dithiophosphonates

Since an early report on the structure of a Ni(II) dithiophosphonate complex,[33] $[Ni\{S_2PPh(OEt)\}_2]$, these complexes have grown to become the most studied metal for this ligand system.[34-51] This can partly be attributed to the tendency of the derivatives to adopt favourable packing orientations. Most examples exhibit a *trans* configuration of the ligand substituents with an inversion centre present on the square planar Ni(II) atom. The *cis* configuration remains elusive and examples of the *cis* isomer created solely by coordination, i.e. not induced by secondary interactions, have not been found in literature. An interesting feature of the square planar Ni(II) complexes is the ability to accommodate secondary ligands and subsequently form an adduct, an example of this was reported by Aragoni *et al.* with an adduct containing pyridine and aminopyridines forming a 6-coordinate Ni(II) complex, shown in Figure 1.5 a.[52] This was further exploited for the formation of polymeric type complexes, obtained from the reaction of Ni(II) dithiophosphonates with N-donor linkers, shown in Figure 1.5 b.[53,54] The topology of the polymers were shown to be tuneable based on the properties of the linker deployed. Karakus et al. reported neutral Ni(II) dithiophosphonate polymers which were prepared with inorganic sulfide bridges between the pyridyl groups.[55]

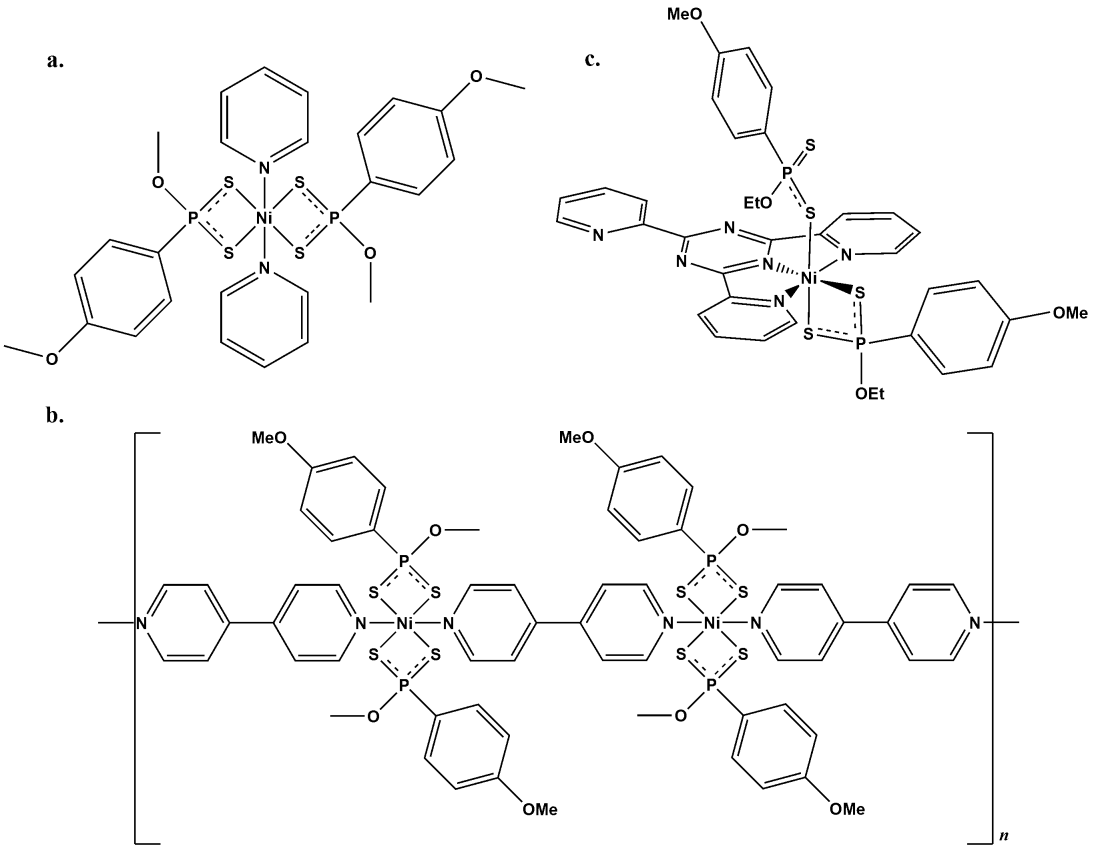

Figure 1.5. a) Octahedral Ni(II) complex containing neutral N-donor ligands at the axial positions. **b)** Coordination polymers as a result of bipyridine coordination. **c)** Combination of dithiophosphonates with bulky 2,4,6-tris(2-pyridyl)-1,3,5-triazine.

The coordination can also be influenced by the occupancy of the coordination sphere. In mixed-ligand systems generated by the reaction of complexes with secondary ligands, the dithiophosphonates have been shown to accommodate different coordination patterns. This was apparent in the reaction of a Ni(II) complex, of the type $[Ni(S_2P(4\text{-}C_6H_4OMe)(OMe))_2]$, with a bulky ligand (2,4,6-tris(2-pyridyl)-1,3,5-triazine). The unusual octahedral nickel complex contains both monodentate and isobidentate coordination modes, shown in Figure 1.5c.[44,45] A report on the application of bis(dithiophosphonates) to the formation of dinuclear Ni(II) complexes, lacked a X-ray structure determination.[55] However, in the present study two dinuclear Ni(II) complexes were isolated and structurally characterised, one of which was formed from a bis(dithiophosphonate) ligand and adopts the rare *cis* configuration.

1.3.3 Copper dithiophosphonates

Cu(I) complexes containing only dithiophosphonate ligands are limited, with only one structure reported by Zhang and co-workers.[28] The structure contains an idealised tetrahedron of copper atoms stabilised by a trimetallic tri-connective ferrocenyl dithiophosphonate, shown in Figure 1.6b. Interestingly, this structure presents the only tetranuclear Cu(I) dithiophosphonate cluster reported.

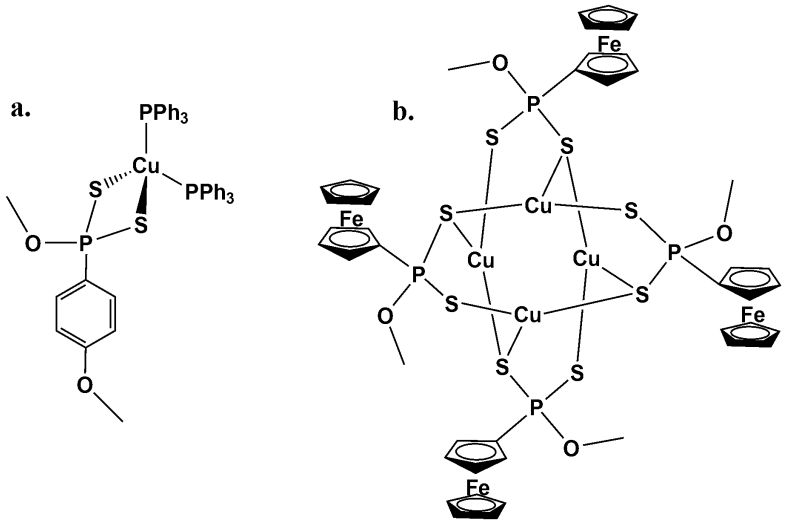

Figure 1.6. a) Mononuclear tetrahedral Cu(I) complex with neutral phosphine ligands**. b)** First tetranuclear Cu(I) cluster.

Mononuclear complexes of the type $[Cu\{S_2P(4\text{-}C_6H_4OR)(OMe)\}(PPh_3)_2]$ were obtained from the addition of a $[PPh_3CuNO_3]$ precursor to a dithiophosphonate, Figure 16a.[56] A similar synthetic route was adopted for the preparation of ferrocenyl derivatives, with the complexes subsequently embedded into nanofibers and applied as antimicrobial agents.[57] Although not a traditional dithiophosphonate, a related reaction involved the direct addition CuOBu and PPh_3 to LR, this resulted in the formation of a dinuclear Cu(I) complex of the type $[Cu_2(\mu_2\text{-}ArS_2P\text{–}O\text{–}PS_2Ar)(PPh_3)_4]$.[58] In the same report the use of a bisphosphine (dppa = Ph_2NHPPh_2) resulted in the formation of a tetranuclear complex of the type $[Cu_4\{Ar(\mu_2\text{-}S)2P\text{–}O\text{–}P(\mu_2\text{-}S)_2Ar\}_2(dppa)_2]$. This thesis reports on a series of tetranuclear Cu(I) dithiophosphonates, synthesised in aqueous conditions.

1.3.4 Silver dithiophosphonates

A mononuclear Ag(I) dithiophosphonate complex has been reported, Figure 1.7a. The complex contains a neutral phosphine ligand and a ferrocenyl dithiophosphonate, which enables the stabilisation of the tetrahedral coordinated metal centre.[59] In 2006, a dinuclear Ag(I) complex containing a unique trigonal planar Ag(I) atom was reported by Haiduc et al. and is shown in Figure 1.7 b.[60] In addition, the Ag, S, and P atoms assemble to form a hetero-atomic macrocycle.

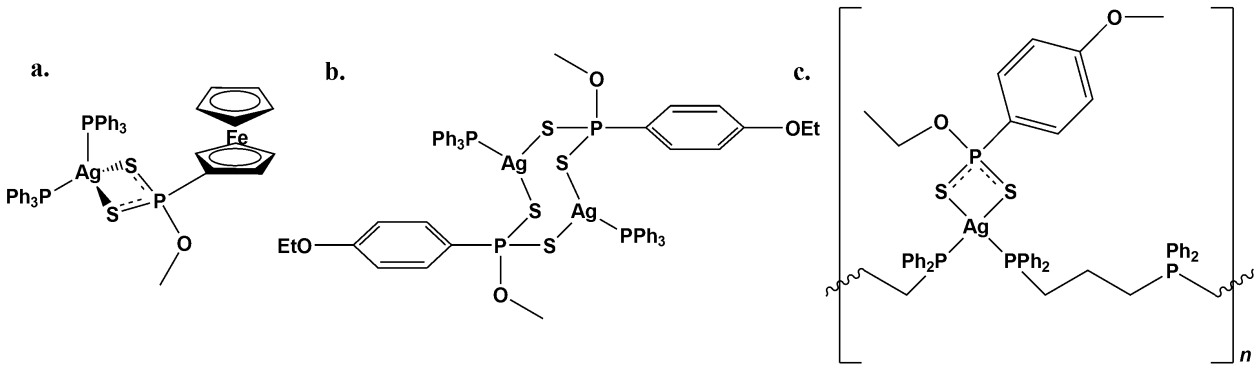

Figure 1.7. a) A mononuclear Ag(I) complex with tetrahedral geometry. **b)** Dinuclear Ag(I) complex with bimetallic dithiophosphonate and neutral PPh_3. **c)** Ag(I) coordination polymer containing isobidentate dithiophosphonate and bis(phosphine) linkers.

Sun and Huang reported an interesting example of the combination of phosphines and dithiophosphonates, with the resultant complex forming a 1D polymer, shown in Figure 1.7c.[61] The polymer contains a bisphosphine linker which connects dithiophosphonate chelated Ag(I) metal centres. The reaction of metal carboxylates with LR and dppm results in the formation of unique tetranuclear silver clusters of the type $[Ag_4\{\mu_4\text{-}ArP(O)S_2\}_2(dppm)_4]$ (dppm = $CH_2(PPh_2)_2$).[62] In the same study the authors noted addition of PPh_3 instead of the bisphosphine resulted in the formation of the largest silver cluster known for this ligand system, of the type $[Ag_{28}(\mu_6\text{-}S)_2\{ArP(O)S_2\}_{12}(PPh_3)_{12}]$. Currently no silver complexes or clusters stabilised only by dithiophosphonates is known, suggesting that stabilisation requires an ancillary ligand. This is in stark contrast to the related (but symmetrical) dithiophosphates. An interesting tetranuclear Ag(I) cluster stabilised solely by dithiophosphonate ligands is reported in the current study.

1.3.5 Gold

A significant factor in Au(I) chemistry is the potential presence of aurophilic interactions. Dithiophosphonates have been described as a useful architecture for the study of these interactions.[63] It is therefore pertinent to describe these interactions before describing literature of previously reported gold dithiophosphonate complexes.

1.3.5.1 Aurophilicity and its implications on Au(I) chemistry

Au(I) complexes have been shown to deviate from conventional patterns , this is due to the closed-shell d^{10} metal centres which bind to each other at distances slightly larger than those present in Au metal. The bond energies in these Au···Au interactions are comparable to the strength in hydrogen bonding, and has resulted in a plethora of coordination compounds which have interesting structural features.[64] The unique characteristics can be attributed to the aurophilic interactions, which arise from electron relativistic and correlation effects.[65] The relativistic effect is most pronounced for Au metal when compared to neighbouring elements in the periodic table, and is indeed a local maximum for the coinage (Group 11) metals.[66] The relativistic effect is a result of the increased acceleration of the valence electrons (which approach the speed of light), induced by the increase in the proton population of the Au nuclei.[67] This results in the contraction of the *s* and *p* orbitals, with a subsequent expansion of the *d* orbital, which ultimately reduces the energy gap between the *6s* and *5d* orbitals significantly.[68] Theoretical calculations that have qualitatively and quantitatively reviewed this phenomenon are numerous.[69,70] Since their first discovery, the analogy between Au···Au contacts and hydrogen bonding has been drawn.[71] The most apparent and early examples of this phenomena, was demonstrated by Schmidbaur in the late 1980's, in which several auromethanes were synthesised and structurally characterised.[72,73] The formation of hexakis(triphenylphosphaneauro)methane dication $[(Ph_3PAu)_6C]^{2+}$, an arrangement which consists of linear Ph_3P-Au-C in a octahedral pattern around a hypervalent carbon, shows the ability of the aurophillic interactions to stabilise the formation of a polyauriomethanes.[74, 75]

The isolability of $[AuPR_3]^+$ with H^+ had become apparent with the spectroscopic and theoretical investigations of hypercoordinate gold analogues of the first row elements i.e.

ammonium, phosphonium, arsonium, and oxonium cations, which possessed remarkable stability.[76,77] An examination of the gold structures, deposited in the Cambridge Structural Database, assign 2.5 – 4 Å as a range for Au···Au contacts.[78]

Two-coordinate linear Au(I) complexes are well studied in gold chemistry.[79] Due to its low coordination, Au(I) forms neutral and ionic complexes of the general formula X-Au-Y (X=Y=neutral or anionic ligands).[68] The intermolecular Au···Au interactions result in the formation of polymeric chains, type **B** and **C** in Figure 1.8. The interaction becomes more pronounced in dinuclear networks and can be differentiated as either inter or intra-molecular Au···Au interactions, of the type **D** and **E**.[63,80] The close proximity of two Au(I) centres in dinuclear systems has been exploited for the study of Au···Au interactions.[81] A comprehensive study on the reactivity and luminescent characteristics of dinuclear dithiophosphonates has been reported.[82,83] The study allowed for the detection of intermolecular Au···Au interactions from their solid-state emission profiles.[83]

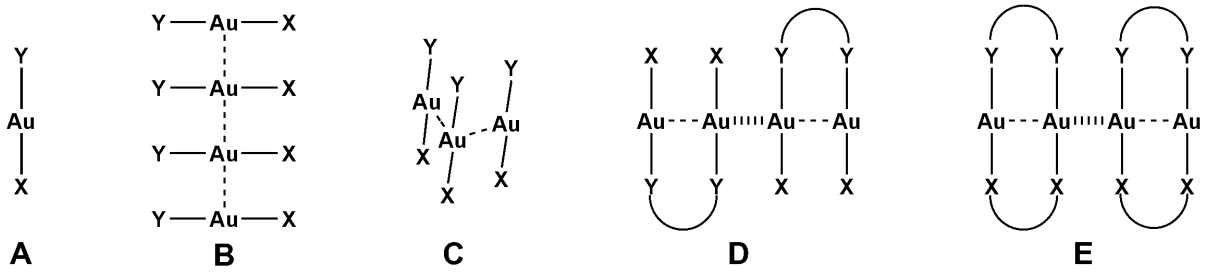

Figure 1.8. Au(I) interactions based on linear **A** results in unsupported interactions of the type **B** and **C**; dinuclear units result in **D** (semi-supported) and **E** (fully supported)[63]

1.3.5.2 Gold dithiophosphonates

It should be noted that the study of mononuclear gold dithiophosphonates are limited, with only one Au(III) complex structurally identified, of the type $[Au\{S_2PPh(OH)\}_2]Cl$, Figure 1.9a.[84] The complex displays two ligand confirmations in the solid state, with both the *cis* and *trans* isomers present in the unit cell. The complex was prepared from the reaction between [AuCl(tht)] and a large excess of $Na[S_2P(OH)Ph]$. Mononuclear Au(I) dithiophosphonates can

be obtained from the reaction of phosphine bearing Au(I) starting materials with dithiophosphonate ligands.

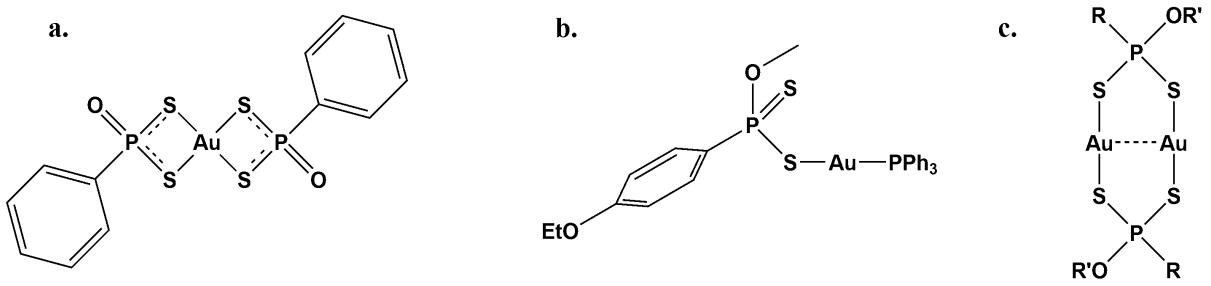

Figure 1.9. Multiple coordination modes in gold dithiophosphonates **a)** Isobidentate coordination in mononuclear Au(III) complex, **b)** Linear mononuclear Au(I) with monodentate coordination, **c)** Dinuclear Au(I) complex with bimetallic biconnective ligands.

Such is the case for the example prepared from the reaction of $[ClAuPPh_3]$ and $NH_4[S_2P(OMe)(p\text{-}C_6H_4OEt)]$ which results in the formation of the Au(I) complex of the type $[Au\{S_2P(OCH_3)(p\text{-}C_6H_4OEt)\}(PPh_3)]$, Figure 1.9b.[56] A second method for the preparation of a mononuclear Au(I) complexes involves the addition of PPh_3 to an isolated dinuclear complex, of the type $[Au\{S_2P(C_6H_4OMe)(OC_5H_9)\}]_2$, in a 4:1 molar ratio.[85] The resultant product has a completely different and rare geometry, with the tetra-coordinate Au(I) atom at the centre of a distorted tetrahedral. Since the initial report on dinuclear Au(I) dithiophosphonate complexes of the type $[Au\{S_2PR(OR')\}]_2$ in 1998,[82] a significant number of variations in the alkyl substituent of dithiophosphonates have been reported,[83,84,86] a general structure is given in Figure 1.9c. The first example was a silyl derivative, of the type $[Au\{S_2P(4\text{-}C_6H_4OMe)(OSiPh_3)\}]_2$. The $[Au\{S_2PR(OR')\}]_2$ type complexes and its reactivity towards bis(phosphines) was investigated and strong evidence proposed the formation of a new hetero-bridged dinuclear complex of the type$[Au_2(dppm)\{S_2P(O)(R)\}]$.[84] Later unsaturation on the ligand was introduced in the form of allyl alcohol and the corresponding Au(I) complex was reported, together with the first luminescence data for dinuclear complexes stabilised by the S-P-S fragment.[86] A subsequent computational study, on the same complex, looked at the Au···Au contacts (both inter- and intra-molecular) in relation to the luminescence profile.[87] Muniz and co-workers were able to assign the phosphorescence to a Ligand to Ligand-Metal charge-transfer (LL-MCT) interaction, (occurring between the sulfur,

phosphorus and gold atoms) which is consistent with the previously obtained experimental data.

In 2002 the first ferrocenyl derivative was reported and isomerisation effects present in solution were described.[83] Without exception all examples crystallise in the *trans* configuration, represented in Figure 1.9c. However, in solution isomerisation to the *cis* conformation becomes apparent, as indicated by ^{31}P NMR. Low temperature NMR experiments indicated that the energy barrier for the isomerisation was significantly low.[83] Furthermore, solid state magic angle spinning NMR investigations indicated the presence of only one isomer in the solid-state, and isomerisation only occurred in solution. In the same study, the use of the bulky chiral menthol as the parent alcohol resulted in the formation of a remarkable non-centrosymmetric Au(I) complex, which crystalized in the monoclinic space group $P2_1$. The molecular structure displays an unusual anti-parallel arrangement of the S-Au-S fragment planes, termed 'crossover'. Karakus et al. prepared a series of ferrocenyl analogues which contained relatively bulky bornyl, myrtenyl and adamantly substituents.[88] The chiral bornyl substituent also resulted in the formation of an overall non-centrosymmetric arrangement and crystals grew in the triclinic space group *P*1. However, the authors noted that all other substituents, except the bornyl group, occupied centrosymmetric positions and no deviation in the parallel S-Au-S coordination planes are observed. A novel topology for Au(I) complexes, which contains eight Au(I) centres is described in Chapter 3.

1.3.6 Palladium dithiophosphonates

The first Pd(II) dithiophosphonates was reported in 1981 and was of the type $[Pd\{S_2P(C_6H_5)(OC_2H_5)\}_2]$, shown in Figure 1.10.[89] The Pd(II) atom is 4-coordinate with square planar geometry and resembles the Ni(II) derivatives, with a centre of inversion present on the Pd(II) atom.

Woollins *et al.* reported two ferrocenyl derivatives,[90] $[Pd\{S_2P(Fc)(OMe)\}]_2$ and in 2004[91] $[Pd\{S_2P(Fc)(OEt)\}_2]$, both gave a square planar geometry around the Pd(II) centre and crystallised in the P21/n space group, Figure 1.10b. Interestingly, in 2010 a report on the same complex, $[Pd\{S_2P(Fc)(OMe)\}_2]$, with the same coordination geometry around the Pd(II) centre, revealed a different orientation of the cyclopentadienyl (Cp) substituent on the

ferrocene, with the latter having an eclipsed conformation of the Cp rings and the initial report having a staggered confirmation.[59]

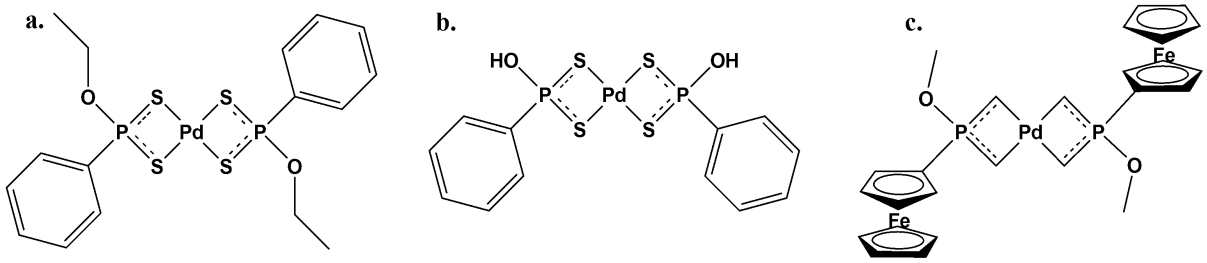

Figure 1.10. a) First Pd(II) complex reported. **b)** *cis*-Pd(II) complex stabilized by hydrogen bonds. **c)** Square-planar Pd(II) complex with ferrocenyl ligands**.**

Aragoni *et al.* reported Pd(II) complexes of the type [Pd{$S_2P(4\text{-}C_6H_4OMe)(OCH_3)$}$_2$], which were also centrosymmetric[92] and later reported an interesting example of the rare *cis* configuration of dithiophosphonate complexes, Figure 1.10c.[93] The Pd(II) complex adopted the configuration due to the formation of extensive hydrogen bonds with ethylenediamine and water. In this thesis a novel Pd(II) dithiophosphonate complex with unusual NMR activity is reported.

1.3.7 Cadmium dithiophosphonates

Gray et al. described the synthesis and structure of a cadmium dithiophosphonate complex, shown in Figure 1.11a.[90] The dinuclear complex has two distinct coordination modes with the ligand, and both chelating and bimetallic biconnective modes are present. The Cd(II) centres are 4-coordinate with a tetrahedral geometry whilst 5-coordinate Cd(II) complexes have also been reported.[41,93,94] All complexes are dinuclear with the ligands coordinating in both bidentate and mondentate patterns, Figure 1.11b.[95] Noteworthy is that the ligand displays a triconnective trimetallic coordination mode. The combination of dithiophosphonates and N-donor ligands has been reported, Figure 1.11c.[96-100] These complexes are octahedral in geometry and the Cd(II) metal is 6-coordinate. Therefore, the variation in coordination in cadmium complexes, due to the large size of the Cd centre, can be utilised to demonstrate the flexibility of the dithiophosphonate ligand. In this study a novel Cd(II) coordination polymer is reported.

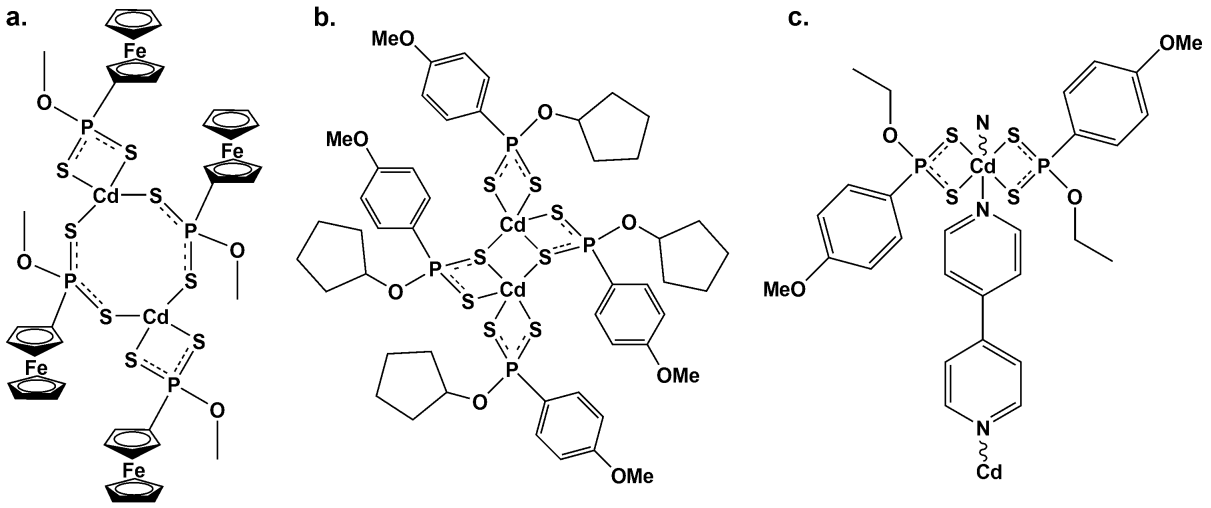

Figure 1.11. Cd(II) complexes bearing various coordination modes **a)** A Cd(II) complex containing both chelating and bimetallic coordination. **b)** Trimetallic tri-connective mode for Cd(II). **c)** Coordination polymer for Cd(II) with bipyridine.

1.4 Supramolecular chemistry

The ability of the ligand to provide strongly covalent and secondary dative coordinative interactions bridging multiple metal centres, directs toward *supramolecular chemistry*. This term was first outlined and defined by Lehn as *"the chemistry of molecular assemblies and of the intermolecular bond"*.[101] Two fundamental approaches to produce assemblies are apparent in the literature and are based on the type of interactions present in the assembly i.e. i) non-covalent interactions which include hydrogen bonding[102], van der Waals, hydrophobic and π-π stacking[103] and ii) directional metal-ligand and metal-metal interactions.[104] The supramolecular structure therefore relies on the coordination geometry of the metal, functional groups present and properties which direct the assembly.[105] The design strategy therefore incorporates two functional subunits of *donors* and *acceptors,* the former refers to organic based ligands which require a minimum of two binding sites and the latter refers to metals which host the coordination sites.[104] Depending on the bite angles and the coordination number of the metal centre several different structures can be obtained, as shown in Figure 1.12.[105]

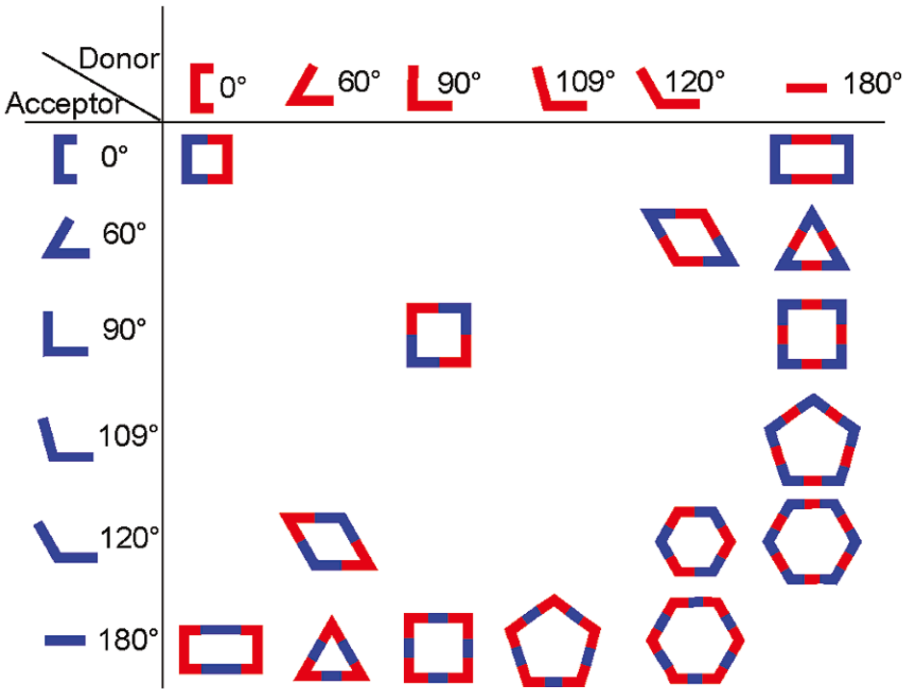

Figure 1.12. Donor and acceptor methodology for accessing Supramolecular Architectures, as adapted from ref. 105.

1.5 Luminescence

Luminescence can be defined as the emission of photons (infrared, ultraviolet or visible) from electronically excited species. In comparison with incandescence, luminescence can be described as cold-body radiation. The origin of the excitation is applied to the naming of the phenomenum, for example **chemi**luminescence arises from a chemical reaction, and several types have been reported[106], some of which are represented in Figure 1.13 below.

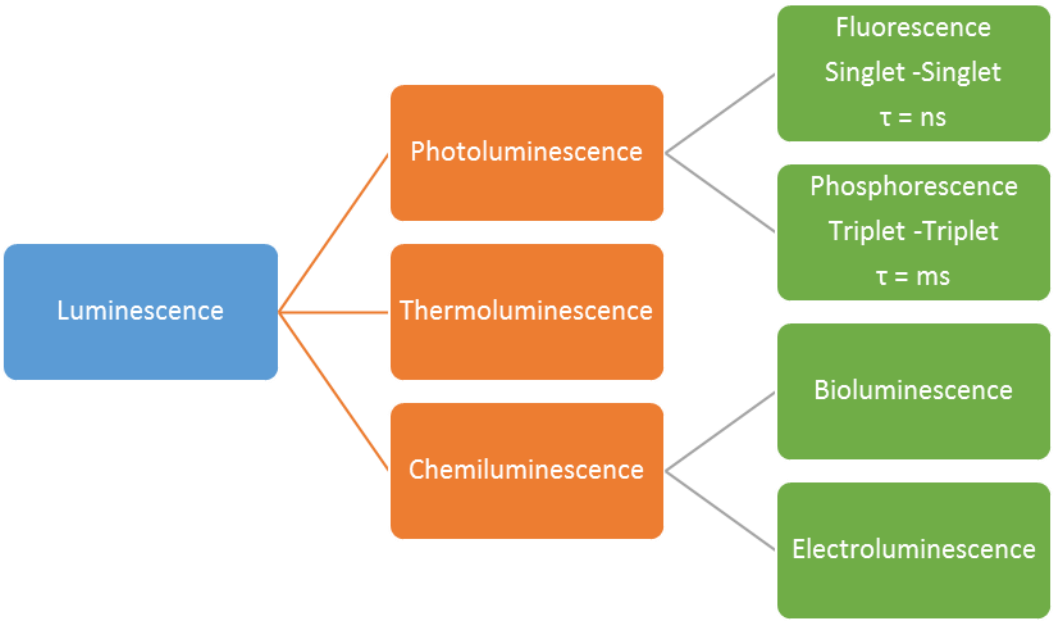

Figure 1.13. Illustration of different types of luminescence phenomena.

1.5.1 Photoluminescence

In the current study the focus will be on **Photo**luminescence, and as the name suggests it deals with the absorption of photons i.e. light. This absorption results in the excitation of the molecule and the subsequent relaxation processes causes an emission, Figure 1.14.

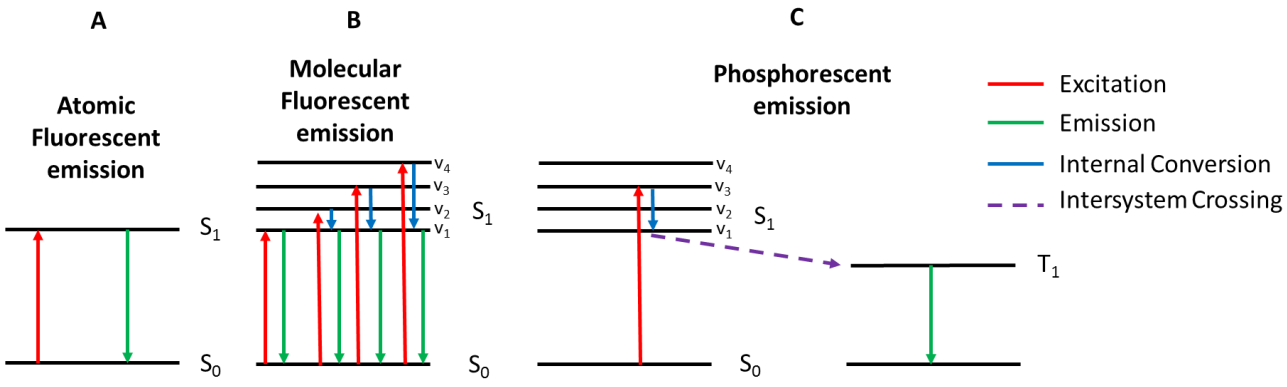

Figure 1.14. Illustration of the photoluminescence process. Arrows represent electronic movement. In an ideal monatomic system resonance fluorescence occurs (excitation ν = emission ν) **(A)**; molecules contain vibrational energy levels and emission occurs after energy loss to internal conversion **(B)**; an intersystem crossing results in delayed emission, phosphorescence **(C)**.

In an ideal mono-atomic system resonance fluorescence occurs, and the excitation and emission frequency are equal, Figure 1.14(**A**). In molecular systems, vibrational energy levels are present and excitation to these levels is followed by internal conversion (non-radiative transition) with the resultant emission being lower in energy, Figure 1.14(**B**). This was first outlined by Stokes in the 19th century in a paper entitled *"On the refrangibility of Light"*. [107] The process of fluorescence is defined as an electronic relaxation composed of two steps. The first step involves the internal conversion of energy (thermal or vibrational) and relaxation to the lowest level of the excited state. Due to this loss of energy the second phase is the emission of a photon, which has lower energy than the incident photon which caused the excitation. Thus the emission is red shifted relative to the excitation. To his credit, the difference between the excitation wavelength and the emission wavelength is known as the *Stokes shift* and the stipulation that an emission should always occur at longer wavelengths relative to its excitation. Importantly, the spin multiplicity is retained in fluorescence, whereas in phosphorescence a change in multiplicity occurs.[108] Therefore an *internal conversion* occurs and is followed by a transition to a triplet excited state before emission to ground state, Figure 1.14(**C**). This second non-radiative transition is an *intersystem crossing* which involves the transition between two isoenergetic vibrational levels of differing multiplicity ($S_1 \rightarrow T_1$). When the relaxation pathway involves a transition, such that the excited triplet state returns to the excited singlet sate ($T_1 \rightarrow S_1$) before emission ($S_1 \rightarrow S_0$), then the resultant process is termed delayed fluorescence and not phosphorescence.[109]

1.5.2 Luminescence in transition metal complexes

The mechanism in these systems are often associated with a *Charge Transfer*. This transfer occurs between the molecular orbital of the ligand and the empty or full *d* orbitals of the transition metal. The transitions are described by the point of origin and its movement through the electronic system, Figure 1.15, demonstrates the situation for an octahedral complex.

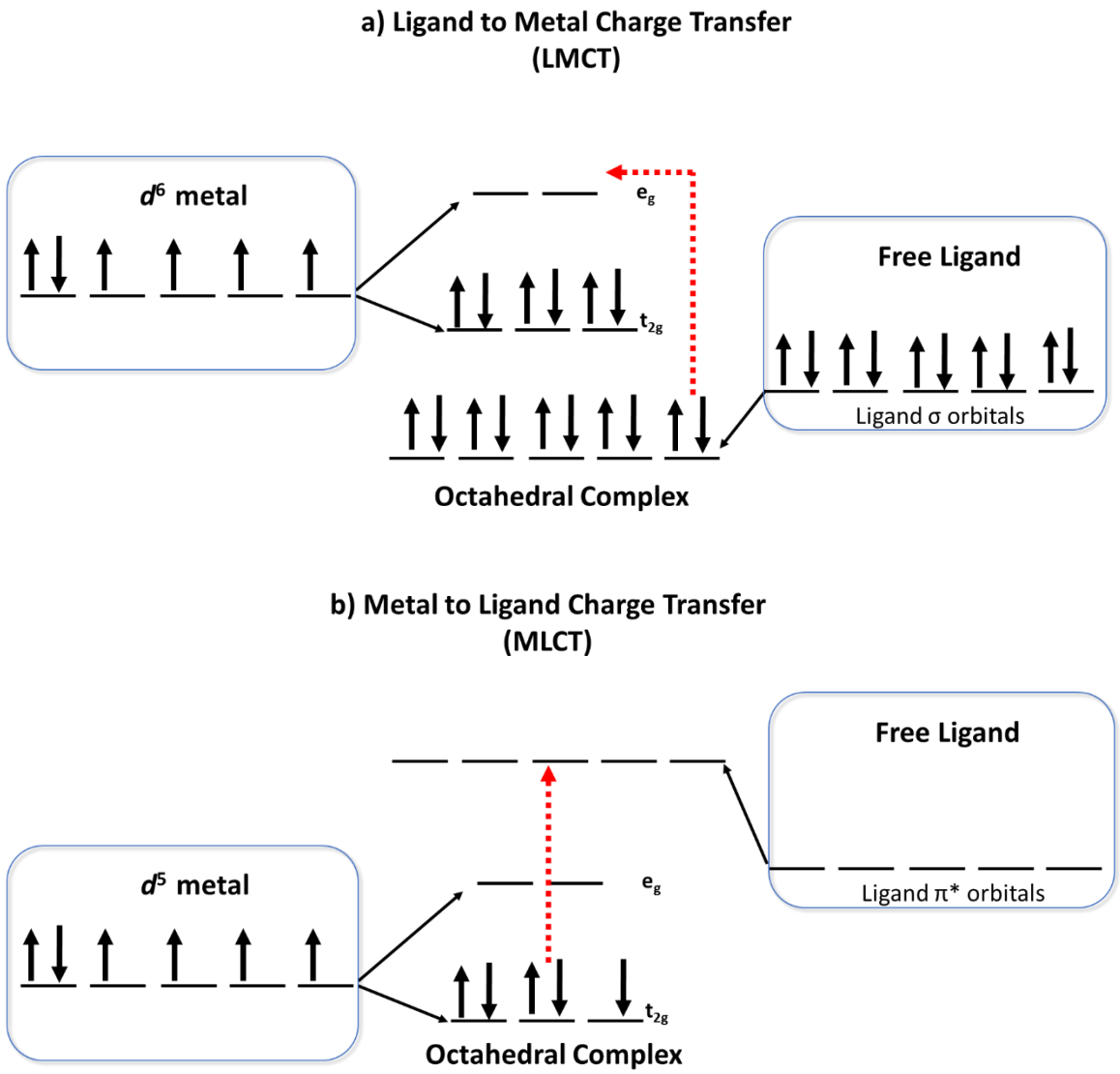

Figure 1.15. Illustration of charge transfer in generic octahedral complexes, with the aid of Crystal field theory. **a)** Transfer of electrons originating from the full σ orbital of the ligand to the empty e_g orbital of the metal. **b)** Transfer of electrons originating e_g orbital of the metal to the empty π* orbital of the ligand.

The application of luminescent organometallic complexes are diverse and include chemosensing ,[110] biomolecular and cellular probes,[111,112] monitoring of industrial important polymerization,[113] and organic light-emitting devices (OLED).[114,115] Reviews on luminescent organometallic compounds have been reported.[116-118]

In the present study, the luminescent characteristics of d^{10} systems of the coinage metals (Au(I), Ag(I) and Cu(I)) was investigated. The luminescent characteristics of dinuclear Au(I)

dithiophosphonate systems have been investigated previously and the Au···Au interactions gave rise to unique and characteristic luminescence patterns.[119] The emission bands were assigned to a LMCT mechanism. However, to the best of our knowledge no luminescent data has been reported for the silver and copper counterparts. However, related derivatives of the Cu(I) complexes have shown rich photophysical properties that has been reported.[120] Other tetranuclear Cu(I) clusters have shown interesting thermochromic[121] and mechanochromic[122] luminescent behaviours.

1.6. Aims

The aims of the study are as follows:

- Design and synthesis of novel ligands which contain multiple coordination moieties on a common backbone.
- Evaluate the coordinative ability of bifunctional ligands by complexation to a diverse range of transition metals.
- Confirm the structural and physical characteristics of the newly synthesized complexes and ligands.
- Identify novel systems, which can provide access to functional materials for luminescent applications.

1.7 Objectives

The primary objectives of the study are as follows:

- To incorporate the known chemistry of dithiophosphonates into the rational design of novel bifunctional ligand systems, which possess the flexibility to accommodate a wide range of metal centres.
- Demonstrate the flexibility of the ligands in terms of their aptitude to accommodate electronically and geometrically different metal centres.

- To gain insight into the complexes, solution and solid state dynamics, with the use of NMR, MS and importantly single crystal X-ray crystallography.
- Provide quantitative data for the physical properties of these systems and provide new synthesis methodologies which simplify their preparation.

1.8 Summary

Overall this thesis seeks to investigate new boundaries and test the limitations of dithiophosphonate and demonstrate its ability to act as an effective building block in the preparation of unique metal architectures. To this end the study drifts away from the norm, which involves the varying of substituents on the ligand base. In this investigation an emphasis is placed on the ability of the ligand to accommodate a diverse range of metal centres and seeks to explore the implications of the various metal centres instead.

The focus of Chapter 2 is the evaluation of diols and a tetrol in the synthesis of disulfide bridged dithiophosphonates. These include its reactivity and redox capabilities, which led to formation of novel heterocycles of two sizes. Ferrocene is incorporated into the study to elucidate the electrochemical behaviour of resulting complexes and more importantly introduce crystallographically favourable substituents for the evaluation of the ligand characteristics. In Chapter 3, a novel approach to dithiophosphonates was adopted, wherein two dithiophosphonate moieties were incorporated onto a common chiral and flexible backbone. The flexibility of this ligand is displayed in its ability to accommodate various metals with differing coordination numbers and oxidation states. The combination of the bis(dithiophosphonate) and metallophilic interactions found in Group 11 metals proved fruitful and a series of multi-metallic complexes, with varying nuclearity and topology were structurally characterised. The Cu(I) complex provides the first example of a Cu_4L_2 configuration for a tetranuclear copper system and the tetranuclear Ag(I) cluster represents the first silver cluster stabilised solely by dithiophosphonates. Complexation to Au(I) afforded a completely new architecture for any transition metal complex known previously. Furthermore the coordination of the newly developed ligand to Au(III) and Ni(II) centres displayed the ability to stabilize metals with varying oxidation states. Chapter 4 seeks to

address the lack of dithiophosphonate chemistry in the realm of tetranuclear Cu(I) clusters and reports the first luminescence data for a series containing seven tetranuclear Cu(I) clusters, of the type Cu_4L_4. Importantly, the chapter seeks to identify a synthetic route which can produce luminescent Cu(I) materials in aqueous environments without requiring protection from oxidation. Chapter 5 looks at an alternative approach to the formation of a bifunctional ligand, and involves the grafting of an N-donor ligand (pyridine) onto a dithiophosphonate backbone. The novel ligand afforded several new metal complexes including the first Co(II) dithiophosphonate. Furthermore, the Co(II) and Cd(II) complexes were found to be coordination polymers. In the case of Ni(II), the complex displayed two configurational isomers with different crystal morphologies. Chapter 6 outlines the impact of the newly prepared systems and how they have created an avenue for future investigations.

1.9 References

1. G. A. Petroianu, *Die Pharmazie*, 2010, **65**, 776-780.
2. F. López-Muñoz, P. García-García and C. Alamo, *J. Clin. Pharm. Ther.*, 2009, **34**, 67-77.
3. T. T. Marrs, R. L. Maynard and F. Sidell, *Chemical warfare agents: toxicology and treatment*, John Wiley & Sons, 2007.
4. N. Yanagisawa, H. Morita and T. Nakajima, *J. Neuro. Sci.*, 2006, **249**, 76-85.
5. I. P. Alimarin, V. R. Tat'yana and M. I. Vadim, *Rus. Chem. Rev.*, 1989, **58**, 863.
6. T. Colclough, *Ind. Eng. Chem. Res.,* 1987, **26**, 1888-1895.
7. R. S. Edmundson, *Dictionary of Organophosphorus Compounds*, Chapman and Hall, New York, 1988.
8. I. Haiduc, D. B. Sowerby and S.-F. Lu, *Polyhedron*, 1995, **14**, 3389-3472.
9. I. Haiduc and D. B. Sowerby, *Polyhedron*, 1996, **15**, 2469-2521.
10. W.E. van Zyl and J. P. Fackler, *Phosphorus, Sulfur, Silicon Rel. Elem.*, 2000, **167**, 117-132.
11. P. Fay and H. P. Lankelma, *J. Am. Chem. Soc.*, 1952, **74**, 4933-4935.
12. P. E. Newallis, J. P. Chupp and L. C. D. Groenweghe, *J. Org. Chem.*, 1962, **27**, 3829-3831.
13. J. P. Chupp and P. E. Newallis, *J. Org. Chem.*, 1962, **27**, 3832-3835.
14. H. Fritz, P. Hug, S. O. Lawesson, E. Logemann, B. S. Pedersen, H. Sauter, S. Scheibye and T. Winkler, *Bull. Soc. Chim. Belg.*, 1978, **87**, 525-534.

15. B. S. Pedersen, S. Scheibye, K. Clausen and S. O. Lawesson, *Bull. Soc. Chim. Belg.*, 1978, **87**, 293-297.
16. B. S. Pedersen, S. Scheibye, N. H. Nilsson and S. O. Lawesson, *Bull. Soc. Chim. Belg.*, 1978, **87**, 223-228.
17. M. P. Cava and M. I. Levinson, *Tetrahedron*, 1985, **41**, 5061-5087.
18. T. Ozturk, E. Ertas and O. Mert, *Chem. Rev.*, 2007, **107**, 5210-5278.
19. M. R. S. J. Foreman, A. M. Z. Slawin and J. D. Woollins, *J. Chem. Soc., Dalton Trans.*, 1996, 3653-3657.
20. P. T. Wood and J. D. Woollins, *J. Chem. Soc., Chem. Comm.*, 1988, 1190-1191.
21. T. B. Rauchfuss and G. A. Zank, *Tetrahedron Lett.*, 1986, **27**, 3445-3448.
22. W. Przychodzeń, *Eur. J. Org. Chem.*, 2005, 2002-2014.
23. T. Nishio, *J. Chem. Soc., Chem. Com.*, 1989, 205-206.
24. L. Legnani, L. Toma, P. Caramella, M. A. Chiacchio, S. Giofre, I. Delso, T. Tejero and P. Merino, *J. Org. Chem.*, 2016, **81**, 7733-7740.
25. W. E. van Zyl and J. D. Woollins, *Coord. Chem.Rev.*, 2013, **257**, 718-731.
26. A. E. Reed and P. v. R. Schleyer, *J. Am. Chem. Soc.*, 1990, **112**, 1434-1445.
27. W. E. van Zyl, J. M. Lopez-de-Luzuriaga and J. P. Fackler, *J. Mol. Struct.*, 2000, **516**, 99-106.
28. S.-L. Liu, X.-Y. Wang, T. Duan, W.-H. Leung and Q.-F. Zhang, *J. Mol. Struct.*, 2010, **964**, 78-81.
29. C. W. Liu, M. D. Irwin, A. A. Mohamed and J. P. Fackler, *Inorg. Chim. Acta*, 2004, **357**.
30. A. R. Gataulina, D. A. Safin, T. R. Gimadiev and M. V. Pinus, *Transition Met. Chem.*, 2008, **33**, 921-924.
31. E. G. Sağlam, *Inorg. Chim. Acta*, 2015, **434**, 188-197.
32. H.-L. Liu, H.-Y. Mao, C. Xu, H.-Y. Zhang, H.-W. Hou, Q.-A. Wu, Y. Zhu, B.-X. Ye and L.-J. Yuan, *Polyhedron*, 2004, **23**, 1799-1804.
33. H. Hartung, *Z. Chem.*, 1967, **7**, 241.
34. M. Arca, A. Cornia, F. A. Devillanova, A. C. Fabretti, F. Isaia, V. Lippolis and G. Verani, *Inorg. Chim. Acta*, 1997, **262**, 81-84.
35. Y. Ozcan, S. Ide, M. Karakus and H. Yilmaz, *Acta Cryst.*, 2002, **C58**, m388-m389.
36. Y. Ozcan, S. Ide, M. Karakus and H. Yilmaz, *Anal Sci*, 2002, **18**, 1285-1286.

37. M. D. Santana, G. Garcia, C. M. Navarro, A. Abel Lozano, J. Perez, L. Garcia and G. Lopez, *Polyhedron*, 2002, **21**, 1935-1942.

38. E, Kır, E.; Yalımlı, Ş.; Kurtulmuş, S.; Aydın, A. and Yılmaz, H, *Phosphorus, Sulfur, Silicon Rel. Elem.,* **2015,** *190* (2), 178.

39. I. P. Gray, H. L. Milton, A. M. Z. Slawin and J. D. Woollins, *Dalton Trans.*, 2003, 3450-3457.

40. C. M. Thomas, A. Neels, H. Stoeckli-Evans, G. Suss-Fink, *J. Organomet. Chem.*, 2001, **633**, 85-90.

41. I. P. Gray, A. M. Z. Slawin and J. D. Woollins, *Dalton Trans.*, 2004, 2477-2486.

42. G. Sanchez, J. Garcia, D. J. Meseguer, J. L. Serrano, J. Perez, E. Molins and G. Lopez, *Inorg. Chim. Acta*, 2004, **357**, 677-683.

43. M. Karakus and H. Yilmaz, *Russ. J. Coord. Chem.*, 2006, **32**, 437-443.

44. M. C. Aragoni, M. Arca, F. A. Devillanova, M. B. Hursthouse, S. L. Huth, F. Isaia, V. Lippolis, A. Mancini, S. Soddu and G. Verani, *Dalton Trans.*, 2007, 2127-2134.

45. M. C. Aragoni, M. Arca, M. Crespo, F. A. Devillanova, M. B. Hursthouse, S. L. Huth, F. Isaia, V. Lippolis and G. Verani, *Dalton Trans.*, 2009, 2510-2520.

46. S. Sewpersad, B. Omondi and W. E. Van Zyl, *Acta Cryst.*, 2012, **E68**, m1534.

47. S. Sewpersad, B. Omondi and W. E. Van Zyl, *Acta Cryst.,* 2012, **E68**, m1483.

48. S. Sewpersad and W. E. Van Zyl, *Acta Cryst.*, 2012, **E68**, m1457.

49. A. Saadat, A. Banaee, P. McArdle, K. Zare, K. Gholivand and A. A. Ebrahimi Valmoozi, *J. Chem. Sci.*, 2014, **126**, 1125-1133.

50. E. G. Saglam, A. Ebinc, C. T. Zeyrek, H. Unver and T. Hokelek, *J. Mol. Struct.*, 2015, **1099**, 490-501.

51. A. Banaei, A. Saadat, M. Mohammad Goli, P. McArdle, E. Pourbasheer and P. Pargolghasemi, *Heteroat. Chem.*, 2016, **27**, 353-360.

52. M. C. Aragoni, M. Arca, F. Demartin, F. A. Devillanova, C. Graiff, F. Isaia, V. Lippolis, A. Tiripicchio and G. Verani, *J. Chem. Soc., Dalton Trans.*, 2001, 2671-2677.

53. M. C. Aragoni, M. Arca, N. R. Champness, M. De Pasquale, F. A. Devillanova, F. Isaia, V. Lippolis, N. S. Oxtoby and C. Wilson, *CrystEngComm*, 2005, **7**, 363-369.

54. M. C. Aragoni, M. Arca, N. R. Champness, A. V. Chernikov, F. A. Devillanova, F. Isaia, V. Lippolis, N. S. Oxtoby, G. Verani, S. Z. Vatsadze and C. Wilson, *Eur. J. Inorg. Chem.*, **2004**,10, 2008-2012.

55. M. Karakus and H. Yilmaz, *Rus. J. Coord. Chem.*, 2006, **32**, 437-443.
56. I. Haiduc, G. Mezei, R. Micu-Semeniuc, F. T. Edelmann and A. Fischer, *Z. Anorg. Allg. Chem.*, 2006, **632**, 295-300.
57. M. Karakus, Y. Ikiz, H. I. Kaya and O. Simsek, *Chem. Cent. J.*, 2014, **8**, 1-8.
58. W. F. Shi and A. Rothenberger, *Eur. J. Inorg. Chem.*, 2005, 2935.
59. X.-Y. Wang, H.-T. Shi, Q. Ma and Q.-F. Zhang, *Z. Naturforsch., B: J. Chem. Sci.*, 2010, **65**, 32-36.
60. I. Haiduc, G. Mezei, R. Micu-Semeniuc, F. T. Edelmann and A. Fischer, *Z. Anorg. Allg. Chem.*, 2006, **632**, 295.
61. D. Sun and R.-B. Huang, *Acta Cryst.*, 2011, **C67**, m315-m317.
62. W. F. Shi, R. Ahlrichs, C. E. Anson, A. Rothenberger, C. Schrodt and M. Shafaei-Fallaha, *Chem. Commun.*, 2005, 893.
63. H. Schmidbaur and A. Schier, *Chemical Society Reviews*, 2012, **41**, 370-412..
64. A. Grohmann and H. I. G. S. Schmidbaur, *Gold: Progress in Chemistry, Biochemistry and technology.*, John Wiley & Sons Ltd., West Sussex, England, 1999.
65. P. Pyykkö, *Angew. Chem. Int. Ed.*, 2004, **43**, 4412-4456.
66. P. Pyykkö, *Angew. Chem. Int. Ed.*, 2002, **41**, 3573-3578.
67. F. Scherbaum, A. Grohmann, B. Huber, C. Krüger and H. Schmidbaur, *Angew. Chem. Int. Ed.*, 1988, **27**, 1544-1546.
68. H. Schmidbaur, *Gold Bull.*, 1990, **23**, 11-21.
69. H. Schmidbaur, *Gold Bull.*, 2000, **33**, 3-10.
70. P. Schwerdtfeger, *Heteroatom Chem.*, 2002, **13**, 578-584.
71. W. Rapson, *Gold Bull.*, 1989, **22**, 19-20.
72. F. Scherbaum, B. Huber, G. Müller and H. Schmidbaur, *Angew. Chem. Int. Ed.*, 1988, **27**, 1542-1544.
73. H. Schmidbaur, W. Graf and G. Müller, *Angew. Chem. Int. Ed.*, 1988, **27**, 417-419.
74. H. Schmidbaur, G. Weidenhiller and O. Steigelmann, *Angew. Chem. Int. Ed.*, 1991, **30**, 433-435.
75. H. Schmidbaur, *Pure Appl. Chem.*, 1993, **65**, 691-698.
76. J. Li and P. Pyykko, *Inorg. Chem.*, 1993, **32**, 2630-2634.
77. O. D. Haeberlen, H. Schmidbaur and N. Rosch, *J. Am. Chem. Soc.*, 1994, **116**, 8241-8248.

78. S. S. Pathaneni and G. R. Desiraju, *J. Chem. Soc., Dalton Trans.*, 1993, 319-322.
79. M. Gimeno and A. Laguna, *Gold Bull.*, 2003, **36**, 83-92.
80. S. L. Lawton, W. J. Rohrbaugh and G. T. Kokotailo, *Inorg. Chem.*, 1972, **11**, 2227-2233.
81. H. Schmidbaur, *Chem. Soc. Rev.*, 1995, **24**, 391-400.
82. W. E. van Zyl, R. J. Staples and J. J. P. Fackler, *Inorg. Chem. Commun.*, 1998, **1**, 51-54.
83. W. E. van Zyl, J. M. López-de-Luzuriaga, A. A. Mohamed, R. J. Staples and J. P. Fackler, *Inorg. Chem.*, 2002, **41**, 4579-4589.
84. H. H. Murray, G. Garzon, R. G. Raptis, A. M. Mazany, L. C. Porter and J. P. Fackler, Jr., *Inorg. Chem.*, 1988, **27**, 836-842.
85. A. Maspero, I. Kani, A. A. Mohamed, M. A. Omary, R. J. Staples and J. P. Fackler, Jr., *Inorg. Chem.*, 2003, **42**, 5311-5319.
86. W. E. Van Zyl, J. M. López-de-Luzuriaga and J. P. Fackler, *J. Mol. Struct.*, 2000, **516**, 99-106.
87. J. Muniz, L. E. Sansores, A. Martinez and R. Salcedo, *J. Mol. Struct. THEOCHEM*, 2007, **820**, 141.
88. M. Karakus, P. Lönnecke, M. Hildebrand and E. Hey-Hawkins, *Z. Anorg. Allg. Chemie*, 2011, **637**, 983-987.
89. J. P. Fackler Jr and L. D. Thompson Jr, *Inorg. Chimi. Acta*, 1981, **48**, 45-52.
90. I. P. Gray, H. L. Milton, A. M. Z. Slawin and J. D. Woollins, *Dalton Trans.*, 2003, 3450-3457.
91. I. P. Gray, A. M. Z. Slawin and J. D. Woollins, *Z. Anorg. Allg. Chemie*, 2004, **630**, 1851.
92. M. C. Aragoni, M. Arca, F. Demartin, F. A. Devillanova, C. Graiff, F. Isaia, V. Lippolis, A. Tiripicchio and G. Verani, *Eur. J. Inorg. Chem.*, 2000, 2239-2244.
93. M. C. Aragoni, M. Arca, F. Demartin, F. A. Devillanova, F. Isaia, V. Lippolis and G. Verani, *Inorg. Chim. Acta*, 2005, **358**, 213-216.
94. W. Shi, M. Shafaei-Fallah, C. E. Anson and A. Rothenberger, *Dalton Trans.*, 2006, 3257-3262.
95. M. Karakus, H. Yilmaz, Y. Ozcan and S. Ide, *Appl. Organomet. Chem.*, 2004, **18**, 141-142.
96. F. Devillanova, C. Aragoni, M. Arca, S. L. Huth and M. B. Hursthouse, *Univ. of Southampton, Crystal Structure Report Archive*, 2006, 247.

97. F. Devillanova, C. Aragoni, M. Arca, S. L. Huth and M. B. Hursthouse, *Univ. of Southampton, Crystal Structure Report Archive*, 2006, 246.
98. F. Devillanova, C. Aragoni, M. Arca, S. L. Huth and M. B. Hursthouse, *Univ. of Southampton, Crystal Structure Report Archive*, 2006, 245.
99. F. Devillanova, C. Aragoni, M. Arca, M. B. Hursthouse and S. L. Huth, *Univ. of Southampton, Crystal Structure Report Archive*, 2006, 235.
100. F. Devillanova, C. Aragoni, M. Arca, M. B. Hursthouse and S. L. Huth, *Univ. of Southampton, Crystal Structure Report Archive*, 2006, 248.
101. J. M. Lehn, *Supramolecular chemistry: concepts and perspectives*, New York, 1995.
102. T. Steiner, *Angew. Chem. Int. Ed.*, 2002, **41**, 48-76.
103. M. W. George, E. S. Eric, J. P. Mathias, C. T. Seto, D. N. Chin, M. Mammen and D. M. Gordon, *Acc. Chem. Res.*, 1995, **28**, 37-44.
104. P. J. Stang and B. Olenyuk, *Acc. Chem. Res.*, 1997, **30**, 502-518.
105. R. Chakrabarty, P. S. Mukherjee and P. J. Stang, *Chem. Rev.*,2011, **11**, 6918.
106. B. Valeur and M. N. Berberan-Santos, *Molecular fluorescence: principles and applications*, John Wiley & Sons, 2012.
107. G. G. Stokes, *Philosophical Transactions of the Royal Society of London*, 1852, **142**, 463-562.
108. C. R. Ronda, *Luminescence: from theory to applications*, John Wiley & Sons, 2007.
109. E. G. Yukihara and S. W. McKeever, *Optically stimulated luminescence: fundamentals and applications*, John Wiley & Sons, 2011.
110. X. He and V. W.-W. Yam, *Coord. Chem. Rev.*, 2011, **255**, 2111-2123.
111. K. K.-W. Lo, A. W.-T. Choi and W. H.-T. Law, *Dalton Trans.*, 2012, **41**, 6021-6047.
112. K. K.-W. Lo, *Top. Organomet. Chem.*, 2010, **29**, 115-158.
113. A. J. Lees, *Coord. Chem. Rev.*, 1998, **177**, 3-35.
114. M.-C. Tang, A. K.-W. Chan, M.-Y. Chan and V. W.-W. Yam, *Top Curr Chem (J)*, 2016, **374**, 46.
115. K. M.-C. Wong, M. M.-Y. Chan and V. W.-W. Yam, *Adv. Mater.*, 2014, **26**, 5558-5568.
116. A. J. Lees, *Chem. Rev.*, 1987, **87**, 711-743.
117. V. W.-W. Yam, V. K.-M. Au and S. Y.-L. Leung, *Chem. Rev.*, 2015, **115**, 7589-7728.
118. V. W.-W. Yam, *Pure Appl. Chem.*, 2013, **85**, 1321-1329.

119. W. E. van Zyl, J. M. Lopez-de-Luzuriaga, A. A. Mohamed, R. J. Staples and J. P. Fackler, Jr., *Inorg. Chem.*, 2002, **41**, 4579-4589.

120. R. S. Dhayal, J.-H. Liao, H.-N. Hou, R. Ervilita, P.-K. Liao and C. W. Liu, *Dalton Trans.*, 2015, **44**, 5898-5908.

121. Q. Benito, X. F. Le Goff, G. Nocton, A. Fargues, A. Garcia, A. Berhault, S. Kahlal, J.-Y. Saillard, C. Martineau, J. Trébosc, T. Gacoin, J.-P. Boilot and S. Perruchas, *Inorg. Chem.*, 2015, **54**, 4483-4494.

122. Q. Benito, X. F. Le Goff, S. Maron, A. Fargues, A. Garcia, C. Martineau, F. Taulelle, S. Kahlal, T. Gacoin, J.-P. Boilot and S. Perruchas, *J. Am. Chem. Soc.*, 2014, **136**, 11311-11320.

Chapter 2
Diol and tetrol precursors to heterocycles in oxidative –S-S- coupling reactions

2.1 Introduction

Ferrocene has remained an iconic organometallic and sandwich compound ever since its structure was confirmed in 1952.[1] Ferrocene and derivatives thereof have been involved in numerous fundamental and applied research endeavours ranging from biomedical,[2] biosensors,[3] catalysis,[4] supramolecular materials[5] and others.[6]

Lawesson's Reagent (**I**) is obtained from the reaction between P_4S_{10} and anisole, and primarily used as a reagent to convert ketones to thiones,[7] its subsequent use as an excellent precursor to form dithiophosphonic acids is now well established. The chemistry of ferrocene is related to that of electron-rich aromatics, a fact already established in the year of its discovery.[8] Woollins and co-workers were the first to observe that replacing anisole with ferrocene in refluxing xylene forms the associated stable dimer (**II**) in good yield[9] and fundamental in forming interesting ferrocenyl heterocycles.[10] The reaction between (**II**) and a vast number of primary or secondary alcohols paved the way for the isolation of numerous ferrocenyl-based dithiophosphonate complexes of the type $[M\{S_2PFc(OR)_x]$ (M = transition metal; Fc = ferrocenyl, x = 1-3) by some of us[11] and others.[12] Dithio-organophosphorus compounds have found application in diverse and important industrial areas ranging from anti-oxidant additives in the oil- and petroleum industry,[13] agricultural pesticide derivatives,[14] metal ore extraction reagents and flotation agents in the mining industry.[15]

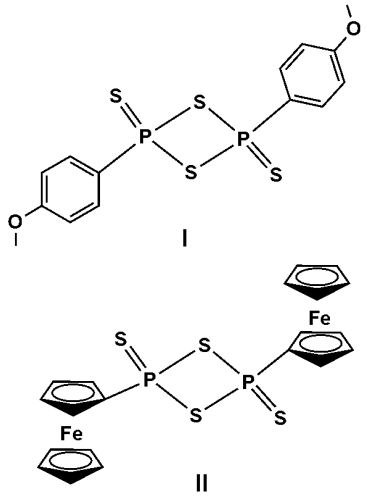

Figure 2.1. Lawesson's reagent (I) and its ferrocenyl analogue (II).

Within the context of green chemistry, it was recently suggested that a structural modification in organophosphorus compounds to reduce toxicity could be achieved by replacing the present oxono analogues as acetylcholinesterase (AChE) inhibitors by the less reactive thiono analogues.[16] A disulfide functionalized bis-ferrocene urea acyclic receptor and urea appended upper rim calix[4]arene receptors has been reported for the fabrication of SAM redox-active anion sensors.[17] Oxidation of $[S_2PR(OR')]^-$salts can be readily achieved with a mild oxidizing agent such as I_2 (with or without activated KI) in aqueous or methanolic solution leading to disulfane products of the type PR(OR')(S)S-SPR(OR')(S) (R = alkyl, aryl). The reaction of bis(thiophosphoryl)disulfanes, with metal precursors have been reviewed[18] whilst for the corresponding bis(thiophosphonyl)disulfanes a number of oxidized S-S coupled compounds have been reported.[19] All such compounds are derived from reaction with simple alcohols (MeOH, EtOH, i-PrOH, etc.) and all form intermolecular S-S oxidative couplings because intramolecular bonding is chemically not possible. As early as the 1970's, the use of diols and polyols to form disulfides was introduced.[20] Through the reaction between Lawesson's reagent and diols new stable di-ammonium salts were formed,[21] which were possibly converted into disulfides but lack verification through structural studies. The oxygen counterpart (phosphonyl peroxides) of the type [(RO)Ph(O)P-O-O-P(O)Ph(OR)] (R = n-butyl) are known, but due to their inherent instability, their study is limited to thermal and photochemical decomposition pathways.[22] By contrast, the disulfide bond is generally considered a strong covalent bond, despite a large variation in the bond lengths that can be achieved, which at extremes vary from 1.89 Å in gaseous disulfur[23] to 2.39 Å in anhydrous sodium dithionite.[24] Interestingly, a recent study performed DFT calculations on a series of diphosphadithiatetrazocines of the type $R'RP(NSN)_2PRR'$ and was scrutinized by topology analysis. Contrary to a regular disulfide bond, it was found that the cross-ring connection is only a secondary electron-sharing bond, about half as strong as a common S−S linkage and the regular disulfide bond itself is best described as a charge-shift bond.[25]

The formation of interlocking rings as a plausible topological motif formed part of the motivation for the present study. Increasing the number of central $[CH_n]_m$ (n = 0, 1, 2; m = 2 or 3) groups increase the length of the sidearms leading to larger C/O/P/S-rich cycles upon S-S coupling which could either i) form interlocking independent molecular rings when the cycle becomes sufficiently large or ii) become a large coordination polymer network through a combination of *intra*- and *inter*molecular S-S coupling.

This study report on the reactions between di- and tetra-ols each with (**II**) (Scheme 2.1) forming ammonium dithiophosphonate salts **L1**-**L3**, followed by iodine oxidization forming the respective disulfide products **1**-**3** achieved through oxidative intramolecular S-S coupling, with representative solid state structures reported for the first time. The solution and solid-state MAS NMR ^{31}P NMR results and concentration dependent electrochemical studies performed on the ferrocene-based disulfide dithiophosphonate, are reported.

2.2 Results and discussion

2.2.1 Synthesis

The dithiophosphonate salts **L1**, **L2** and **L3** were prepared by the direct addition of the respective alcohols to **II** and subsequent deprotonation, Scheme 2.1. In cases where the alcohol is in a liquid phase no additional solvent is required. Therefore liquid ethanediol (or ethylene glycol) was added directly to **II**, with the solids pentaerythritol or *trans*-1,2-cyclohexanediol requiring a small amount of toluene. In all cases the reaction was essentially complete once dissolution of all solids took place. The respective dithiophosphonic acids formed were deprotonated *in-situ* with the weak base ammonia at 0°C (ice bath) forming two *di*- and one *tetra*-ammonium (Fc)dithiophosphonate salt derivatives **L1**-**3**, as shown in Scheme 2.1. All of the above salts were found to be relatively stable and could be stored indefinitely under a N_2 atmosphere. Prolonged exposure to air eventually lead to the distinct smell of H_2S being released. The salts were subsequently oxidized by iodine in a methanol solution forming the disulfide heterocyclic products **1**-**3** as yellow powders through oxidative *intra*molecular S-S coupling. The disulfides were found to be soluble in chlorinated solvents.

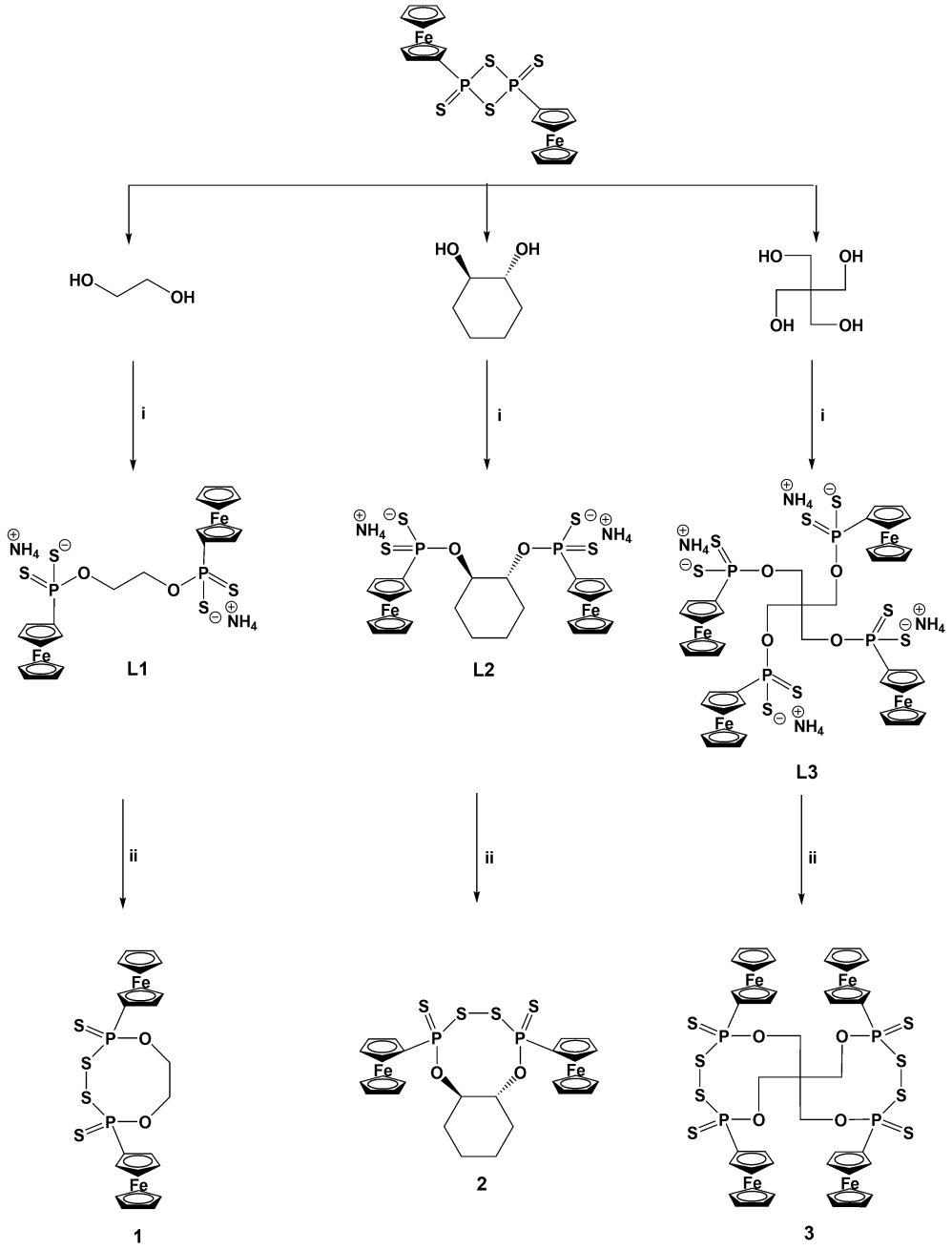

Scheme 2.1. Synthesis of C/O/P/S cycles *via* oxidative intramolecular S-S coupling. Conditions: **i)** Toluene, 70°C until complete dissolution, then ammonia gas at 0°C, **ii)** Iodine in MeOH at room temperature.

2.2.2 Solution and solid state NMR

The unsubstituted cyclopentadienyl ring in all cases gave a singlet peak, with the substituted ring giving two sets of signals for the pair of equivalent protons. The ^{1}H NMR showed peaks in the expected region, with the exception of compound **L1**. Normally ethylene glycol would have singlet peaks for the CH_2 groups due to symmetry arguments but we found for **L1** that

the CH_2 groups reveal triplets suggesting the molecule has a disrupted symmetry, J_{H-H} = 10.8 Hz. The ^{31}P NMR spectra of **L1**-**L3** gave singlet peaks at 94.17, 89.48 and 96.20 ppm which lies within the expected range.[11c] The ^{31}P NMR spectra of **1**-**3** also showed singlet peaks in the same range which suggests a single isomer and configuration is present in solution. Previously reported compounds with intermolecular S-S bridges described the possibility of the formation of two distinct isomers due to the chirality at the P atom. The rotational freedom of the single S-S bridge accounted for the presence of distinct P environments, depending on the orientation of the remaining groups on the P atom. In our case the additional linkage, via the alkane O-C-C-O present, restricts this rotational freedom upon formation of the S-S bridge, and directs the formation to a single absolute configuration at the P centres. In the solid-state, the packing energy nullifies molecular fluxionality and only one configuration was identified. The corresponding ^{31}P MAS NMR spectrum (Figure 2.2) shows a singlet peak resonating at 92.3 ppm. The spinning sidebands were distinguished from the relevant peak by varying the spin-rate of the rotor. The local environments around the P atoms were unperturbed by adjacent dinuclear units and are magnetically equivalent, leading to the observed single peak. Therefore, it is proposed that fixed configuration is present both in solution and the solid state.

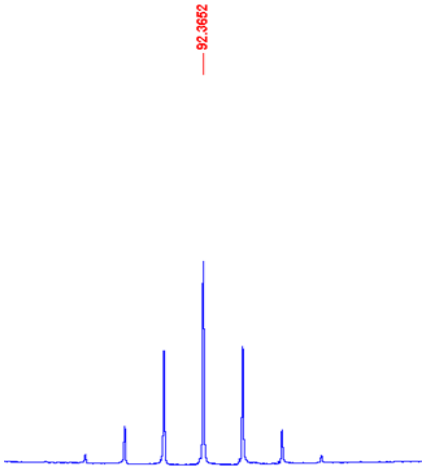

Figure 2.2. Solid state ^{31}P MAS NMR spectrum with spinning side-bands.

In addition, the structural dynamics of the S=PSSP=S geometries has been studied and classified.[19] Three distinct geometries are possible, *anti-anti* where both S atoms point away from the disulfide bridge; *syn-syn* where both point towards the disulfide bridge; and *anti-syn*

which is a hybrid of the aforementioned geometries, Figure 2.3. Variation in the geometry of the P_2S_4 backbone has several contributing factors. In this study compounds **1**-**3** all display *anti-anti* geometries.

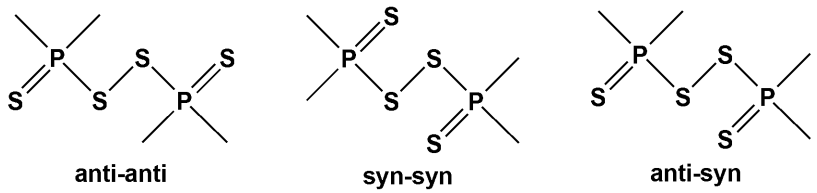

Figure 2.3. Possible geometries for the P_2S_4 backbone.

2.3 Solid state analysis

Selected bond lengths and angles for compounds **1, 2, 3** are shown in Table 2.1 and important X-ray crystallographic data and parameters presented in Table 2.2. Complex **1** crystallizes in the monoclinic space group C2/c. A perspective view of compound **1** is shown in Figure 2.4. The cyclopentadienyl (Cp) rings of the ferrocene moiety occupy an eclipsed conformation relative to each other. Interestingly the unique 8 membered hetrocycle [-S-P-O-C-C-O-P-S-] formed is the first of its type to be reported. The average P=S and P-S bond lengths are 1.927 and 2.102 Å respectively, and shows no deviation from the expected values. A portion of its packing in the crystal structure is shown in Figure 2.5. An interesting observation for **1** is an unusually high number of formula units that can be related to the symmetry in the unit cell (indicated by the high *Z* value). The ethandiol fragment allows for a high packing efficiency as compared to **2** and **3**. This allowed for the formation of well-ordered molecular sheets within the crystal lattice.

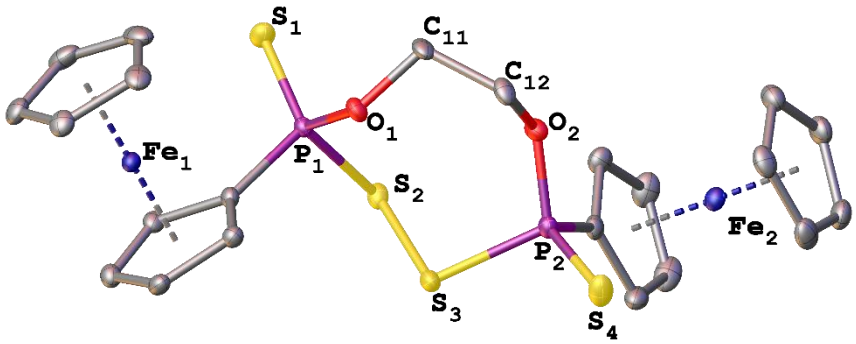

Figure 2.4. Thermal ellipsoid drawing (50% probability) of **1**. Hydrogen atoms are omitted for clarity.

Table 2.1. Selected bond distances (Å), angles (°) and torsion angles (°) for **1**-**3**with e.s.d. in parentheses.

Compound **1**			
S(2)-S(3)	2.0697(10)	P(1)-O(1)	1.584(2)
P(1)-S(2)	2.1015(15)	P(2)-O(2)	1.587(2)
P(2)-S(3)	2.1022(10)	S(1)-P(1)-S(2)	105.23(4)
P(1)=S(1)	1.9255(10)	S(4)-P(2)-S(3)	105.61(4)
P(2)=S(4)	1.9282(10)	O(1)-P(1)-S(1)	119.38(9)
S(1)-P(1)-S(2)-S(3)		172.01	
P(2)-S(3)-S(2)-P(1)		-101.19	
Compound **2**			
S(1A)-S(2A)	2.0633(13)	P(1A)-O(1A)	1.5863(19)
P(1A)-S(1A)	2.1178(11)	P(2A)-O(2A)	1.5854(18)
P(1B)-S(1B)	2.1088(9)	S(2A)-S(1A)-P(1A)	101.19(4)
P(1A)=S(3A)	1.9219(11)	S(1A)-S(2A)-P(2A)	102.49(4)
P(2A)=S(4A)	1.9160(11)	O(1A)-P(1A)-S(3A)	119.03(8)
S(2A)-S(1A)-P(1A)-S(3A)		172.93(5)	
S(1A)-S(2A)-P(2A)-S(4A)		163.79(4)	
P(1A)-S(1A)-S(2A)-P(2A)		-97.37(4)	
Compound **3**			
S(1)-S(2)	2.071(2)	P(2)=S(4)	1.923(2)
S(5)-S(6)	2.066(2)	P(3)=S(7)	1.919(2)
P(1)-S(1)	2.1046(19)	P(4)=S(8)	1.9244(19)
P(2)-S(2)	2.1048(19)	P(1)-O(1)	1.596(4)
P(3)-S(5)	2.0986(19)	P(2)-O(2)	1.594(4)
P(4)-S(6)	2.1082(19)	P(3)-O(3)	1.587(4)
P(1)=S(3)	1.9119(19)	P(4)-O(4)	1.593(3)
S(2)-S(1)-P(1)-S(3)		176.13(8)	
S(1)-S(2)-P(2)-S(4)		-175.55(8)	
S(6)-S(5)-P(3)-S(7)		176.82(9)	
S(5)-S(6)-P(4)-S(8)		-174.65(8)	
P(3)-S(5)-S(6)-P(4)		-107.42(8)	

Table 2.2. X-ray crystallographic data for compounds **1**, **2** and **3**.

Compound	**1**	**2**	**3**
Formula	$C_{22}H_{22}Fe_2O_2P_2S_4$	$C_{26}H_{28}Fe_2O_2P_2S_4$	$C_{45}H_{40}Fe_4O_4P_4S_8 \cdot 2CH_2Cl_2$
Fw	620.28	674.36	1418.38
Crystal System	Monoclinic	Monoclinic	Orthorhombic
Space group	C2/c	$P2_1/c$	P b c a
a, Å	57.4371(9)	17.7370(9)	27.4485(13)
b, Å	7.41200(10)	15.2384(8)	14.5982(7)
c, Å	41.5300(6)	21.1581(11)	28.2672(14)
a, deg.	90	90	90
b, deg.	104.2230(10)	100.1970(10)	90
g, deg.	90	90	90
V, $Å^3$	17138.4(4)	5628.4(5)	11326.6(9)
Z	28	8	8
ρ_{calcd}, g cm^{-3}	1.442	1.592	1.664
T, K	100(2)	173(2)	173(2)
Completeness, %	99.5	99.7	99.6
Reflections collected	205410	45238	52043
Independent reflections	21515	10286	12757
R_1a, wR_2b [I>2σ(I)]	0.0381, 0.0964	0.0318, 0.0784	0.0596, 0.1616
R_1a, wR_2b (all data)	0.0442, 0.00993	0.0426, 0.0849	0.1035, 0.1894
Goodness of fit	1.204	1.025	1.052
Largest diff. peak and hole, e/$Å^3$	0.585 and -0.565	0.614 and -0.325	1.930 and -1.299

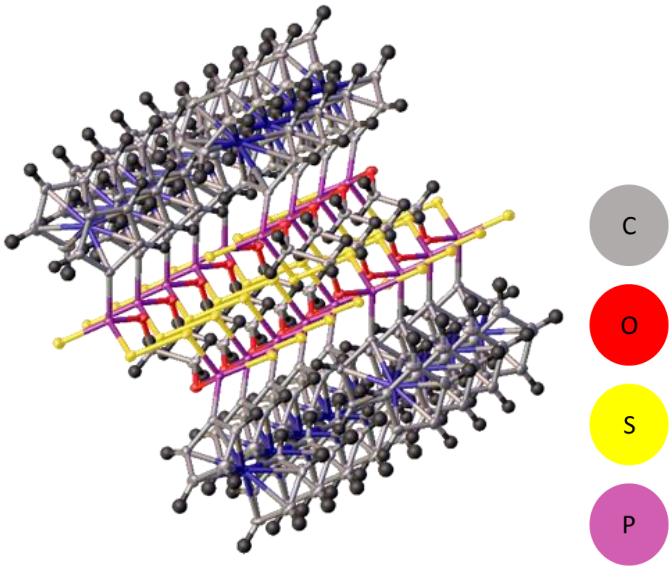

Figure 2.5. Portion of the crystal structure packing for **1**.

Compound **2** crystallizes in the monoclinic space group, $P2_1/c$, with a unit cell consisting of 8 molecules. Selected bond lengths and angles are shown in Table 2.1. A perspective view of complex **2** is shown in Figure 2.6. The Cp rings are eclipsed, with the cyclohexane ring in the chair conformation, Figure 2.7a. The oxygen atoms on the cyclohexane ring are in a gauche conformation (O-C-C-O torsion angles *ca.* 73°), with both substituents in the axial position. Average P=S and P-S bond lengths are 1.921 and 2.111 Å respectively, and shows no deviation from the expected values. Careful inspection of the two P atoms in terms of stereochemistry indicates that both have the same absolute configuration. The heterocycle present in **1** and **2** is shown in Figure 2.7b. Notably a structural overlay analysis of the heterocyclic rings in **1** and **2** reveals that they are isostructural. In addition only a slight deviation in the orientation of the ferrocene units are observed. This indicates that the impact of the cyclohexyl backbone on the overall configuration of the molecule is minimal.

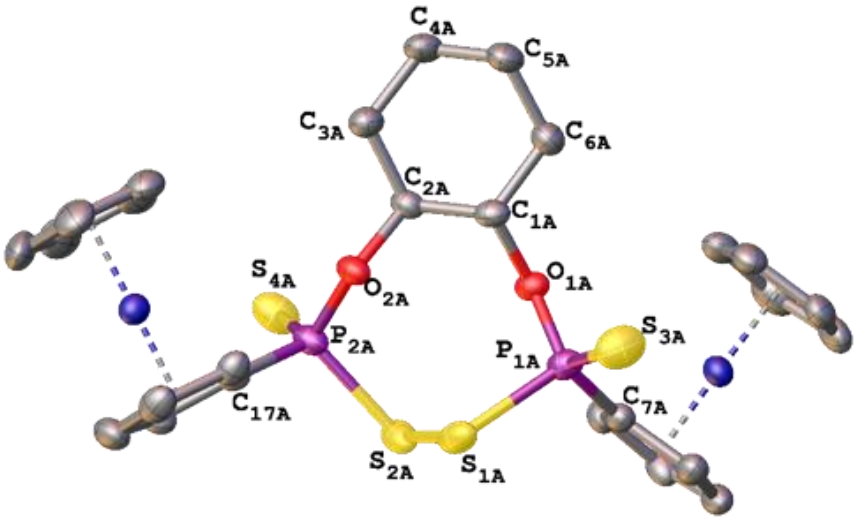

Figure 2.6. Thermal ellipsoid drawing (50% probability) of **2**. Hydrogen atoms are omitted for clarity.

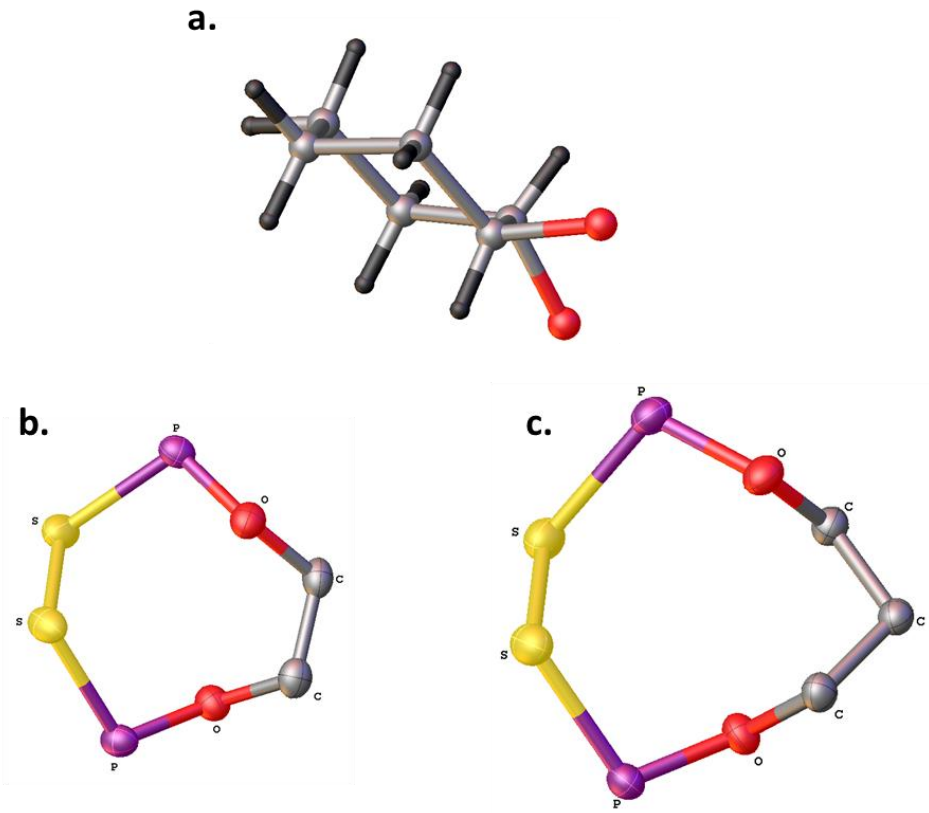

Figure 2.7. a) Chair conformation of cyclohexyl group present in **2. b)** 8 membered hetrocycle present in **1** and **2**. **c)** 9 membered heterocycle present in **3**.

Compound **3** crystallizes in the orthorhombic space group Pbca with two solvate molecules of CH_2Cl_2. The P atoms both have the same absolute configuration. The P=S and P-S bond lengths are not significantly different from **4** and **5**, measuring 1.923 and 2.105 Å respectively. The S-S coupling results in the formation of two 9-membered heterocycles with one common atom which lies on the centroid (Atom C_1), shown in Figure 2.8. Interestingly the ferrocene moieties differ in their conformation with both staggered and eclipsed forms present in the same molecule. This accounts for the large uncertainty in the position of the carbons on the Cp substituents.

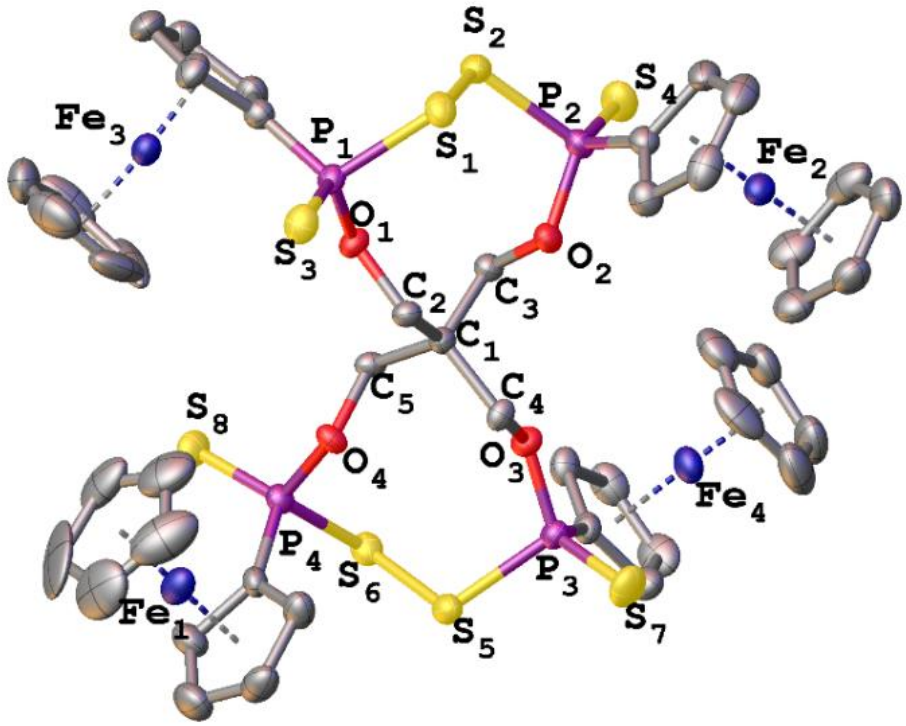

Figure 2.8. Thermal ellipsoid drawing (50% probability) of 6. Hydrogen atoms and CH_2Cl_2 solvate molecules omitted for clarity.

2.4 Electrochemistry

Cyclic voltammetry was used to investigate the reversibility of the ferrocenium-ferrocene redox couple. Measurements were taken at the Pt electrode in a 1 M solution of $[NBu_4][PF_6]$. Dichloromethane was used as solvent due to its inertness towards ferrocenium-type ions. Pertinent cyclic voltammetric data is summarized in Table 2.3.

Table 2.3. Electrochemical Data for Heterocycles

Compound	**Ferrocene**	**1**	**3**
$\mathbf{E_{pf}}$	303	512	417
$\mathbf{i_{pf}}$	9.87	7.98	6.64
$\mathbf{E_{pr}}$	202	393	298
$\mathbf{i_{pr}}$	-10.8	-9.20	-27.9
$\mathbf{i_{pr}/\ i_{pf}}$	1.15	1.15	4.20
$\mathbf{\Delta E = E_{pf} - E_{pr}}$	101	119	119

[a] All the potential and current values are quoted in mV and μA, for a scan rate of 50 mV/s.

Macrocycles **1** and **3** exhibit a reversible oxidation of the ferrocene moieties that deviate from the standard ferrocene. This shift to a higher potential, as compared to ferrocene, can be attributed to the electron withdrawing nature of the substituents on the cyclopentadienyl rings, which reduces the electron density on the metal centre. The loss of electron density by inductive effects impedes the oxidation process and accounts for the increase in the potential. The separation between the cathodic and anodic peaks, ΔE_p were 0.10, 0.12 and 0.12 V, for ferrocene, **1** and **3**, respectively. The compounds show a degree of reversibility with **1** having a ip_a/ip_c that is not significantly greater than unity, 1.15. These values are significantly larger than expected for a two electron reversible process. This deviation can possibly be assigned to the uncompensated resistance given by the low conducting solvent, dichloromethane. A single oxidation process is visible on the voltammograms of the compounds, as shown in Figure 2.9 and 2.10. This implies that the linkage between the ferrocene moieties is nonconductive and blocks electronic communication. The saturation of the S-S bridge and carbon skeleton are a key factor in this regard. Therefore redox activity is restricted to single sites and the charge localized on single redox centres.

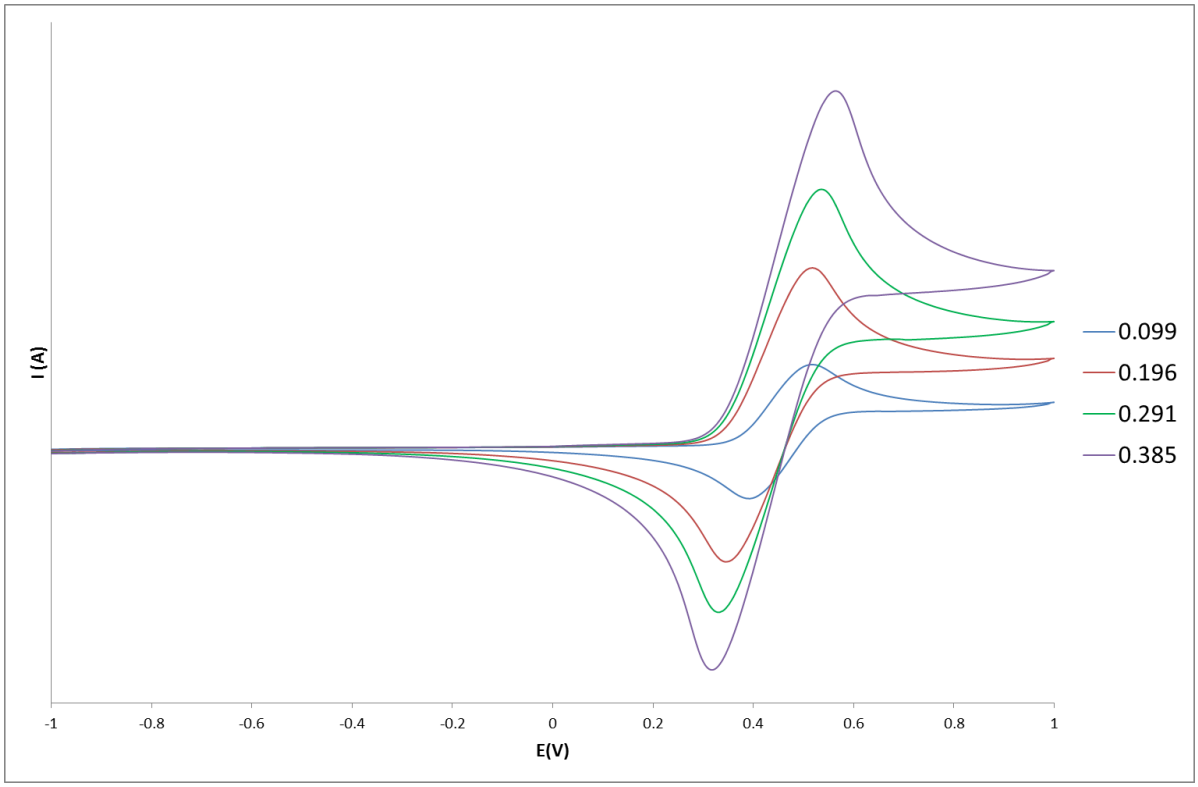

Figure 2.9. Concentration dependent cyclic voltammograms of **1**.

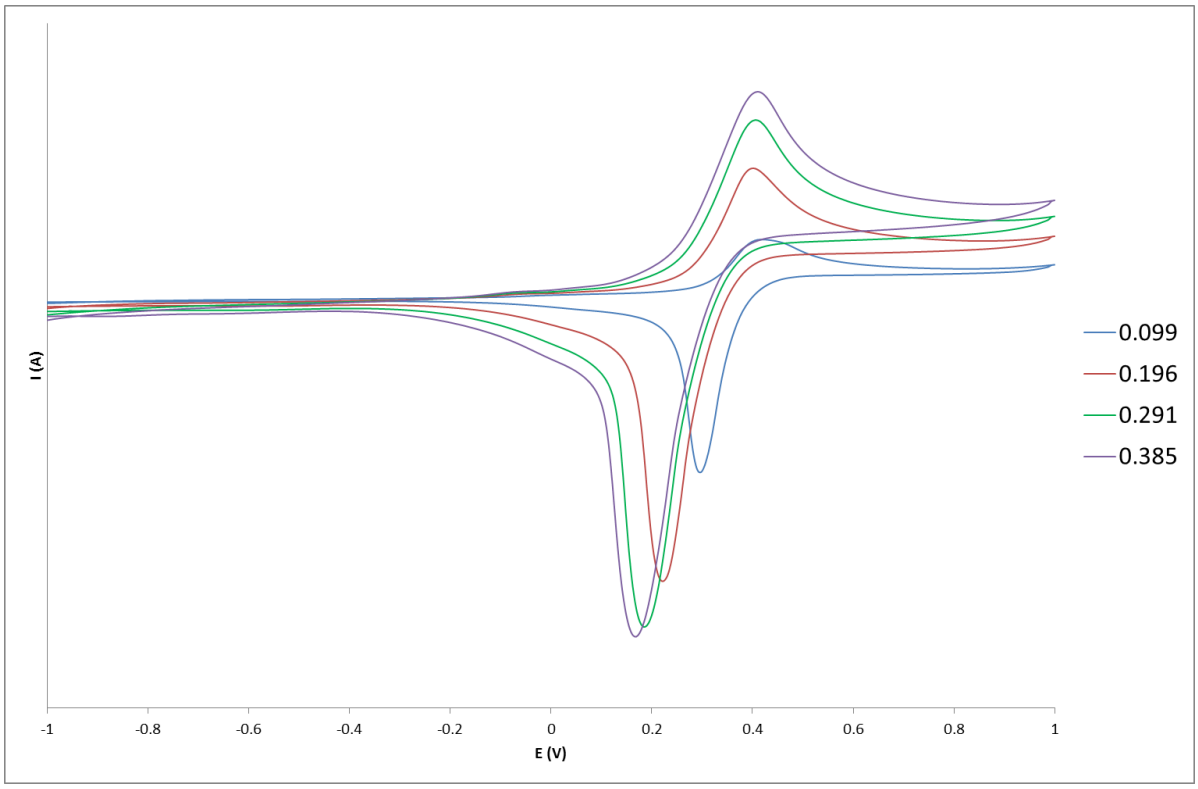

Figure 2.10. Concentration dependent cyclic voltammograms of **3**.

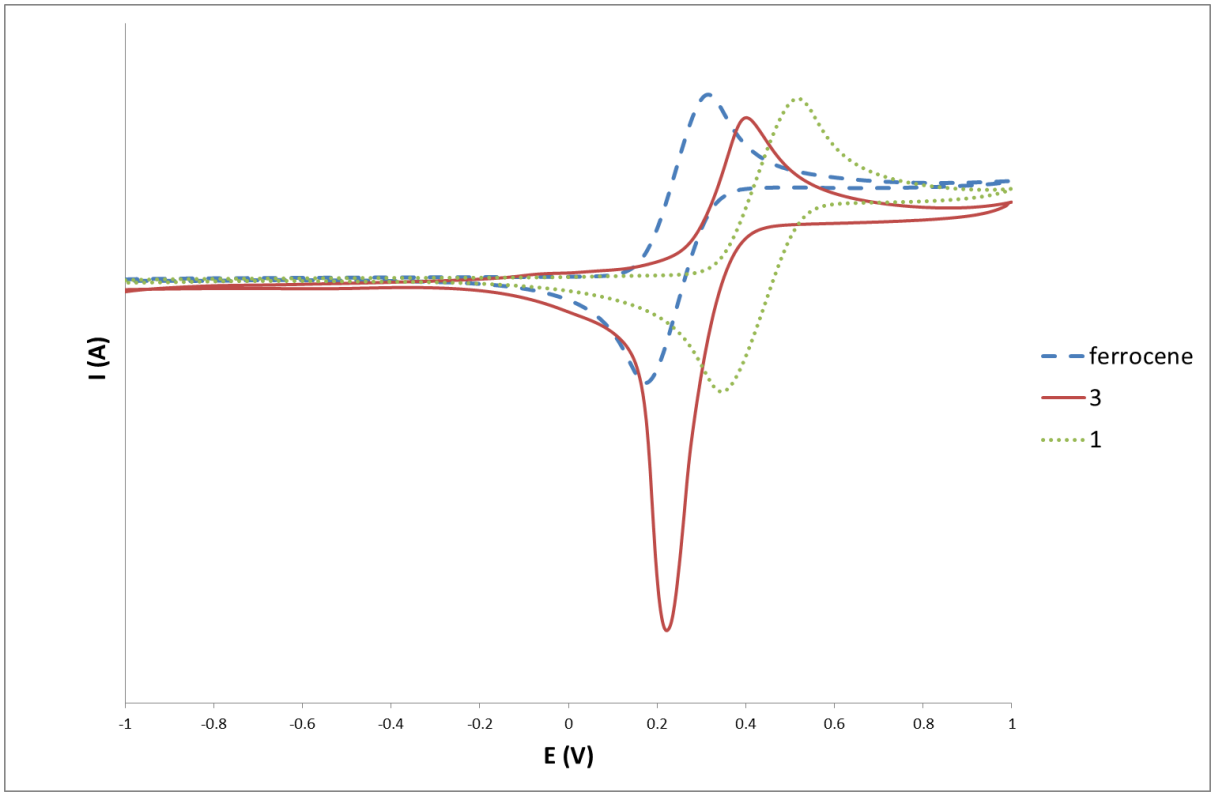

Figure 2.11. Comparative cyclic voltammograms of **1**, **3** and ferrocene.

In summary, this chapter demonstrated the first examples of structurally characterized *intra*molecular S-S coupling of dithiophosphonates, which led to the formation of novel heterocyclic compounds. Variation of the alcohol chain length led to the formation of two ring sizes. X ray analysis showed that the SPPS backbone adopts a single conformation in all cases. Redox activity was investigated and the ferrocene moieties seem to act as independent receptors. In relation to the objectives outlined in Chapter 1, this chapter illustrated the plausibility of multiple dithiophosphonates on a common backbone and outlines synthetic route for ligand synthesis in subsequent chapters.

2.6 Experimental

All commercial chemicals and other reagents were used as received. Phosphorus-pentasulfide, ferrocene, iodine (sublimed), ethanediol, 1,2-*trans*-cyclohexanediol and pentaerythritol were purchased from Sigma Aldrich and used without further purification. Ammonia gas was obtained from Afrox (South Africa). Unless otherwise noted, all reactions and manipulations were carried out under an inert atmosphere with a positive nitrogen gas flow using standard Schlenk techniques. Diethyl ether, THF, benzene, and hexane were distilled under dinitrogen over a Na wire with the formation of a benzophenone ketyl indicator. Dichloromethane was distilled over P_4O_{10}. Methanol and ethanol were distilled from I_2/Mg turnings.

Mass spectral analyses were performed on a Waters API Quattro Micro spectrometer. ^{1}H and $^{31}P\{^{1}H\}$ NMR spectra were recorded on a Bruker Avance 400 MHz spectrometer. NMR data are expressed in parts per million (ppm) downfield shift and for ^{1}H spectra referenced internally to the residual proton impurity in the deuterated solvent ($CDCl_3$ in all cases) whilst ^{31}P spectra chemical shifts are reported relative to a 85% H_3PO_4 in D_2O external standard solution, all at 298 K. Data are reported as chemical shift position (δH), multiplicity, relative integral intensity and assignment. Solid state ^{31}P NMR spectra were obtained on a Bruker 600 MHz spectrometer operating at room temperature with a magic angle spinning (MAS) probe. Melting points were determined using a Stuart SMP3 melting point apparatus. Elemental analyses were performed using a ThermoScientific Flash 2000 CHN Analyzer. Cyclic voltammetry measurements were recorded on a Metrohm 797 Computrace, equipped with a three electrode system: a Pt working electrode, a Ag|AgCl reference electrode and an auxiliary Pt electrode. The Metrohm CT797 Application (Versions 1.3.2.85) software was utilized for both operation and data analysis. The ferrocenyl compounds were dissolved in dichloromethane and added to a tetrabutylammonium hexafluorophosphate (0.1 M) supporting electrolyte solution.

2.6.1 Synthesis of $(NH_4)_2[S_2P(Fc)OCH_2CH_2O(Fc)PS_2]$, (**L1**).

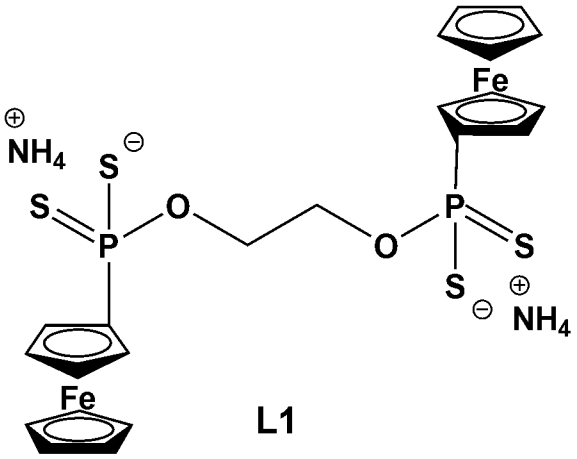

L1

Dry ethanediol (0.200 mL, 3.570 mmol) was added to $(FcP(S)S)_2$ (2.000 g; 3.570 mmol) at 70° C until complete dissolution of solids was observed. The reaction vessel was allowed to cool down to room temp. and then placed in an ice bath and anhydrous NH_3 slowly bubbled through resulting in the formation of a yellow precipitate. The ammonium salt was then dissolved in THF and filtered through anhydrous $MgSO_4$/Celite. The volume of the filtrate was reduced *in* vacuo. Ether was added to precipitate and consolidate the product to yield a bright yellow powder. Yield: 1.157 g (54%). Melting point: 161.4-161.8°C. ^{1}H-NMR ($CDCl_3$) δ: 4.933 – 4.855 (t, 2H, *J* = 10.8 Hz, CH_2); 4.624 – 4.438 (d, 4H, *J* = 55.8 Hz, Fc(4)); 4.315 – 4.289 (d, 4H, *J* = 7.8 Hz, Fc); 4.413 (s, 10H, Fc); 3.998 – 3.909 (t, 2H, *J* = 13.4 Hz, CH_2). ^{31}P-NMR δ: 94.17 (s, 2P, P-S). ESI-MS: *m/z* 620 (100%) $[S_2(Fc)P(OC_2H_4O)P(Fc)S_2]^{2-}$.

2.6.2 Synthesis of $(NH_4)_2[(S_2PFc)_2(trans\text{-}1,2\text{-}O,O'\text{-}C_6H_{10})]$, (**L2**).

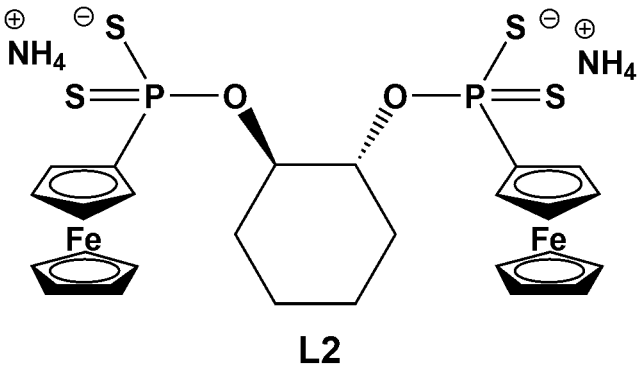

L2

A toluene solution of 1,2-*trans*-cyclohexandiol (0.318 g, 2.740 mmol) was added to $(FcP(S)S)_2$ (1.500 g, 2.677 mmol) at 70° C and heated until complete dissolution of solids was observed. The reaction vessel was then placed in an ice bath and anhydrous NH_3 slowly bubbled through resulting in the formation of a yellow precipitate. The ammonium salt was then dissolved in THF and filtered through anhydrous $MgSO_4$/Celite. The volume of the filtrate was reduced *in* vacuo. Ether was added to precipitate and consolidate product to yield a caramel-yellow powder. Yield: 1.236 g (65%). Melting point: 154.4°C (dec). ^{1}H-NMR ($CDCl_3$) δ: 1.-1.49 (t, 2H, *J* = 10.21 Hz, CH_2); 1.61 – 1.77 (m, 2H, CH_2); 1.82 – 1.93 (m, 2H, CH_2); 2.24-2.37 (m,

2H, CH_2); 4.34 (s, 10H, Fc(5)); 4.44-4.51 (d, 4H, *J* = 11.29 Hz , Fc); 4.59 (s, 2H, CH); 4.77-4.93 (m, 4H, Fc);. ^{31}P NMR δ: 89.48 (s, 2P).

2.6.3 Synthesis of $(NH_4)_4[C\{CH_2OPS_2(Fc)\}_4]$, (**L3**).

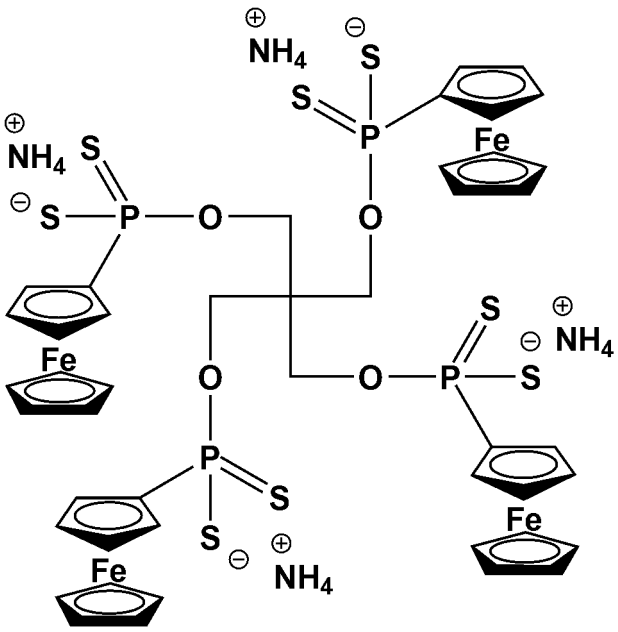

L3

A toluene solution of pentaerythritol (0.244 g, 1.785 mmol) was added to $(FcP(S)S)_2$ (2.000 g; 3.570 mmol) at 70° C and heated until complete dissolution of solids was observed. The reaction vessel was then placed in an ice bath and anhydrous NH_3 slowly bubbled through resulting in the formation of a yellow precipitate. The ammonium salt was then dissolved in THF and filtered through anhydrous $MgSO_4$/Celite. The volume of the filtrate was reduced *in* vacuo. Ether was added to precipitate and consolidate product to yield a bright yellow powder. Yield: 1.953 g (83%). Melting point: 192.4-193.0°C. ^{1}H-NMR ($CDCl_3$) δ: 4.729 – 4.626 (d, 8H, *J* = 30.9 Hz, Fc); 4.548 – 4.499 (d, 8H, *J* = 14.7 Hz, Fc); 4.330 – 4.306 (t, 4H, *J* = 3.6 Hz, CH_2); 4.153 (s, 20H, Fc); 2.161 – 2.154 (t, 4H, *J* = 1.1 Hz, CH_2). ^{31}P NMR δ: 96.20 (s, 4P, P-S). ESI-MS: *m/z* 1252 (15%) $[S_4(Fc)_2P_2(O_2C_5H_8O_2)P_2(Fc)_2S_4]^{4-}$. Anal. Calc. for $C_{45}H_{64}Fe_4N_4O_4P_4S_8$: C 40.67; H 4.85 N 2.11 %. Found: C 40.15; H 4.56; 1.76 %.

2.6.4 Synthesis of [{-$CH_2OP(S)(Fc)S$-}$_2$], (**1**).

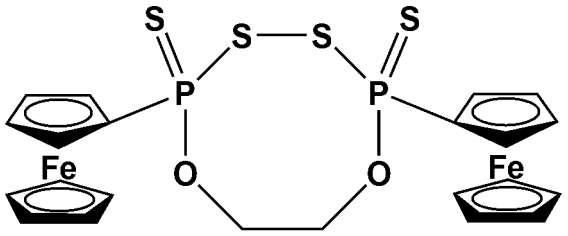

1

The dithiophosphonate salt (**L1**) (0.200 g, 0.075 mmol) was dissolved in MeOH. I_2 (0.021 g, 0.083 mmol) was added to the salt solution. A yellow precipitate formed immediately and was stirred for a further 20mins to ensure completion. The product was collected by vacuum filtration and dried *in vacuo* to yield a bright yellow powder Yield: 0.068 g (72%). Melting point: 186.6-187.0°C. ^{1}H-NMR ($CDCl_3$) δ: 5.103 – 5.020 (t, 4H, *J* = 12.5 Hz, CH_2); 4.784 – 4.598 (d, 2H, *J* = 55.8 Hz, Fc); 4.483 – 4.452 (d, 2H, *J* = 9.3 Hz, Fc); 4.308 (s, 10H, Fc); 4.159 – 4.093 (t, 2H, *J* = 9.9 Hz, CH_2). ^{31}P NMR δ: 93.26 (s, 2P, P-S). ESI-MS: *m/z* 620 (100%) [$S(Fc)P(OC_2H_4O)P(Fc)S$]. Single crystals suitable for X-ray studies were obtained from the slow evaporation of dichloromethane solution.

2.6.5 Synthesis of [(S_2P-Fc)$_2$(*trans*-1,2-O,O'-C_6H_{10})], (**2**).

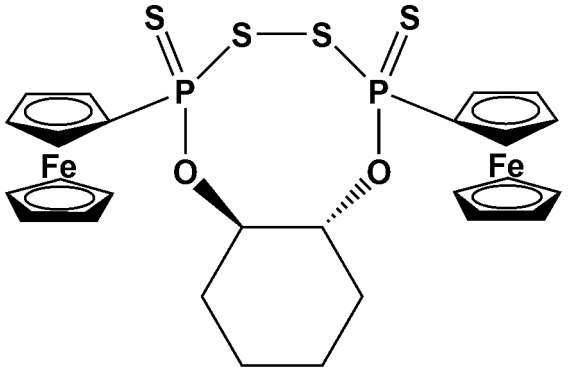

2

The bis(dithiophosphonate) salt (**L2**) (1.054 g, 1.483 mmol) was dissolved in MeOH. I_2 (0.381 g, 1.504 mmol) was added to the salt solution. A yellow precipitate formed immediately and was stirred for a further 20 mins to ensure completion of the reaction. The product was collected by vacuum filtration and dried *in vacuo* to yield a bright yellow powder. Yield: 0.810 g (81%). Melting point: 149.8 – 150.2 °C. ^{1}H-NMR ($CDCl_3$) δ: 1.42-1.49 (t, 2H, *J* = 10.21 Hz, CH2); 1.61 – 1.77 (m, 2H, CH_2); 1.82 – 1.93 (m, 2H, CH_2); 2.24 – 2.37 (m, 2, CH_2); 4.34 (s, 10H, Fc); 4.44 – 4.51 (d, 4H, *J* = 11.29 Hz , Fc) 4.59 (s, 2H, CH); 4.77 – 4.93 (m, 4H, Fc); ^{31}P NMR δ: 89.48 (s, 2P, P-S), Anal. Calc. for $C_{26}H_{28}Fe_2O_2P_2S_4$ (674.40): C 46.30; H 4.18 %. Found: C 45.82; H 4.28 %. Single crystals suitable for X-ray studies were obtained from the slow diffusion of hexane into a concentrated dichloromethane solution of **2**.

2.6.6 Synthesis of [C{$CH_2OP(S)(Fc)S$}$_4$], (**3**).

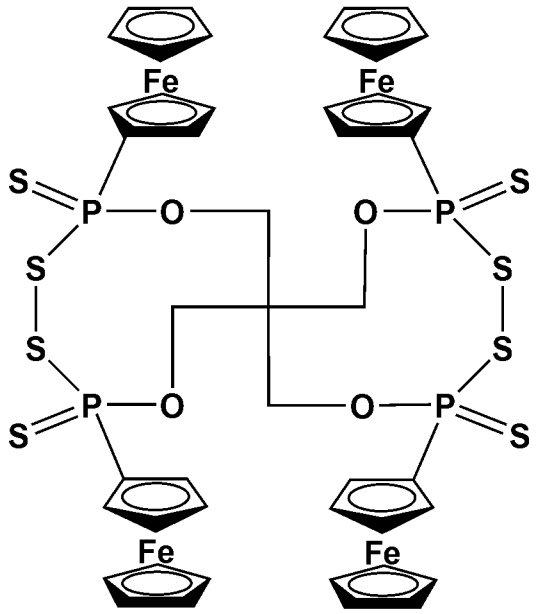

3

The tetra(dithiophosphonate) salt (**L3**) (3.000 g, 2.265 mmol) was dissolved in MeOH. I_2 (1.150 g, 4.529 mmol, 2 molar equiv.) was added to the salt solution. A yellow precipitate formed immediately and was stirred for a further 20 mins to ensure completion of the reaction. The product was collected by vacuum filtration and dried *in vacuo* to yield a bright yellow powder Yield: 2.518 g (89%). Melting point: 199.8-200.2°C (dec). 1H-NMR ($CDCl_3$) δ: 4.738 – 4.630 (d, 4H, *J* = 32.4 Hz, Fc(4)); 4.551 – 4.505 (d, 4H, *J* = 13.8 Hz, Fc(4)); 4.387 – 4.360 (d, 4H, *J* = 8.1 Hz, Fc); 4.319 (s, 20H, Fc); 4.219 – 4.190 (d, 4H, *J* = 8.7 Hz, Fc); 1.621 – 1.485 (t, 8H, *J* = 20.7 Hz, CH_2); 1.230 – 1.193 (t, 8H, *J* = 11.1 Hz, CH_2). ^{31}P-NMR δ: 95.2927 (s, 4P, P-S). ESI-MS: *m/z* 1255 – 1252 (100%) [$C_{45}H_{48}Fe_4O_4P_4S_8$]. Single crystals suitable for X-ray studies were obtained from the slow evaporation of dichloromethane solution.

2.6.7 X-ray structure determination

Crystals were mounted on glass fibers with epoxy resin, and all geometric and intensity data were collected on a Bruker APEXII CCD diffractometer equipped with graphite monochromated Mo-Kα radiation (λ = 0.71073 Å). The data reduction was carried out with SAINT-Plus software.[26] The SADABS program was used to apply empirical absorption corrections.[27] All structures were solved by direct methods and refined by full-matrix least-squares on F^2 with SHELXTL software package[28] found in SHELXTL/PC version 5.10.[29] Thermal ellipsoid plots are generated with *OLEX2*.[30]

2.7 References

1. Wilkinson, G.; Rosenblum, M.; Whiting, M.C.; Woodward, R. B. *J. Am. Chem. Soc*. 1952, ***74***, 2125–2126. (b) Fischer, E. O.; Pfab, W. *Z. Naturforsch. B* 1952, ***7***, 377–379.
2. (a) Metzler-Nolte, N.; Salmain, M. In Ferrocenes; Petr, S., Ed.; Wiley: Weinheim, 2008; Chapter 13, pp 499-639. (b) Wlassoff, W. A.; King, G.C. *Nucleic Acids Res*. 2002, ***30****(12)*, e58. (c) Metzler-Nolte, N.; Van Staveren, D.R. *Chem. Rev*. 2004, ***104***, 5931-5985; (d) Hartinger, C.G.; Metzler-Nolte, N.; Dyson, P.J. *Organometallics* 2012, ***31***, 5677−5685.
3. (a) Bayly, S.R.; Beer, P.D.; Chen, G.Z. In Ferrocenes; Petr, S., Ed.; Wiley: Weinheim, **2008**; Chapter 8, pp 281-318. (b) Astruc, D.; Daniel, M.-C.; Ruiz, J. *Chem. Commun* **2004**, 2637–2649.
4. (a) Arrayas, R.G.; Adrio, J.; Carretero, J.C. *Angew. Chem., Int. Ed.* 2006, **45**, 7674–7715; (b) Le Roux, E.; Malacea, R.; Manoury, E.; Poli, R.; Gonsalvi, L.; Peruzzini, M. *Adv. Synth. Catal*., 2007, ***349***, 309–313. (c) Malacea, R.; Manoury, E.; Routaboul, L.; Daran, J.-C.; Poli, R.; Dunne, J.P.; Withwood, A.C.; Godard, C.; Duckett, S.B. *Eur. J. Inorg. Chem*. **2006**, 1803–1816.
5. (a) Yang, H.-B.; Ghosh, K.; Zhao, Y.; Northrop, B. H.; Lyndon, M. M.; Muddiman, D. C.; White, H. S.; Stang, P. J. *J. Am. Chem. Soc.* 2008, ***130***, 839-841.
6. Santi, S.; Bisello, A.; Cardena, R.; Donoli A. *Dalton Trans*., 2015, ***44***, 5234–5257. (b) Nguyen, P.; Gómez-Elipe, P.; Manners, I. *Chem. Rev.* 1999, ***99***, 1515-1548.
7. (a) Nizamov, I.S.; Bityeva, E.S.; Al'fonsov, V.A. *Russ. J. Gen. Chem*. 1993, **63**, 1840. (b) Ozturk, T.; Ertas, E.; Mert, O. *Chem. Rev.* 2007, **107**, 5210.
8. Woodward, R. B.; Rosenblum, M.; Whiting, M. C. *J. Am. Chem. Soc*. 1952, ***74***, 3458–3459.
9. Foreman, M.R.S.; Slawin, A.M.Z.; Woollins, J.D. *J. Chem. Soc., Dalton Trans*. **1996**, 3653.
10. (a) Foreman, M.R.S.; Slawin, A.M.Z.; Woollins, J.D. *J. Chem. Soc., Chem. Commun*. **1997**, 855. (b) Foreman, M.R.S.; Slawin, A.M.Z.; Woollins, J.D. *J. Chem. Soc., Chem. Commun*. **1997**, 1269. (c) Foreman, M.R.S.; Slawin, A.M.Z.; Woollins, J.D. *Phosphorus, Sulfur, Silicon Rel. Elem.*, 1997, ***125***, 469. (d) Foreman, M.R.S.; Slawin, A.M.Z.; Woollins, J.D. *J. Chem. Soc., Dalton Trans.* **1999**, 1175.

11. (a) Van Zyl, W.E. *Comments Inorg. Chem*., 2010, ***31***, 13-45. (b) Van Zyl, W.E.; Woollins, J.D. *Coord. Chem. Rev*., 2013, ***257***, 718-731. (c) Van Zyl, W.E.; Fackler, J.P. *Phosphorus Phosphorus, Sulfur, Silicon Rel. Elem.*, 2000, ***167***, 117-132. (d) Van Zyl, W.E.; López-de-Luzuriaga, J.M.; Mohamed, A.A.; Staples, R.J.; Fackler, J.P. *Inorg. Chem.*, 2002, ***41,*** 4579-4589. (e) Van Zyl, W.E.; Staples, R.J.; Fackler, J.P., Jr. *Inorg. Chem. Commun.* 1998, ***1***, 51-54. (f) Van Der Walt, H.; Muller, A.; Staples, R.J.; Van Zyl, W.E. *Acta Cryst.* 2010, ***E66***, m1364.
12. (a) Gray, I.P.; Milton, H.L.; Slawin, A.M.Z.; Woollins, J.D. *Dalton Trans*. **2003**, 3450. (b) Karakus, M.; Aydogdu, Y.; Celik, O.; Kuzucu, V.; Ide, S.; Hey-Hawkins, E. *Z. Anorg. Allg. Chem.* 2007, **633**, 405. (c) Wang, X.-Y.; Li, Y.; Ma, Q.; Zhang, Q.-F. *Organometallics* 2010, ***29***, 2752. (d) Thomas, C.M.; Neels, A.; Stoeckli-Evans, H.; Suss-Fink, G. *J. Organomet. Chem*. 2001, ***633,*** 85. (e) Wang, X.Y.; Shi, H.-T.; Zhang, Q.-F. *Chin. J. Struct. Chem.* 2011, ***30***, 380. (f) Karakus, M.; Lonnecke, P.; Yakhvarov, D.; Hey-Hawkins, E.; *Z. Anorg. Allg. Chem*. 2004, ***630***, 1444. (g) Gray, I.P.; Slawin, A.M.Z.; Woollins, J.D. *Z. Anorg. Allg. Chem*. 2004, ***630***, 1851. (h) Barranco, E.M.; Crespo, O.; Gimeno, M.C.; Jones, P.G.; Laguna, A. *Inorg. Chem*. 2008, ***47***, 6913. (i) Liu, S.-L.; Wang, X.-Y.; Duan, T.; Leung, W.-H.; Zhang, Q.-F. *J. Mol. Struct*. 2010, ***964***, 78.
13. (a) Klaman, D. Lubricants and Related Products, Verlag-Chemie, Weinheim, **1984**. (b) Barnes, A.M.; Bartle, K.D.; Thibon, V.R.A. *Tribology Internat*., 2001, ***34***, 389. (c) Nicholls, M.A.; Dob, T.; Norton, P.R.; Kasrai, M.; Bancroft, G.M. *Tribology Internat*. 2005, ***38***, 15. (d) Spikes, H.A. *Lubrication Sci.*, 2008, ***20***, 103.
14. (a) Patnaik, P. A Comprehensive Guide to Hazardous Properties of Chemical Substances, John Wiley & Sons, 3rd edition, Hoboken NJ, **2007**. (b) Gaines, T.B. *Toxicol. Appl. Pharmacol*., 1969, ***14***, 515.
15. Bromberg, L.; Lewin, I.; Warshawsky, A. *Hydrometallurgy*, 1993, ***33***, 59.
16. Voutchkova, A.M.; Osimitz, T.G.; Anastas, P.T. *Chem. Rev*., 2010, ***110***, 5845.
17. Cormode, D.P.; Evans, A.J.; Davis, J.J.; Beer, P.D. *Dalton Trans.*, 2010, ***39***, 6532–6541
18. Haiduc, I.; Goh, L.Y. *Coord. Chem. Rev*., 2002, ***224***, 151.
19. (a) Gray, I.P.; Slawin, A.M.Z.; Woollins, J.D. *New J. Chem*. 2004, ***28***, 1383. (b) Lopusinski, A.; Luczak, L.; Michalski, J.; Koziol, A.E.; Gdaniec, M. *Chem. Commun*. **1991**, 889. (c) Przychodzen, W. Chojnacki, *J. Heteroatom Chem*. 2008, ***19***, 271. (d) Knopik, P.;

Luczak, L.; Potrzebowski, M.J.; Michalski, J.; Blaszczyk, J.; Wieczorek, M.J. *J. Chem. Soc., Dalton Trans*. **1993**, 2749.

20. Grishina, O.N.; Kosova, L.M.; Lipatova, I.P.; Shagidullin, R.R. *Zh. Obsch. Khim*. 1970, ***40***, 66. (b) Grishina, O.N.; Andreev, N.A. *Zh. Obsch. Khim*. 1975, ***45***, 2093.
21. Przychodzen, W. *Phosphorus, Sulfur, Silicon Rel. Elem.*, 2004, **179**, 1621.
22. Korth, H.G.; Lommes, P. *Chem. Ber*. 1992, ***125***, 2419.
23. Gibson, K.J.; Leonard, N.J. *Biochemistry* 1984, ***23***, 78.
24. Dunitz, J.D. *Acta Cryst*. 1956, ***9***, 579.
25. Jacobsen, H. *Inorg. Chem*. 2013, ***52***, 11843.
26. SAINT V4.043: Software for the CCD Detector System, Bruker Analytical X-ray System, Madison, WI, 1995
27. Sheldrick, G.M. SADABS, University of Gottingen, Gottingen, Germany, 1996.
28. SHELXL-97: Sheldrick, G.M. Program for the Refinement of Crystal Structure, University of Göttingen, Göttingen, Germany, 1997.
29. SHELXL 5.10 (PC version): Program Library for Structure Solution and Molecular Graphics, Bruker analytical X-ray System, Madison, WI, 1998.
30. Dolomanov, O.V.; Bourhis, L.J.; Gildea, R.J. ; Howard, J.A.K; Puschmann, H. *J. App. Cryst*. 2009, ***42***, 339–341.

Chapter 3
Chiral Dithiophosphonates: Teaching an old dog new tricks

3.1 Introduction

Previous investigations into the reaction of diols, noncyclic (1,2-ethanediols and 1,4-butanediols)[1] and aromatic (*o*-dihydroxybenzene derivatives),[2] with diphosphetane dimers resulted in the formation of a mixture of products. The reaction was carried out in acetonitrile at 80 °C and elimination of H_2S during the reaction resulted in the formation S-S bond linkages, by thermal redistribution.[3] The isolation of bis-dithiophosphonic acids in the form of ammonium salts with iodine oxidation, and the subsequent formation of –S-S- bonds to form disulfide rings, has been reported[4] and explored in Chapter 2. However, the ligation potential of the salts, in most cases, was not a priority and literature containing complexes with bis(monoanionic) dithiophosphonate ligands is limited.[5-7] More importantly these reports lack structural characterisation. Recognizing the possibility of creating completely novel systems with respect to the dithiophosphonate motif, this work explores diols related to isomeric saturated cyclic alkanes in particular, and *en route* to the preparation of multinuclear metal complexes.

3.1.1 Ligand design

In the realm of coordination-driven assembly, two significant factors are the *acceptor* (coordination site) and the *donor* (ligand) (outlined in Chapter 1, Section 1.4). The *donor* can be broadly defined as being linear units which contain coordination sites at 180° relative to each other or angular units which possess coordination sites at desirable angles to each other. The possibility of generating a system in which the donor could satisfy a multitude of acceptors by adopting different geometries and conformations is of particular interest. Consequently, an ideal candidate for such a coordination study would have a molecular backbone which could generate various angles and still confer certain rigidity.

To this end we sought to incorporate the cyclohexane molecule into the backbone of the ligand. Cyclohexane can occupy different orientations with free rotation around the sp^3 hybridized carbon atoms and C-C bond angles of 109.5°. The conformations include the chair, half chair twist boat and true boat. The chair conformation is the most energetically favored for the unsubstituted ring followed by the twist boat and boat confirmations, Figure 3.1.

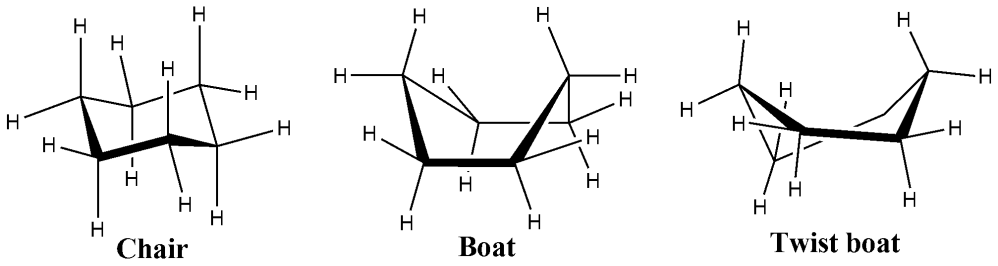

Figure 3.1. Conformations of unsubstituted cyclohexane.

The next factor to consider is the position of the substituents which also plays a significant role in accessibility to the conformations. A 1,2-substitution was chosen not only to keep the coordinating moieties in close proximity but also to more likely result in a concrete molecular entity, i.e. not a coordination polymer. Two isomers are possible for the di-substituted 1,2-cyclohexandiol, i.e. *cis* or *trans*, shown in Figure 3.2. In both cases the substituents can occupy either axial or equatorial positions. The benefit of the *trans*-isomer over the *cis* isomer is the possibility of two distinct enantiomers (or ring conformations as a result of ring inversion), shown in Figure 3.2. The plane of symmetry present in the *cis* derivative infers that the *meso* compound would not afford the same chirality.

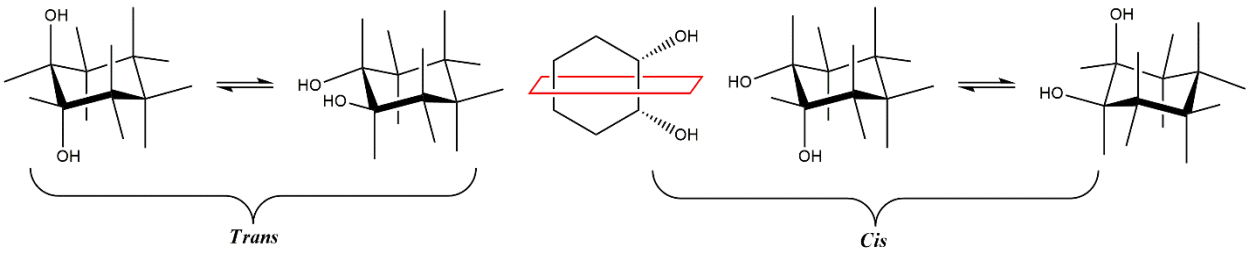

Figure 3.2. Representation of *cis*- and *trans*-1,2-cyclohexandiol. Ring inversion of the *trans* isomer gives rise to an enantiomer, which is not possible for symmetric *cis* which has a mirror plane (shown in red).

An example of the ligand used with great success in this study, and which meets the above requirements, is shown in Figure 3.3.

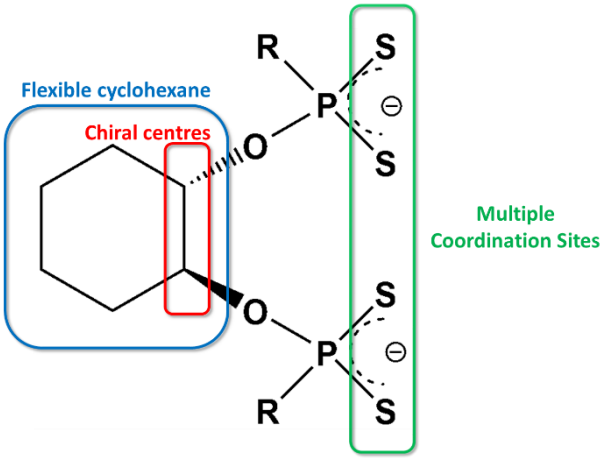

Figure 3.3. Incorporation of ligand design characteristics into the dithiophosphonate moiety.

3.1.2 Metal architectures

The combination of the newly synthesized bis(dithiophosphonate) ligands, and the coinage metals (which have a known affinity to form metal-metal interactions) affords the opportunity to prepare novel multi-nuclear complexes. In the current context the possible geometries need to be outlined. Herein we describe the chemistry of Group 11 metal (Cu, Ag and Au) clusters previously reported.

3.1.3 Tetranuclear Ag(I) topologies

Recently the implications of argentophilic interactions has been reviewed.[8] These interactions play a role in the formation of multinuclear networks. However, unlike its Au(I) counterpart, Ag(I) complexes are rarely 2-coordinate and examples contain bulky ligands which inhibit intermolecular interactions.[8] The Ag···Ag interaction nevertheless plays a role in the formation of poly-nuclear Ag(I) complexes. Analysis of previously reported structures, yields four dominant tetranuclear arrangements of Ag(I) atoms, shown in Figure 3.4.

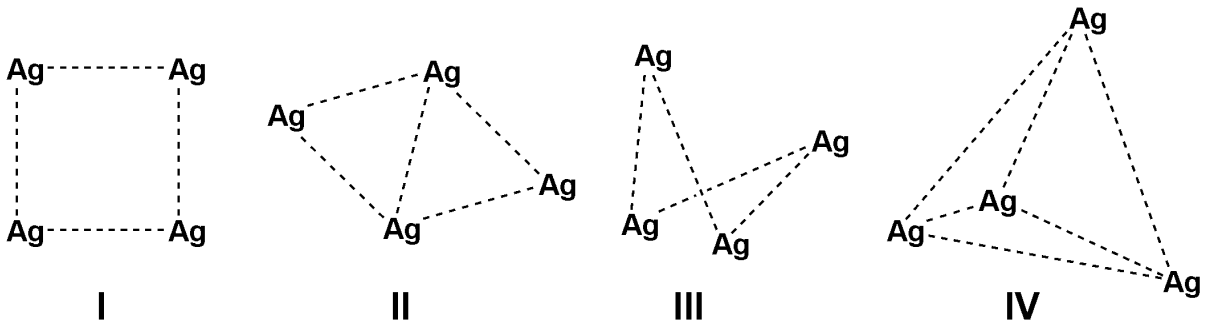

Figure 3.4. Ag(I) metal frameworks observed in literature.

It should be noted that the phosphor-1-1-dithiolates are not a well-established ligand system for the stabilization of tetranuclear Ag clusters, although numerous Ag clusters of higher nuclearity are known. One example is a mixed S/Se dichalcogenophosphinato ligand which was used to prepare a cluster of the type $[Ag(SSeP^{i}Pr_2)]_4$, with geometry of type **IV**.[9] A search of literature yielded no examples of tetranuclear Ag(I) clusters stabilized by dithiophosphonates. Nonetheless the architecture has been shown to be supported by a diverse group of ligands and some examples are discussed here.

Selbin and coworkers showed that the geometry is not limited to specific ligand type, as the dithiobenzoate ligands were capable of stabilizing both type **I** and **III** architectures.[10] The earliest structural report of a square arrangement (type **I**) was as early as 1978,[11] and other examples are known in literature.[12-15] An interesting example of type **I** was stabilized by iron carbonyl bridges which resulted in the formation of a mixed metal cluster, of the type $[Ag_4\{\mu_2\text{-}Fe(CO)_4\}]^{4-}$.[16] Halides have been shown to possess the ability to aid in the stabilization of type **I** arrangements, with chloride,[17] bromide[18] and iodide.[19] One example contained chloride in two different environments, with four bridging (μ_2) chloride ions at the perimeter and one μ_4-Cl present at the centre of the silver atoms. [17] Yam and co-workers reported a series of chalcogen (μ_4) centred square arrays which were shown to have interesting photophysical properties.[20] Increasing interaction of diagonal Ag(I) atoms resulted in the type **II** [21] [22] motif. Reaction of acetylide ligands of the type [LiCCPh] with $[CpAgPPh_3]$ is one such example.[23] A distorted tetrahedron with four Ag contacts (type **III**) has been reported. [24] Ferrocene was incorporated with the use of 1,1'-bis[(2-hydroxybenzylidene)thiocarbonohydrazono-1-ethyl]ferrocene as a ligand.[25] Helicate stabilized structures of type **IV** have been prepared from a pentatopic ligand which coordinated *via* briding sulfur atoms to the Ag core. [26] It

appears that chalcogens in general are effective in stabilizing Ag frameworks and thiolates with trigonal-planar coordination to the silver atoms (type **IV**) have been reported.[27] Type **IV** clusters are notably not the dominant form of tetranuclear Ag(I) frameworks and a lack of such clusters with phosphor-1-1-dithiolate ligands provides a great opportunity to demonstrate the flexibility of this novel ligand system. Herein we report the first dithiophosphonate stabilized tetranuclear Ag(I) cluster to be structurally reported.

3.1.4 Gold metallacycles

Metallatriangles are well established supramolecular architectures and examples are known for a large number of transition-metals; they all contain three metal atoms within a metallacycle that approximates to the shape of a triangle.[28] Gold triangles contain three gold atoms within the triangle and commonly form from Au(I) precursors with bidentate 1,2-C,N or N,N monoanionic ligands (linkers) through coordination-driven self-assembly, Figure 3.5.[29] Such gold triangles are typically 9-membered metallacycles which invariably contain intramolecular Au···Au interactions due to the small size of the triangle.

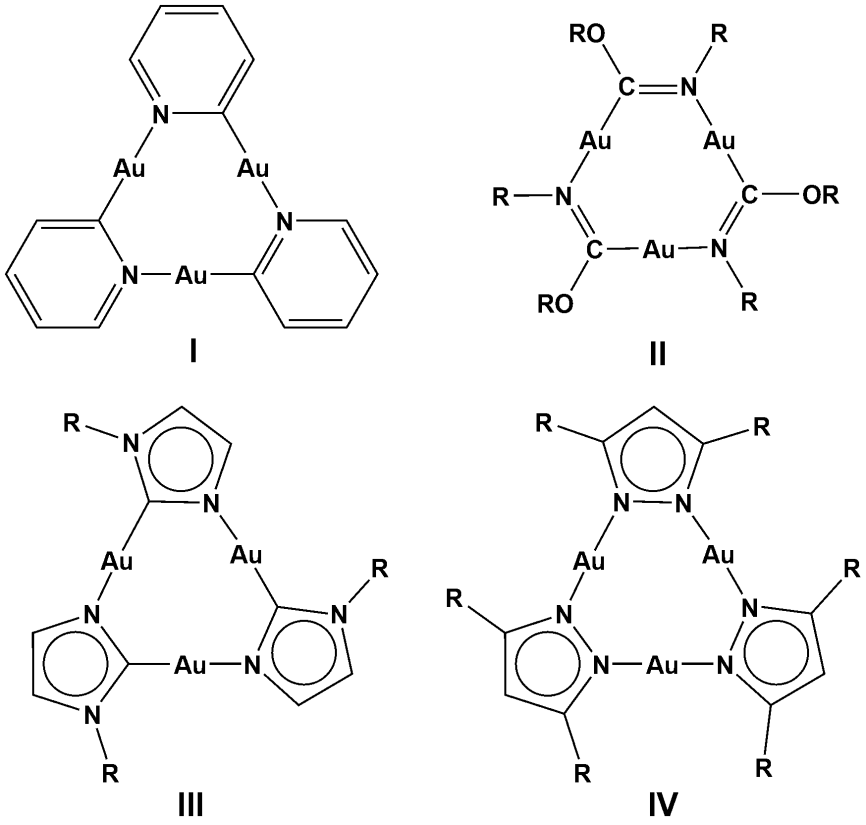

Figure 3.5. Known Au(I) metallatriangles.

The first cyclic gold triangle was reported by Vaughan in 1970 (**I**) and contains bridging 2-pyridyl linkers;[30] this triangle is also a useful precursor for entry into Au(I) carbene chemistry.[31] Other gold triangles followed, and include linkers forming carbeniates[32-34] (**II**) (which include complexes advancing luminescence and polymorphism properties),[35, 36] and imidazolates (**III**).[37, 38] A significant number of gold triangles from substituted pyrazolates (**IV**) have also been reported.[39-41]

3.1.5 Oxidative addition reactions

Oxidative addition (OA) reactions of small molecules across dinuclear Au(I) complexes of the type $[Au(CH_2)_2PR_2]_2$ (**A**)[42, 43] and $[Au(CH_2)(S)PR_2]_2$ (**B**) [44, 45] and $[Au(NRCHNR)]_2$ (**C**)[46] have been well established.

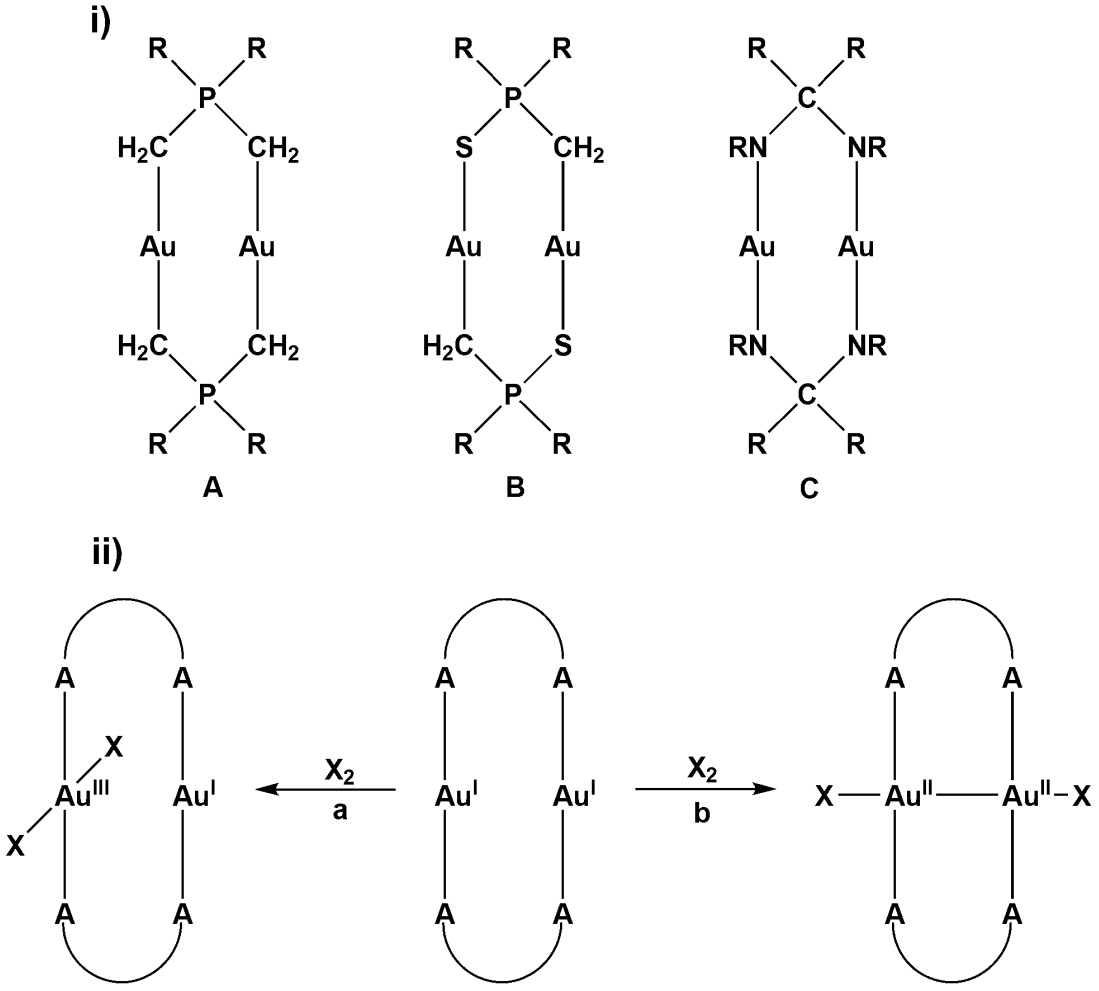

Scheme 3.1. **i)** Ylides which have previously shown oxidative addition reactions with small molecules, **ii)** Oxidative addition across dinuclear units resulting in heterovalent or homovalent species.

These systems contain C-P-C (**A**), C-P-S (**B**) and N-C-N (**C**) bridging monoanionic ligands and upon oxidation all readily form homovalent dinuclear Au(II)/Au(II) complexes with a formal σ-bond between the d^9 gold(II) centres. In the less studied bridging S-C-S case, $[Au_2\{S_2CC(CN)_2\}]^{2-}$ complex which does add X_2 (halide or other small molecule) but importantly, the negative charge of the resulting Au(II) complex appears to greatly improve its stability.[47,48] For the related S-C-S bridging neutral dithiocarbamate complexes of the type $[AuS_2CNR_2]_2$, an OA reaction had been suggested, but was found to be too unstable to isolate at room temperature.[49] Recently, the addition of the elusive F_2 across type (**C**) had been achieved.[50] Alternatively, oxidation of these dinuclear units can also lead to heterovalent Au(I)/Au(III) systems achieved simply through a change in solvent polarity where only one of the gold centres become oxidized. Either way, in all above OA cases the dinuclear unit remains intact.

Importantly, OA reactions for dinuclear Au(I) complexes containing solely bridging S-P-S ligands are rare (further discussion follows in Section 3.2.4). A closely related example to achieve this feat is the mixed ligand complex $[Au_2\{(CH_2)_2PMe_2\}\{S_2PPh_2\}]$, which adds Cl_2 reversibly.[51] Indeed, the complex $[Au(S_2P(OH)Ph)_2]Cl$ is the first structurally characterized mononuclear Au(III) complex with a S-P-S chelating ligand.[52] The complex was prepared from the reaction between [AuCl(tht)] and a large excess of $Na[S_2P(OH)Ph]$. Clearly, oxidation of the Au(I) centre occurred, but oddly no oxidant added across it (the ligand charge remained unchanged), and it is thus not clear which chemical species became reduced in the process.

3.2. Results and discussion

3.2.1 Ligand synthesis

The reaction of Lawesson's Reagent with *trans* 1,2 cyclohexanediol results in the quantative formation of the corresponding dithiophosphonic acid (Scheme 3.2). Subsequent deprotonation of the acid with NH_3 leads to the formation of the corresponding dithiophosphonate ammonium salt.

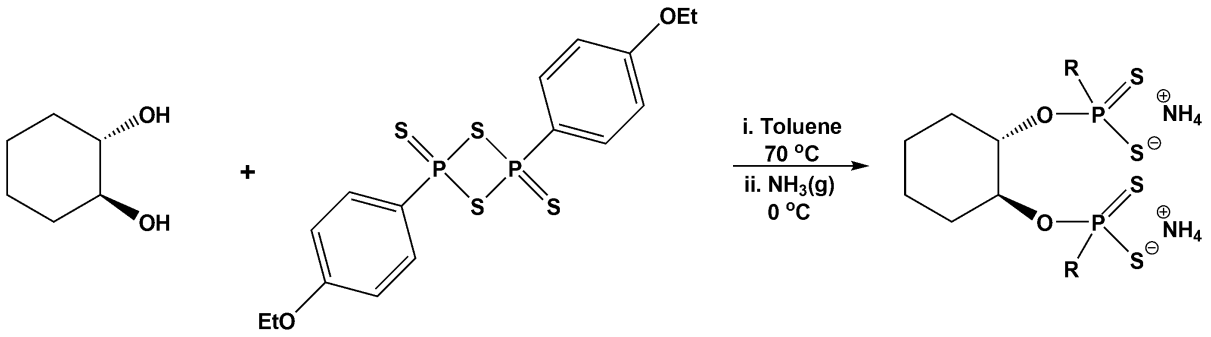

Scheme 3.2. Reaction of LR and *trans*-1,2-cyclohexandiol (R = $C_6H_5(OEt)$).

Compared to previously described reactions of diols,[1, 2] the reaction results in the sole formation of a bis(monoanionic) group. This could be attributed to the controlled amount of flexibility provided by the saturated cyclic alcohol and the *trans* isomer allows for reactions to occur on opposite faces relative to the ring. Obviously the *cis* ligand was also tested, and indeed leads to a quantitative yield of the ligand product, but subsequent metal complex formation proved challenging as no single crystals could be successfully grown, which we ascribe to undesirable crystal packing effects. The saturation of the alcohol is a key factor, as electronic communication between the reaction centres are negated and the two potential chelating units can act independently. The configuration is such that the two phosphorus environments are chemically equivalent, with a single resonance at 105 ppm in the ^{31}P NMR spectrum. Diols offer new perspectives in forming dithiophosphonates because it: i) introduces two monoanionic dithio moieties within close proximity, ii) introduces potentially intricate isomers in that either *R* or *S* isomer formation can occur on each P atom in theory. In practice, however, the least congested (stable) option is typically favoured (this offers a

distinctly different but less predictable molecular structure outcome when compared to "flat diols" such as 1,2-dihydroxybenzene), and iii) increases ligand flexibility due to sp^3 hybridized C atoms that abound.

Complexation to coinage metals offers a good starting point in the description of the ligand capabilities. Complexes of Cu(I), Ag(I) and Au(I) will be described here. It should be noted that the metallophilic interactions increases down the Group 11 coinage metals, and its impact will therefore be investigated. The copper and silver complexes result in the formation of a tetrahedron core with metal atoms, while the gold results in the formation of a new hexanuclear triangle.

3.2.2 Tetranuclear Cu(I) cluster

The reaction of $[NH_4]_2[(S_2P\text{-}1,4\text{-}C_6H_4OEt)_2(\textit{trans}\text{-}1,2\text{-}O,O'\text{-}C_6H_{10})]$ with $Cu(CH_3CN)_4PF_6$ (molar ratio 1:2) in THF led to the formation of the first tetranuclear cluster with a Cu_4L_2 configuration, Scheme 3.3.

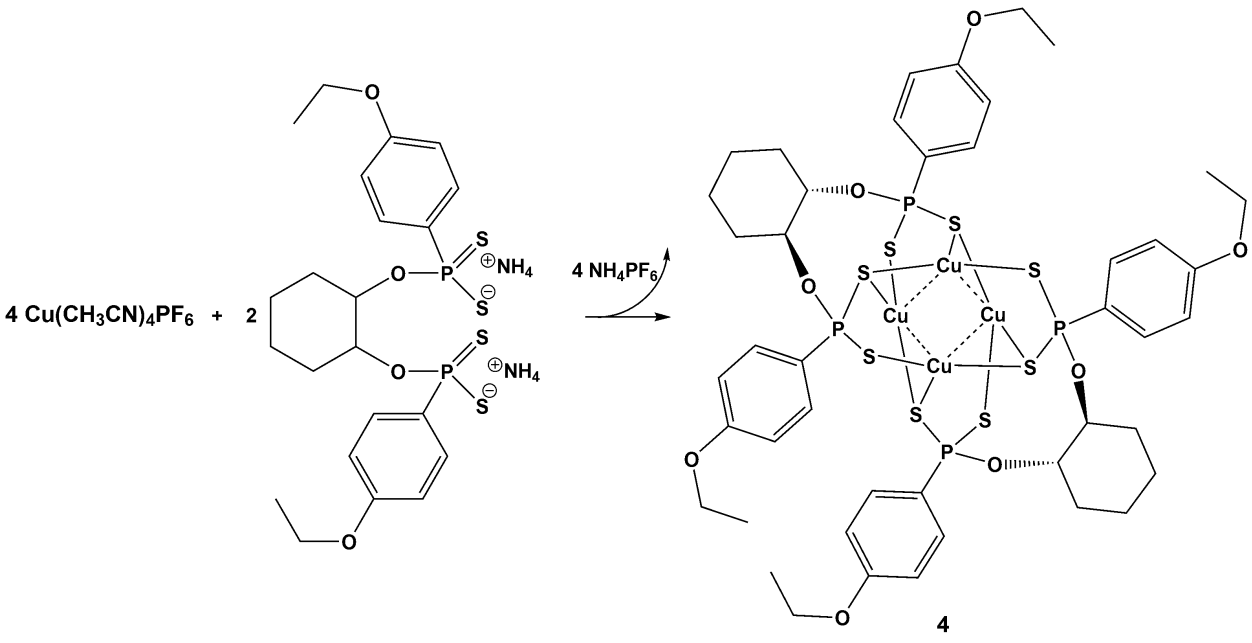

Scheme 3.3. Synthesis of tetranuclear Cu(I) cluster (**4**).

The ^{31}P NMR spectrum displays a single peak at 104.39 ppm, shown in Figure 3.6. Unlike its counterparts the chemical environments around each P atom is identical. The configuration of the cluster is therefore persistent in solution. The ^{1}H-NMR shows no significant deviation

from the free ligand. The cluster shows stability in air but is susceptible to oxidation upon prolonged exposure.

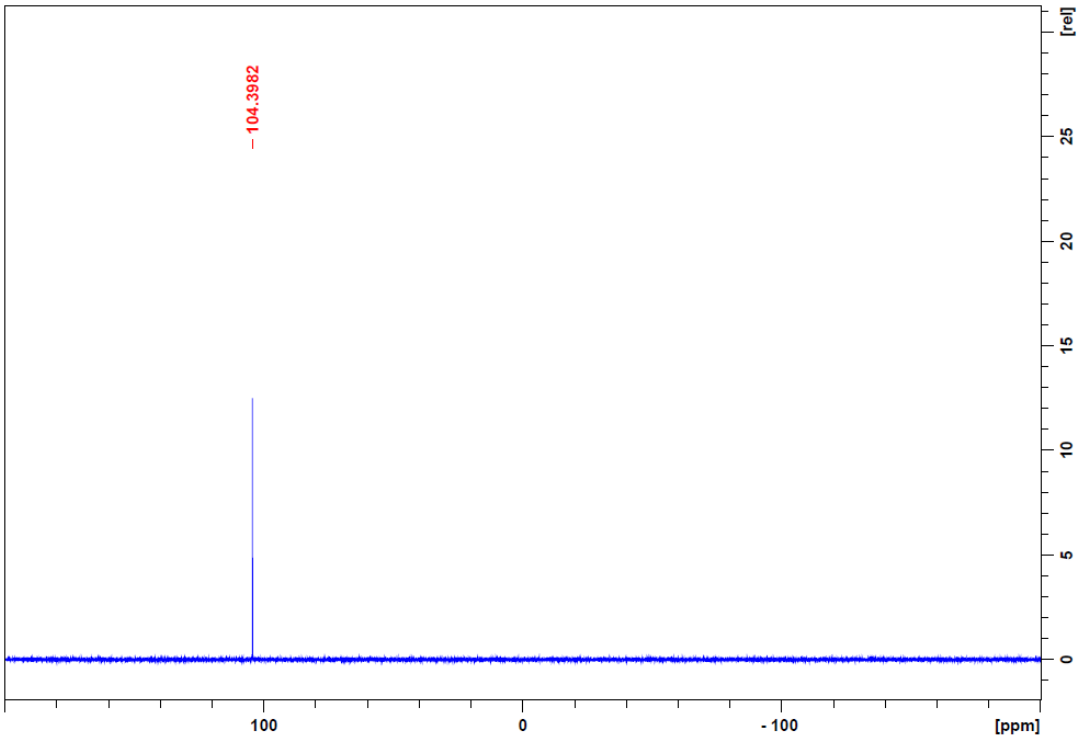

Figure 3.6. ^{31}P-NMR spectrum of **4** in $CDCl_3$.

Crystals of **4** showed a lack of stability at room temperature, and thus indicated that solvates were present in the lattice, slowly leaking out. Compound **4** crystallizes in the triclinic space group P-1, with two molecules of **4** and three solvates in the unit cell, shown in Figure 3.7. Selected bond lengths and angles can be found in Table 3.1. The solvate molecules occupy non-symmetric positions in the lattice and therefore causes a reduction in the overall symmetry of the system.

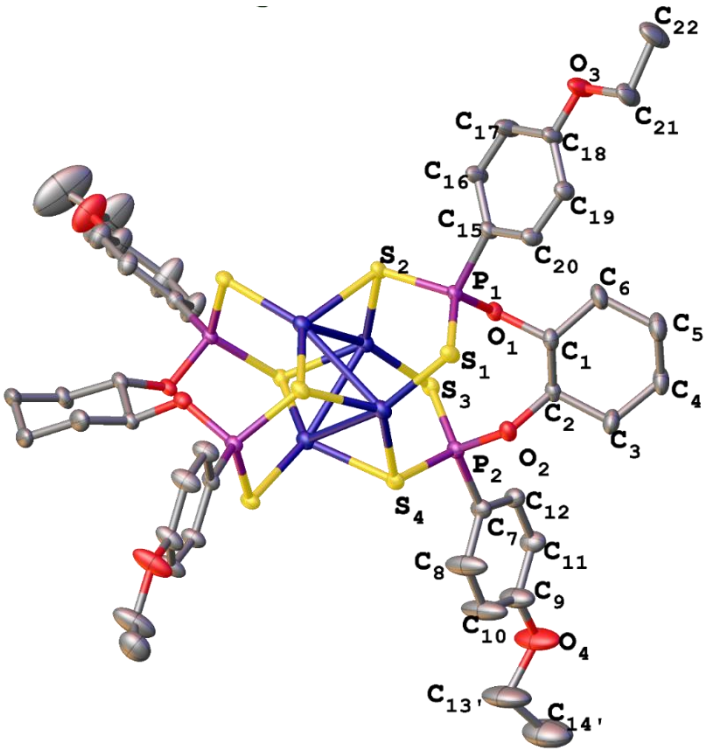

Figure 3.7. Molecular structure of **4**, thermal ellipsoids drawn at 35% probability, hydrogens omitted for clarity. Central Cu atoms are blue.

The metal framework reveals a core of four copper atoms arranged in a distorted tetrahedron. The tetrahedron is stabilized by four sulfur bridged metal Cu···Cu contacts with average distance of 2.7 Å, shown in Figure 3.8a. The non-bridged Cu atoms are at a distance of 3.08 Å, which is significantly longer than the sum of the van der Waals radius of two Cu atoms (2.8 Å) and not within the range reported for Cu-Cu (based on a search of the CCDC 2.632-2.978 Å).

The average S-P-S bite angles of the ligand are 116°, with each S-P-S moiety capping a triangular face of the tetrahedron. The intra-ligand S···S bite distance is 3.417 Å, with Cu-S bond distances of 2.292 Å. Each S-P-S moiety coordinates in a trimetallic, tri-connective (μ_2-S; μ_1-S) coordination mode and is shown in Figure 3.8b. Although the charge is delocalized across the S-P-S fragment, differential P-S bond lengths exists with the P-S_1 bond (2.058 Å) being slightly longer than the P-S_2 bond (1.979 Å). The *ca* 8 pm elongation arises as a direct result of the denticity, with $S_{(2)}$ bridging two Cu atoms a resultant loss of electron density occurs in the corresponding P-S bond. The inherent flexibility of the cyclohexyl groups allows for S-P-S fragments freedom to bind to all four copper atoms. The cyclohexyl groups are in a chair confirmation with oxygen substituents on the ring in a *gauche* confirmation (O-C-C-O

torsion angle *ca.* 63°), shown in Figure 3.8c. These chelating ligands can be described as having two S-P-S fragments *tethered* to each other, which results in the copper tetrahedron becoming somewhat distorted.

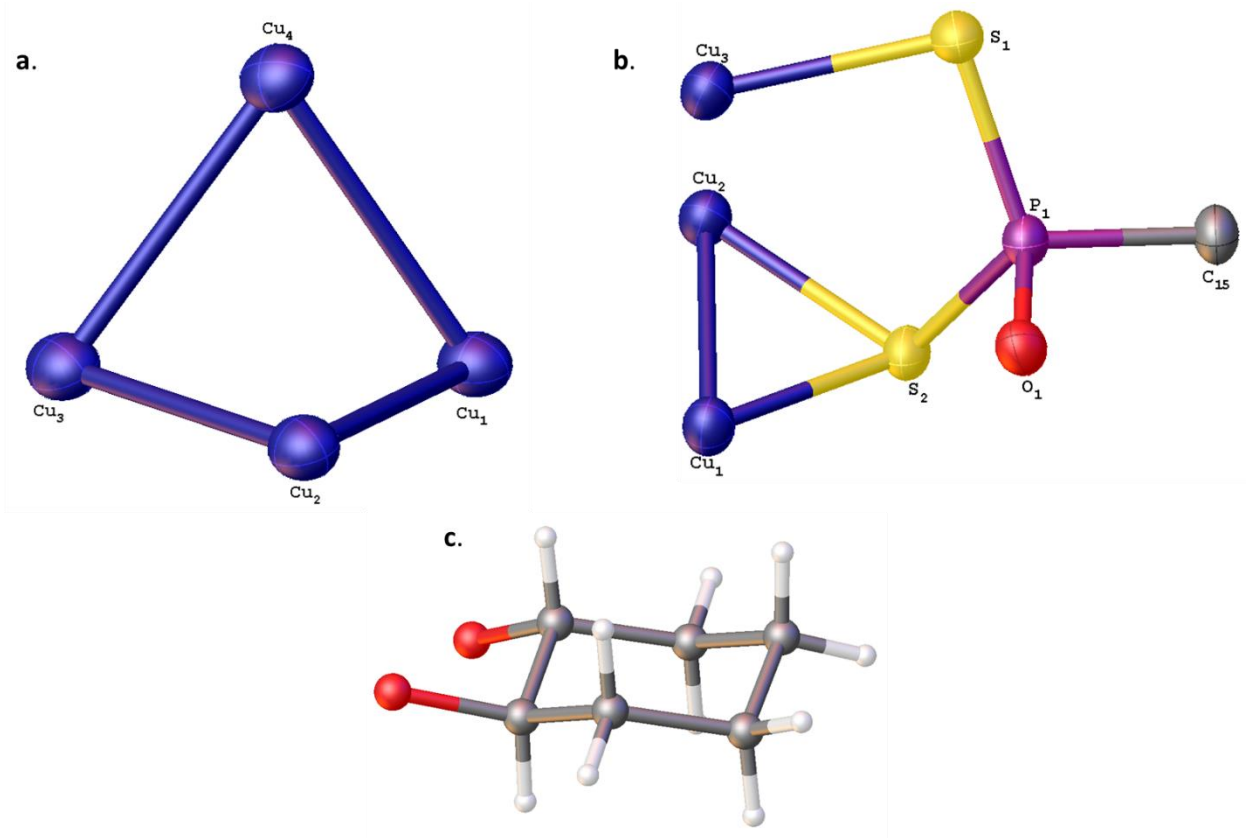

Figure 3.8. a) Tetra-nuclear Cu(I) core present in compound **4** with ligands omitted for clarity **b)** Trimetallic triconnective bonding mode present for each S-P-S moiety **c)** Chair conformation of cyclohexyl groups with oxygen atoms in *gauche* conformation present in **4**.

3.2.3 Tetranuclear Ag(I) cluster

The addition of 2 equivalents $[Ag(CH_3CN)_4]PF_6$ to $[NH_4]_2[(S_2P\text{-}1,4\text{-}C_6H_4OEt)_2(\textit{trans}\text{-}1,2\text{-}O,O'\text{-}C_6H_{10})]$ in THF led to the formation of the first tetranuclear Ag(I) cluster stabilized by dithiophosphonates, Scheme 3.4.

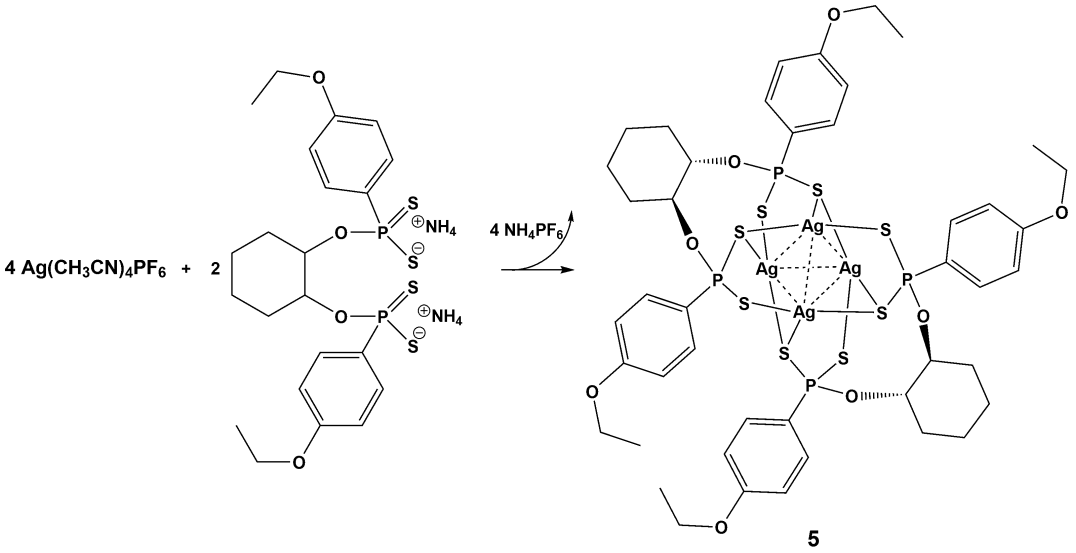

Scheme 3.4. Synthesis of a tetranuclear Ag(I) cluster (**5**).

Once formed, the complex is very unstable in the presence of light and prone to decomposition. This decomposition is clearly visible in solutions exposed to light, with the appearance of metallic silver deposits with mirror formation. This decomposition is confirmed by the ^{31}P NMR which displayed two peaks, Figure 3.9. One peak at 100.66 ppm which corresponds to the cluster and is not significantly different from its copper counterpart. The second peak at 105 ppm corresponds to chemical shift of the free ligand. The UV/light sensitivity of **5** did not affect the growth of single crystals from solution, and Xray analysis was possible. A short collection strategy at 100 K was possible, presumably due to the highly symmetric space I $4_1/a$ found. A molecular representation of **5** is shown in Figure 3.10. Selected bond lengths and angles can be found in Table 3.1.

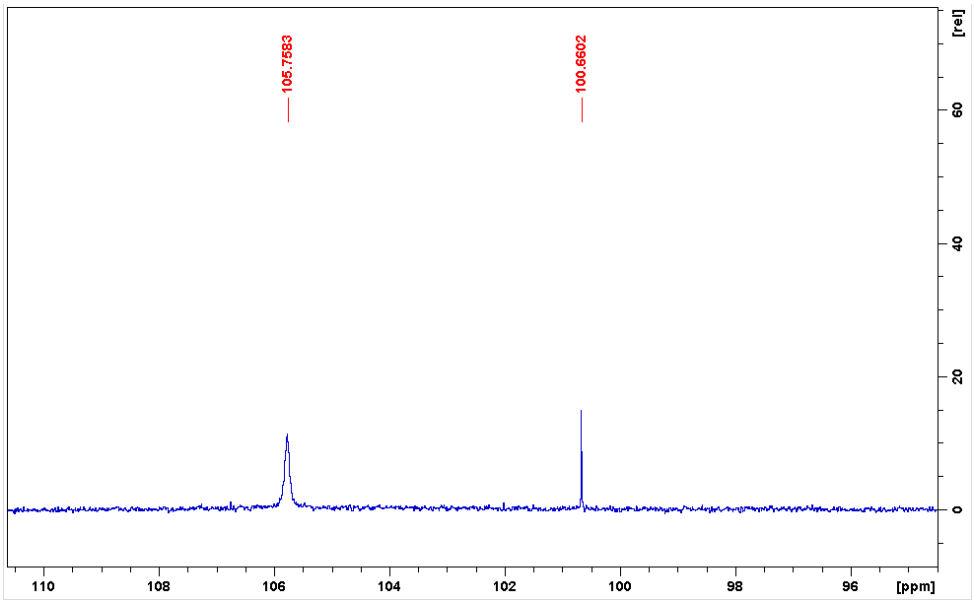

Figure 3.9. Decomposition of **5** in solution **as** seen in the ^{31}P NMR spectrum.

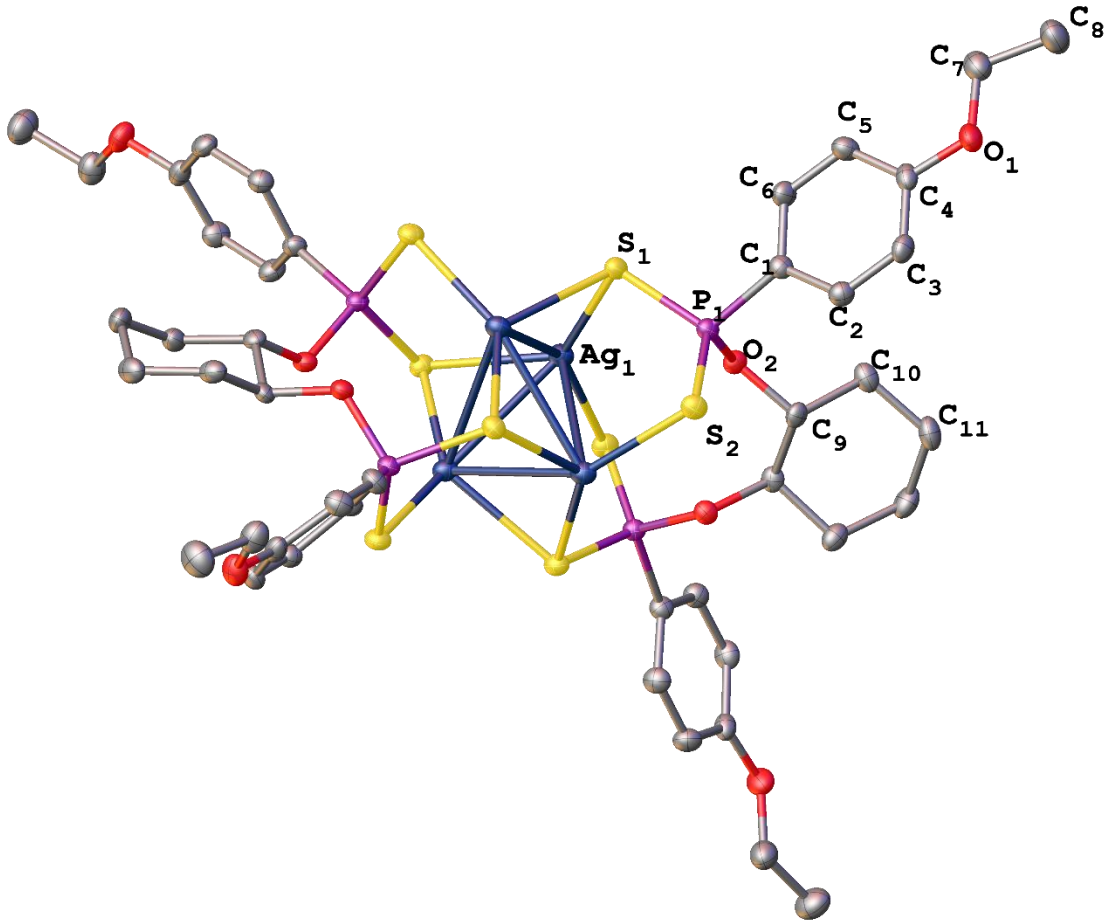

Figure 3.10. Molecular representation of **5** with ellipsoid drawn at 35 % probability and hydrogen atoms omitted for clarity.

The Ag core in **5** is significantly different from its Cu(I) counterpart with the tetrahedron stabilized by 6 Ag···Ag metal contacts, Figure 3.11. Two distinct contacts can be identified: 1) four shorter contacts bridged by sulfur with a distance of 3.023 Å and 2) two longer non-bridged Ag atoms at a distance of 3.346 Å, which is marginally shorter than the sum of the van der Waals radii of two Ag atoms (3.44 Å).

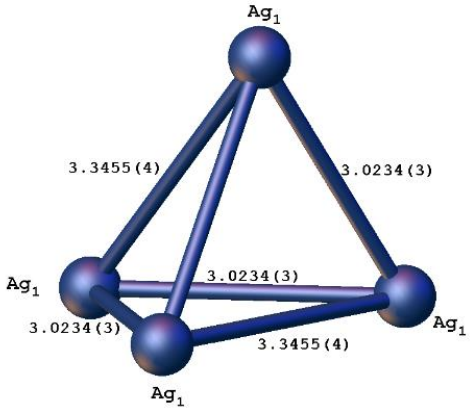

Figure 3.11. Ball and stick representation of the Ag(I) core present in **5.**

However, no solvates are present in the crystal lattice. This allows for a better interpretation of the symmetry present in the molecular units and the unit cell as a whole. The Ag cluster crystallizes in the tetragonal space group $I4_1/a$, with the asymmetric unit containing one quarter of a complete Ag_4 cluster, shown in Figure 3.12a. The introduction of the cyclohexane into the dithiophosphonates has introduced symmetry within the bis(dithiophosphonate). When focusing on the ligand, a C_2 rotation axis is present between the 1,2 and 4,5 positions on the cyclohexane ring, shown in Figure 3.12b.

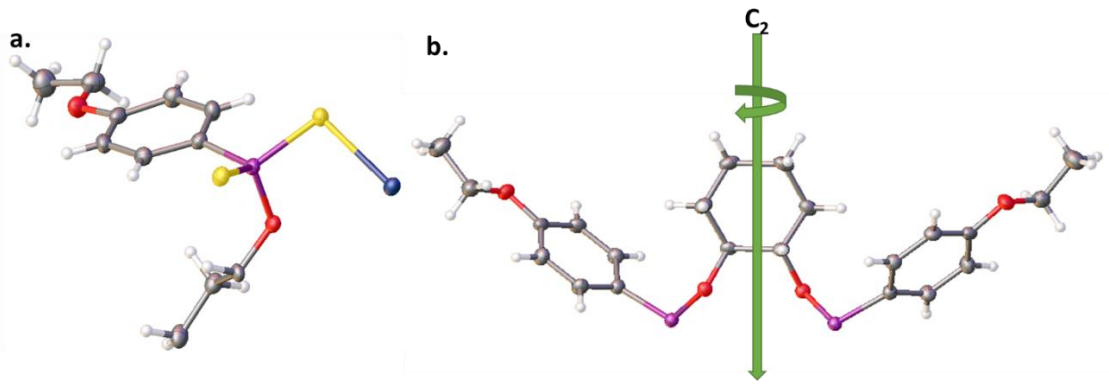

Figure 3.12. a) Asymmetric unit present **5** which represents a quarter of the molecule.**b)** Representation of the rotational axis present in ligand conformation observed in **5**.

Table 3.1. Selected bond lengths (Å) and bond angles(°), for **4** and **5,** with e.s.d. in brackets.

4		**5**	
P(1)-S(1)	1.983(2)	P(1)-S(1)	2.0308(9)
P(1)-S(2)	2.042(2)	P(1)-S(2)	1.9810(9)
P(2)-S(3)	1.981(2)	O(2)-P(1)	1.6071(18)
P(2)-S(4)	2.043(2)	Ag(1)-S(1)	2.4685(7)
O(1)-P(1)	1.593(5)	Ag(1)-Ag(1)^{2}	3.0233(3)
Cu(1)-Cu(2)	2.6989((12)	Ag(1)-Ag(1)^{1}	3.3455(4)
Cu(1)-Cu(4)	2.7301(11)	P(1)-S(1)-Ag(1)	98.48(3)
Cu(2)-Cu(3)	2.7214(12)	S(2)-P(1)-S(1)	116.74(4)
Cu(3)-Cu(4)	2.7202(12)		
S(1)-P(1)-S(2)	115.79(79)		

3.2.3 Hexanuclear Au(I) metallatriangle

The reaction of $(NH_4)_2[(S_2P\text{-}1,4\text{-}C_6H_4OEt)_2(\textit{trans}\text{-}1,2\text{-}O,O'\text{-}C_6H_{10})]$ with [AuCl(tht)] (tht = tetrahydrothiophene) (molar ratio 1:2) in THF at room temperature led to the formation of a novel 27-membered metallatriangle **6** of the type $[Au_2\{S_2P\text{-}1,4\text{-}C_6H_4OEt)_2(\textit{trans}\text{-}1,2\text{-}O,O'\text{-}C_6H_{10})\}]_3$, as outlined in Scheme 3.5. As such, it is three times larger than any of the aforementioned Au(I) triangles (Section 3.1.4), and contains three dinuclear Au(I) units. Notably, of the 27 atoms within the ring, only 6 are C atoms, the remaining 21 atoms comprise the heteroatoms O, P, S, and Au. Metallatriangles containing dinuclear units were hitherto unknown for gold and limited to very few metals in general.[53-57]

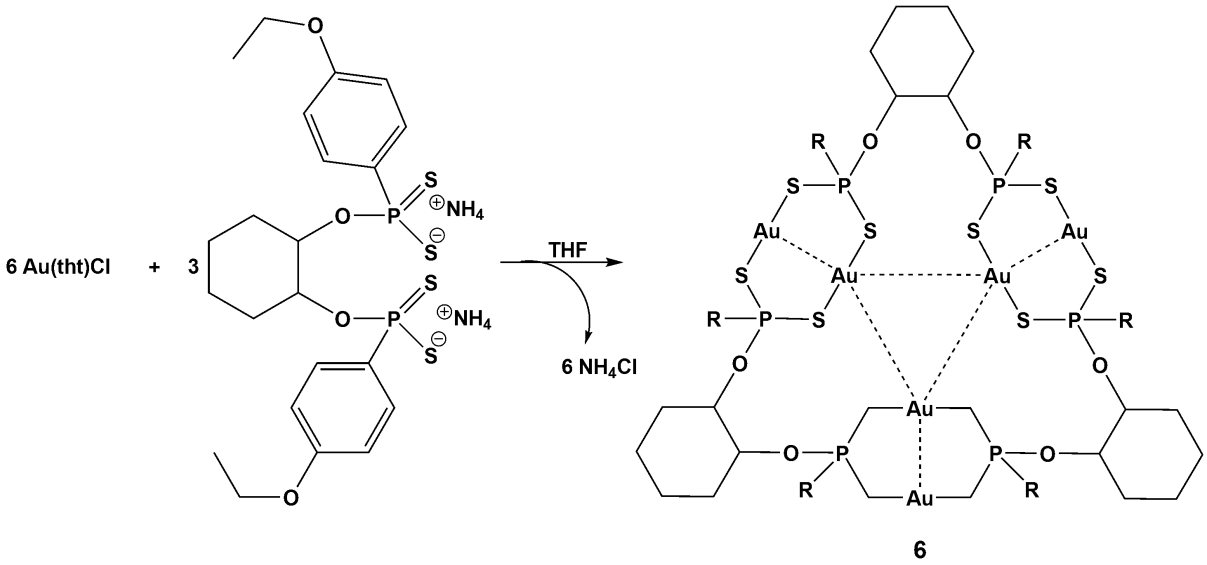

Scheme 3.5. Formation of **6**, $[Au_2S_2P\text{-}1,4\text{-}C_6H_4OEt)_2(\textit{trans}\text{-}1,2\text{-}O,O'\text{-}C_6H_{10})]_3$.

Dinuclear complexes of the type $[AuS_2R(OR')]_2$ are known to be present as both *syn* and *anti*-isomers in solution, generating a duplication of peaks in NMR experiments, one for each isomer. The solution structure of **6** appears complex as revealed by the decoupled ^{31}P NMR spectrum, showing ten unidentified singlet peaks within the region 92 – 106 ppm, which are all in the expected region for this complex type.[58-60] Complex **6** seems susceptible to forming rearrangement/isomerization products in deuterated chloroform. Previous studies have shown that a dynamic equilibrium can exist in solution between different supramolecular assemblies and are observable on the NMR time scale, as described for Pd(II) and Pt(II) complexes.[61,62] Repeating the NMR experiment in deuterated-dmso solvent reduced the number of peaks and hence increased the solution stability. However, it still revealed two singlet peaks resonating at 99.39 and 13.42 ppm. The former is undoubtedly assigned to **6** as it falls in the region found for the Cu(I) and Ag(I) systems. It also suggests that the *syn* and *anti* isomerization does not take place, similar to the above examples. Unfortunately the latter peak appears persistent but could not be unambiguously identified. Resorting to solid-state MAS ^{31}P NMR, the bulk purity of **6** was confirmed with a singlet peak resonating at 95.60 ppm, Figure 3.13.

In summary, NMR demonstrates that solution rearrangement/isomerization processes are at work. The peak at 13.42 ppm aside, we are reluctant to wholly ascribe these phenomena to decomposition since the same (presumably pure) gold starting material was used for further oxidative addition reactions.

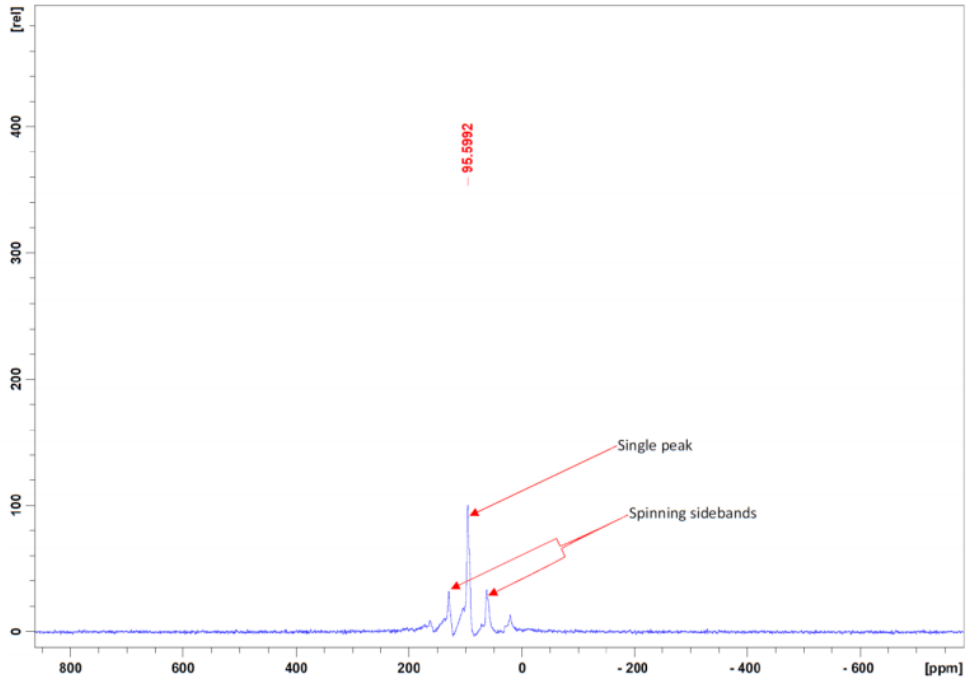

Figure 3.13. Solid state MAS ^{31}P NMR spectrum of **6**.

Crystals of **6** revealed a tetragonal space group $I4_1/a$, with a CH_2Cl_2 solvate present. The geometry of the complex is completely different from its Cu and Ag counterparts. A molecular representation is shown Figure 3.14 and bond lengths/angles presented in Table 3.2. The difference in structure can be attributed to several factors, which include but are not limited to the following:

1. The preferred coordination geometry of 2-coordinate Au(I) is linear.
2. An increase in size of the metal centres have made it impossible for the ligand to accommodate the required orientation.
3. Short intramolecular Au···Au contacts contribute significantly to the formation of a triangle's stability.

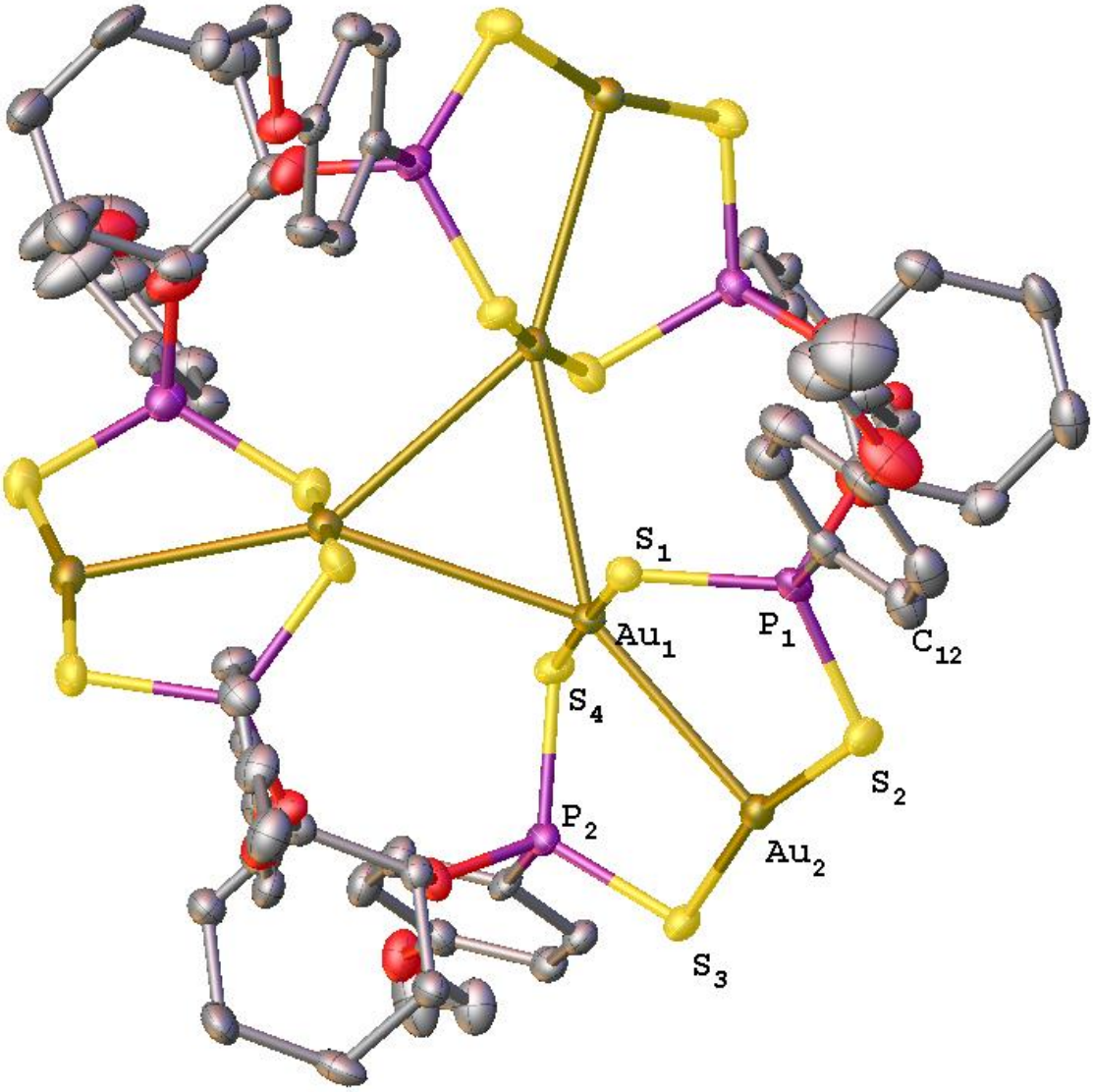

Figure 3.14. Molecular structure of complex **6**: thermal ellipsoids drawn at the 35% probability level, solvates and H atoms omitted for clarity.

Complex **6** exhibits two different types of intramolecular Au···Au interactions: a) an interaction between the gold atoms within each of the three dinuclear units at an average distance of *ca.* 3.0 Å, and b) interactions between each gold atom and the two gold atoms situated across the cavity at a slightly longer average distance of *ca*. 3.3 Å, Figure 3.15a. There are no significant intermolecular Au···Au interactions within **6**. The Au···Au interactions are of sufficient magnitude that all the Au(I) atoms are coplanar. Likewise the intramolecular Au···Au interactions across the cavity add additional stability to the extent that it twists the molecule to retain the triangular architecture; for example the S-Au-S linkages are essentially

linear in some cases (179°), whilst in others significantly distorted (165°). Within each dinuclear unit the S-Au-S axes do not run parallel to each other and torsion angles of *ca* 19 ° for S-Au···Au-S are present. This results in a significantly large *cross-over* for a *fully supported* dinuclear unit, Figure 3.15b.[60] The S-P-S fragment coordinated in *bimetallic biconnective* mode, with the the S-P bond lengths of equal magnitude *ca* 2.02 Å, indicating complete delocalization of the S-P π bond.

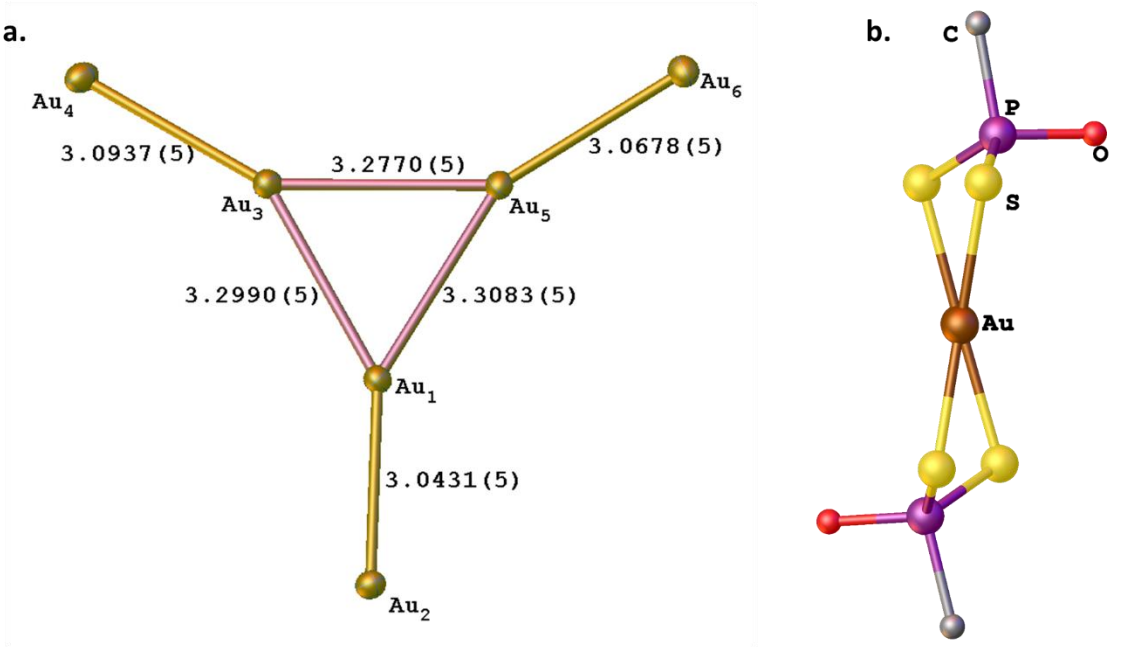

Figure 3.15. a) Topology of Au(I) atoms present in **6** with Au···Au contacts labeled. **b)** A single dinuclear unit present in **6** indicating the distortion of the S-Au-S planes (*cross-over*).

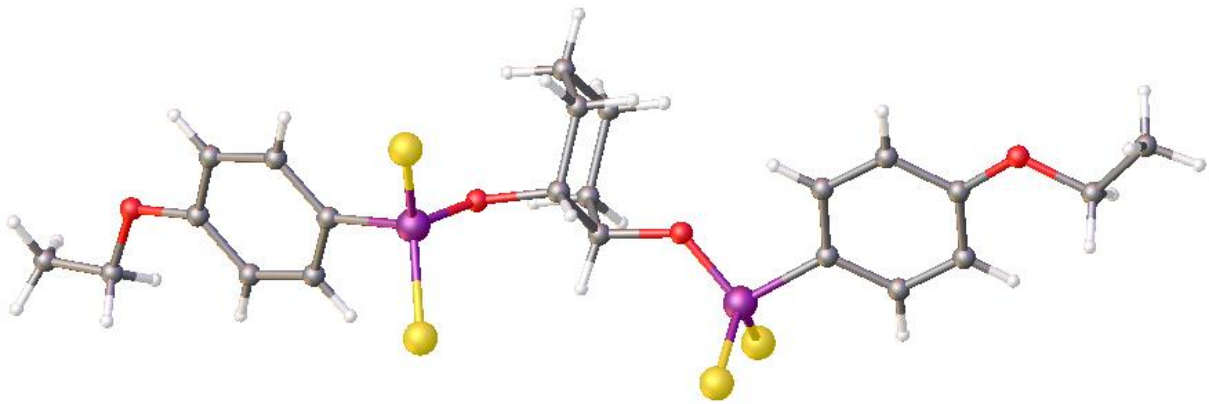

Figure 3.16. The antiperiplanar arrangement of the cyclohexyl group with ligands engaged in coordination on opposite sides relative to the ring.

The cyclohexyl groups are also in a chair conformation as in aforementioned examples, however, the arrangement of the axial and equatorial substituents on the ring differ, with an *anit-periplanar* confirmation present (O-C-C-O average torsion *ca.* 173 °), shown if Figure 3.16. Interestingly, the rotational axis described for the Ag(I) complex is still present with the S-P-S coordination fragments occupying opposite sides relative to the cyclohexyl ring.

The molecular units pack to form an aesthetically appealing and interesting arrangement, Figure 3.17a. Intriguingly, closer inspection of the arrangement of the metallatriangles relative to each other, reveals a rotation of the individual assemblies as one moves down the crystallographic plane akin to helical packing, shown in Figure 3.17b.

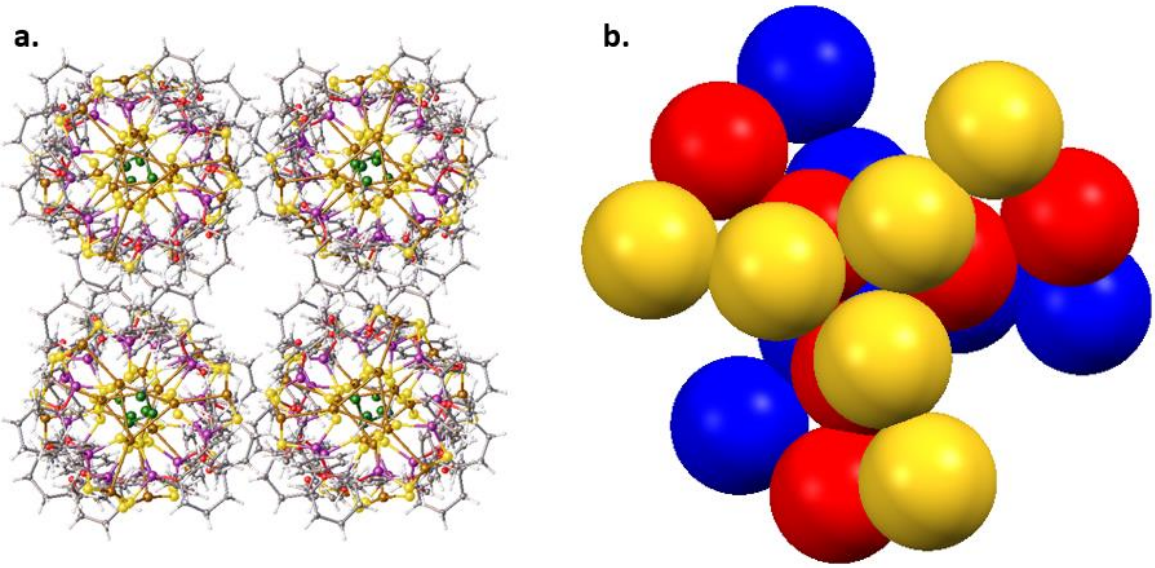

Figure 3.17. a) Crystal packing present in **6**. **b)** the long range order of the Au(I) triangles with the 1st layer in yellow, 2nd in red and 3rd in blue.

Table 3.2. Selected bond lengths (Å) and bond angles (°), for **6** and **7,** with e.s.d. in brackets.

6		**7**	
P(1)-S(1)	2.018(3)	P(1)-S(1)	2.031(2)
P(1)-S(2)	2.015(3)	P(1)-S(2)	2.033(2)
P(2)-S(3)	2.017(3)	P(2)-S(3)	2.030(2)
P(2)-S(4)	2.026(3)	P(2)-S(4)	2.033(2)
O(7)-P(1)	1.590(6)	O(1)-P(1)	1.568
Au(1)-S(1)	2.298(2)	Au(1)-Br(1)	2.4309(7)
Au(1)-Au(2)	3.0431(5)	Au(1)-Br(2)	2.4288(7)
Au(1)-Au(3)	3.2990(5)	Au(1)-S(2)	2.3270(16)
Au(1)-Au(5)	3.3083(5)	Au(1)-S(1)	2.3325(16)
Au(3)-Au(4)	3.0937(5)	S(1)-P(1)-S(2)	100.23(9)
Au(3)-Au(5)	3.2770(5)	S(3)-P(2)-S(4)	99.49(9)
Au(5)-Au(6)	3.0678(5)		
S(2)-Au(2)-S(3)	165.99(8)		
S(5)-Au(3)-S(8)	176.97		

3.2.4 Dinuclear Au(III) dithiophosphonate

Complex **6** is a large metallatriangle and also contains three well-separated dinuclear Au(I) units; making **6** an ideal candidate for testing of heretofore unknown OA products. Treatment of **6** with Br_2 in CH_2Cl_2 caused an immediate colour change from pale yellow to red. Unlike **6** which resulted in the complicated ^{31}P NMR spectrum described above, that of complex **7** was simple and formed only one singlet peak resonating at 101 ppm assigned to the two equivalent P atoms, shown in Figure 3.18. Based on the stoichiometry used, it formed exactly 3 equivalents of the red complex **7** without additional side-products, Scheme 3.6.

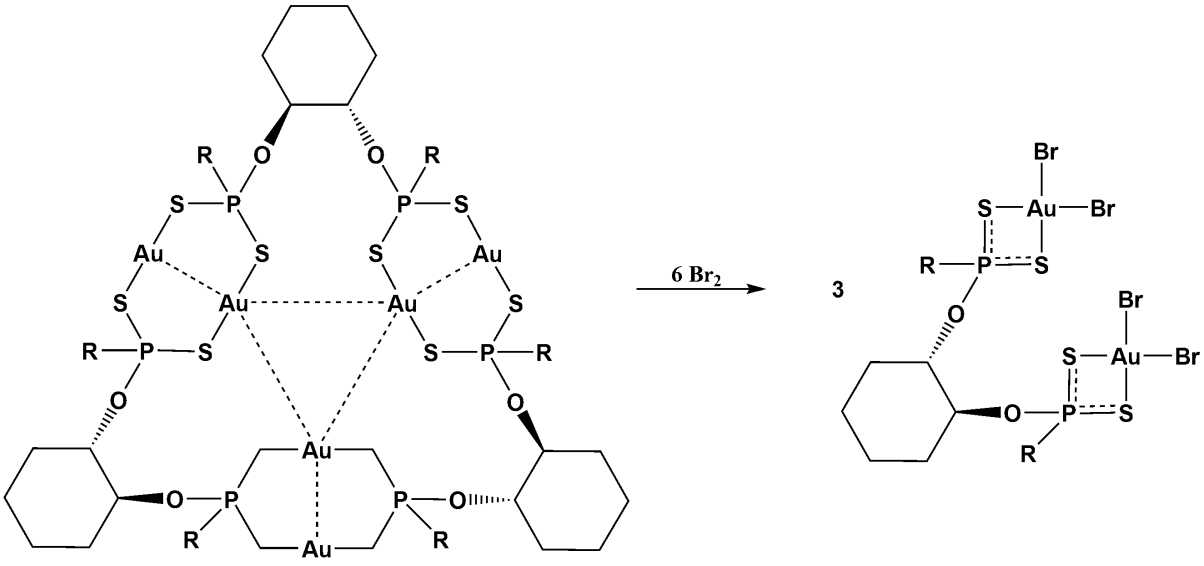

Scheme 3.6. Reaction of **6** with Br_2 and formation of **7.**

Whereas **6** was the first complex with a neutral Au_2S_4 manifold to induce *any* kind of reaction with a halogen, complex **7** is the first complex containing both a S-P-S chelating (S,S) ligand and a halogen ligand across a Au(III) centre obtained through an OA reaction, or indeed any other means.

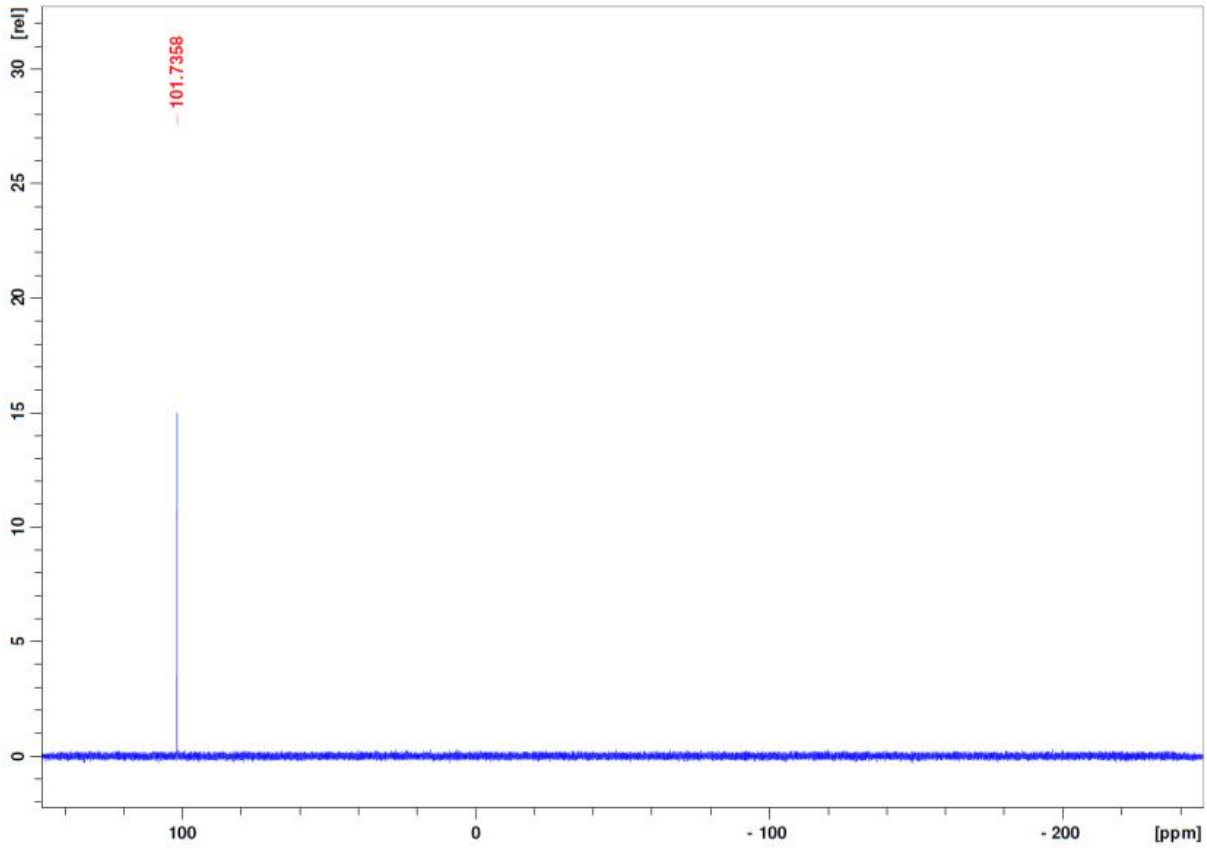

Figure 3.18. ^{31}P-NMR spectrum of **7** displaying a single peak, indicating magnetically equivalent P atoms.

Importantly, the OA reaction departed significantly from that observed for types (**A)** and (**B)** and (**C**) described above (Section 3.15). The dinuclear units of **6** ruptured into 3 equivalent and stable complexes, each containing two well separated Au(III) centres (*i.e.* a non-classical dinuclear Au(III) complex). Further, any notion of an isolable, Au-Au stabilized Au(II)/Au(II) major product that ought to resemble the quintessential OA products of (**A**), (**B**), or (**C**) either never formed or had been circumvented through a different reaction mechanism. At present, no evidence suggests a reaction sequence leading to **7** included a Au(II) intermediate. The driving force for the formation of **7** could derive from either electronic or steric factors. The fact that OA reactions readily form dinuclear Au(II) complexes from types (**A**), (**B**), or (**C**), but are distinctly absent for *neutral* complexes with S-X-S (X = C or P) bridging ligands suggests the latter contribute an electronic structure whereby OA reactions are negatively affected by Au-Au bond formation.[63] Steric factors usually play no role, but in the case of **6** it is useful to note that should OA with Br_2 occur across the dinuclear Au(I) units, it would create two essentially linear Br-Au-Au-Br moieties with two of the four Br atoms pointed to the centre of

the complex which has no available space. Therefore in this case, the steric hindrance may have contributed to the rupturing of the complex. Complex **7** represents the first gold complex containing both S-P-S chelates and halogen ligands, Figure 3.19. Selected bond lengths and angles are presented in Table 3.2.

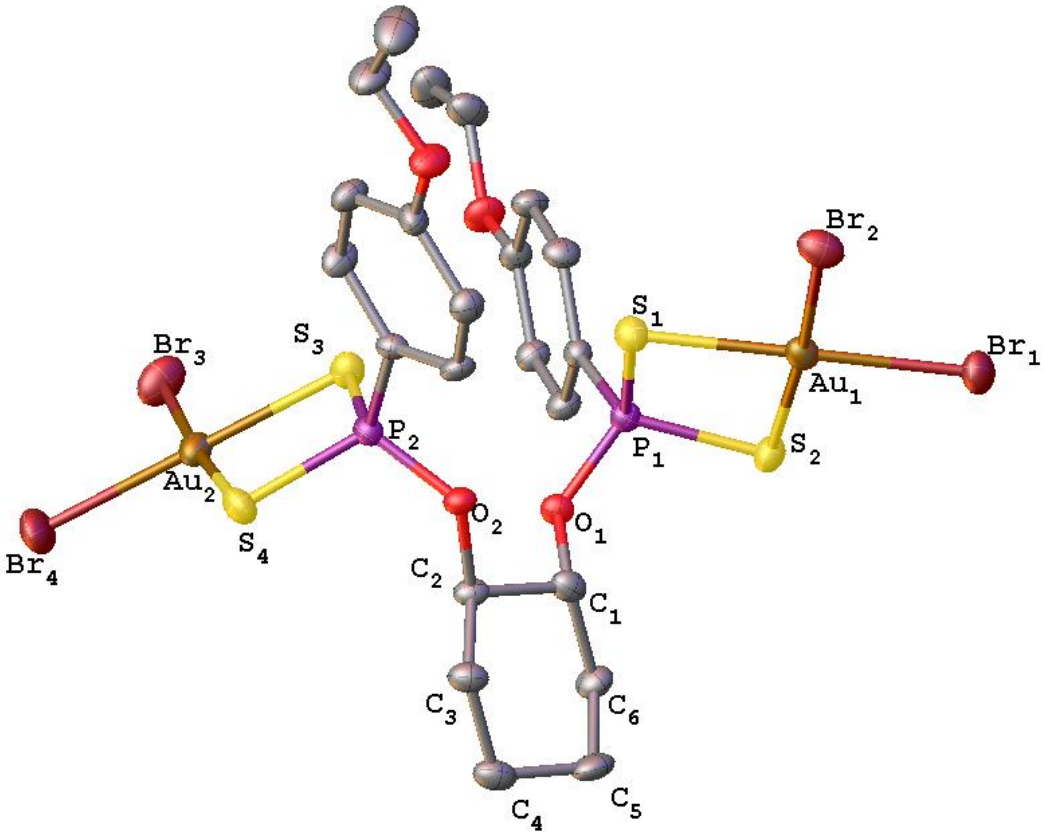

Figure 3.19. Molecular representation of **7,** thermal ellipsoids drawn at the 50% probability level, H atoms omitted for clarity.

Following publication of the hexanuclear Au(I) complex and its oxidative addition reaction[64] described in this thesis, Van Zyl and Liu investigated this further.[65] Importantly, the report supports the direct formation of a Au(III) square-planar complex. The Au(III) complex was isolated from the addition of iodine to a discrete dinuclear Au(I) complex, which contained symmetric S-P-S bridging moieties, shown in Figure 3.20.[65] It was furthermore demonstrated that the reaction is chemically reversible in that the more difficult reductive elimination process could be achieved with Sn(IV).

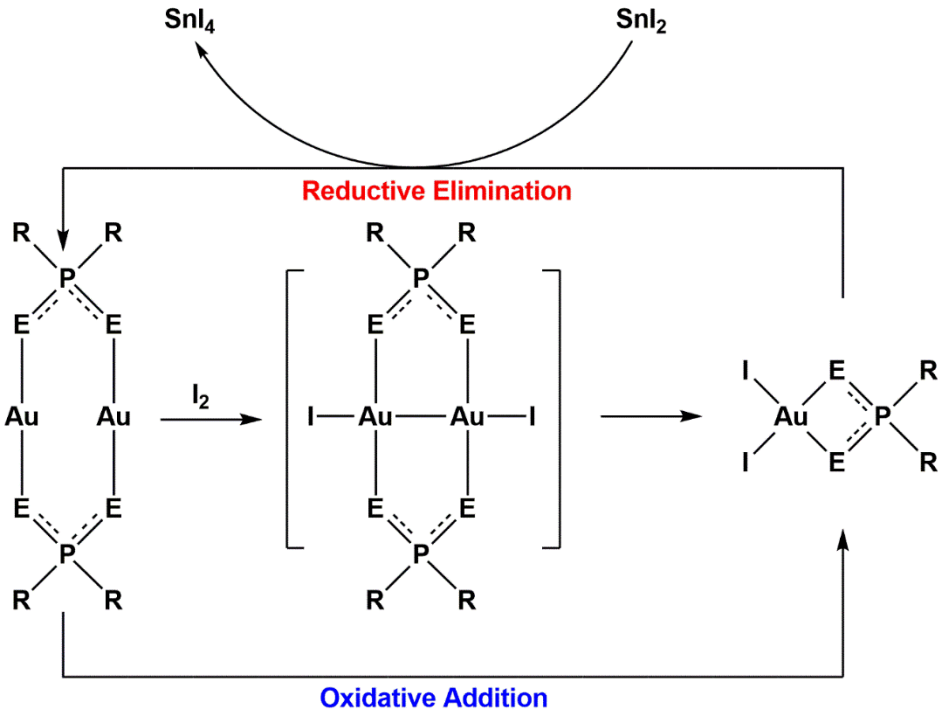

Figure 3.20. Reversible oxidative addition observed for related symmetric dinuclear Au(I) complexes, (ref. 65).

3.2.5 Cofacial dinuclear Ni(II) complex

It is suggested that the presence of metallophilic interactions amongst the Group 11 metals had some role to play, and were contributing factors to the formation of above described clusters. The question was thus posed: What would happen when such interactions were not present in the system? In the next section, we turned our attention to a Ni(II) system, which is not known to have metal-metal interactions.

The stability of the ligand is observed by its ability to form metal complexes even in water (aqueous) media. Thus, the addition of $NiCl_2{\cdot}6H_2O$ dissolved in water to a methanolic/water solution of $(NH_4)_2[(S_2P\text{-}1,4\text{-}C_6H_4OEt)_2(\textit{trans}\text{-}1,2\text{-}O,O'\text{-}C_6H_{10})]$, resulted in the immediate formation of a purple precipitate, characterized as $[Ni_2S_2P\text{-}1,4\text{-}C_6H_4OEt)_2(\textit{trans}\text{-}1,2\text{-}O,O'\text{-}C_6H_{10})]_2$, Scheme 3.7.

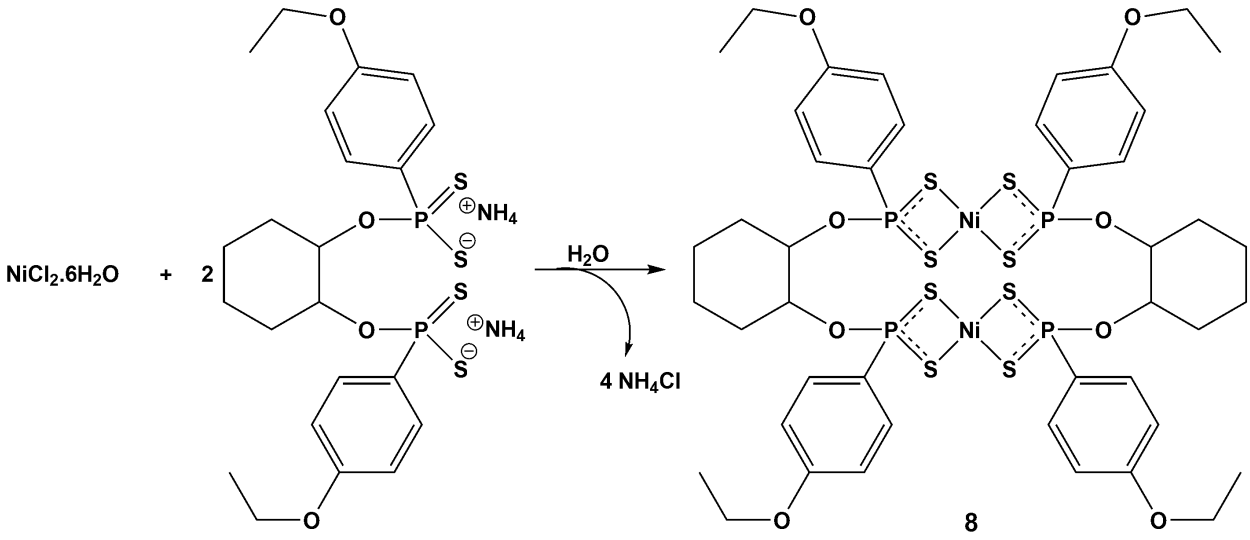

Scheme 3.7. Application of ligand in an aqueous medium and formation of a cofacial Ni(II) complex.

The novel cofacial dinuclear hetero-atomic macrocycle consists of 18 atoms, only 4 of which are carbon atoms and the remaining consisting of O, P, S and Ni atoms. The ^{31}P NMR spectrum showed two resonance peaks, at 98.9 and 96.9 ppm. This is due to the presence of two isomeric forms in solution, which is known to occur for Ni(II) dithiophosphonate complexes.[66] The ^{1}H-NMR displayed poor resolution due to severe overlap of peaks and could not be assigned. The mass spectrum further confirmed the predicted structure with the detection of the sodium adduct of the complex. Complex **8** was found to be stable under ambient conditions, unlike the coinage metal analogues.

In the solid-state, complex **8** crystallises in the monoclinic space group P21/c with the asymmetric unit consisting of one half of the molecule, shown in Figure 3.21. Selected bond lengths and angles are presented in Table 3.3. Each 4-coordinate metal centre has a distorted square-planar geometry which is expected for dithiophosphonate Ni(II) complexes.[66-70] The isobidentate S-P-S fragments (bite angle *ca.* 102 °) chelate the Ni(II) centre and equivalent P-S bond lengths (*ca*. 2.0 Å) indicate a complete delocalization of the P-S π bond. The chair conformation of the cyclohexane is maintained with the oxygen atoms in an anti-periplanar configuration. The free rotation around the O-P bond becomes apparent when compared to complex **6**, with the coordinating fragments now pointed in the same direction unlike in **6** where they pointed in opposite directions. The elusive *cis* configuration in **8** is supported by the conformation of the ligand. A 2002 report described a related Ni(II) dithiophosphonate

complex, but in that case the *cis* configuration was enforced and aided through an extensive network of hydrogen bonds.[71] The distance between the Ni(II) centres is 4.9 Å and the perceived cavity is inaccessible due to the packing of the molecules in the crystal lattice, Figure3.22.

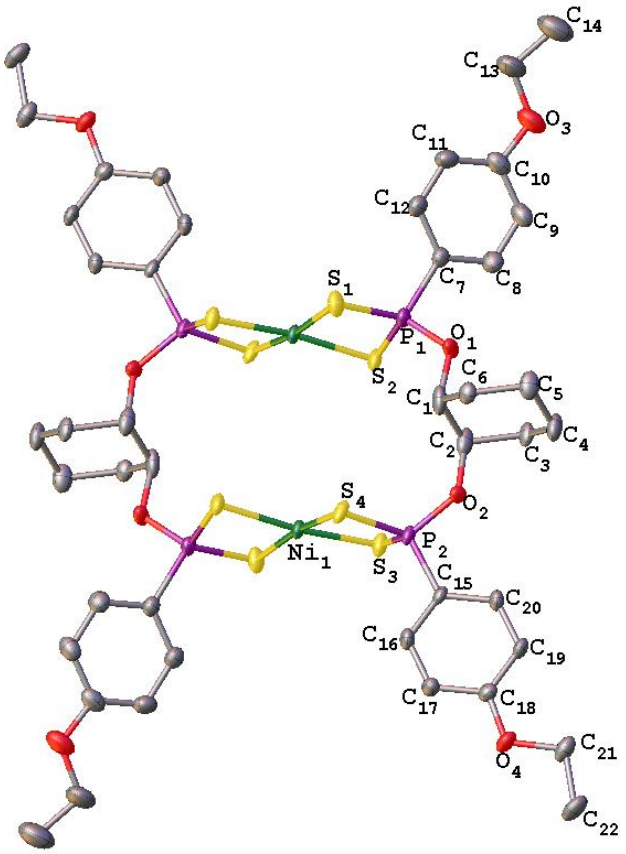

Figure 3.21. Molecular representation of **8**: Thermal ellipsoids drawn at 35 % probablity and H atoms removed for clarity.

A peculiar anomaly was observed during the growth of crystals of complex **8**. Two different crystal morphological types were obtained from the same vessel under the same conditions, i.e. blue needles and purple prismatic crystals. Normally this occurrence would imply a gross difference in compositional structure. However, X-ray analysis of the two different crystals revealed a non-selective random inclusion and exclusion of CH_2Cl_2, leading to blue needles and purple prism-like crystals, respectively. The ability of the molecule to incorporate one mole of CH_2Cl_2 into a particular growth pattern and exclude it from neighbouring crystals from the same crystal growth environment is indeed unique, and difficult to explain. The large

excess CH_2Cl_2 is absent during the synthesis process, and thus only incorporated into the structure during the crystal growth process.

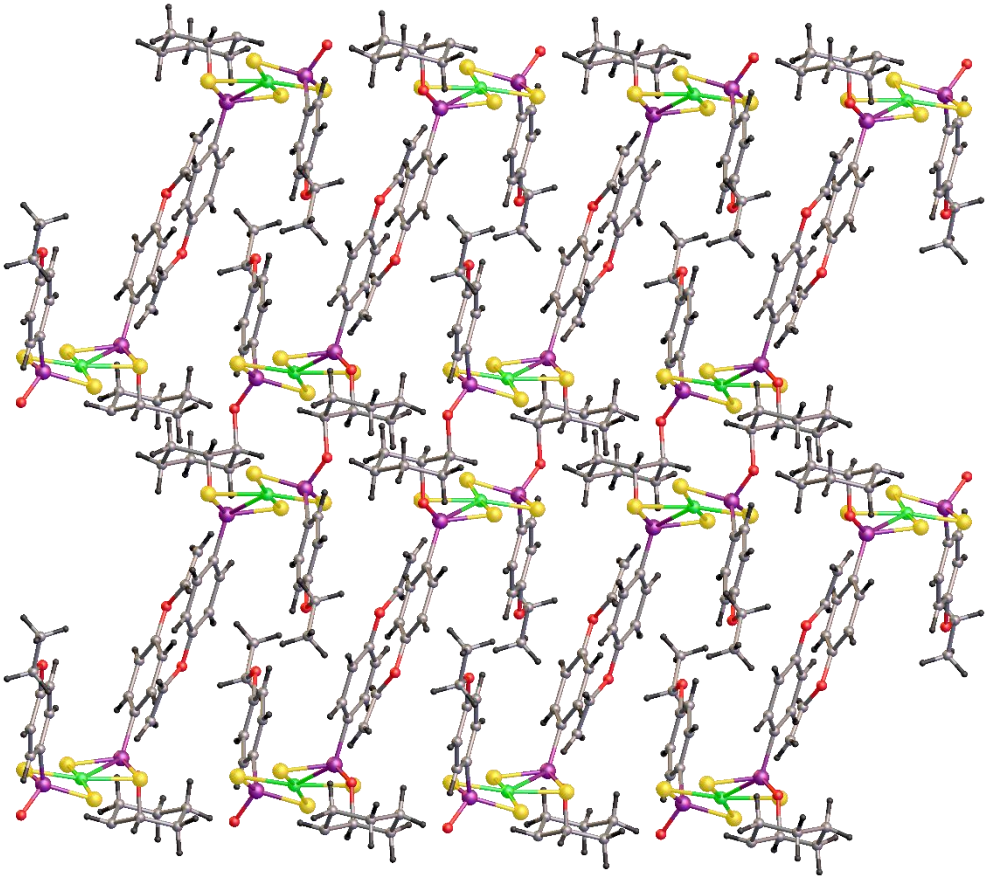

Figure 3.22. Packing in crystal lattice of **8** viewed along the *b*-axis.

The structure containing the solvent is shown in Figure 3.23. The solvent does not lie within the cavity across the Ni centres, which has been shown to act as a recognition site in related cofacial dinuclear complexes.[72] Two short contacts present between, Cl-O 3.2 Å and H-S 2.9 Å, disrupt the packing and act as *molecular spacers.* The data of the two structures are, unsurprisingly, quite similar.

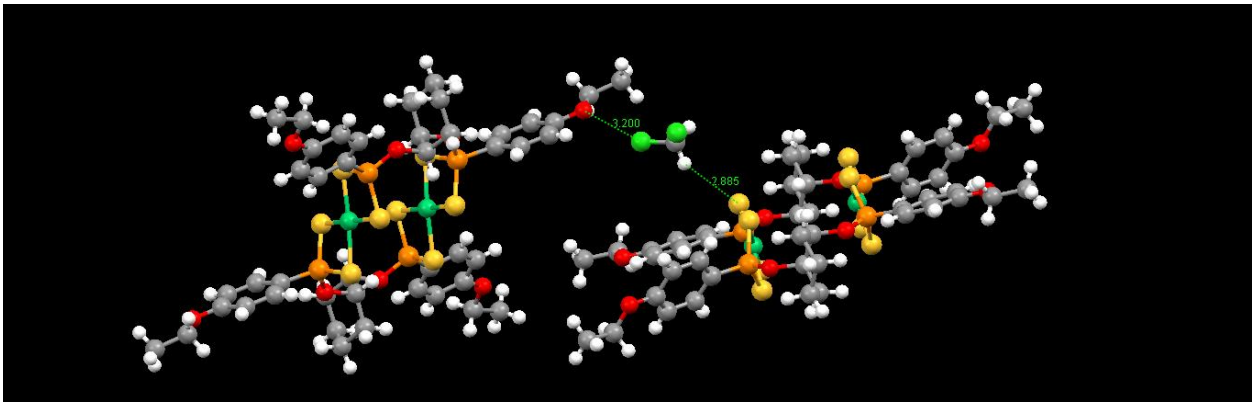

Figure 3.23. Ball and stick representation of two molecular units of **8** and its interaction CH_2Cl_2

Table 3.3. Selected bond lengths (Å) and bond angles(°) for **8**, with e.s.d. in brackets.

P(1)-S(1)	1.995(2)
P(1)-S(2)	2.001(2)
P(2)-S(3)	2.003(2)
P(2)-S(4)	1.996(2)
O(1)-P(1)	1.587(4)
Ni(1)-S(1)	2.2329(18)
Ni(1)-S(2)	2.2255(16)
Ni(1)-S(3)	2.2178(17)
Ni(1)-S(4)	2.2143(16)
S(1)-P(1)-S(2)	102.82(9)

Table 3.4. Details of Xray crystal data collection and refinement for **4**-**6**.

Compound	4	5	6
Emperical formula	$C_{44}H_{56}Cu_4O_8P_4S_8$ 3(CH_2Cl_2)	$C_{44}H_{56}Ag_4O_8P_4S_8$	$C_{66}H_{84}Au_6O_{12}P_6S_{12}(CH_2Cl_2)$
Mw	1602.18	1524.73	2906.6
Temperature[K]	150	173(2)	173(2)
Size [mm]	0.43 x 0.40 x 037	0.16 x 0.089 x 0.046	0.24 x 0.16 x 0.09
Cryst. System	Triclinic	Tetragonal	Tetragonal
Space Group	P-1	I 41/a	I 41/a
a[Å]	13.5793(5)	12.8185(3)	26.7928(18)
b[Å]	13.6609(5)	12.8185(3)	26.7928(18)
c[Å]	19.7817(7)	32.9696(16)	54.090(4)
α[°]	103.0832(8)	90	90
β[°]	107.6626(8)	90	90
γ[°]	91.5606(8)	90	90
V[Å^3]	3387.6(2)	5417.4(3)	38828(5)
Z	2	4	16
ρcal [g cm^{-3}]	1.571	1.870	1.989
Absorption coefficient [mm^{-1}]	1.861	1.816	9.495
***F*(000)**	1628.0	2880	21984
***Θ*range [°]**	2.23 to 50	1.7 to 28.39	1.7 to 25.4
Data/restraints/parameters	11794/715/705	2712/0/155	17883/0/952
Goodness of fit F^2	1.052	1.040	1.061
Final *R* indices [$I > 2\sigma(I)$]	R_1 = 0.0726, wR_2 = 0.2188	R_1 = 0.0228, wR_2 = 0.0581	R_1 = 0.0357, wR_2 = 0.0911
***R* indices (all data)**	R1 = 0.0845, wR2 = 0.2343	R_1 = 0.0326, wR_2 = 0.0600	R_1 = 0.0590, wR_2 = 0.1045
Largest diff peak/hole [e/ Å^3]	4.16/-1.66	0.49/-0.47	2.69/-1.64

Table 3.5. Details of Xray crystal data collection and refinement for **7**-**8**.

Compound	**7**	**8**	**8.CH_2Cl_2**
Emperical formula	$C_{22}H_{28}Au_2Br_4O_4P_2S_4$	$C_{22}H_{26}NiO_4P_2S_4$	$C_{23}H_{28}NiO_4P_2S_4Cl_2$
Mw	1260.20	603.32	690.26
Temperature[K]	173(2)	173(2)	173(2)
Size [mm]	0.12 x 0.12 x 0.07	0.20 x 0.12 x 0.07	0.33 x 0.30 x 0.164
Cryst. System	Monoclinic	Monoclinic	Monoclinic
Space Group	P 21/c	P 21/c	P 21/c
a[Å]	11.2132(8)	15.1505(19)	17.2228(9)
b[Å]	15.3143(11)	11.5775(14)	11.8570(6)
c[Å]	19.9458(15)	15.6508(19)	15.7181(9)
α[°]	90	90	90
β[°]	92.7980	91.715(2)	105.936(3)
γ[°]	90	90	90
V[$Å^3$]	3421.1(4)	2744.0(6)	3086.4(3)
Z	4	4	4
ρcal [g cm^{-3}]	2.447	1.460	1.485
Absorption coefficient [mm^{-1}]	13.604	1.154	1.204
***F*(000)**	2336	1248	1424
***Θ*range [°]**	1.68 to 25.35	2.19 to 25.26	1.23 to 25.37
Data/restraints/parameters	6250/0/345	4947/0/287	5646/0/327
Goodness of fit F^2	1.019	1.021	1.061
Final *R* indices [$I > 2\sigma(I)$]	R_1 = 0.0299, wR_2 = 0.0617	R_1 = 0.0608, wR_2 = 0.1334	R_1 = 0.0673, wR_2 = 0.1918
***R* indices (all data)**	R_1 = 0.0469, wR_2 = 0.0673	R_1 = 0.1111, wR_2 = 0.1555	R_1 = 0.0817, wR_2 = 0.2070
Largest diff peak/hole [e/ $Å^3$]	1.007/-0.710	0.750/-0.813	2.570/-2156

3.3 Luminescence

The luminescent properties of the complexes prepared from the coinage metals were evaluated. Unfortunately, cluster **5** was not amenable to luminescence studies, due to the decomposition of the compound during exposure to an excitation source (both the solution and solid state). No luminescent characteristics of Cu(I) dithiophosphonates has been reported in literature. Herein the first luminescent data will be reported for this system and in the next chapter several Cu(I) dithiophosphonates will be described and compared to literature.

In the solid-state, the emission was measured at room temperature (RT) and at 77 K (liquid nitrogen). The cluster does not show significant thermochromatic behaviour. However, the reduction in temperature causes an increase in the intensity and a narrowing of the emission band. This arises due to a reduction in energy loss due to molecular vibrations and increase in the radiative relaxation pathway. The broad, indistinguishable characteristics of the emission bands indicate charge transfer between the ligand and the metal. The origin of the transfer is tentatively assigned to the metal core (MLCT) due the similarity observed in the emission profile for related Cu(I) architectures.[73]

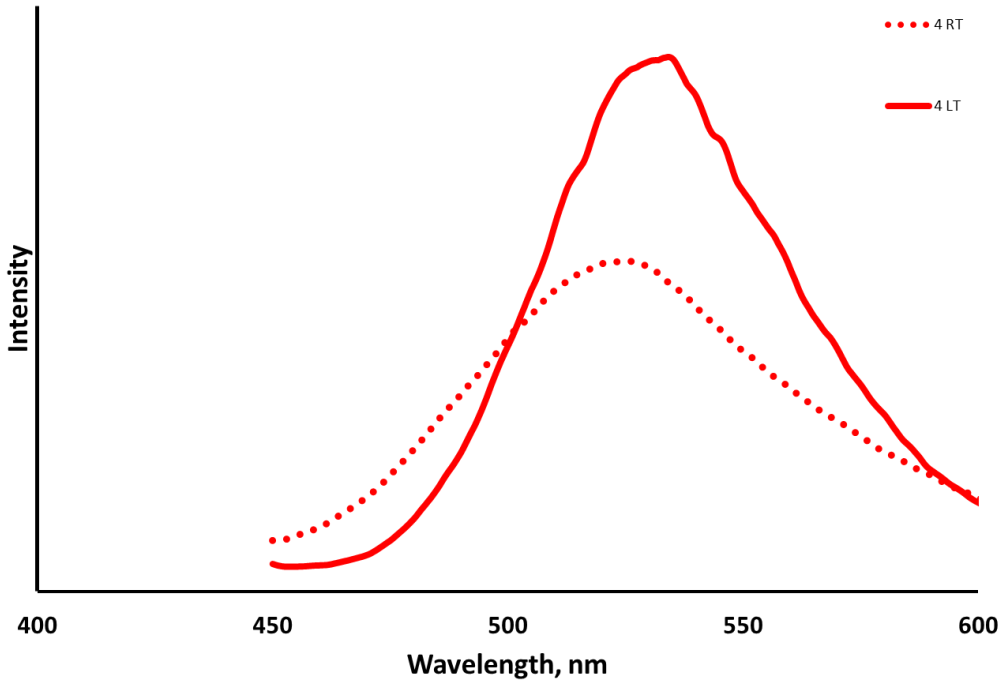

Figure 3.24. Emission profile of **4** at 298 K (RT) and 77 K (LT).

The emission is stable over a range of excitation wavelengths, shown in Figure 3.25, with a maximum emission (λ^{em} (nm) = 520 nm) obtained at an excitation wavelength of 368 nm.

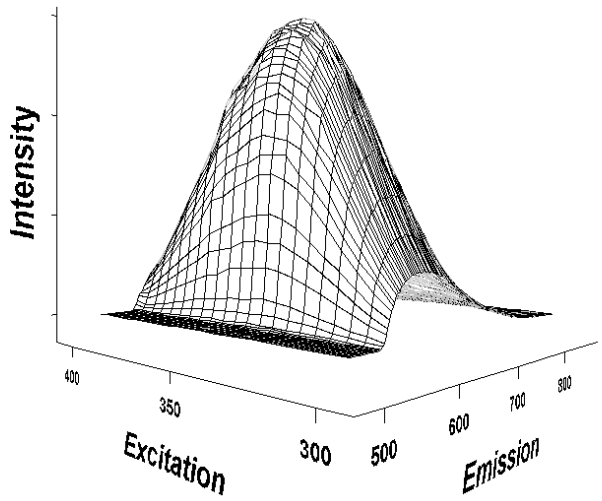

Figure 3.25. 3D graphic of emission spectra at 298 K for cluster **4** measured with excitations between 350 and 400 nm.

The rich photochemical properties of d^{10} Au(I) complexes has attracted considerable attention[74] and lays the foundation for their potential application in chemo-sensing,[75] and fabrication of optoelectronic devices.[76] Of special interest is the relationship between the observed emission and the presence of weak intermolecular Au(I)···Au(I) interactions between neighbouring gold centres[77] and perceived applications.[78,79] The luminescence properties of dinuclear Au(I) dithiophosphonate complexes have previously been studied in detail.[80,81] When substituents on the sulfur ligands do not produce significant electronic perturbations, as in the present study, luminescence of dinuclear Au(I) dithiolate systems shows an emission that arises from a S-Au charge-transfer transition, LMCT, with possible contribution from the metal-metal bond formed in the excited state, LMMCT. The LMMCT emission bands become strongly influenced by the weak intermolecular Au···Au distances. Complex **6** had a maximum emission in the solid-state (λ_{max}= 488 nm) at 298 K. The excitation and emission spectra of **6** is shown in Figure 3.26.

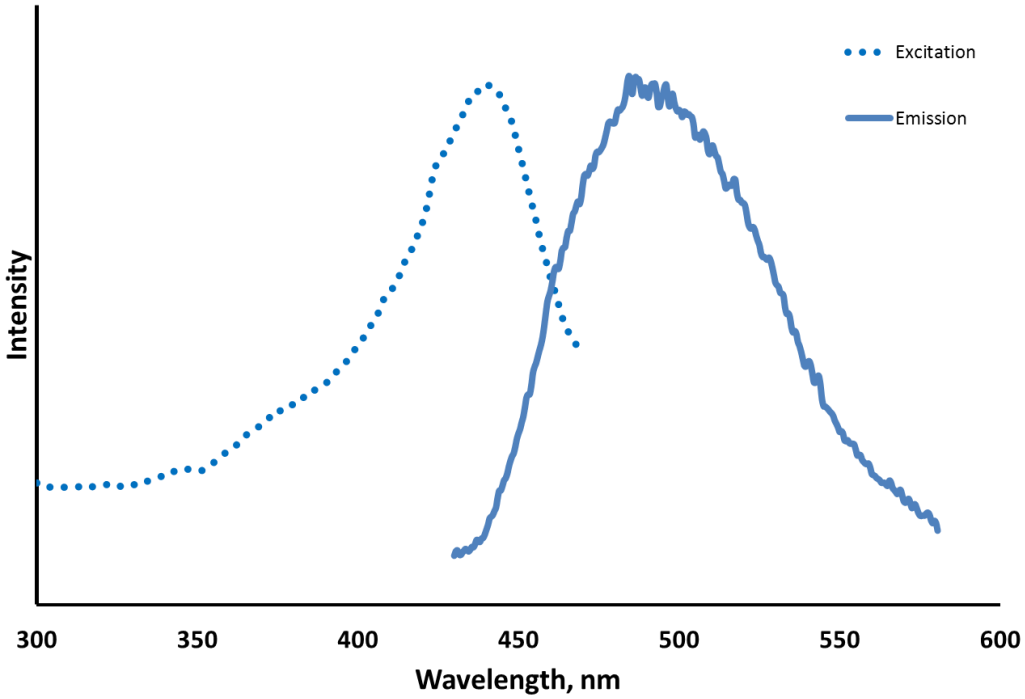

Figure 3.26. Excitation and emission profiles for **6** at 298 K.

In summary, this chapter involved the design and synthesis of a novel bis(dithiophosphonate) ligand based on a flexible, chiral and saturated backbone. The flexibility of the ligand was found to be crucial in the formation of poly-nuclear metal frameworks. Variability in the donor angle is a result of two factors: 1) The ring inversion affords both gauche and antiperiplanar conformations, therefore the coordination fragment can occupy axial or equatorial positions. 2) Sterically unrestricted rotation about the O-P bond further affords variability in the angle of incident coordination. The proposed design strategy and subsequent application was successful, since it was demonstrated that the ligand is capable of accommodating wide variety of metal centres, with varying coordination number and geometry. The Cu(I) cluster can be described as the first cluster to have a Cu_4L_2 configuration. Its Ag(I) counterpart is the first dithiophosphonate stabilised Ag(I) framework reported to date. The hexanuclear Au(I) cluster is the largest metallatriangle and the reactivity of the gold macrocycle was demonstrated, by the reaction with bromine. This led to the isolation of the first Au(III) complex produced by the oxidative addition across a S-P-S framework, which has been further investigated by others. The cofacial dinuclear nickel complex synthesized, has

demonstrated unique solvent interactions, which enabled the isolation of two morphologically different crystal types from the same growth chamber. Ultimately this chapter addressed the objective outline in Chapter 1, and the 1,2-*trans*-cyclohexyl ring was found to be both flexible and capable of accommodating metal centres with varying geometries or oxidation states.

3.4 Experimental

Unless otherwise stated, all reactions were carried out under an inert atmosphere using standard Schlenk techniques. Phenetole, phosphorus-pentasulfide, 1,2-*trans*cyclohexandiol, hexafluorophosphoric acid, Cu(I) oxide, and Ag(I) oxide were obtained from Sigma Aldrich. Nickel (II) chloride was purchased from SAARCHEM. Gold solution (dissolved in aqua regia) was a gift from Rand Refineries. Ammonia gas was purchased from Afrox (South Africa). LR, [Au(tht)]Cl, $[Cu(CH_3CN)_4]PF_6$ and $[Ag(CH_3CN)_4]PF_6$ were prepared according to literature methods.[59,82,83] Diethyl ether, tetrahydrofuran, benzene, and hexane were distilled under dinitrogen over a Na wire with the formation of a benzophenone ketyl indicator. Dichloromethane was distilled over P_4O_{10}.

^1H and ^{31}P-NMR spectra were recorded on a Bruker Advance 400 MHz spectrometer at 298 K. NMR data are expressed in parts per million (ppm). ^1H spectra are referenced internally to residual proton impurity in the deuterated solvents ($CDCl_3$ in all cases). ^{31}P NMR spectra chemical shifts were referenced relative to an 85% H_3PO_4 in D_2O external standard solution. Data are reported as resonance position (δ_H), multiplicity, assignment, and relative integral intensity. Solid state ^{31}P NMR spectra were obtained on a Bruker 600 MHz spectrometer operating at room temperature with a magic angle spinning (MAS) probe. Melting points were determined with an Electrothermal 9100 melting point apparatus. Luminescence spectra were recorded on a Perkin–Elmer LS-55 spectrometer equipped with a front surface accessory.

3.4.1 Synthesis of $(NH_4)_2[(S_2P\text{-}1,4\text{-}C_6H_4OEt)2(trans\text{-}1,2\text{-}O,O'\text{-}C_6H_{10})]$,(**L4**).

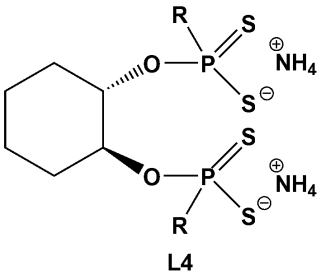

L4

A Schlenk flask was charged with $(4\text{-}C_6H_4OEtP(S)S)_2$ (1.5g, 3.48mmol) and placed under vacuum for 30 minutes. The solid was heated to 70 °C, *trans*-1,2-$C_6H_{10}(OH)_2$ (1.5g, 3.48mmol) and toluene (2 mL) was added. The temperature was maintained at 70 °C for 60 minutes, until dissolution of all the solids had been observed. The clear residue was cooled to room temperature, before being placed in an ice bath for 10 minutes. Anhydrous NH_3(g) was bubbled through the residue with vigorous agitation, which caused the immediate precipitation of a white salt. Yield 1.986 g (98%).Melting Point 85.2-85.4 °C. ^{1}H NMR (400 MHz, $CDCl_3$): δ (ppm) *J*(Hz) 1.39(m, CH, 2H), 1.41 (t, CH_3, 6H, $J_{H\text{-}H}$ = 6.98), 1.63 (m, CH, 2H), 1.78 (m, CH, 2H), 2.18 (d, CH, $J_{H\text{-}H}$ = 12.61 Hz), 4.06 (q, CH_2, 4H, $J_{H\text{-}H}$ = 6.98), 4.92 (m, OCH, 2H), 6.93 (dd, ArCH, 4H, $J_{H\text{-}H}$ = 8.84, $J_{P\text{-}H}$ = 3.84), 7.88 (dd, ArCH, 4H, $J_{H\text{-}H}$ = 8.82, $J_{P\text{-}H}$ = 13.95). ^{31}P-NMR (400 MHz, $CDCl_3$) ppm: 105.0

3.4.2 Synthesis of $[Cu\{(S_2P(1,4\text{-}C_6H_4OMe)(O,O\text{-}trans\text{-}1,2\text{-}C_6H_{10})\}]_4$, (**4**).

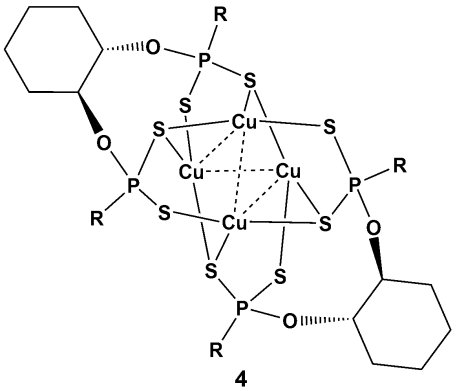

4

A Schlenk flask was charged with $(NH_4)_2[(S_2P\text{-}1,4\text{-}C_6H_4OEt)2(trans\text{-}1,2\text{-}O,O'\text{-}C_6H_{10})]$ (342mg, 1.00 mmol) and dry THF (10 mL). To the clear solution $[Cu(CH_3CN)_4]PF_6$ (746 mg, 2.00 mmol) dissolved in acetonitrile (5 mL) was added and the reaction stirred for 30 min, resulting in the formation of a turbid yellow solution. The solvent was removed *in vacuo*, followed by extraction with 20 mL of dichloromethane. The extract was filtered through a composite of Celite/anhydrous $MgSO_4$. The volume of the filtrate was reduced *in vacuo.* A pale yellow powder was consolidated and washed with diethyl ether (2 x 5 mL). Single crystals suitable for X-ray diffraction studies were grown by slow diffusion of hexane layered onto a concentrated CH_2Cl_2 solution. Yield 526 mg (78 %) Melting Point: 180.6-181.0 °C. ^{1}H NMR (400 MHz, $CDCl_3$): δ (ppm) *J*(Hz) 1.03(m, CH, 2H), 1.22 (m, CH, 2H), 1.40 (t, CH_3, 6H, $J_{H\text{-}H}$ = 6.98),

1.57 (m, CH, 2H), 2.18 (m, CH, 2H), 4.06 (q, OCH_2, 4H, J_{H-H} = 6.98), 4.63 (m, OCH, 2H), 6.88 (dd, ArCH, 4H, J_{H-H} = 8.84 J_{P-H} =3.84), 7.94 (dd, ArCH, 4H, J_{H-H} = 8.82, J_{P-H} = 13.95). ^{31}P-NMR (400 MHz, $CDCl_3$): 104.3982.

3.4.3 Synthesis of [Ag{(S_2P(1,4-C_6H_4OMe)(O,O-*trans*-1,2-C_6H_{10})}]$_4$, (**5**).

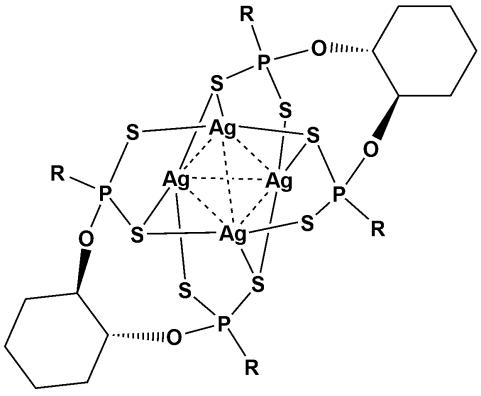

5

A Schlenk flask was charged with $(NH_4)_2$[(S_2P-1,4-C_6H_4OEt)2(trans-1,2-O,O'-C_6H_{10})] (158 mg, 0.46 mmol) and dry THF (10 mL). To the clear solution [Ag($CH_3CN)_4$]PF_6 (208 mg, 0.5 mmol) dissolved in acetonitrile (5 mL) was added and the reaction stirred for 15 min, resulting in the formation of a turbid orange-yellow solution. The solvent was removed *in vacuo*, followed by extraction with 10 mL of dichloromethane. The extract was filtered through a composite of Celite/anhydrous $MgSO_4$. The volume of the filtrate was reduced *in vacuo.* A yellow powder was consolidated and washed with diethyl ether (2 x 5 mL). Single crystals suitable for X-ray diffraction studies were grown by slow diffusion of hexane layered onto a concentrated CH_2Cl_2 solution. Yield 220 mg (76 %). Melting Point: 101.2-102.0 °C (decomposed). ^{31}P-NMR (400 MHz, $CDCl_3$): δ (ppm) 100.66.

3.4.4 Synthesis of $[Au_2\{(S2P\text{-}1,4\text{-}C_6H_4OEt)_2(trans\text{-}1,2\text{-}O,O'\text{-}C_6H_{10})\}]_3$,(**6**).

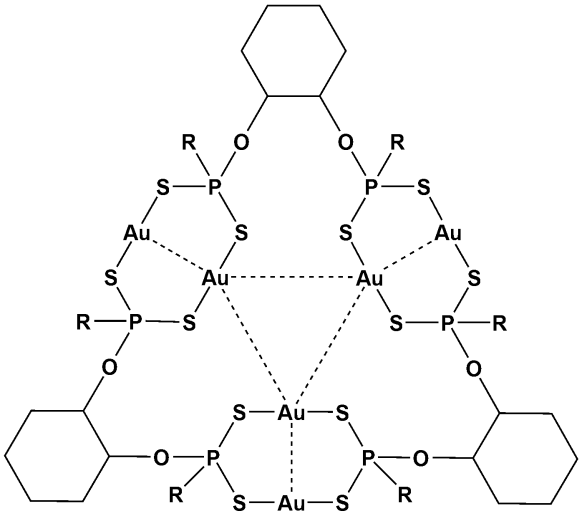

6

A Schlenk flask was charged with $(NH_4)_2[(S_2P\text{-}1,4\text{-}C_6H_4OEt)_2(trans\text{-}1,2\text{-}O,O'\text{-}C_6H_{10})]$ (400mg, 0.687mmol) and dry tetrahydrofuran (40 mL). To the clear solution AuCl(tht) (440mg, 1.374mmol) (tht=tetrahydrothiophene) was added and the reaction stirred for 30 min, resulting in the formation of a turbid yellow solution. The solvent was removed in *vacuo,* followed by extraction with 50 mL of dichloromethane. The extract was filtered through a composite of Celite/anhydrous $MgSO_4$. The volume of the filtrate was reduced in *vacuo*. A yellow powder was consolidated and washed with diethyl ether (2 x 5 mL). Yield 580mg (90 %) of yellow powder soluble in chlorinated organic solvents. Single crystals suitable for X-ray diffraction studies were grown by slow diffusion of hexane layered onto a concentrated DCM solution of **6**. Melting Point: 160.2-161.0 °C. ^{31}P-NMR ($CDCl_3$) ppm: 92.94, 94.03, 95.61, 96.37, 99.51, 99.85, 100.09, 101.03, 101.34, 106.12

3.4.5 Synthesis of $[Au_2Br_4\{(S2P\text{-}1,4\text{-}C_6H_4OEt)_2(trans\text{-}1,2\text{-}O,O'\text{-}C_6H_{10})\}]$, (**7**)

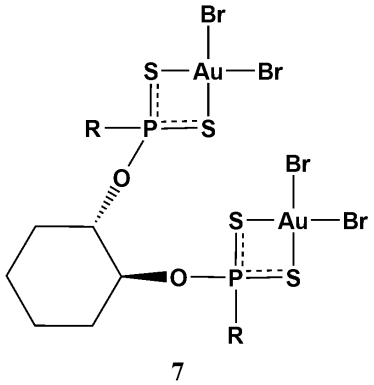

7

A Schlenk flask was charged with **1** (427mg, 0.15mmol), and dichloromethane (20 mL). To the clear solution bromine (15 µL, 0.30 mmol) was added and stirred for 30 min. Solvent was removed in *vacuo.* A red crystalline powder was obtained. Yield 567mg (86.4%). Single crystals suitable for X-ray diffraction studies were grown by slow diffusion of hexane layered onto a concentrated DCM solution of **7**. Melting Point 152.4-153.2 °C ^{1}H-NMR (CDCl3) ppm: ^{1}H NMR (400 MHz, $CDCl_3$): δ (ppm) *J*(Hz) 1.03(m, CH, 2H), 1.22 (m, CH, 2H), 1.40 (t, CH_3, 6H, $J_{H\text{-}H}$ = 6.98), 1.57 (m, CH, 2H), 2.18 (m, CH, 2H), 4.08 (q,

OCH_2, 4H, $J_{H\text{-}H}$ = 6.98), 4.91 (m, OCH, 2H), 7.04 (dd, ArCH, 4H, $J_{H\text{-}H}$ = 8.92 $J_{P\text{-}H}$ =3.84), 7.81 (dd, ArCH, 4H, $J_{H\text{-}H}$ = 8.91, $J_{P\text{-}H}$ = 13.95).^{31}P-NMR ($CDCl_3$) ppm: 101.7.

3.4.6 Synthesis of [Ni{(S2P-1,4-$C_6H_4OEt)_2$(trans-1,2-O,O'-C_6H_{10})}]$_2$, (**8**).

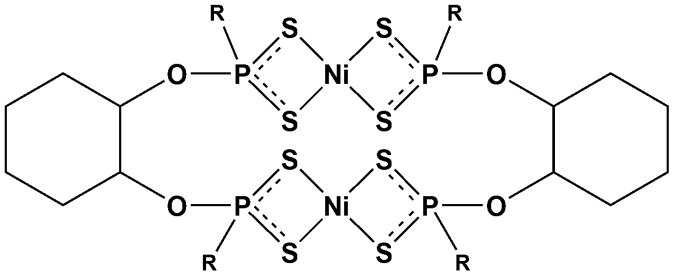

8

A beaker was charged with $(NH_4)_2$[(S_2P-1,4-$C_6H_4OEt)_2$(*trans*-1,2-O,O'-C_6H_{10})] (392 mg, 0.673 mmol) and dissolved in methanol (40 mL). To the beaker $NiCl_2{\cdot}6H_2O$ (160 mg, 0.673 mmol), dissolved in deionized water (5mL), was added and stirred for 20 min. The resultant purple precipitate was filtered under vacuum and dried in air. Single crystals suitable for X-ray diffraction studies were grown by slow diffusion of hexane layered onto a concentrated DCM solution of **6**. Yield 356mg (88%) Melting Point 172.4-173.2 °C. ^{31}P-NMR ($CDCl_3$) ppm: 96.9, 98.9. ESI-MS (m/z) (cal.) 1230.9255 (1230.9296) for ([Ni{($S_2PC_6H_4OEt)_2$(O,O-C_6H_{10})}]$_2$ + Na^+).

3.5 References

1. R. Shabana, F. H. Osman and S. S. Atrees, *Tetrahedron*, 1993, **49**, 1271-1282.
2. R. Shabana, F. H. Osman and S. S. Atrees, *Tetrahedron*, 1994, **50**, 6975-6988.
3. M. C. Demarcq, *J. Chem. Soc., Dalton Trans.*, 1988, 2221-2224.
4. W. Przychodzeń, *Phosphorus, Sulfur, Silicon Rel. Elem.*, 2004, **179**, 1621-1633.
5. G. Hua, Y. Li, A. M. Z. Slawin and J. D. Woollins, *Tetrahedron*, 2008, **64**, 5442-5448.
6. M. Karakus, H. Yilmaz and E. Bulak, *Russ. J. Coord. Chem.*, 2005, **31**, 316-321.
7. W. Przychodzen, *Phosphorus, Sulfur Silicon Relat. Elem.*, 2004, **179**, 1621-1633.
8. H. Schmidbaur and A. Schier, *Angew. Chem. Int. Ed.*, 2015, **54**, 746-784.
9. A. Panneerselvam, C. Q. Nguyen, M. A. Malik, P. O'Brien and J. Raftery, *J. Mater. Chem.*, 2009, **19**, 419-427.

10. J. A. Schuerman, F. R. Fronczek and J. Selbin, *Inorg. Chim. Acta*, 1989, **160**, 43-52.
11. A. N. Nesmeyanov, N. N. Sedova, Y. T. Struchkov, V. G. Andrianov, E. N. Stakheeva and V. A. Sazonova, *J. Organomet. Chem.*, 1978, **153**, 115-122.
12. M. D. Irwin, H. E. Abdou, A. A. Mohamed and J. J. P. Fackler, *Chem.Commun.*, 2003, 2882-2883.
13. R. Richter, F. Dietze, S. Schmidt, E. Hoyer, W. Poll and D. Mootz, *Z. Anorg. Allg. Chem.*, 1997, **623**, 135-140.
14. E. Hartmann and J. Strähle, *Z. Anorg. Allg. Chem.*, 1990, **583**, 31-40.
15. E. M. Meyer, S. Gambarotta, C. Floriani, A. Chiesi-Villa and C. Guastini, *Organometallics*, 1989, **8**, 1067-1079.
16. V. G. Albano, F. Azzaroni, M. C. Iapalucci, G. Longoni, M. Monari, S. Mulley, D. M. Proserpio and A. Sironi, *Inorg. Chem.*, 1994, **33**, 5320-5328.
17. S. Miao, W.-R. Yao, D.-S. Guo and Q.-F. Zhang, *J. Mol. Struct.*, 2003, **660**, 159-165.
18. V. J. Catalano, H. M. Kar and J. Garnas, *Angew. Chem. Int. Ed.*, 1999, **38**, 1979-1982.
19. M. Brill, E. Kuhnel, C. Scriban, F. Rominger and P. Hofmann, *Dalton Trans.*, 2013, **42**, 12861-12864.
20. V. W.-W. Yam, K. K.-W. Lo, C.-R. Wang and K.-K. Cheung, *Inorg. Chem.*, 1996, **35**, 5116-5117.
21. Y. Wang and N. Okabe, *Acta Cryst.*, 2005, **C61**, m263-m265.
22. J. C. Garrison, R. S. Simons, C. A. Tessier and W. J. Youngs, *J. Organomet. Chem.*, 2003, **673**, 1-4.
23. C. Brasse, P. R. Raithby, M.-A. Rennie, C. A. Russell, A. Steiner and D. S. Wright, *Organomet.*, 1996, **15**, 639-644.
24. M. M. Habtu, S. A. Bourne, K. R. Koch and R. C. Luckay, *New J. Chem*, 2006, **30**, 1155-1162.
25. C.-J. Qiao, D. Ding, J. Li, L. Gu, Y. Xu and Y.-T. Fan, *Inorg. Chem. Commun.*, 2009, **12**, 1057-1060.
26. M. R. Bermejo, A. M. González-Noya, R. M. Pedrido, M. J. Romero and M. Vázquez, *Angew. Chem. Int. Ed.*, 2005, **44**, 4182-4187.
27. G. Henkel, P. Betz and B. Krebs, *Angew. Chem. Int. Ed.*, 1987, **26**, 145-146.
28. E. Zangrando, M. Casanova and E. Alessio, *Chem. Rev.*, 2008, **108**, 4979-5013.
29. A. Burini, A. A. Mohamed and J. P. Fackler, *Comments Inorg. Chem.*, 2003, **24**, 253-280.

30. L. G. Vaughan, *J. Am. Chem. Soc.*, 1970, **92**, 730-731.
31. H. G. Raubenheimer, J. G. Toerien, G. J. Kruger, R. Otte, W. van Zyl and P. Olivier, *J. Organomet. Chem.*, 1994, **466**, 291-295.
32. F. Bonati and G. Minghetti, *Angew. Chem. Int. Ed.*, 1972, **11, 429-**.
33. G. Minghetti and F. Bonati, *Inorg. Chem.*, 1974, **13**, 1600-1602.
34. J. E. Parks and A. L. Balch, *J. Organomet. Chem.*, 1974, **71**, 453-463.
35. A. L. Balch, M. M. Olmstead and J. C. Vickery, *Inorg. Chem.*, 1999, **38**, 3494-3499.
36. J. C. Vickery, M. M. Olmstead, E. Y. Fung and A. L. Balch, *Angew. Chem. Int. Ed.*, 1997, **36**, 1179-1181.
37. B. Bovio, S. Calogero, F. E. Wagner, A. Burini and B. R. Pietroni, *J. Organomet. Chem.*, 1994, **470**, 275-283.
38. A. Burini, R. Bravi, J. P. Fackler, R. Galassi, T. A. Grant, M. A. Omary, B. R. Pietroni and R. J. Staples, *Inorg. Chem.*, 2000, **39**, 3158-3165.
39. B. Bovio, F. Bonati and G. Banditelli, *Inorg. Chim. Acta*, 1984, **87**, 25-33.
40. G. Minghetti, G. Banditelli and F. Bonati, *Inorg. Chem.*, 1979, **18**, 658-663.
41. H. H. Murray, R. G. Raptis and J. P. Fackler, *Inorg. Chem.*, 1988, **27**, 26-33.
42. A. Grohmann and H. I. G. S. Schmidbaur, *Gold: Progress in Chemistry, Biochemistry and Technology.*, John Wiley & Sons Ltd., West Sussex, England, 1999.
43. H. Schmidbaur and A. Schier, *Comprehensive Organometallic Chemistry III*, Elsevier, New York, 2007.
44. J. P. Fackler, E. Galarza, G. Garzon, A. M. Mazany, H. H. Murray, M. A. Omary, R. G. Raptis, R. J. Staples, W. E. van Zyl, S. Wang, E. Cerrad and M. Laguna, *Inorg. Synth.*, 2002, **33**, 171.
45. A. M. Mazany and J. P. Fackler, *J. Am. Chem. Soc.*, 1984, **106**, 801-802.
46. A. A. Mohamed, H. E. Abdou and J. P. Fackler Jr, *Coord. Chem. Rev.*, 2010, **254**, 1253-1259.
47. M. N. I. Khan, J. P. Fackler, C. King, J. C. Wang and S. Wang, *Inorg. Chem.*, 1988, **27**, 1672-1673.
48. M. N. I. Khan, S. Wang and J. P. Fackler, *Inorg. Chem.*, 1989, **28**, 3579-3588.
49. D. C. Calabro, B. A. Harrison, G. T. Palmer, M. K. Moguel, R. L. Rebbert and J. L. Burmeister, *Inorg. Chem.*, 1981, **20**, 4311-4316.

50. D. Y. Melgarejo, G. M. Chiarella, J. P. Fackler, L. M. Perez, A. Rodrigue-Witchel and C. Reber, *Inorg. Chem.*, 2011, **50**, 4238-4240.
51. W. E. van Zyl, J. M. López-de-Luzuriaga, J. P. Fackler and R. J. Staples, *Can. J. Chem*, 2001, **79**.
52. H. H. Murray, G. Garzon, R. G. Raptis, A. M. Mazany, L. C. Porter and J. P. Fackler, *Inorg. Chem.*, 1988, **27**, 836-842.
53. F. A. Cotton, L. M. Daniels, C. Lin and C. A. Murillo, *J. Am. Chem. Soc.*, 1999, **121**.
54. F. A. Cotton, C. Lin and C. A. Murillo, *Inorg. Chem.*, 2001, **41**.
55. F. A. Cotton, C. A. Murillo and X. Wang, *Inorg. Chem.*, 2004, **43**.
56. G. Suss-Fink, J. L. Wolfender, F. Neumann and H. Stoeckli-Evans, *Angew. Chem. Int. Ed.*., 1990, **29**.
57. B. Wisser, A.-C. Chamayou, R. Miller, W. Scherer and C. Janiak, *CrystEngComm.*, 2008, **10**, 461-464.
58. A. Maspero, I. Kani, A. A. Mohamed, M. A. Omary, R. J. Staples and J. P. Fackler, *Inorg. Chem.*, 2003, **42**, 5311-5319.
59. W. van Zyl and J. P. Fackler, *Phosphorus, Sulfur, Silicon Rel. Elem.*, 2000, **167**, 117-132.
60. W. E. van Zyl, J. M. López-de-Luzuriaga, A. A. Mohamed, R. J. Staples and J. P. Fackler, *Inorg. Chem.*, 2002, **41**, 4579-4589.
61. M. Fujita, O. Sasaki, T. Mitsuhashi, T. Fujita, J. Yazaki, K. Yamaguchi and K. Ogura, *Chem.Commun.*, 1996, 1535-1536.
62. M. Schweiger, S. R. Seidel, A. M. Arif and P. J. Stang, *Inorg. Chem.*, 2002, **41**, 2556-2559.
63. F. John P, Jr., *Polyhedron*, 1997, **16**, 1-17.
64. M. N. Pillay, B. Omondi, R. J. Staples and W. E. van Zyl, *CrystEngComm*, 2013, **15**, 4417-4421.
65. Y.-C. Lee, Y.-R. Lin, B.-Y. Liou, J.-H. Liao, N. K. Gusarova, B. A. Trofimov, W. E. van Zyl and C. W. Liu, *Dalton Trans.*, 2014, **43**, 663-670.
66. I. P. Gray, A. M. Z. Slawin and J. D. Woollins, *Dalton Trans.*, 2004, 2477-2486.
67. M. C. Aragoni, M. Arca, Neil R. Champness, Aleksey V. Chernikov, Francesco A. Devillanova, F. Isaia, V. Lippolis, Neil S. Oxtoby, G. Verani, Sergey Z. Vatsadze and C. Wilson, *Eur.J. Inorg. Chem.*, 2004, **2004**, 2008-2012.

68. M. C. Aragoni, M. Arca, M. Crespo, F. A. Devillanova, M. B. Hursthouse, S. L. Huth, F. Isaia, V. Lippolis and G. Verani, *Dalton Trans.*, 2009, 2510-2520.

69. M. C. Aragoni, M. Arca, F. Demartin, F. A. Devillanova, C. Graiff, F. Isaia, V. Lippolis, A. Tiripicchio and G. Verani, *J. Chem. Soc., Dalton Trans.*, 2001, 2671-2677.

70. M. Karakus and H. Yilmaz, *Russ. J. Coord. Chem.*, 2006, **32**, 437-443.

71. V. G. Albano, M. C. Aragoni, M. Arca, C. Castellari, F. Demartin, F. A. Devillanova, F. Isaia, V. Lippolis, L. Loddo, G. Verani, *Chem. Comm.,* **2002**, 1170-1171.

72. A. R. Gataulina, D. A. Safin, T. R. Gimadiev and M. V. Pinus, *Trans. Met. Chem.*, 2008, **33**, 921-924.

73. P.-K. Liao, C.-S. Fang, A. J. Edwards, S. Kahlal, J.-Y. Saillard and C. W. Liu, *Inorg. Chem.*, 2012, **51**, 6577-6591.

74. L. Balch Alan and A. L. Balch, *Structure and Bonding (Berlin, Germany)*, 2007, **123**, 1-40.

75. X. He and V. W.-W. Yam, *Coord. Chem.Rev.*, 2011, **255**, 2111-2123.

76. V. K.-M. Au, K. M.-C. Wong, D. P.-K. Tsang, M.-Y. Chan, N. Zhu and V. W.-W. Yam, *J. Am. Chem. Soc.*, 2010, **132**, 14273-14278.

77. M. A. Rawashdeh-Omary, M. A. Omary, H. H. Patterson and J. P. Fackler, *J. Am. Chem. Soc.*, 2001, **123**, 11237-11247.

78. M. Mansour and M. A. Mansour, *J. Am. Chem. Soc.*, 1998, **120**, 1329-1330.

79. Y. Kunugi, K. R. Mann, L. L. Miller and C. L. Exstrom, *J. Am. Chem. Soc.*, 1998, **120**, 589-590.

80. W. E. van Zyl, J. M. Lopez-de-Luzuriaga, A. A. Mohamed, R. J. Staples and J. P. Fackler, Jr., *Inorg. Chem*, 2002, **41**, 4579-4589.

81. W. E. Van Zyl, J. M. López-de-Luzuriaga and J. P. Fackler, *J. Mol. Struct.*, 2000, **516**, 99-106.

82. R. Uson, A.Laguna, M. Laguna., *Inorg. Syth*, 1989, **26**, 85-86.

83. G. J. Kubas, B. Monzyk, A. L. Crumblis, *Inorg. Syth*, 1990, **28**, 68-70.

Chapter 4
Luminescent tetranuclear Cu(I) dithiophosphonate clusters

4.1 Introduction

The chemistry of dithiophosphonate ligands stabilising Cu(I) is limited, with only one reported example of the type $[Cu(OMe)Fc(\mu\text{-}S)(\mu^3\text{-}S)]_4$ prepared from the reaction between $Na[S_2PFc(OMe)]$ and $[Cu(CH_3CN)_4][ClO_4]$.[1] This excludes the 2-coordinate linear copper systems which have been reported, and which are isolated as triphenylphosphine adducts. This is yet another system which has been developed for its symmetric counterparts, with reports of complexes containing the diselenophosphorates,[2] carbamates[3] and diselenocarbamates.[4] An important factor in our case is the asymmetry of the dithiophosphonate ligand. It is reasonable to assume that in coordinative systems of this nature, the symmetry of the ligand backbone will play a significant role in the crystallisation and isolation of stable copper clusters.

In this chapter we sought to report on a series tetranuclear Cu(I) clusters of the type Cu_4L_4 and discuss their optical properties. We also developed an alternative synthesis strategy which requires no preparation of a Cu(I) precursor and takes advantage of the redox activity of both a Cu(II) centre and a dithiophosphonate ligand.

4.1.1 Cu(I) topologies: In bidentate sulfur systems (S-X-S)

The coordination chemistry of Cu(I), within bidentate sulfur systems, has given rise to mulit-nuclear clusters containing Cu_4 (**A**),[5-7] Cu_6 (**B**)[8] and Cu_8 (**C**)[9,10] cores with the ligands displaying tri-metallic tri-connective (**A** and **B**) and tetra-metallic tetra-connective (**C**) coordination modes.

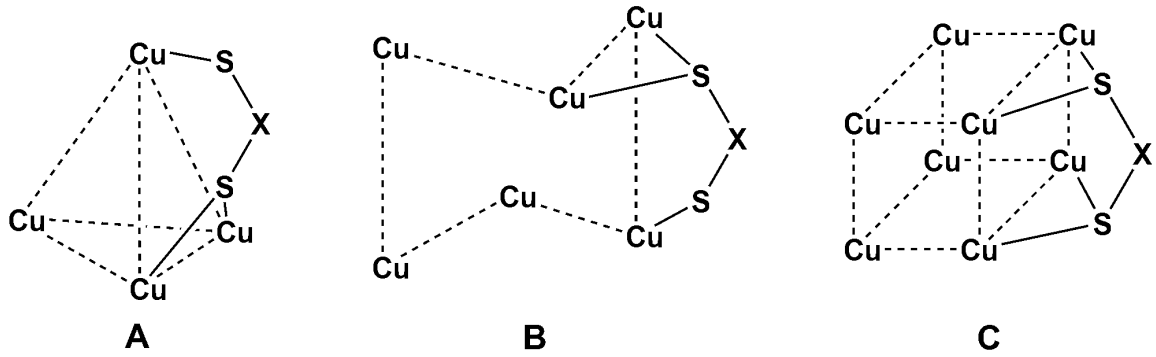

Figure 4.1. Illustration of poly-nuclear Cu(I) clusters with bidentate ligands.

It should be noted that much larger clusters have been reported, which involved the incorporation of hydrides into the structure, with a Cu_{20} and Cu_{32} of the type $[Cu_{20}H_{11}\{S_2P(OiPr)_2\}_9]$ and $[Cu_{32}(H)_{20}\{S_2P(OiPr)_2\}1_2]$ respectively.[11,12]

In the current study, our focus is on the preparation of clusters of type **A**. Since a 1972 structural investigation into the topology of **A** with dithiophosphorate ligands, little attention has been given to physical properties of these clusters nor to their preparation.[5] In fact, a search of the structural database reveals only a few examples of clusters stabilized by S-P-S fragments, 3 of which contain the same ligand and configuration as the aforementioned example.[13]

4.2 Results and discussion

4.2.1 Synthesis and solution characterisation

It was found that Cu(I) dithiophosphonate clusters, of the type $[Cu\{S_2P(1,4\text{-}C_6H_4OMe)(OR)\}]_4$, can by synthesized at room temperature via two different methods. The preparation of the dithiophosphonate salts, in both cases, followed facile methods previously described.[14] Firstly, we adopted a more conventional route which involved the reaction of a cuprous precursor, of the type $[Cu(CH_3CN)_4]PF_6$, with one stoichiometric equivalent of the corresponding alkyl dithiophosphonate, Scheme 4.1.

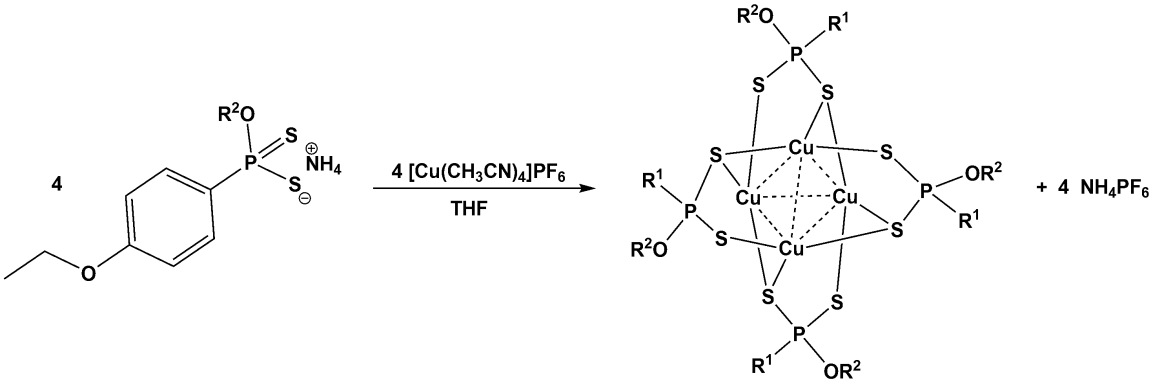

Scheme 4.1. Conventional approach to the synthesis of tetranuclear Cu(I) clusters.

$[Cu(CH_3CN)_4]PF_6$ is a widely used precursor for the non-aqueous synthesis of cuprous complexes. However, its fragility to degradation in the presence of water due to its hygroscopic nature is well known.[15] It is for this reason that complexation needs to be carried out in dry oxygen-free environments. To circumvent the need for 'dry' solvents or oxygen free reaction conditions, this study embarked on a new procedure to produce clusters *via* a self-redox reaction in aqueous solutions with an inexpensive cupric chloride precursor, shown in Scheme 4.2. This method provides access to luminescent species and should facilitate a wider application in future studies.

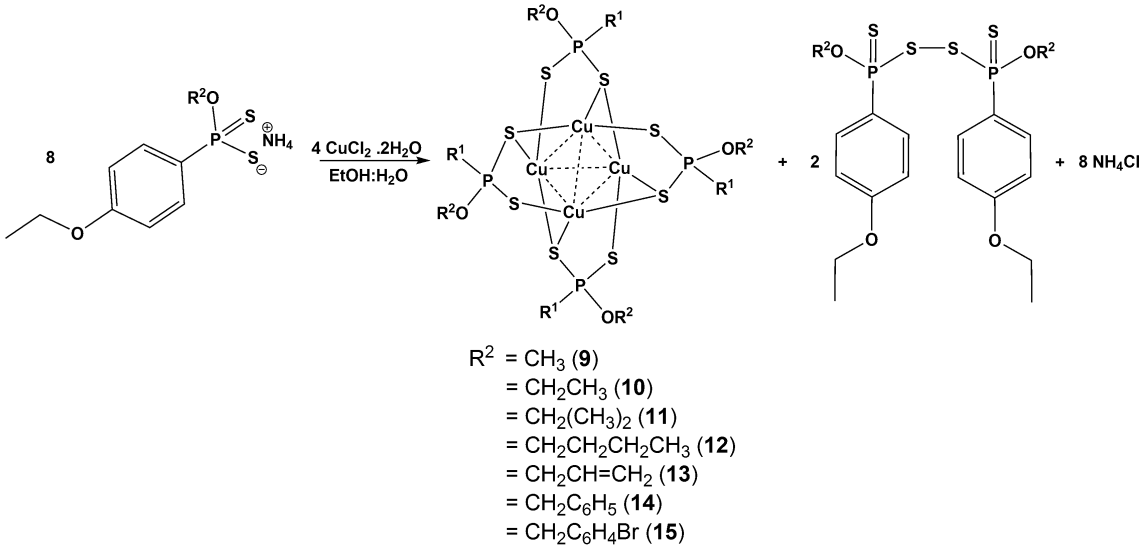

Scheme 4.2. Synthesis of tetranuclear cluster with a Cu(II) metal source in aqueous solutions, at room temperature.

In Chapter 2 we noted that the oxidation of $[S2PR(OR')]^-$salts can readily be achieved with a mild oxidizing agent such as I_2 in aqueous or methanolic solution leading to disulfide products of the type PR(OR')(S)S-SPR(OR')(S) (R = alkyl, aryl).[16] Upon mixing of the dithiophosphonate ligand and $CuCl_2$ salt solutions, a brown colour appears which dissipates rapidly with the simultaneous formation of a pale yellow precipitate. The separation of the cluster and the disulfide can be achieved with relative ease due to the difference in their solubility (and polarity). Separation by column chromatography can be deployed to obtain both the cluster and disulfide. However, if only the cluster is required (as in the present case) washing the precipitate, firstly with water followed by hexane results in high purity products. The identity of the disulfide was confirmed by NMR spectra which corresponds to reported chemical shifts.[16]

The use of transition metals, including Cu(II) complexes for the oxidation of thiols to disulfides have been reported over a century ago.[17] Significantly the self-redox reaction has been reported and reviewed for related symmetric ligands, but has not been exploited for the preparation and isolation of clusters.[18] Originally it was thought that the electron transfer from the ligand to metal complex resulted in the formation of a Cu(I) species and a corresponding sulfur radical, with the recombination of 2 radicals resulting in the formation of a disulfide.[19] After extensive electron paramagnetic resonance (EPR) studies, a different

reaction sequence was proposed.[20] Investigations could not find evidence of radicals to support previously mentioned mechanism and concluded that the reaction proceeds via an associative mechanism between Cu(II) complexes as shown in Figure 4.2.[21]

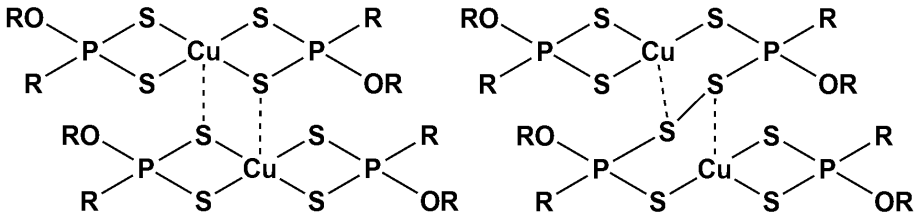

Figure 4.2. Associative pathway for the self-redox reaction resulting in the formation of Cu(I) centre.

Importantly, self-redox occurs *via* direct contact between the metal centres and super-exchange between copper atoms via bridging ligands.[18] The reduction of Cu(II) to Cu(I) therefore occurs with the concomitant oxidation of the ligand to form a disulfide. The intermediate which involves the association of two square planar complexes is governed mainly by steric contributions of the ligand.[18] In both mechanisms the reaction proceeds *via* the initial formation Cu(II) complex and to the best of our knowledge no square planar Cu(II) complexes stabilized solely by dithiophosphonate ligands, of the type [Cu(II)L_2], have been reported. In this study the reduction is rapid and complete identification of a Cu(II) intermediate is therefore challenging. The initial Cu(II) complex would be paramagnetic (NMR inactive) and the subsequent redox reaction should result in the formation of diamagnetic Cu(I) and disulfide (NMR active). However, due to the rapid kinetics of the reaction, attempts to monitor the formation of such products were unsuccessful. Furthermore, the water medium in which the reaction occurs, prevents monitoring at low temperatures, which would significantly reduce the kinetics. At this stage we can tentatively assign the dark coloured species to a Cu(II) intermediate which is not stable for extended periods and dissipates rapidly. The clear difference between dithiophosphonates and its symmetric counterparts is the reduction in symmetry in our system, caused by the asymmetric nature of the ligand. Complexes of symmetric dithiolates contain Cu(II) intermediate with C_4 rotation axis whereas dithiophosphonates possess a lower C_2 rotation axis perpendicular to the square planar

coordination plane. This could account for the lack of stability of the Cu(II) intermediate and is advantageous for the current purpose.

With a focus on the preparation and isolation of Cu(I) clusters with the modified procedure, we are able to produce a diverse group of Cu(I) clusters shown in Table 4.1.

Table 4. 1 ^{31}P NMR data for clusters **9**-**15.**

Cluster	**R**	**^{31}P NMR (δ)**
9	CH_3	103.3
10	CH_2CH_3	100.2
11	$CH(CH_3)_2$	98.5
12	$CH_2CH_2CH_2CH_3$	100.2
13	$CH_2CH{=}CH_2$	101.5
14	$CH_2C_6H_5$	101.6
15	m-$CH_2C_6H_4Br$	102.6

All the clusters are relatively stable once isolated, with high solubility in polar chlorinated solvents. ^{1}H and ^{31}P NMR and mass spectroscopy confirmed the structural characteristics of the clusters, which all have a Cu_4L_4 configuration.

The diverse group of ligands prepared allows for a comparison of the coupling between H and P nuclei in dithiophosphonate ligands. Three $J_{P\text{-}H}$ coupling constants can be distinguished for cluster **9**, shown in Figure 4.3a. The coupling is largely proximity based with the 15 Hz coupling of methylene protons to the ^{31}P nuclei being the largest, followed by the coupling to the ortho-aromatic protons and meta-aromatic protons, at 13 and 3 Hz respectively. The broadening of resonances for protons located on the carbon adjacent to the oxygen atom are

a consequence of multiple couplings. In cluster **9** no vicinal protons are present and a well resolved doublet is observed, shown in Figure 4.3b, unlike **10** and **13** where the coupling cannot be quantified due to the combination of J_{P-H} and J_{H-H} of adjacent vicinal protons**.** Furthermore, the combination of the vicinal J_{H-H} and J_{P-H} couplings, resulted in a **dd** for the aromatic protons.

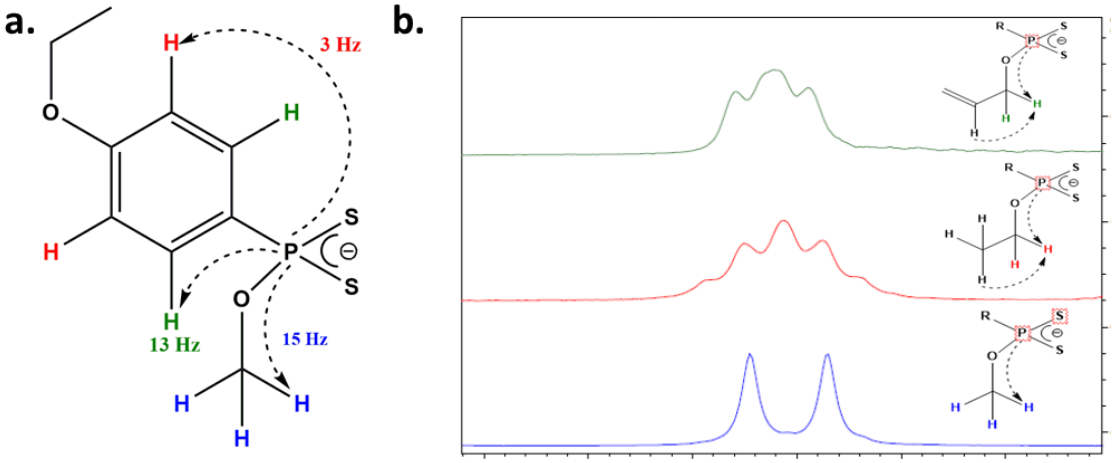

Figure 4.3. a) Representation of of J_{P-H} coupling present in dithiophosphonates. **b**) 15 Hz J_{P-H} doublet for methyl protons (blue), broadening of alkyl resonances for ethyl (red) and allyl (green).

A single set of resonances in the ^{1}H spectra were observed for each compound, suggesting an identical chemical environment around each of the four ligands. A common feature of complexes containing the asymmetric dithiophosphonate motif is the isomerization that could occur in solution leading to different configurations. The decoupled ^{31}P NMR for all clusters showed a single peak within range of 100 ppm, displayed in Table 4.1. This confirms the rigidity of the cluster in solution. The mass spectrometry played a key role in the characterisation of the clusters since CH elemental analysis would only provide a empirical formula CuL, and not the structurally ascertained composition, Cu_4L_4. We noted that the growth of crystals for these clusters depends significantly on the substituent on the alcohol and symmetry is not the only factor that can influence the efficiency of crystal growth.

4.2.2 Structural analysis

Selected bond lengths and angles are presented in Table 4.2, with collection and refinement parameters shown in Table 4.3. Cluster **11** crystallizes in a body centred lattice in a tetragonal space group, $I4_1/a$, and a molecular representation is shown in Figure 4.4.The space group is significantly different from the $P2_12_12_1$ and Pn seen in the related symmetric isopropyl derivatives of the dithiophosphate[5] and diselenophosphate[2] clusters, respectively. The introduction of the anisole group on the P atom, creates a sterically saturated environment around the phosphorus atom, thus limiting the rotation of the C-O bond and the resultant loss of freedom forces the isopropyl group to occupy equivalent orientations on each ligand and therefore within the crystal lattice. The asymmetric unit therefore consists of exactly one quarter of the molecule. This implies that each Cu(I) atom is crystallographically equivalent, and the ligands occupy equivalent orientations and positions.

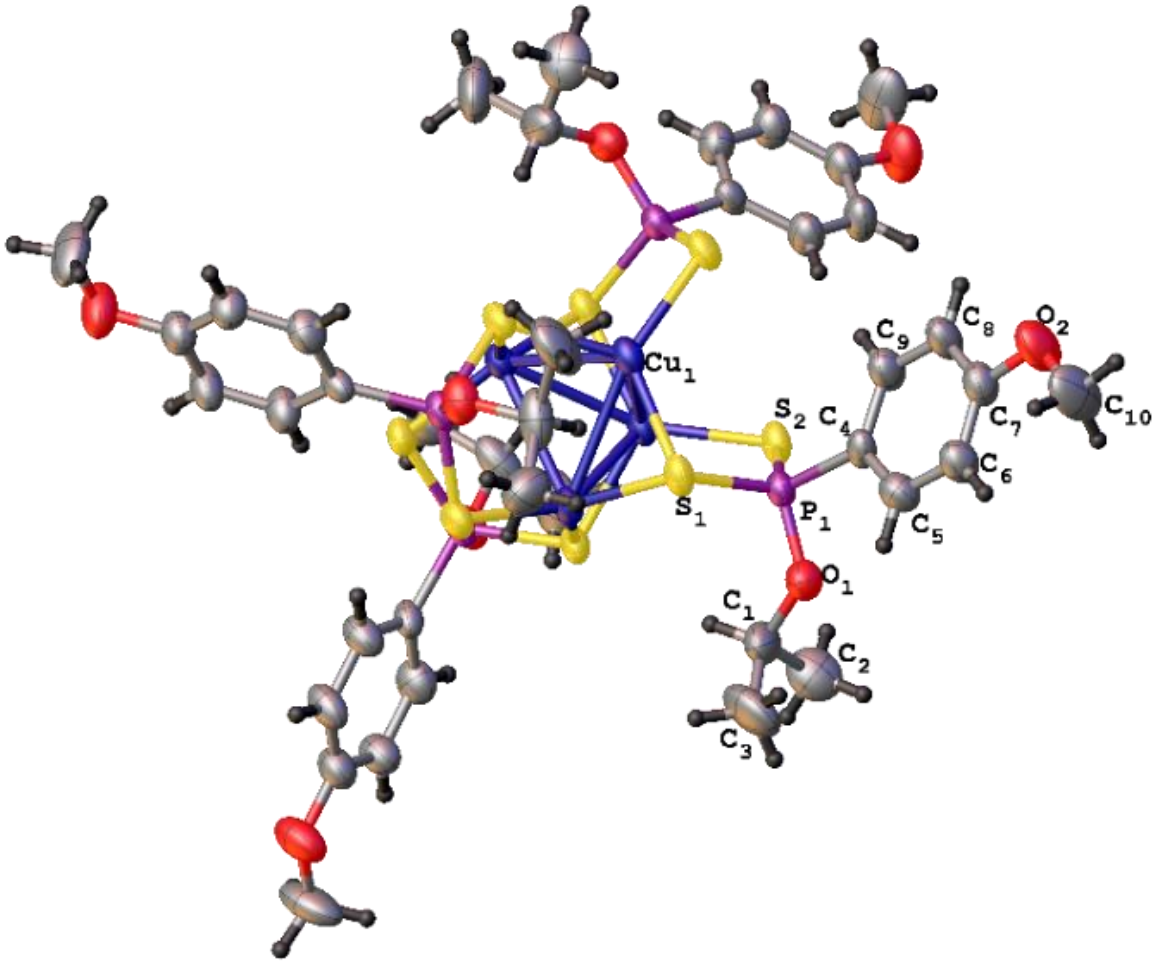

Figure 4.4. Molecular representation of **11**, thermal ellipsoids drawn at 35 % probability.

The metal framework reveals a core of four copper atoms arranged in a trigonal pyramidal arrangement, shown in Figure 4.5. The tetrahedron is stabilized by six Cu···Cu contacts, which can be further divided into types: **i**) four shorter contacts that are bridged by sulfur at 2.757 Å and **ii**) two non-bridged metal contacts, measuring 2.904 Å, the latter being significantly longer than the sum of the van der Waals radius of two Cu atoms (2.8 Å).

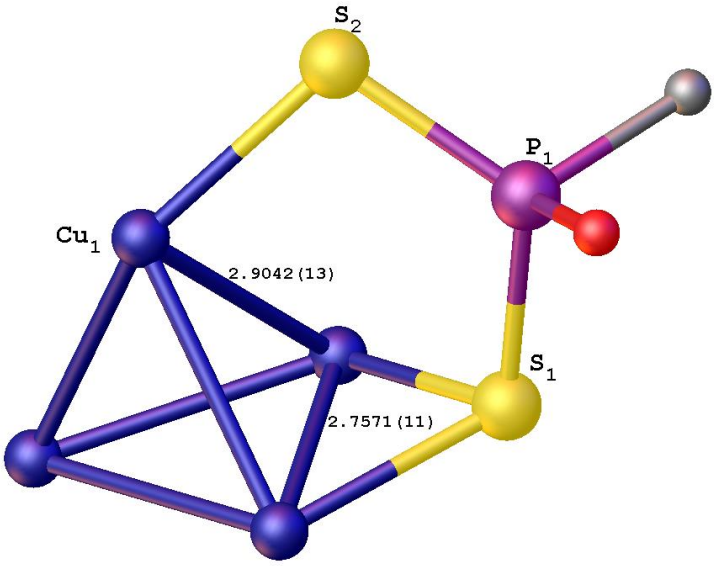

Figure 4.5. Representation of tri-metallic tri-connective coordination mode of ligand, and Cu(I) core with two different Cu···Cu contacts. (ligand substituents omitted for clarity.

An empirical comparison of the Cu···Cu distances can be achieved with Pauling's expression developed for inter-nuclear distances in metal bonds.[22,23] Bond orders for **i** (1.18) and **ii** (0.67) thus indicate that the three copper atoms act cooperatively to stabilize the fourth (i.e. two bridged contacts (**ii**) and one non-bridged contact (**i**)). The propensity for Cu(I) centres to cluster has been shown to be driven by both Cu(I) interactions and stereochemical aspects of the ligand.[24] Mono-anionic dithiophosphonate ligands, with bite angles at *ca*. 115.70°, cap each triangular face of the tetrahedron resulting in closed d^{10} electronic configuration on the copper atoms. The intra-ligand S···S bite distance is 3.417 Å, with Cu-S bond distances of 2.292 Å. Each ligand coordinates in a trimetallic, tri-connective (μ_2-S; μ_1-S) coordination mode. Although the charge is delocalized across the S-P-S fragment, differential P-S bond lengths exists with the P-S_1 bond (2.058 Å) being relatively longer than the P-S_2 bond (1.979 Å). The *ca.* 8 pm elongation arises as a direct result of the denticity, with S_1 bridging two Cu

atoms and as a resultant loss of electron density occurs in the corresponding P-S bond. This arrangement plays a role in the formation of unique and characteristic luminescent patterns.

Table 4. 2. Bond distances (Å) and angles (°) for **11** and **14** with e.s.d. in brackets.

11		**14**	
P(1)-S(1)	2.057	P(1)-S(1)	2.0481(18)
P(1)-S(2)	1.978	P(1)-S(2)	1.954(2)
P(1)-O(1)	1.574	P(1)-O(2B)	1.468(7)
P(1)-C(4)	1.777(6)	P(1)-C(1)	1.894(5)
Cu(1)-Cu(1)^{1}	2.7572(11)	Cu(1)-Cu(2)	2.7600(10)
Cu(1)-Cu(1)^{2}	2.7571(11)	Cu(1)-Cu(1)^{1}	2.9494(13)
Cu(1)-Cu(1)^{3}	2.9042(15)	Cu(2)-Cu(2)^{1}	2.9353(14)
S(2)-P(1)-S(1)	115.72(9)	S(2)-P(1)-S(1)	117.06(8)
Cu(1)^{1}-Cu(1)-Cu(1)^{3}	58.220(14)	Cu(1)^{1}-Cu(2)-Cu(2)^{1}	57.93

Cluster **14** crystallizes in the monoclinic space group C2/c, Figure 4.6. The overall loss of symmetry can be attributed to the disorder present in the ligands. The metal core bears a great similarity to **11**. However, in **14,** two crystallographically independent Cu(I) sites are apparent. This results in the slight variation of the Cu···Cu contacts with two values for the bridged contacts (2.754 and 2.760 Å) and the non-bridged contacts (2.949-2.935 Å). It should be noted that the deviation is not significant and the electronic argument presented for **11**

still holds true. A slight increase in the bite angle of the S-P-S fragment, ca. 117 °, is noted. This could be due to the increase in the sterically more demanding substituents, which influence the tetrahedral configuration on the P atom. The length of the P-S bonds can be described in the similar manner as **11,** with magnitudes of 2.048 and 1.954 Å for the P-S_1 and P-S_2 bonds, respectively.

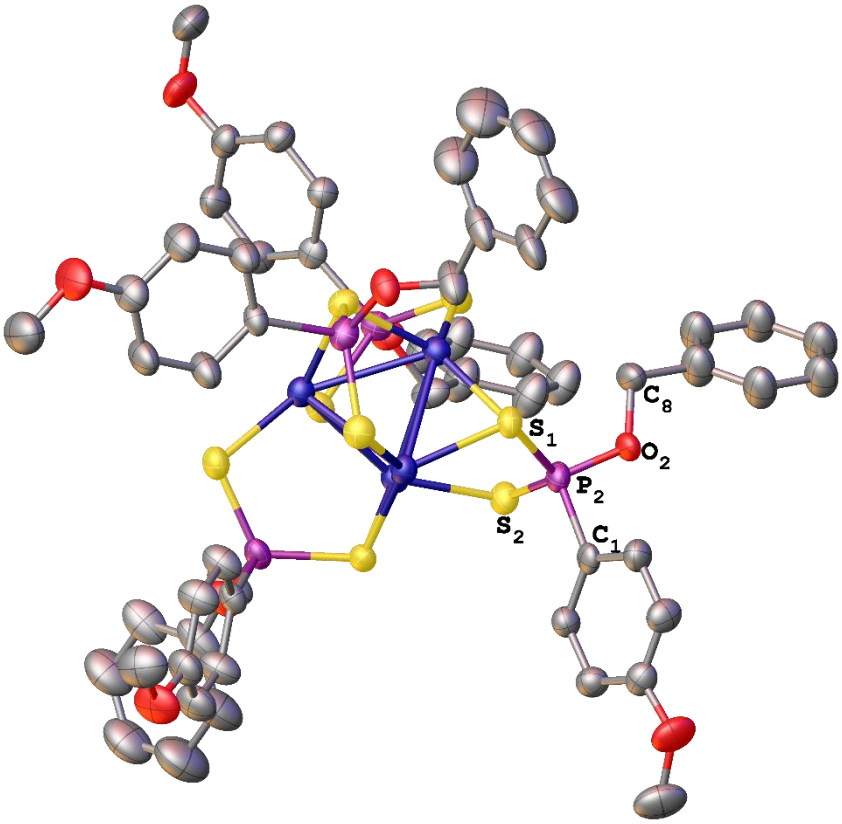

Figure 4.6. Molecular structure of **14**, thermal ellipsoids drawn at 35% probability, hydrogens omitted for clarity.

Interestingly, the O-benzyl and anisole groups interchangeable occupy equivalent positions in the crystal lattice, resulting in a static positional disorder, shown in Figure 4.7. The disorder can be related to the similarity in the size, composition ($C_6H_5OCH_3$ and $C_6H_5CH_2O$) and geometry of the two substituents.

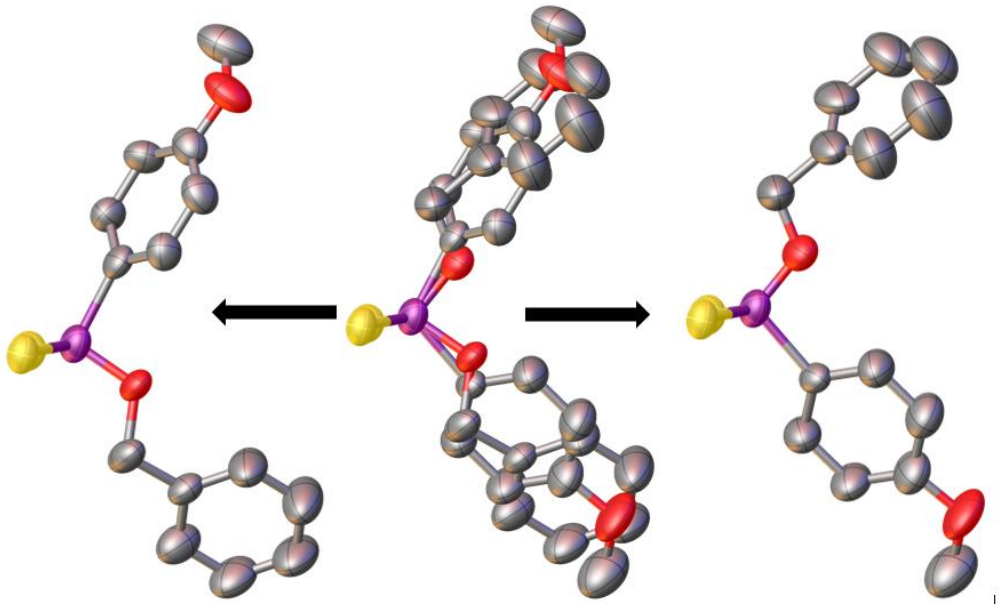

Figure 4.7. Separation of disorder present on **14**, thermal ellipsoids drawn at 35% probability, hydrogens omitted for clarity.

Since the crystals were stable (photograph of crystal shown in Figure 4.8), it can be presumed that the difference between the two confirmations does not significantly impact on the overall lattice energy. In the preparation of cluster **15** we tried to remove this position exchange and introduced a bromide substituent on the meta position of the benzyl ring. However, we were unable to obtain suitable crystals for X-ray analysis. The inability to grow suitable crystals of **15**, could be assigned to the loss of the positional exchange between the two groups present in **14**. It can be said that the combination of benzyl and anisole substituents creates a sort of *faux* symmetry between the two groups, which is responsible for an improvement in crystal growth. The secondary coordination sphere (space behind the coordinating S-P-S fragment) is sterically restrictive, with certain groups being able to occupy space more efficiently. This has proven to be dominant factor in successful crystallization and stability of other derivatives which were not of adequate quality for data collection.

Table 4.3. Collection and Refinement Data for **11** and **14**.

Cluster	**11**	**14**
Empirical formula	$C_{40}H_{56}Cu_4O_8P_4S_8$	$C_{56}H_{56}Cu_4O_8P_4S_8$
Mw	1299.37	1491.52
Temperature[K]	296	296
Size [mm]	0.22 × 0.21 × 0.12	0.420 x 0.350 x 0.210
Cryst. System	Tetragonal	Monoclinic
Space Group	$I4_1/a$	C2/c
a[Å]	20.955(3)	29.275(7)
b[Å]	20.955(3)	14.725(3)
c[Å]	12.350(2)	20.737(5)
α[°]	90.00	90
β[°]	90.00	134.715(10)
γ[°]	90.00	90
V[$Å^3$]	5422.8(15)	6352(3)
Z	4	4
ρcal [g cm^{-3}]	1.592	1.560
Absorption coefficient [mm^{-1}]	2.019	1.735
F(000)	2656.0	3040.0
Θrange [°]	3.82 to 50.22	3.39 to 50
Number of data/restraints/parameters	2416/0/145	5601/596/497
Goodness of fit F^2	1.042	1.030
Final R indices [I > 2σ(I)]	R_1 = 0.0471, wR_2 = 0.1298	R_1 = 0.0462, wR_2 = 0.1174
R indices (all data)	R_1 = 0.0796, wR_2 = 0.1531	R_1 = 0.0775, wR_2 = 0.1367
Largest diff peak/hole [e/ $Å^3$]	0.53/-0.32	0.51/-0.330

4.2.3 Luminescence

Herein we report the first luminescence data for a series of tetranuclear Cu(I) dithiophosphonate clusters. The solid-state photophysical data are summarized in Table 4.4. A yellow-green emission colour was noted for all clusters, Figure 4.8.

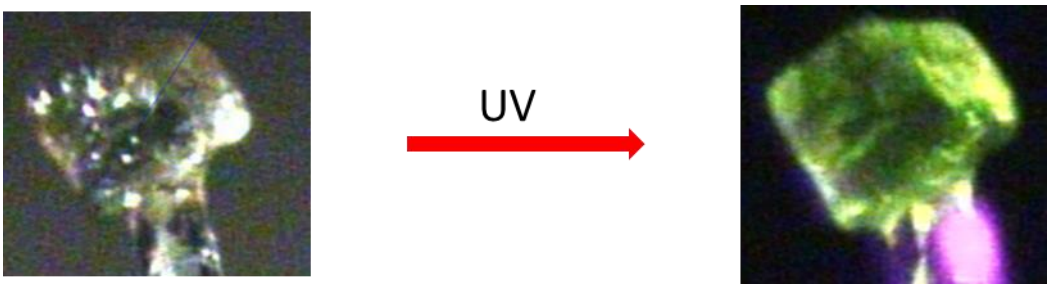

Figure 4.8. Image of emission from single crystal of cluster **14**.

The broad, indistinguishable characteristics of the emission bands are consistent with a MLCT, with a contribution from the Cu···Cu interactions (3d → 3d transitions).[11] Variation in the substitution on the dithiophosphonate ligand does not greatly influence the position of the emission band, shown in Figure 4.9. This indicates π→π* transitions in the anisole or benzyl groups do not contribute to the emission. Thus the emission can be assigned to be as a result of the core and the primary coordination sphere, with a lifetime dependent on the ability of the ligand to stabilize the excited state.

The radiative lifetime of the emissive states proved to be single exponentials with an average of 11.98 μs. The duration of the lifetime and the relatively large Stokes shift indicates phosphorescence with decay from a triplet excited state. Tetra-nuclear clusters of the configuration $Cu_4X_4L_4$ (X=halide, L=neutral ligand) have been well studied[25-30] and recent examples display mechanochromism[31] and thermochromism.[32] In the present study the emission band position remains constant over a wide temperature range (297 K- 77 K) indicating no thermochromatic behavior. The reduction in temperature does however cause an increase in intensity and narrowing of the emission band, which is in line with a reduction in energy loss due to molecular vibrations and in increase in the radiative pathway.

Table 4.4 Photophysical data for clusters **9**-**15**.

Compound	State (T/K)	λ^{ex} (nm)	λ^{em} (nm)	τ (μs)
9	298	364	520	10.99751
10	298	370	519	12.296565
11	298	376	524	12.23359
	77	380	534	
12	298	365	522	11.55972
13	298	368	525	10.53409
14	298	375	524	12.58952
15	298	364	523	13.64788

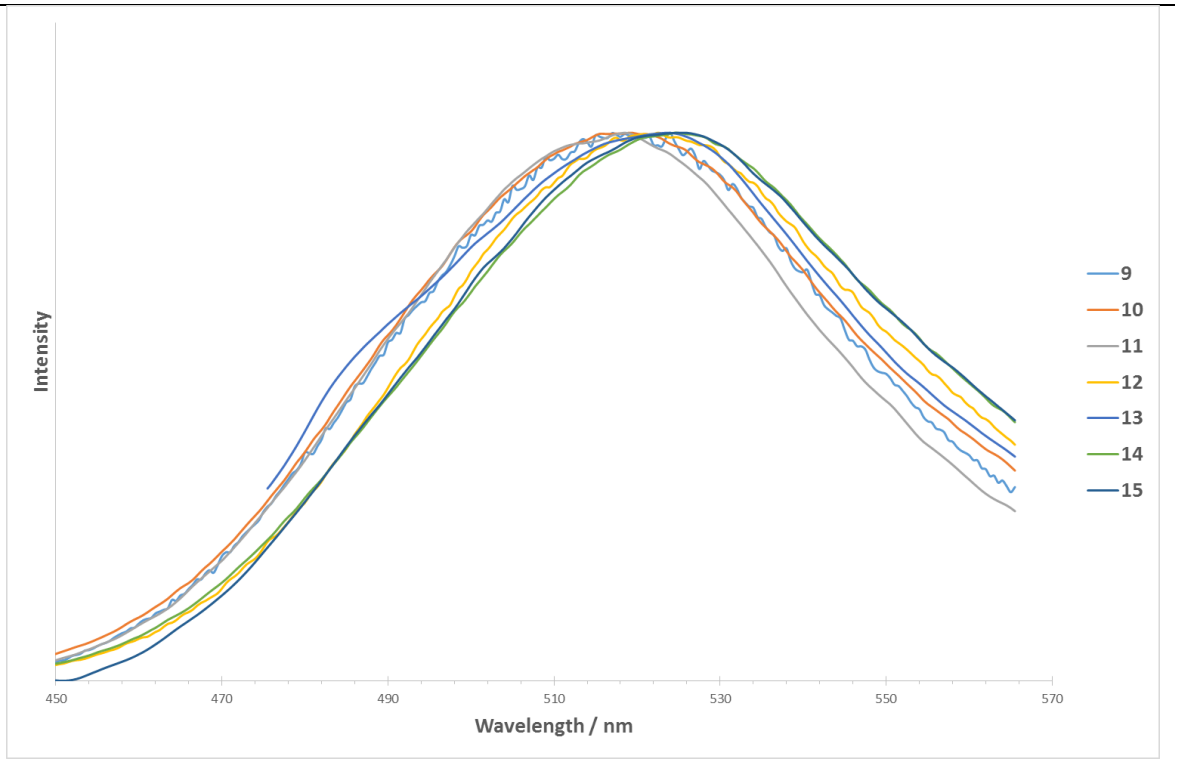

Figure 4.9. Room temperature emission spectra for clusters **9** -**15**.

A recent study described how spectral down-conversion of UV-radiation can optimize the photoelectric transformation in a solar cell, and increase its efficiency.[33] All clusters reported here have also shown down-conversion properties and therefore a solar cell application is possible within a matrix. Of additional benefit is that the clusters show both temperature and excitation independent emission profiles. To this end we incorporated the cluster into a flexible matrix that supports the luminescent characteristics. The powder of **9** was dispersed in polyvinyl alcohol (PVA) and the emission spectrum was found to be similar (λ^{em} = 517 nm) to the solid state emission of the parent cluster (λ^{em} = 520 nm), Figure 4.10.

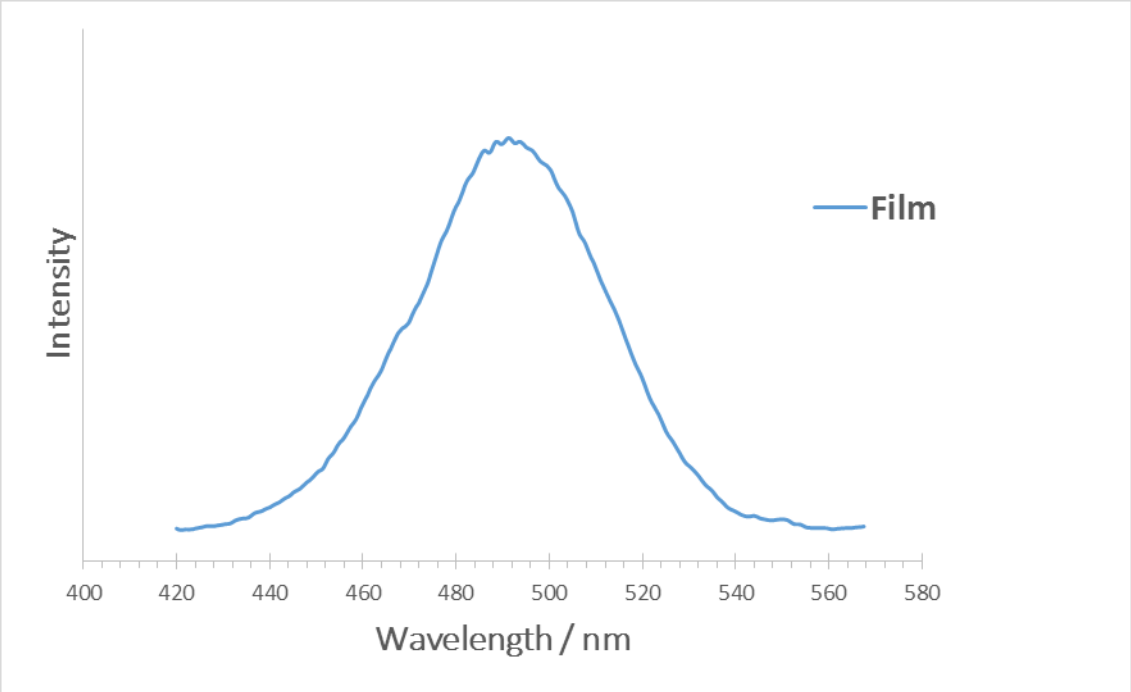

Figure 4.10. Emission spectrum of **9** dispersed in PVA film.

4.2.4 Electronic structure

Cluster **11** has a closed shell configuration, selected frontier virtual and occupied molecular orbitals are shown in Figure 4.11. The calculations were based on the positional data obtained from single crystal X-ray analysis. The RB3LYP functional and 6-31G(d)) basis set was employed. The HOMO and LUMO contain contributions both from the metal core and the

ligands. Importantly, the alkyl substituents on the P atom do not show significant contributions to both the HOMO and LUMO. The LUMO +1 are largely the π*- orbitals on the ligand. The HOMO orbital is mainly localized on the coordinating sulfur atoms and the cluster core. The HOMO-2 and HOMO-3 orbitals are degenerate. The lack of contributions from the alkyl substituents accounts for the similarity in the emission profile observed for all clusters. However, they could play a role in the stabilization of the excited species and therefore influence the emission lifetimes. The HOMO-LUMO band gap determined from Gaussian09 molecular orbital calculations was 3.89 eV.

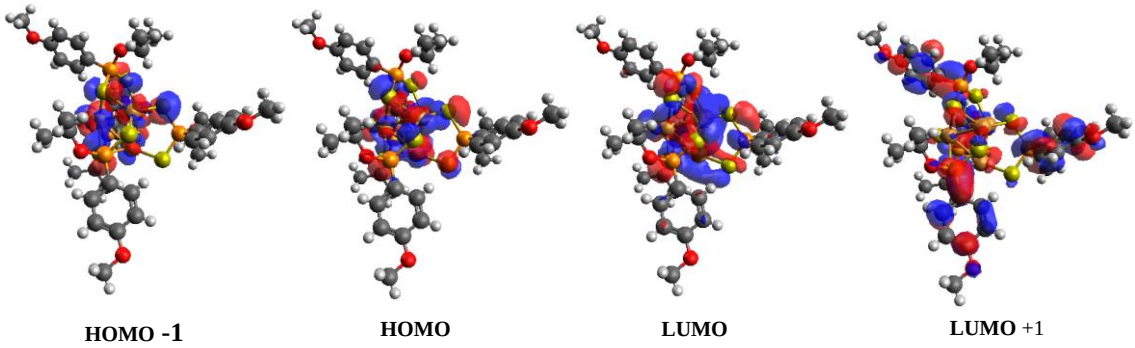

Figure 4.11. Selected frontier molecular orbitals for **11**.

In summary, a new synthesis protocol for the synthesis of tetranuclear Cu(I) clusters has been identified. Structural analysis confirmed the structure of the tetranuclear Cu(I) core to be a tetrahedron. The ligand substituents play a key role in the crystallisation of these derivatives. In particular an interesting case of positional disorder was noted for **14**. Furthermore this series of dithiophosphonates clusters have been shown to be highly luminescent at room temperature. This synthetic route avoids the need for Cu(I) precursors and the sacrificial oxidation of the ligand provides a cost effective alternative to expensive reagents. Therefore in line with an objective to identify synthesis protocols which make available luminescent materials for a broader application, has been identified and found to be effective.

4.3 Experimental

All commercially available reagents were reagent grade and used without further purification. Anisole, phenetole, phosphorus-pentasulfide, hexafluorophosphoric acid, Cu(I) oxide, and Cu(II) chloride were obtained from Sigma Aldrich. Ammonia gas was purchased from Afrox (South Africa). Ligands[14] and $[Cu(CH_3CN)_4]PF_6$,[15] were prepared according to literature methods. ^1H and $^{31}P\{^1H\}$ spectra were recorded on a Bruker Advance 400 MHz spectrometer at 298 K. NMR data are expressed in parts per million (ppm). ^1H spectra are referenced internally to residual proton impurity in the deuterated solvents ($CDCl_3$ in all cases). ^{31}P NMR spectra chemical shifts were referenced relative to an 85% H_3PO_4 in D_2O external standard solution. Data are reported as resonance position (δ_H), multiplicity, assignment, and relative integral intensity. Melting points were determined with an Electrothermal 9100 melting point apparatus. Luminescence spectra were recorded on a Perkin–Elmer LS-55 spectrometer equipped with a front surface accessory. Variable temperature emission spectra were recorded on a Cary Eclipse B10 fluorescence spectrophotometer. Phosphorescence Lifetime measurements were determined from the exponential regression of the intensity values against gate time.[34]

4.3.1 Synthesis of $[Cu\{(S_2P(1,4\text{-}C_6H_4OEt)(OCH_3)\}]_4$, (**9**).

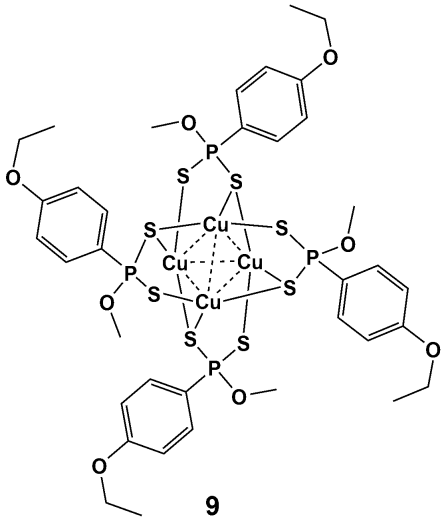

9

A Schlenk flask was charged with $(4\text{-}C_6H_4OEtP(S)S)_2$ (700mg, 1.16 mmol) and placed under vacuum for 10min. The solid was heated to 80 °C before the addition of CH_3OH (110mg, 3.43 mmol). The temperature was maintained for 15 min, until a clear residue was observed. After cooling the residue in an ice bath, anhydrous NH_3 gas was bubbled through the residue, resulting the formation of a white precipitate. The excess ammonia was removed in vacuo and the salt immediately dissolved in ETOH:H_2O (4:1) solution. An aqueous solution of $CuCl_2{\cdot}2H_2O$(280mg, 1.64mmol)

was added dropwise, resulting in a short-lived brown colour which immediately dissipates to yield a yellow precipitate. The precipitate is collected by filtration and washed with water (2 x 5ml) followed by hexane (2 x 5mL). The crude product is recrystallized from dichloromethane to yield a pale yellow powder. Yield = 352mg (70%). Melting point 156.2-156.8 °C. ^{1}H NMR (400 MHz, $CDCl_3$): δ (ppm), J(Hz) 1.42(t, CH_3, 3H, J_{H-H} =6.98), 3.86(d, $POCH_3$, 3H, J_{P-H} = 14.85), 4.07(q, CH_2, 2H, J_{H-H} = 6.99), 6.93 (dd, ArCH, 2H, J_{H-H} = 8.72, J_{P-H} = 3.16), 7.97 (dd, ArCH, 2H, J_{H-H} = 8.66, J_{P-H} = 13.58) ^{31}P NMR (400 MHz, $CDCl_3$): δ (ppm)103.32. ESI-MS (m/z) (cal.) 1264.6251(1264.71) for ([Cu{($S_2P(1,4\text{-}C_6H_4OEt)(OCH_3)$}]$_4$ + Na^+).

Clusters **10** – **15** were prepared in a similar manner to **9**.

4.3.2 Synthesis of [Cu{($S_2P(1,4\text{-}C_6H4OEt)(OCH2CH_3)$}]$_4$, (**10**).

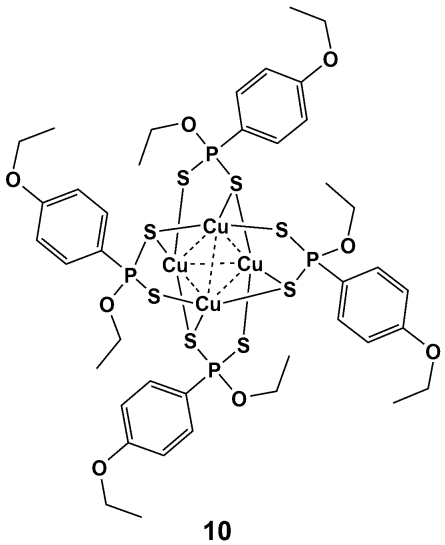

10

Yield = 312mg (83%) Melting Point 158.5-159.3 °C. ^{1}H NMR (400 MHz, $CDCl_3$): δ (ppm), J(Hz) 1.36(t, CH_3, 3H, J_{H-H} =7.02), 1.42(t, CH_3, 3H, J_{H-H} =7.02), 4.06(q, OCH_2, 2H, J_{H-H} =6.98), 4.26(m, $POCH_2$, 2H), 6.92 (dd, ArCH, 2H, J_{H-H} = 8.60, J_{P-H} = 3.44), 7.97 (dd, ArCH, 2H, J_{H-H} = 8.36, J_{P-H} = 13.41) ^{31}P NMR (400 MHz, $CDCl_3$): δ (ppm)100.20. ESI-MS (m/z) (cal.) 1322.7241(1322.77) for ([Cu{($S_2P(1,4\text{-}C_6H_4OEt)(OCH_2CH_3)$}]$_4$ + Na^+).

4.3.3 Synthesis of $[Cu\{(S_2P(1,4\text{-}C_6H_4OMe)(OCH(CH_3)_2)\}]_4$, (**11**).

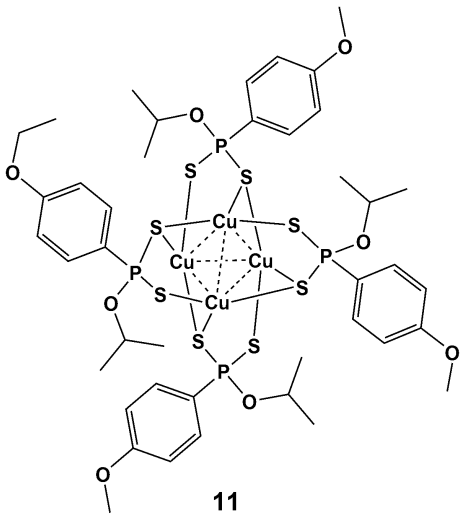

11

Yield = 298 mg (76%). Melting point 160.2-161.4 °C. ^1H NMR (400 MHz, $CDCl_3$): δ (ppm), J(Hz) 1.27(d, CH_3, 6H, $J_{H\text{-}H}$ = 6.04), 3.76(s, OCH_3, 3H), 5.10(m, 1H), 6.82 (dd, ArCH, 2H, $J_{H\text{-}H}$ = 8.74, $J_{P\text{-}H}$ = 3.02), 7.90(dd, 2H, $J_{H\text{-}H}$ = 8.60, $J_{P\text{-}H}$ = 13.40Hz) ^{31}P NMR (400 MHz, $CDCl_3$): δ (ppm) ^{31}P NMR 98.5. ESI-MS (m/z) (cal.) 1376.8203 (1376.84) for ($[Cu\{(S_2P(1,4\text{-}C_6H_4OEt)(OCH_2CH_3)\}]_4 + Na^+$).

4.3.4 Synthesis of $[Cu\{(S_2P(1,4\text{-}C_6H_4OMe)(OCH_2CH_2CH_2CH_3)\}]_4$, (**12**).

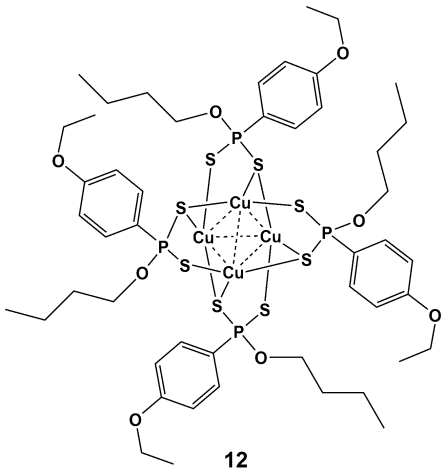

12

Yield = 320mg (78%). Melting point 160.2-160.4°C. ^1H NMR (400 MHz, $CDCl_3$): δ (ppm), J(Hz) 0.92 (t, CH_3, 3H, $J_{H\text{-}H}$ =7.38), 1.42(t, CH_3, 3H, $J_{H\text{-}H}$ =7.02), 1.44(m, CH_2,2H), 1.705(p, CH_2, 2H, $J_{H\text{-}H}$ =6.97), 4.07(q, OCH_2, 2H, $J_{H\text{-}H}$ =6.99), 4.21 (b, OCH_2, 2H) 6.91(dd, ArCH, 2H, $J_{H\text{-}H}$ = 8.75, $J_{P\text{-}H}$ = 3.14), 7.96 (dd, ArCH, 2H, $J_{H\text{-}H}$ = 8.60, $J_{P\text{-}H}$ = 13.49) ^{31}P NMR (400 MHz, $CDCl_3$): δ (ppm)100.15. ESI-MS (m/z) (cal.) 1432.9615 (1432.90) for ($[Cu\{(S_2P(1,4\text{-}C_6H_4OEt)(OCH_2CH_3)\}]_4 + Na^+$).

4.3.5 Synthesis of [Cu{($S_2P(1,4\text{-}C_6H_4OMe)(OCH_2CH{=}CH_2)$}]$_4$,(**13**).

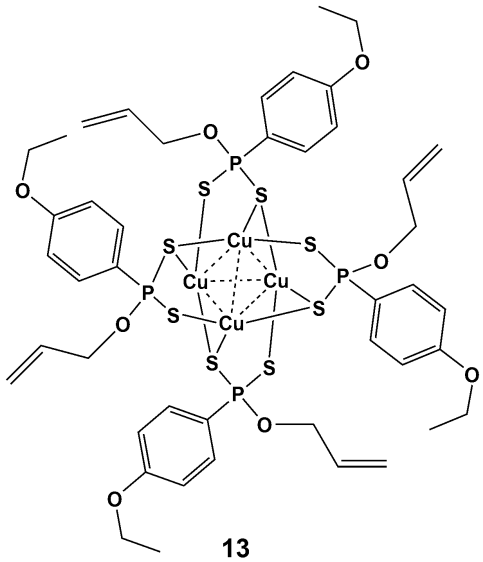

13

Yield = 254 mg (65%). Melting point 159.6-159.8°C ^{1}H NMR (400 MHz, $CDCl_3$): δ (ppm), J(Hz) 1.42(t, CH_3, 3H, $J_{H\text{-}H}$ =6.98), 4.06(q, OCH_2, 2H, $J_{H\text{-}H}$ =7.03), 4.71(m, $POCH_2$, 2H), 5.21 (d, , 1H, $J_{H\text{-}H}$ = 8.60), 5.35 (dd, , 1H, $J_{H\text{-}H}$ = 17.16, $J_{P\text{-}H}$ = 1.40), 5.99(m,CH,1H) 6.92(dd, ArCH, 2H, $J_{H\text{-}H}$ = 8.78, $J_{P\text{-}H}$ = 3.26), 7.98 (dd, ArCH, 2H, $J_{H\text{-}H}$ = 8.70, $J_{P\text{-}H}$ = 13.71) ^{31}P NMR (400 MHz, $CDCl_3$): δ (ppm)101.53. ESI-MS 1366.7764(1366.7773) (m/z) (cal.) for ([Cu{($S_2P(1,4\text{-}C_6H_4OEt)(OCH_2CH{=}CH_2)$}]$_4$ + Na^+).

4.3.6 Synthesis of [Cu{(S2P(1,4-$C_6H_4OMe)(OCH_2C_6H_5)$}]$_4$, (**14**).

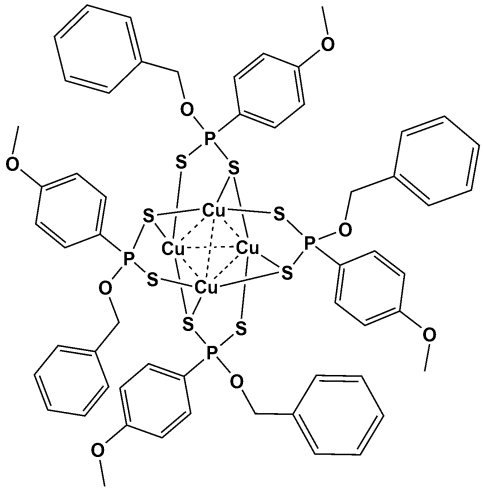

14

Yield = 345mg (77%). Melting point 152.4-153.2°C ^{1}H NMR (400 MHz, $CDCl_3$): δ (ppm), J(Hz) 3.85(s, OCH_3, 3H), 5.29(s,2H), 6.95(dd, ArCH, 2H, $J_{H\text{-}H}$ = 8.78, $J_{P\text{-}H}$ = 3.14), 7.35(d, ArCH, 2H, $J_{H\text{-}H}$ =7.56Hz), 7.44(d, ArCH, 2H, $J_{H\text{-}H}$ = 7.00 Hz), 8.04 (dd, ArCH, 2H, $J_{H\text{-}H}$ = 8.64, $J_{P\text{-}H}$ = 13.65) ^{31}P NMR (400 MHz, $CDCl_3$): δ (ppm) 101.6. ESI-MS (m/z) (cal.) 1512.6606 (1512.78) for ([Cu{($S_2P(1,4\text{-}C_6H_4OMe)(OCH_2C_6H_5)$}]$_4$ + Na^+).

4.3.7 Synthesis of $[Cu\{(S_2P(1,4\text{-}C_6H_4OMe)(OCH_2C_6H_4Br)\}]_4$, (**15**).

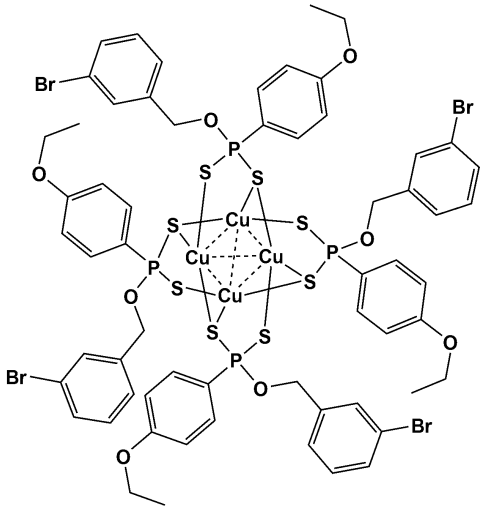

15

Yield = 357mg (67%). Melting point 155.2-156.0°C ^{1}H NMR (400 MHz, $CDCl_3$): δ (ppm), J(Hz) 1.42(t, CH_3, 3H, $J_{H\text{-}H}$ =7.00), 4.07(q, OCH_2, 2H, $J_{H\text{-}H}$ =6.98), 5.21(d, $POCH_2$, $J_{P\text{-}H}$ = 8.12 Hz), 7.19(t, m-ArH, 1H, $J_{H\text{-}H}$ =7.80), 7.56(s, o-ArH, 1H), 7.42(d, p-ArH, 1H, $J_{H\text{-}H}$ = 7.84) , 7.33(d, o-ArH, 1H, $J_{H\text{-}H}$ = 7.72 (dd, ArCH, 2H, $J_{H\text{-}H}$ = 8.76, $J_{P\text{-}H}$ = 3.24), 7.98 (dd, ArCH, 2H, $J_{H\text{-}H}$ = 8.66, $J_{P\text{-}H}$ = 13.79) ^{31}P NMR (400 MHz, $CDCl_3$): δ (ppm)102.60. ESI-MS (m/z) (cal.) 1886.7702 (1886.47) for ($[Cu\{(S_2P(1,4\text{-}C_6H_4OEt)(OCH_2C_6H_4Br)\}]_4 + Na^+$).

4.4 References

1 S.-L. Liu, X.-Y. Wang, T. Duan, W.-H. Leung, Q.-F. Zhang, *J. Mol. Struct.* 2010, **964**, 78-81.

2 Y.-J. Hsu, C.-M. Hung, Y.-F. Lin, B.-J. Liaw, T. S. Lobana, S.-Y. Lu, C. W. Liu, *Chem. Mater.* 2006, **18**, 3323-3329.

3 P.-K. Liao, C.-S. Fang, A. J. Edwards, S. Kahlal, J.-Y. Saillard, C. W. Liu, *Inorg. Chem*. 2012, **51**, 6577-6591.

4 R. S. Dhayal, J.-H. Liao, H.-N. Hou, R. Ervilita, P.-K. Liao, C. W. Liu, *Dalton Trans*., 2015, **44**, 5898-5908.

5 S. L. Lawton, W. J. Rohrbaugh and G. T. Kokotailo, *Inorg. Chem.*, 1972, **11**, 612-618.

6 Fackler, R. J. Staples, C. W. Liu, R. T. Stubbs, C. Lopez and J. T. Pitts, *Pure Appl. Chem.*, 1998, **70**, 839-844.

7 E. Block, H. Kang, G. Ofori-Okai and J. Zubieta, *Inorg. Chim. Acta*, 1990, **167**, 147-148.

8 D. Coucouvanis, C. N. Murphy and S. K. Kanodia, *Inorg. Chem*, 1980, **19**, 2993-2998

9 D. Rusanova, K. E. Christensen, I. Persson, K. J. Pike, O. N. Antzutkin, X. Zou, R. Dupree and W. Forsling, *J. Coord. Chem.*, 2007, **60**, 517-525.

10 C. W. Liu, M. D. Irwin, A. A. Mohamed and J. P. Fackler Jr, *Inorg. Chim. Acta*, 2004, **357**, 3950-3956.

11 R. S. Dhayal, J.-H. Liao, X. Wang, Y.-C. Liu, M.-H. Chiang, S. Kahlal, J.-Y. Saillard, C. W. Liu, *Angew. Chem. Int. Ed.*, 2015, **54**, 13604-13608.

12 R. S. Dhayal, J.-H. Liao, S. Kahlal, X. Wang, Y.-C. Liu, M.-H. Chiang, W. E. van Zyl, J.-Y. Saillard, C. W. Liu, *Chem. - Eur. J.*, 2015, **21**, 8369-8374.]

13 N. D. Yordanov, V. Alexiev, C. Malakova, A. Shishkov, *Trans. Met. Chem.*, 1983, **8**, 210-212.

14 W. E. van Zyl, J. P. Fackler, *Phosphorous, Sulfur, Silicon Rel. Elem.*, 2000, **167**, 117-132.

15 G. J. Kubas, B. Monzyk, A. L. Crumblis, *Inorg. Syth*, 1990, **28**, 68-70.

16 I. P. Gray, A. M. Z. Slawin, J. D. Woollins, New J. Chem. 2004, **28**, 1383-1389.

17 P. Klason, *Berichte der Deutschen Chemischen Gesellschaft*,1887, **20**, 3407-3413.

18 N. D. Yordanov, Trans. Met. Chem. 1997, **22**, 200-207.

19 R. C. Smith, V. D. Reed, W. E. Hill, *Phosphorus, Sulfur, Silicon Rel. Elem.* 1994, **90**, 147-154.

20 N. D. Yordanov, V. Alexiev, C. Malakova, A. Shishkov, *Trans. Met. Chem.*,1983, **8**, 210-212.

21 N. D. Yordanov, D. Shopov, *J. Chem. Soc., Dalton Trans.*, 1976, 883-886.

22 L. Pauling, *J. Am. Chem. Soc.*, 1947, **69**, 542-553.

23 A. Simon, *Angew. Chem. Int. Ed*, 1983, **22**, 95-113.

24 P. K. Mehrotra, R. Hoffmann, *Inorg. Chem*.,1978, **17**, 2187-2189.

25 C. K. Ryu, M. Vitale, P. C. Ford, *Inorg.Chem.*, 1993, **32**, 869-874.

26 P. C. Ford, A. Vogler, *Acc. Chem. Res.*, 1993, **26**, 220-226.

27 Z. Liu, P. I. Djurovich, M. T. Whited, M. E. Thompson, *Inorg. Chem.*, 2012, **51**, 230-236.

28 M. Knorr, F. Guyon, A. Khatyr, C. Strohmann, M. Allain, S. M. Aly, A. Lapprand, D. Fortin, P. D. Harvey, *Inorg. Chem.*, 2012, **51**, 9917-9934.

29 P. Roesch, J. Nitsch, M. Lutz, J. Wiecko, A. Steffen, C. Müller, *Inorg. Chem.*, 2014, **53**, 9855-9859.

30 S. Naik, J. T. Mague, M. S. Balakrishna, *Inorg. Chem.*,2014, **53**, 3864-3873.

31 Q. Benito, X. F. Le Goff, G. Nocton, A. Fargues, A. Garcia, A. Berhault, S. Kahlal, J.-Y. Saillard, C. Martineau, J. Trébosc, T. Gacoin, J.-P. Boilot, S. Perruchas, *Inorg. Chem.*, 2015, 54, 4483-4494.

32 Q. Benito, X. F. Le Goff, S. Maron, A. Fargues, A. Garcia, C. Martineau, F. Taulelle, S. Kahlal, T. Gacoin, J.-P. Boilot, S. Perruchas, *J. Am. Chem. Soc.*, 2014, **136**, 11311-11320.

33 V. P. Afanas'ev, V. N. Vasil'ev, A. I. Ignat'ev, E. V. Kolobkova, N. V. Nikonorov, A. I. Sidorov, V. A. Tsekhomskiĭ, *J. Opt. Technol*. 2013, **80**, 635-641.

34 B. Jackson, H. Donato, *J. Chem. Ed.*, 1993, **70**, 780.

Chapter 5
Complexes of dithiophosphonate-based bifunctional S/N type ligands

The aim of this chapter is to incorporate two different donor atoms for metal coordination on the same ligand framework. In comparison with Chapter 3 which adopted a *homoleptic* approach to the preparation of metal complexes, this chapter explores a more '*heteroleptic* approach', whereby pyridine and dithiophosphonate are combined into one ligand that contains two different sets of donor atoms to coordinate to the metal centre. The coordinative ability of the ligand was evaluated with a diverse group of transition metals.

5.1 Introduction

In the literature survey of Chapter 1 two dominant independent ligands where commonly utilized in combination with dithiophosphonates, these were phosphines and N-donor ligands. These functionalities are compatible with the dithiophosphonate ligand and have been effective in the preparation of coordination polymers.[1-3] The formation of these coordination polymers are due to the cooperative nature of the dithiophosphonate ligand. It is therefore plausible, that the addition of any one of these functionalities to a dithiophosphonate backbone, would have significant potential to generate completely novel systems. The incorporation of pyridine onto the backbone, rather than a phosphine, can be seen as advantageous for the following reasons: 1) the pyridyl coordination group is more resistant to oxidation; 2) the steric effect of auxiliary substituents on the phosphine would be avoided; 3) incorporation of the pyridine group can be readily achieved with the use of alcohols containing a pyridine functionality. Furthermore, studies of free pyridine coordination to dithiophosphonates has received attention both from experimental and computational investigations.[4] Importantly, the linker between the two coordinating groups needs to be of sufficient length and flexibility, such that the ligand can accommodate the coordination geometry of the metal centre. An idealised structure of this ligand is given in

Figure 5.1. This part of the study moved away from the coinage metals, in order to demonstrate the coordinative power of the ligand in the absence of metallophilic contributions.

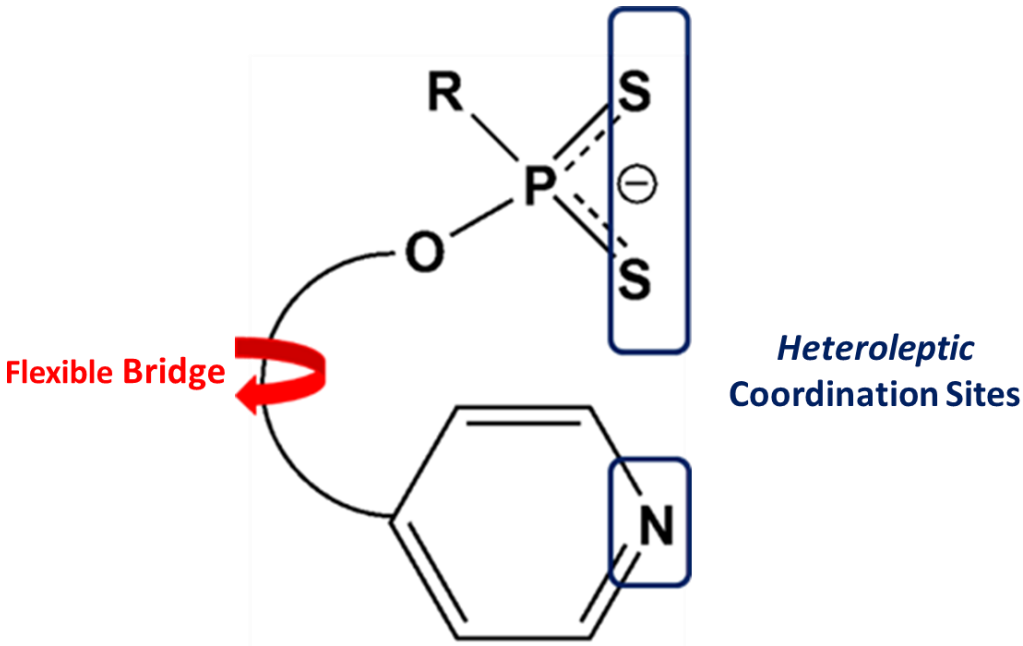

Figure 5.1. Combination of two different donor atoms in a common ligand framework.

5.2 Results and discussion

5.2.1 Ligand preparation

The 2,4-diaryl-1,3-dithiadiphosphetane disulfide dimer, reacts with two stoichiometric equivalents of 2-pyridine ethanol, symmetrically cleaving the dimer, to produce the first generation of dithiophosphonates incorporating the pyridine moiety into the framework of a dithiophosphonate (**L11**), Scheme 5.1.

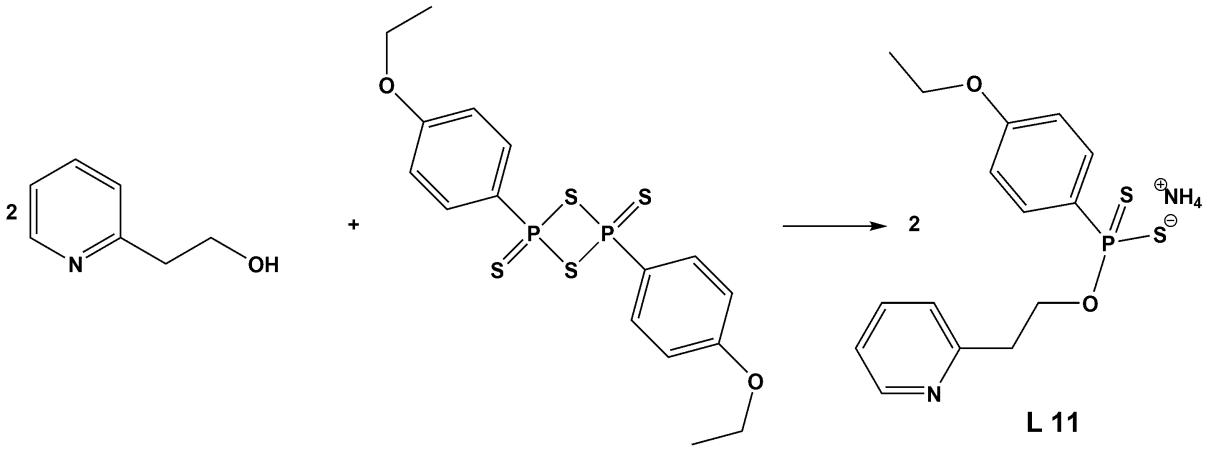

Scheme 5.1. Combination of pyridine and dithiophosphonate.

The relative basicity of the pyridine functionality has an adverse effect on the reaction as compared to linear and branched alkyl alcohols. This is seen in the increased reaction times required and an overall reduction in yield. This could be due to some mechanistic contributions from the pyridine functionality which has basic characteristics. The isolated dithiophosphonate shows a single resonance peak at 107ppm for the P atom which falls within the expected region, 90 to 112ppm, for this ligand class.[5] The introduction of pyridine also presents the opportunity of forming a zwitterion. Therefore, without deprotonation, crystals (**L11z**) were obtained and found suitable for single crystal X-ray analysis. **L11z** crystallises in the monoclinic space group C2/c with two molecules in the asymmetric unit, one of which is shown Figure 5.2. Selected bond lengths and angles can be found in Table 5.1. Electronic neutrality arises from the pyridinium cation and delocalisation of negative charge over the S-P-S fragment (observed in electron density map). The position of the pyridinium proton is not modelled and assigned based on residual electron density. The packing in crystal lattice of **L11z** reveals hydrogen bonding (N-H···S) between the pyridinium proton (H1A) and the S atom of an adjacent molecular unit. The parameters for N-H···S hydrogen bond, for both molecules in the asymmetric unit, are given in Table 5.2. The hydrogen-bonding is a packing director in the crystal lattice and together with the phenetole rings parallel to each other, a layered motif is observed (Figure 5.3). Furthermore, the hydrogen bonding results in differential P-S bond lengths with P-S(1) bond length (1.99 Å) slightly longer than the P-S(2) bond length(1.96).

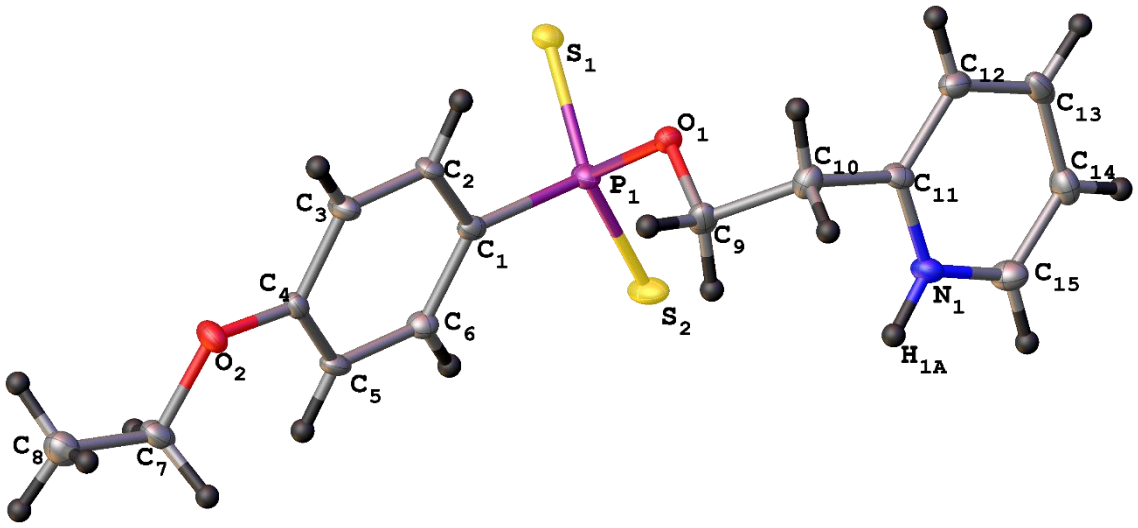

Figure 5.2. Molecular representation of **L11z**: thermal ellipsoids drawn at 50 % probability.

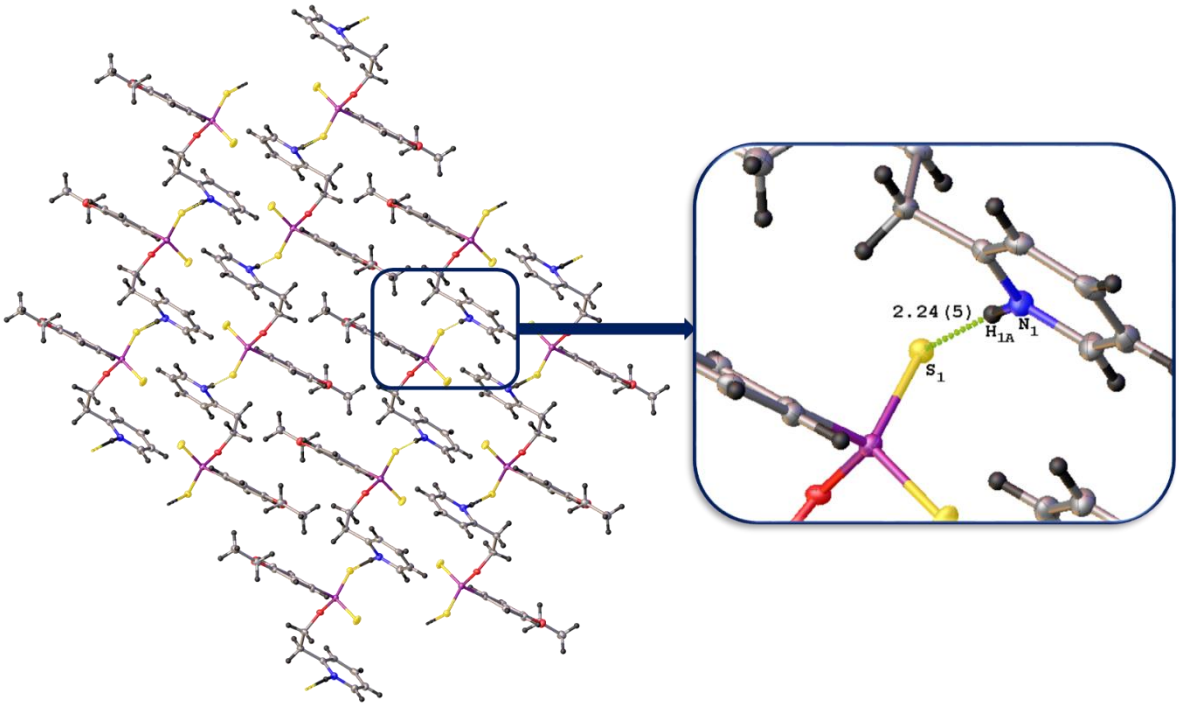

Figure 5.3. Crystal packing observed in **L11z** with hydrogen bonding (inset).

Table 5.1. Selected bond lengths (Å) and angles (°) for **L11z**, with e.s.d. in brackets**.**

P(1)-S(1)	1.9917(17)	P(I)-O(1)	1.626(3)
P(1)-S(2)	1.9648(17)	P(1)-C(1)	1.815(5)
P(2)-S(3)	1.9698(16)	S(1)-P(1)-S(2)	118.35(7)
P(2)-S(4)	1.9899(17)	O(1)-C(9)-C(10)-C(11)	64.3(5)

Table 5.2. Hydrogen bond distances (Å) and angles (°) for **L11z**.

Donor-H···Acceptor	**Donor-H**	**Acceptor-H**	**Donor-Acceptor**	**Angle**
N(1)-H(1A)···S(1)	0.96(6)	2.28(6)	3.227(5)	169.0
N(1)-H(2A) ··S(4)	0.98(5)	2.23(5)	3.205(5)	174.0

5.2.2 Co(II) coordination polymer.

The reaction of **L11** with $[Co(ClO_4)_2]\cdot 6H_2O$ in water/ethanol solution led to the formation of a novel coordination polymer **16**, Scheme 5.2. Extraction with dichloromethane and the subsequent slow evaporation of the solvent resulted in the formation of a highly crystalline material, which did not require re-dissolving for the formation of crystals. Mass spectroscopy confirmed the purity of the material and displayed a molecular peak for the monomer, indicating the lability of the pyridine moiety coordination.

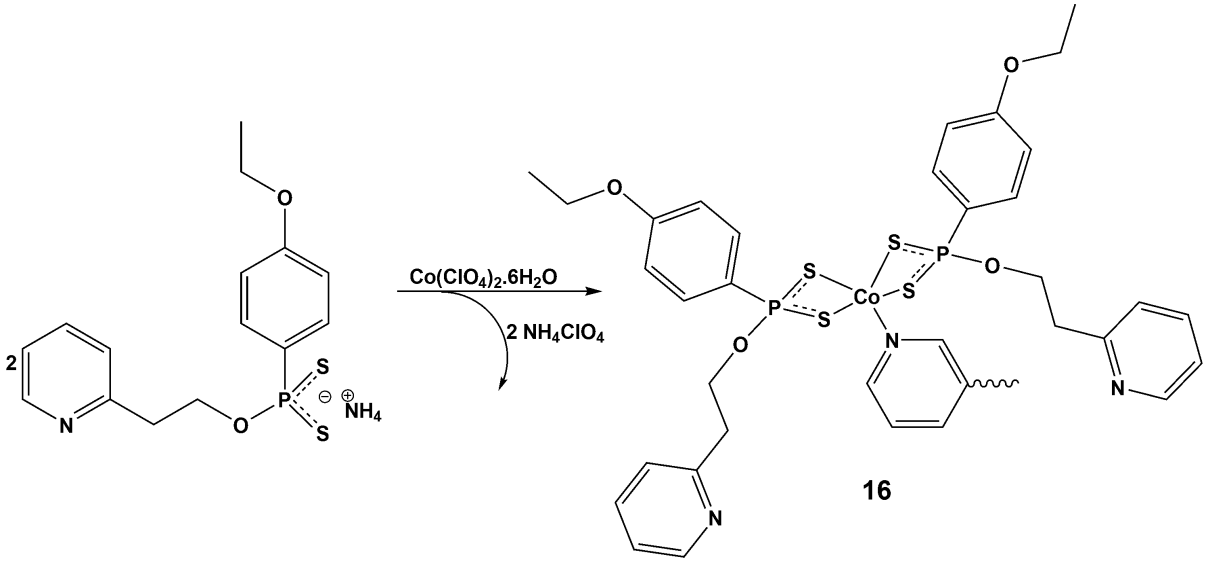

Scheme 5.2. Synthesis of Co(II) coordination polymer in aqueous media.

Complex **16** crystallizes in the monoclinic space group $P2_1/c$, and a molecular representation of the asymmetric unit is shown in Figure 5.4. Selected bond angles and distances can be found in Table 5.3. The structure represents the first report of a Co(II) dithiophosphonate complex. Each Co(II) centre is stabilized by two isobidentate S-P-S fragments and a nitrogen atom. The 5-coordinate cobalt centre is in a distorted trigonal bipyramid arrangement, shown in Figure 5.5.

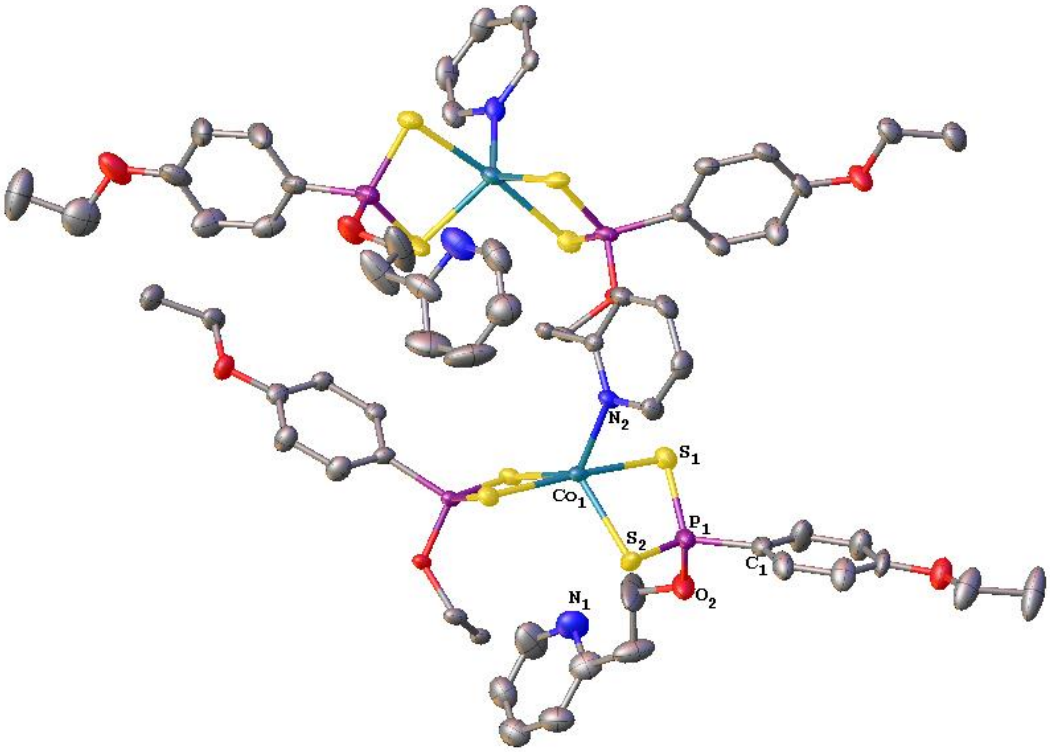

Figure 5.4. Asymmetric unit present in crystal lattice of **16**: Thermal ellipsoids drawn at 35% probability and H atoms omitted for clarity.

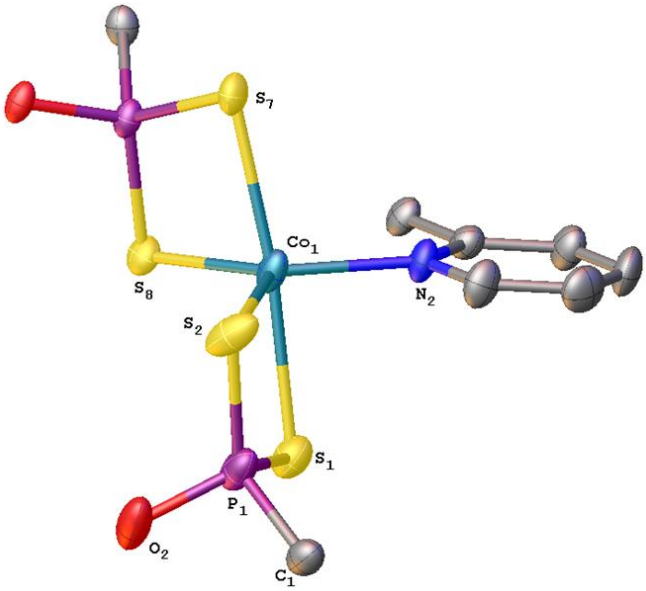

Figure 5.5. Representation of the coordination geometry around each Co(II) centre in **16**.

The axial sulfur atoms deviate from linearity by 8°, with the three equatorial positions all coplanar with the Co(II) atom. The P-S bond lengths are on average *ca.* 2.0 Å, and the S-P-S bite angles are *ca*. 109°. The Co-N bond distance is *ca.* 2.06 Å and within the average seen for the bonding of free pyridine in similar Co(II) systems, 2.057 Å (search of CCDC). The S-P-S coordination is bidentate with one axial and one equatorial sulfur. The ethyl bridge between the pyridine and the dithiophosphonate functionality provides the required flexibility and allows the pyridine moiety adequate freedom to coordinate to an adjacent molecular unit. Interestingly, inspection of the monomer unit shows a *cis* configuration. The coordination of the pyridine to the adjacent molecular unit gives rise to a coordination polymer and polymer expansion is shown in Figure 5.6.

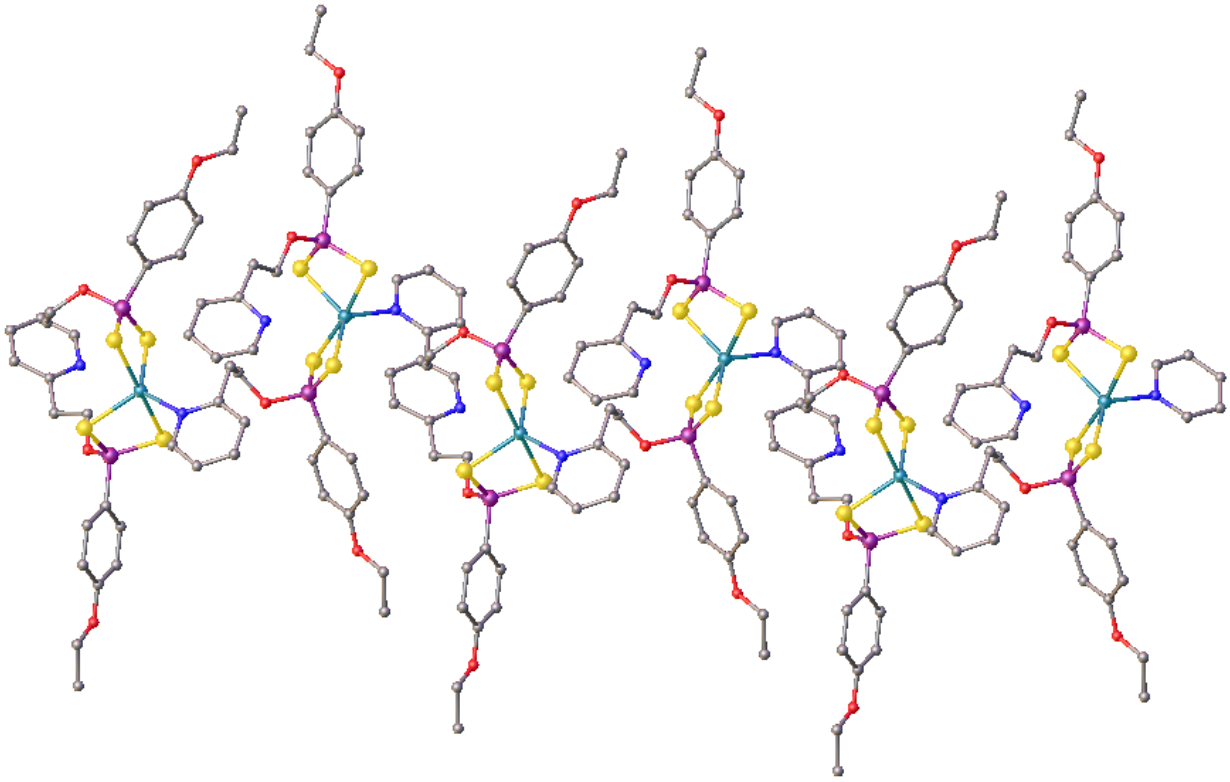

Figure 5.6. Polymer expansion across a single molecular direction for **16**.

Table 5.3. Selected bond lengths (Å) and angles (°) for **16**, with e.s.d. in brackets**.**

P(1)-S(1)	1.967(3)	Co(1)-S(7)	2.498 (2)
P(1)-S(2)	2.009(3)	Co(1)-S(8)	2.360(2)
P(2)-S(3)	1.997(3)	Co(1)-N(2)	2.073(6)
P(2)-S(4)	1.976(3)	S(1)-P(1)-S(2)	109.18(12)
P(1)-O(2)	1.587(6)	S(7)-P(4)-S(8)	108.91(11)
P(1)-C(1)	1.775(8)	S(1)-Co(1)-S(7)	81.98(7)
Co(1)-S(1)	2.581(2)	S(1)-Co(1)-S(7)	173.71(7)
Co(1)-S(2)	2.353(2)	S(1)-Co(1)-N(2)	85.85(17)

5.2.3 Mononuclear and dinuclear Ni(II) dithiophosphonates

The reaction of **L11** with $[Ni(ClO_4)_2]\cdot 6H_2O$ in water/ethanol solution led to the formation of **17**, Scheme 5.3. Complex **17** showed interesting solution characteristics which indicated fluxional behaviour in the coordination of the pyridine moiety. The complex was found to be soluble in chlorinated solvents and gave a purple solution. However, in alcoholic or aqueous environments the compound was found to be insoluble, and the precipitate would be orange. Therefore two different configurational isomers could be isolated.

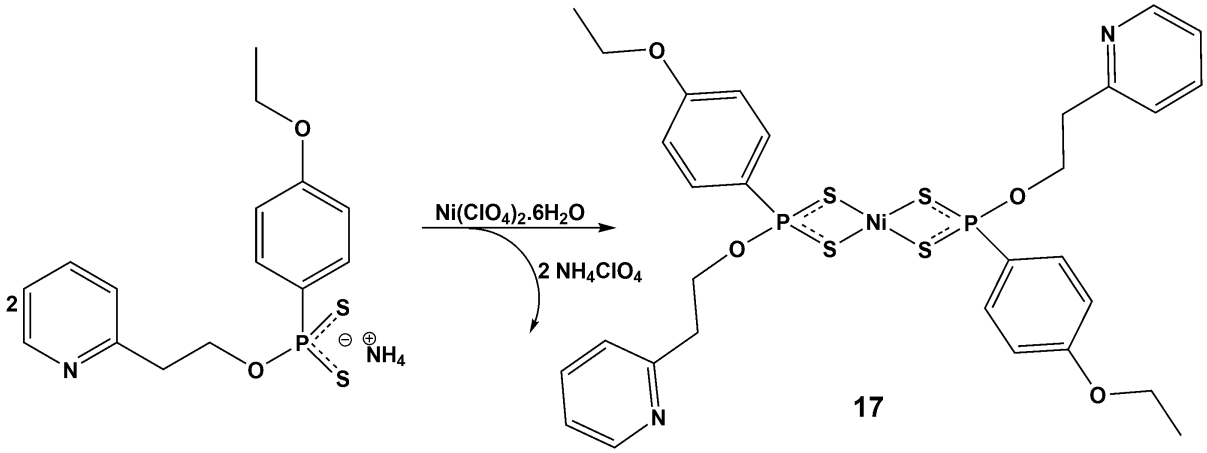

Scheme 5.3. Preparation of Ni(II) complex **17**.

The fluxional behaviour is apparent in the solution NMR experiments, as the system has the possibility of both para- and diamagnetism. The square-planar configuration is NMR active (diamagnetic), while the 5-coordinate species is inactive (paramagnetic). As a result of this, a loss in resolution in the ^{31}P NMR is noted, and a broad peak at *ca* 100 ppm is observed. However, the ^{1}H NMR is reasonably well resolved and corresponds to the 4-coordinate complex. Interestingly, the phosphorus-proton coupling ($J_{P\text{-}H}$) explained for these ligand systems in Chapter 4, is significantly reduced and a comparison of the phenetole aromatic peaks with complex **11**, reveals a loss of the long range $J_{P\text{-}H}$ coupling to the *meta*-protons of the phenetole group, shown in Figure 5.7. The mass spectrum of **17** corresponds to the mononuclear complex, this is due to the lability of the pyridine coordination during ionization.

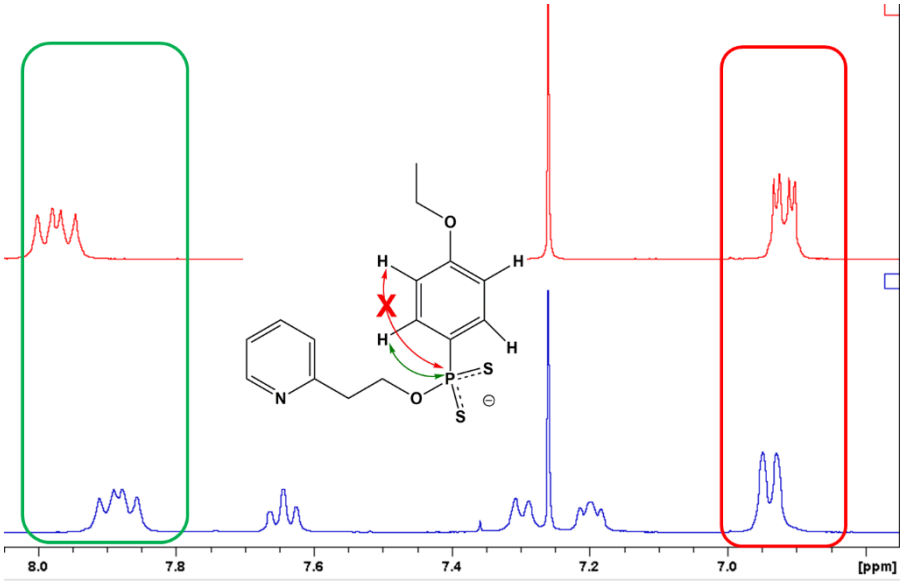

Figure 5.7. Comparison of signals observed for the aromatic protons of the phenetole substituent in **17** (blue) and **11**(red). The reduction in $J_{P\text{-}H}$ coupling is significant.

The behaviour observed in solution was further characterised in the solid state, with two different crystal morphologies, purple (**17a**) and orange (**17b**), isolated from the crystal growth chamber. X-ray diffraction analysis of a purple crystal (**17a**) revealed a triclinic crystal system and space group P-1, shown in Figure 5.8. Selected bond lengths and angles for **17a** and **17b** are presented in Table 5.4.

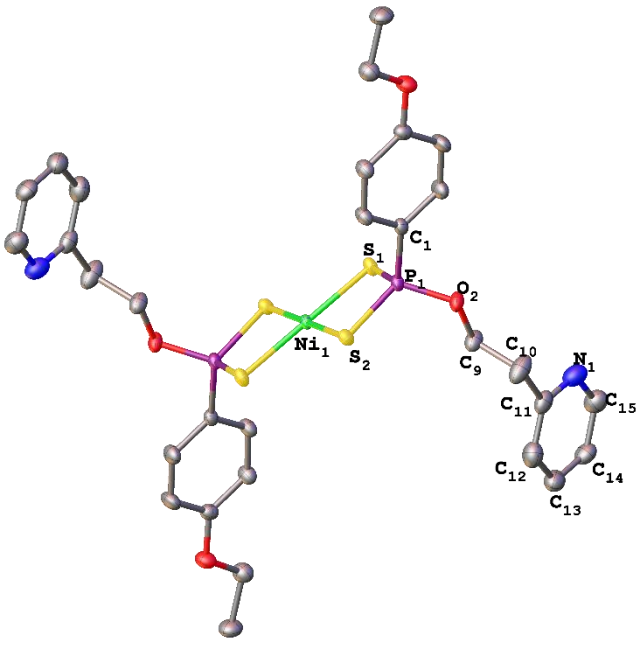

Figure 5.8. Molecular representation of **17a**: Thermal ellipsoids drawn at 35% and hydrogen atoms omitted for clarity.

The nickel atom lies on a centre of inversion, with the asymmetric unit comprising one half of the molecular unit. The configuration is similar to the numerous examples outlined in Chapter 1. The coordination geometry of the complex is square planar and the Ni(II) atom is bound by four sulfur atoms of the two S,S-bidentate ligands. The P-S bond distances are similar, at 2.017 Å and 2.003 Å, indicating an iso-bidentate coordination and complete delocalization of P-S π-bond over S-P-S chelate. The substituents on the phosphorus atom are in a *trans*-configuration, with the pyridine moieties occupying opposites of the coordination plane. Importantly, the pyridyl moiety is non-coordinative in this case.

The orange crystal (**17b**) also crystallized in the triclinic space group P -1. The lattice has two distinct bonding modes, as shown in Figure 5.9. The first is a square-planar Ni complex with the pyridyl groups non-coordinative with *S,S*-bidentate ligands chelating the metal centre and the configuration is isostructural to **17a**. This was confirmed by a structural overlay of the two molecular units, which revealed no significant difference in bond distances and angles.

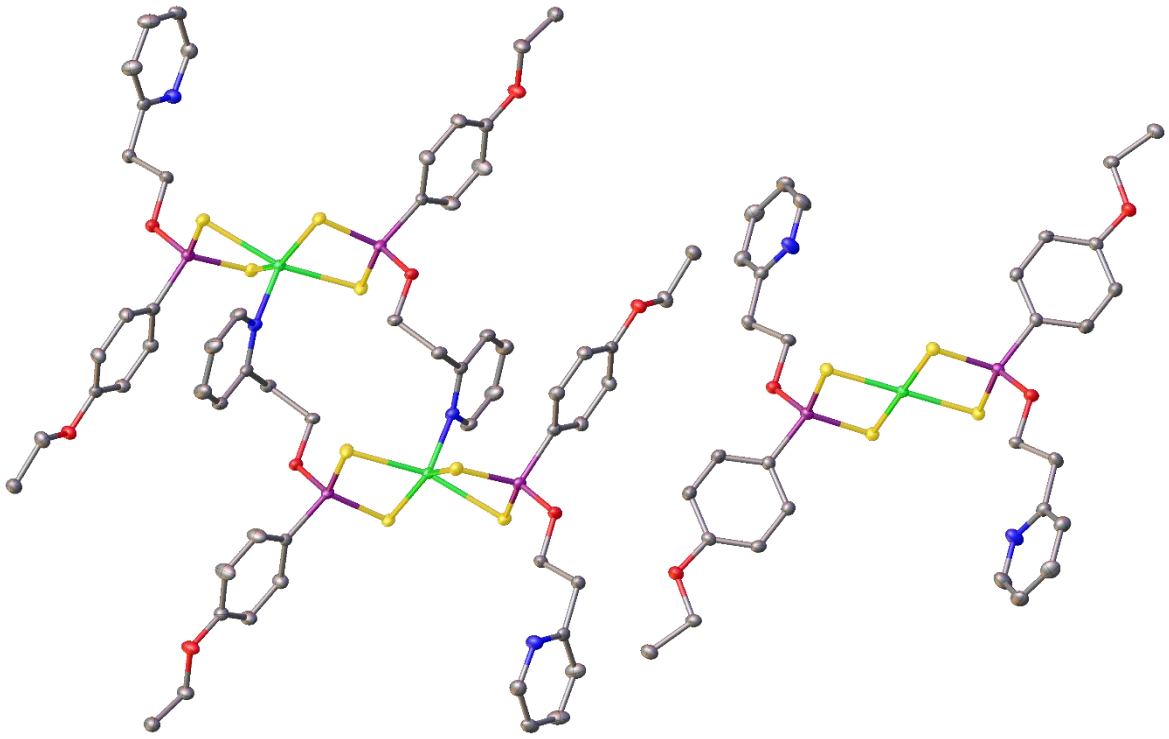

Figure 5. 9. Molecular representation of **17b**: Thermal ellipsoids drawn at 35% and hydrogen atoms omitted for clarity. Two different coordination geometries are present in the unit cell.

The other occupant of the unit cell is significantly different from its counterpart and displays a unique configuration. It contains a dinuclear Ni(II) system which arises from the

coordination of the pyridine moiety, and results in the formation of a 16 atom heterocycle, Figure 5.10 The coordination geometry around the 5-coordinate Ni(II) departs significantly from the 6-coordinate adducts usually formed with N-donor ligands and related Ni(II) complexes.[4,6] The base of the pyramid is formed by four sulfur atoms and the apex is occupied by the nitrogen atom of the pyridyl group of an adjacent molecular unit. Thus resulting in a discrete dinuclear Ni(II) complex. The nickel atom lies 0.513 Å out of the average plane of the sulfur atoms, which is a result of the short Ni-N bond distance of 2.058 Å. The Ni-S distances are *ca.* 2.4 Å and are significantly longer (0.2 Å) than the Ni-S bond distances observed for **17a** and the square planar moiety in the same unit cell. The lengthening of the Ni-S bond is a result of the increased electron density on the Ni(II) centre. A comparison of the S-P-S bite angle (107°) reveals a 6° increase as compared to **17a** and is attributed to the ability of the S-P-S moiety to accommodate pyridyl group. A layered crystal packing sequence of mononuclear/dinuclear/dinuclear/mononuclear is observed in the lattice and shown in Figure 5.11.

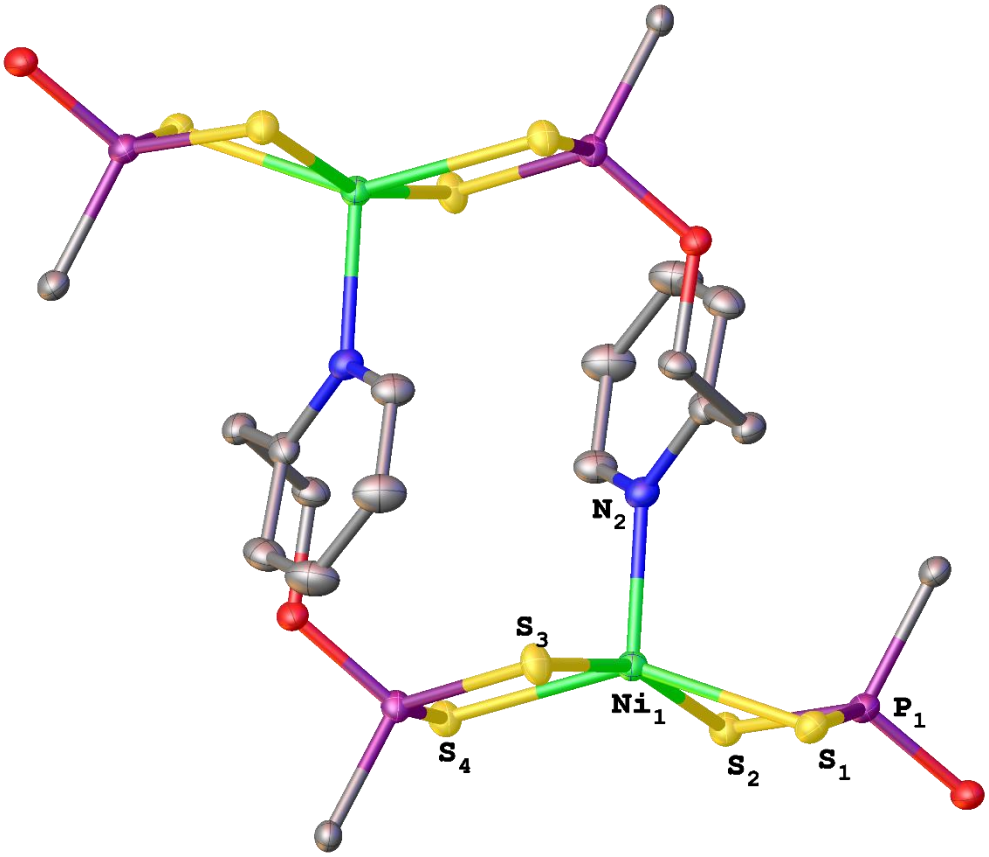

Figure 5.10. Thermal ellipsoid representation of the coordination geometry of the dinuclear complex **17b.** Non-coordinating pyridine and phenetole groups omitted for clarity.

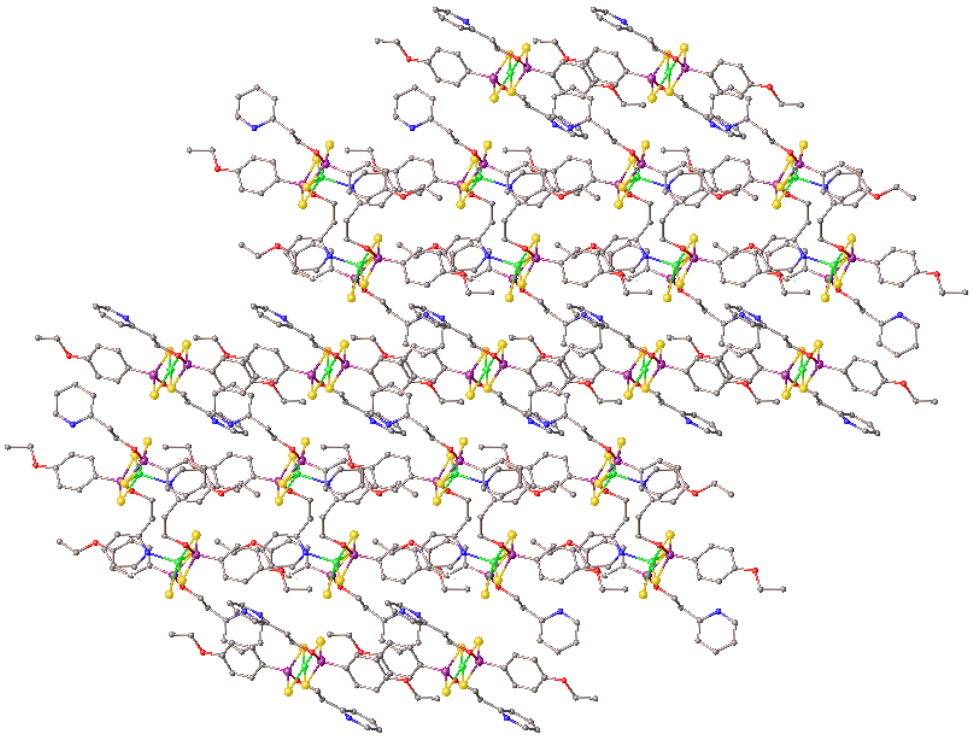

Figure 5.11. Packing in **17b** viewed along the *b*-axis.

Attempts to grow each of the crystal morphologies selectively proved unsuccessful and it is believed an equilibrium occurs during crystal growth which results in the formation of differential crystal morphologies. The ethyl bridge is key to the formation of the dinuclear Ni(II) complex and in an effort to emphasise its importance, a derivative containing the shorter methylene bridge (**18**) was prepared in a similar manner to **17**. Selected bond lengths and angles are presented Table 5.4. The purple crystals of **18** grew in the triclinic space group P-1 and a molecular representation is shown in Figure 5.12. Importantly, the shorter bridge does not accommodate the coordination of the pyridine moiety, and only one crystal morphology is isolated. The square planar geometry showed a *trans* configuration of the pyridyl groups relative to the coordination plane. The P-S bond lengths are similar and are *ca*. 2.0 Å in magnitude, this indicates equalised delocalisation of charge over the S-P-S fragment. The S-P-S bite angle is 102° which is consistent with square planar complexes described in this study.

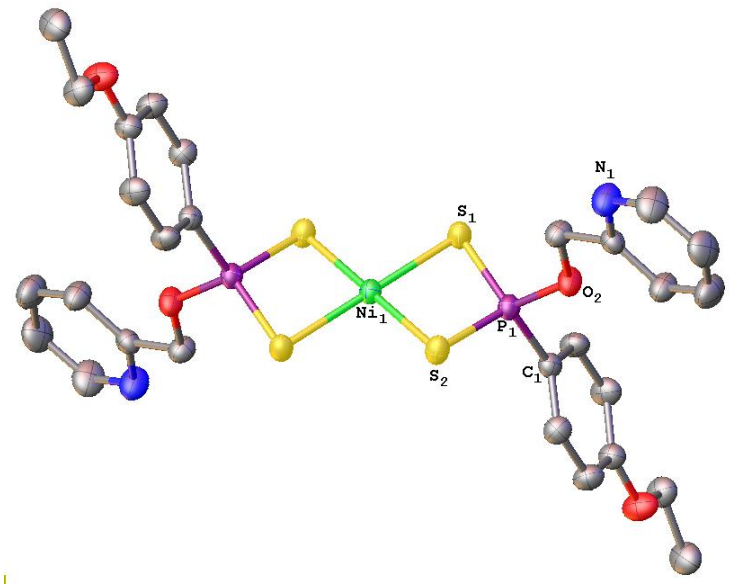

Figure 5.12. Molecular representation of **18**: Thermal ellipsoids drawn at 35 % probability and H atoms omitted for clarity.

Table 5.4. Bond lengths (Å) and angles for **17a**, **17b** and **18**.

17a		**17b**		**18**	
P(1)-S(1)	2.0171(9)	P(1)-S(1)	2.0048(10)	P(1)-S(1)	2.0023(12)
P(1)-S(2)	2.0030(9)	P(1)-S(2)	1.9942(10)	P(1)-S(2)	2.0074(11)
P(1)-O(2)	1.587(6)	P(1)-O(2)	1.6025(18)	P(1)-O(2)	1.5897(15)
P(1)-C(1)	1.775(8)	P(1)-C(1)	1.791(3)	P(1)-C(1)	1.792(2)
Ni(1)-S(1)	2.2263(6)	Ni(1)-S(1)	2.3980(7)	Ni(1)-S(1)	2.2416(8)
Ni(1)-S(2)	2.2348(6)	Ni(1)-S(2)	2.4709(7)	Ni(1)-S(2)	2.2304(9)
S(1)-P(1)-S(2)	101.39(4)	Ni(1)-N(1)	2.058(2)	S(1)-P(1)-S(2)	102.35(4)
S(1)-Ni(1)-S(1)^1	180.0	S(1)-P(1)-S(2)	107.49(4)	S(1)-Ni(1)-S(1)^1	180.00(4)

5.2.4 Mononuclear Pd(II) dithiophosphonate

The coordination variability observed for Ni(II) called for a further investigation for Group 10 metals. The reaction of **L11** with $PdCl_2$ in ethanol led to the formation of the mononuclear complex **19**, Scheme 5.4. Mass spectroscopy confirmed the purity of the material, with the detection of the sodium adduct. The solution dynamics are not visually detectable as seen in **17**. However, the solution NMR experiments proved interesting.

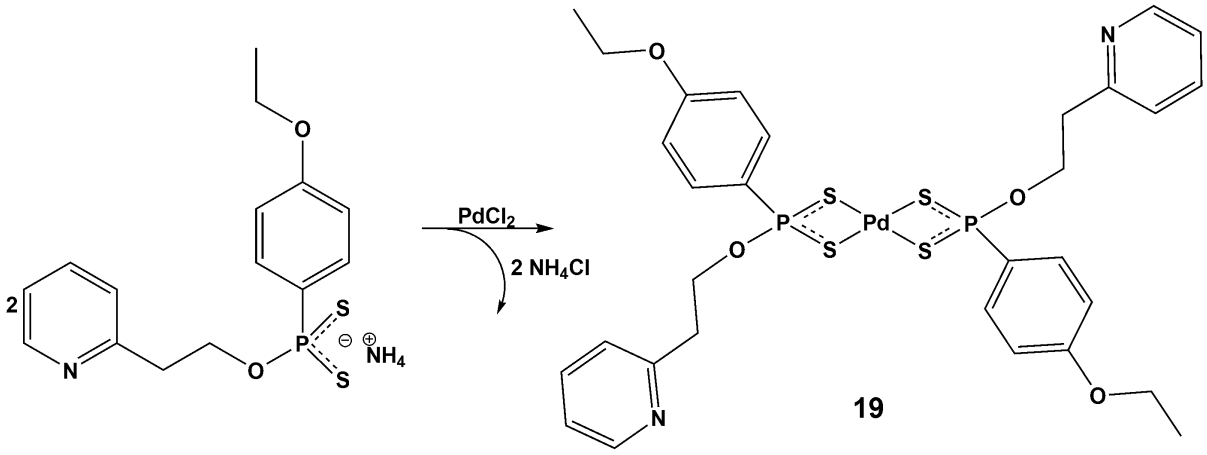

Scheme 5.4. Synthesis of Pd(II) derivative with the use of $PdCl_2$.

The isomerization effects eluded to previously is more pronounced in **19** and as such it is an ideal candidate for further discussion. The ^{31}P-NMR displays a pair of peaks of equal intensity, with a difference of 0.0767 ppm, shown in Figure 5.13. This indicates the energy barrier between the isomeric forms in solution is sufficiently low to allow for an equilibrium between the two isomers. The isomerisation is detectable in the ^{1}H-NMR as well. The integration of the signals in ^{1}H-NMR correspond to the expected complex, however, the multiplicity is interesting. The resonance overlap between the corresponding isomers, which have similar chemical shifts, gives rise to a seemingly *false* multiplicity because it appears to be a quintet but is in fact the overlap of two quartets. So, the expected quartet, which should have a height ratio of 1:3:3:1, in the region of 4 ppm (assigned to the O***CH$_2$***CH$_3$), is experimentally observed as an overlap of two quartets from each isomer. As a result this appears to be a quintet, which has a peak height ratio of 1:4:6:4:1. A graphical explanation of the overlap and a comparison to complex **17**, is shown in Figure 5.14.

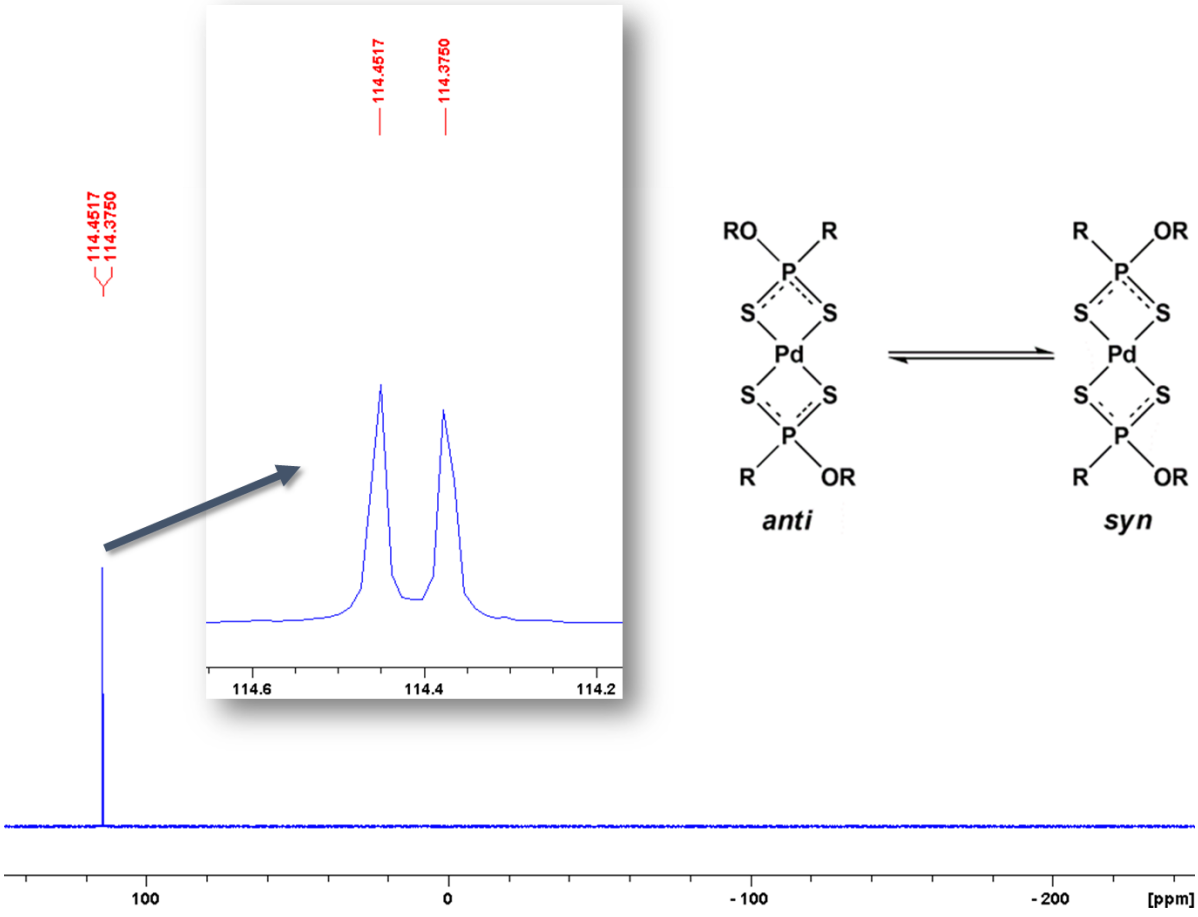

Figure 5. 13 Solution decoupled ^{31}P-NMR spectrum of **19**.

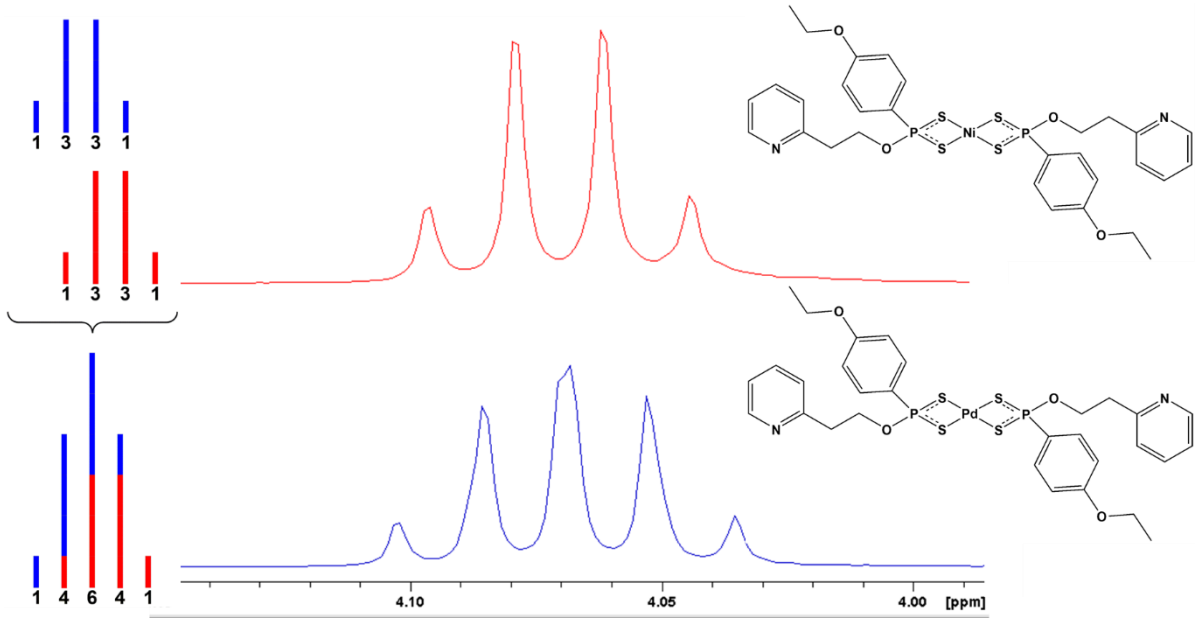

Figure 5. 14. Illustration of the contribution from each isomer, which results in the formation of a quintet (left). ^{1}H-NMR spectrum of **19** (blue) and **17** (red) for comparison.

In the solid state **19** crystalizes in the triclinic space group P-1, and a molecular representation is shown in Figure 5.15. Selected bond lengths and angles are presented in Table 5.5. The complex has a square planar geometry with the bidentate ligands coplanar with the metal centre, i.e. P, S and Pd atoms all lie on the same plane. . Complete electronic delocalization of the P-S π bond occurs over the S-P-S moiety, as indicated by equal P-S bond lengths of 2.0 Å. The S-P-S bite angle measures 103.52 ° with a bite distance of 3.142 Å. Importantly the pyridine moiety is not engaged in coordination, and the substituents are in an *anti*-configuration relative to the Pd(II) centre. Furthermore the pyridine groups do not act as packing directors in the crystal lattice, shown in Figure 5.16. The pyridine unit could thus readily be used as an N atom donor coordination site for a number of other metal centres, such as Cu(I) and Ag(I). Such studies were not pursued in this thesis.

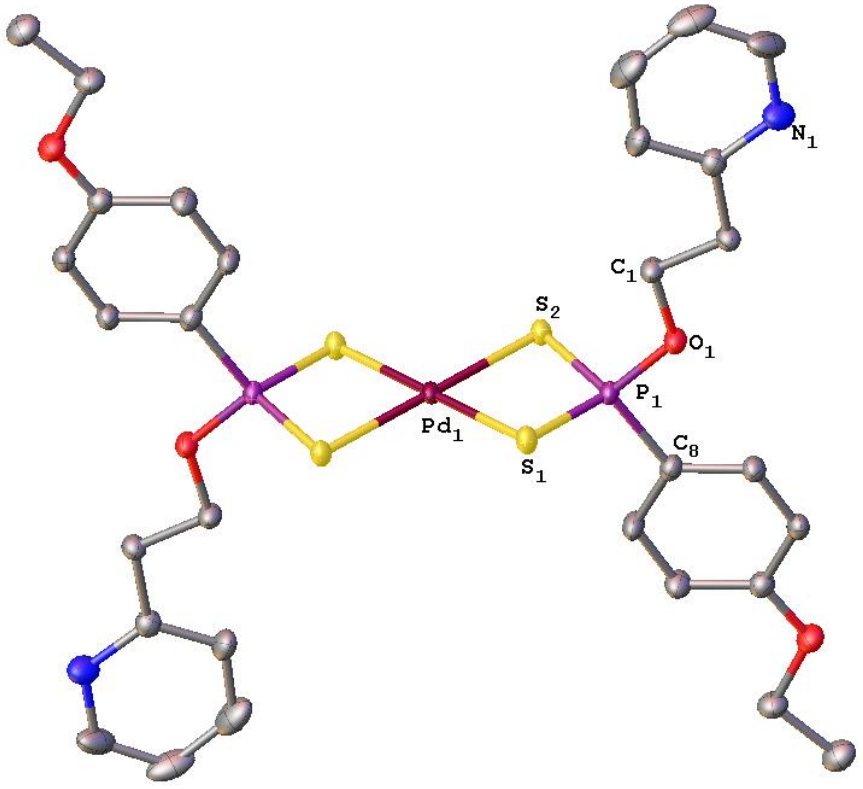

Figure 5. 15. Molecular representation of **19** with thermal ellipsoids drawn at 35 % probablity and H atoms removed for clarity.

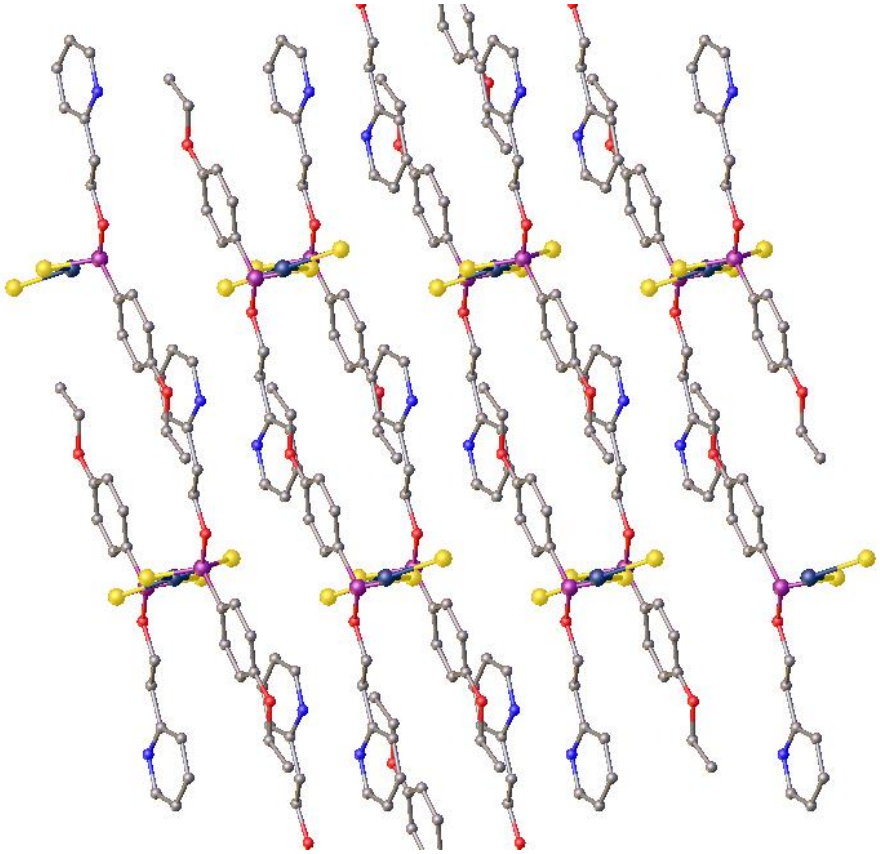

Figure 5.16. Packing in **19** viewed along the *b* axis.

Table 5.5. Selected bond angles (°) and distances (Å) for **19**.

P(1)-S(1)	2.0161(10)	Pd(1)-S(1)	2.3415(7)
P(1)-S(2)^{2}	2.0122(10)	Pd(1)-S(2)	2.3390(7)
P(1)-O(1)	1.575(2)	S(1)-P(1)-S(2)^{1}	102.52(4)
P(1)-C(8)	1.799(3)	S(2)-Pd(1)-S(2)^{1}	180.0

5.2.5 Dinuclear Au(I) dithiophosphonate.

The reaction of **L11** with [Au(tht)]Cl in THF led to the formation of a new dinuclear Au(I) complex, Scheme 5.5. The dinuclear macrocycle with S-P-S moieties follow coordination patterns observed previously in literature.[7]

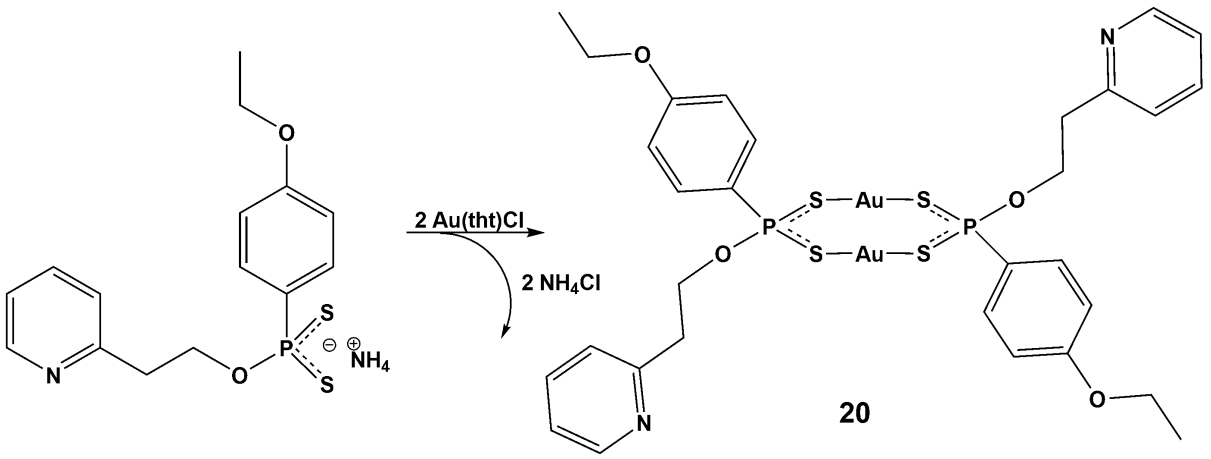

Scheme 5.5. Preparation of dinuclear Au(I) dithiophosphonate in THF.

The isomerization effects are not as pronounced as the Pd(II) example and a greater separation is observed in the ^{31}P NMR with two well resolved resonance peaks 2 ppm apart for complex **2**, 103 ppm and 101ppm. The *anti*-isomer contains an inversion centre which is lost upon reconfiguration to the *syn*.

In the solid state, the lattice energies restrict molecular fluxionality between the isomers and the most stable configuration can be deduced. Solid state magic angle spinning (MAS) NMR experiments aided in the determination of the isomeric composition of the bulk powder. The spectrum shown in Figure 5.17, shows a single peak at 104ppm. The spinning sidebands were distinguished from the relevant peaks by the varying the spin rate of the rotor. The local environments around the P atoms is unperturbed by adjacent dinuclear units and are magnetically equivalent, indicating a single isomer in the solid state.

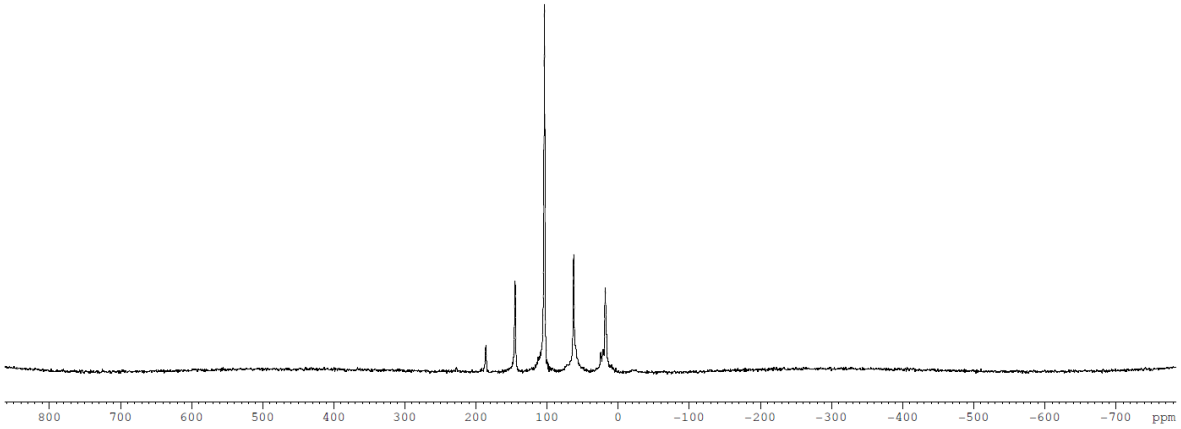

Figure 5.17. Solid state MAS NMR spectrum of **20** collected at 10 kHz.

The single peak corresponds to the *trans*-isomer, isolated and characterised by X-ray crystallography. A molecular representation is shown in Figure 5.18 and selected bond distances and angles are given in Table 5.4.

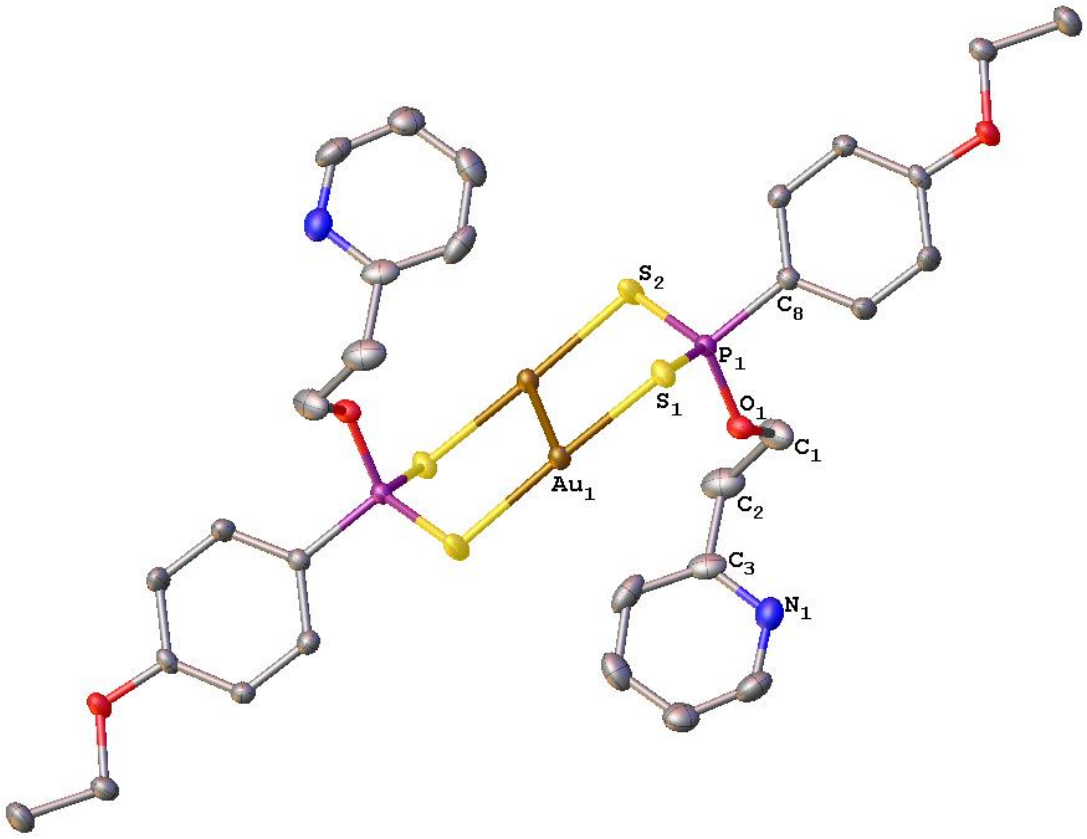

Figure 5.18. Molecular representation of **20**: Thermal ellipsoids drawn at 35% probability and H-atoms omitted for clarity.

Complex **20** crystallises in the monoclinic space group $P2_1/c$. Selected bond lengths and angles are given in Table 5.6. A bimetallic biconnective coordination mode for the ligand is observed, which is as expected for dinuclear Au(I) complexes previously reported.[8] The eight membered neutral macrocycle adopts an elongated chair conformation with the S-Au-S linkages parallel. The P atoms lie on opposite sides of coordination plane, unlike its square planar counterparts (complex **17a**, **18** and **19**), wherein the P atom is planar to the sulfur and metal atoms. The fully supported intramolecular Au···Au interaction of distance 3.105 Å, caused a deviation from linearity in S-Au-S units with angles measures 171.14°. The P-S bond lengths are *ca* 2.0 Å which indicates a complete delocalisation of the P-S π bond. The pyridyl groups are not engaged in metal coordination but do engage in hydrogen bonding with a contact measuring 2.562 Å to a flanking phenylic hydrogen, shown in Figure 5.19. This interaction is of sufficient magnitude to inhibit the formation of intermolecular Au···Au contacts. This secondary interaction directs the packing in the crystal lattice, resulting in a stacked configuration, as shown in Figure 5.20.

Table 5.6. Selected Bond lengths [Å] and angles [°] for **20**.

P(1)-S(1)	2.0138(12)	Au(1)-S(1)	2.969(9)
P(1)-S(2)	2.0149(13)	P(1)-S(1)-Au(1)	101.10(4)
P(1)-O(2)	1.585(2)	S(1)-P(1)-S(2)	117.92(5)
P(1)-C(1)	1.789(3)	S(1)-Au(1)-S(2)[1]	171.14(3)

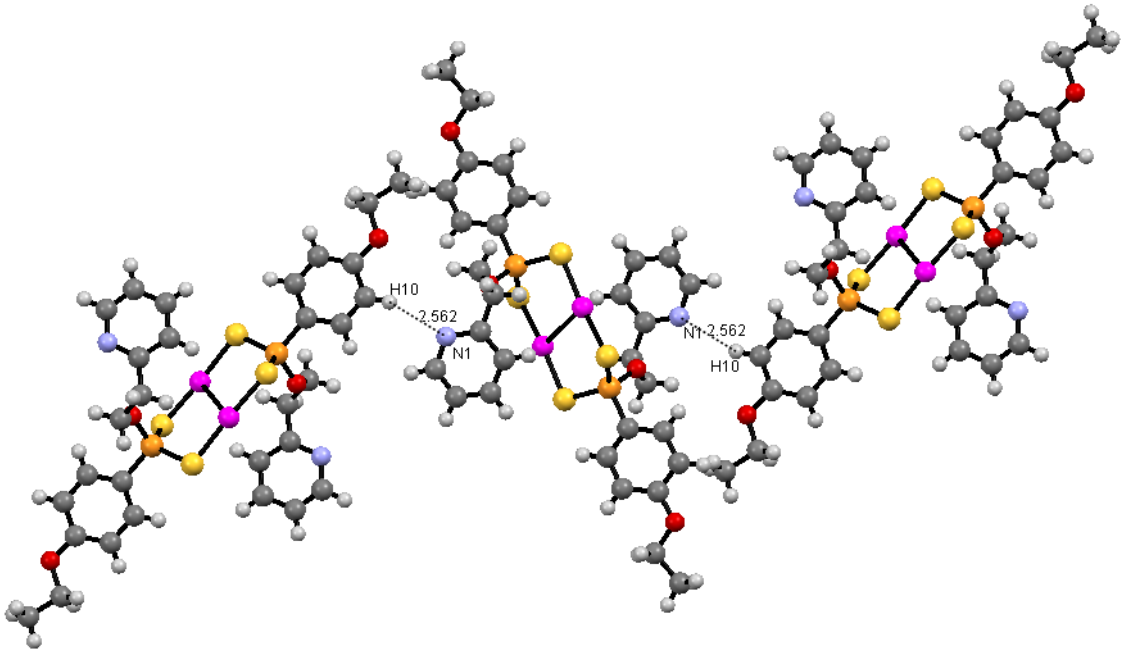

Figure 5.19. Ball and stick representation, illustrating the hydrogen bonding present in **20.**

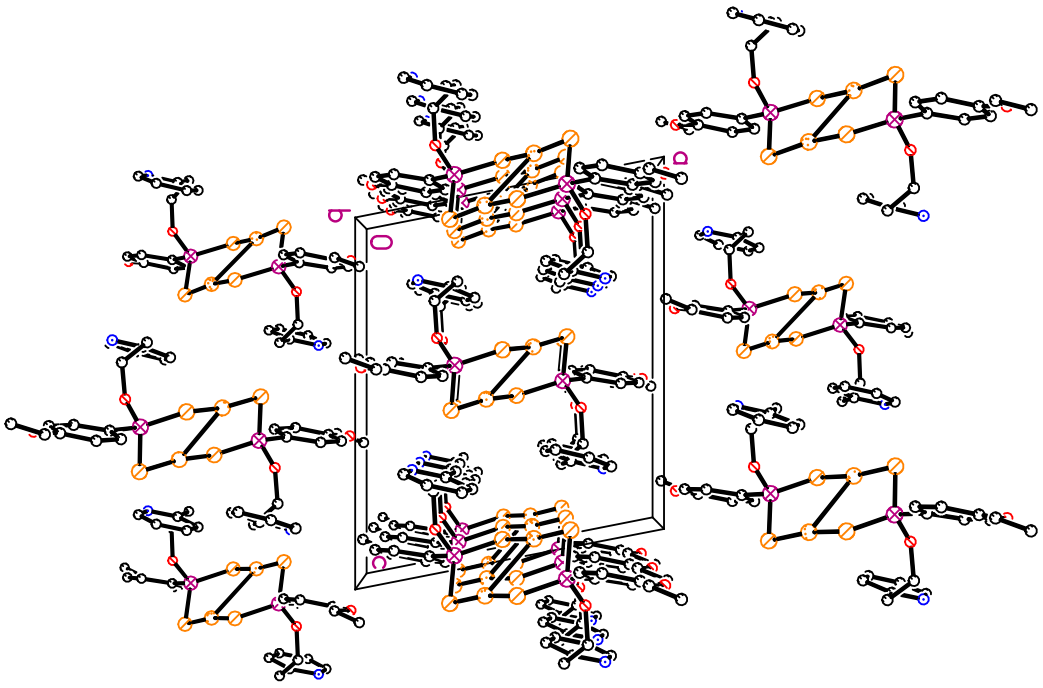

Figure 5.20. ORTEP representation of packing of **20** in crystal lattice shown along the b axis.

5.2.6 Cd(II) coordination polymer.

The cadmium complex was synthesized from a $CdCl_2 \cdot H_2O$ precursor and isolated as a white powder, shown in Scheme 5.6. Unlike the previously described examples, solvent diffusion was needed to obtain crystals suitable for X-ray analysis. The solution NMR experiments confirmed the absence of isomerisation in solution and a single peak is observed in the ^{31}P-NMR at 105.36 ppm. The ^{1}H-NMR displayed a single set resonances with the chemical shifts similar to other complexes described earlier.

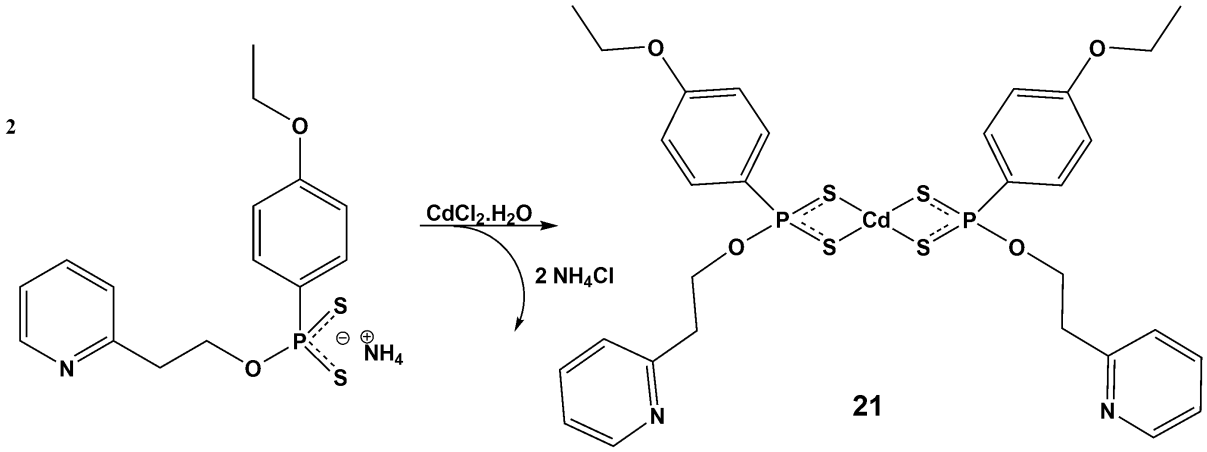

Scheme 5.6. Reaction of **L1** with $CdCl_2$ results in the formation *cis*-dithiophosphonate Cd(II) complex **21**.

Complex **21** crystallises in a monoclinic space group P21/n, and a molecular representation of the asymmetric unit is shown in Figure 5.21. The asymmetric unit in **21** differs from its Co(II) counterpart (**16**), however, the ligand conformation and coordination is similar. The ligands are in a *cis*-configuration and the 5-coordinate Cd(II) centre has distorted trigonal bipyramid geometry. The deviation from linearity of the axial axis S-Cd-S is significant when compared to **16**, with the S-Cd-S angle measuring 165.30 °. There is no significant deviation in the equatorial plane with the coordinating sulfur (2) and nitrogen (1) atoms coplanar with the metal centre. The P-S bond lengths are *ca.* 2.0 Å and the P-S π-bond is delocalised over the S-P-S fragment. The Cd-N bond distance is 2.3 Å and is significantly shorter than the Cd-S bonds, which measure *ca.* 2.6 Å. The coordination of the pyridyl substituent to adjacent molecular unit results in the formation of a coordination polymer, shown in Figure 5.22.

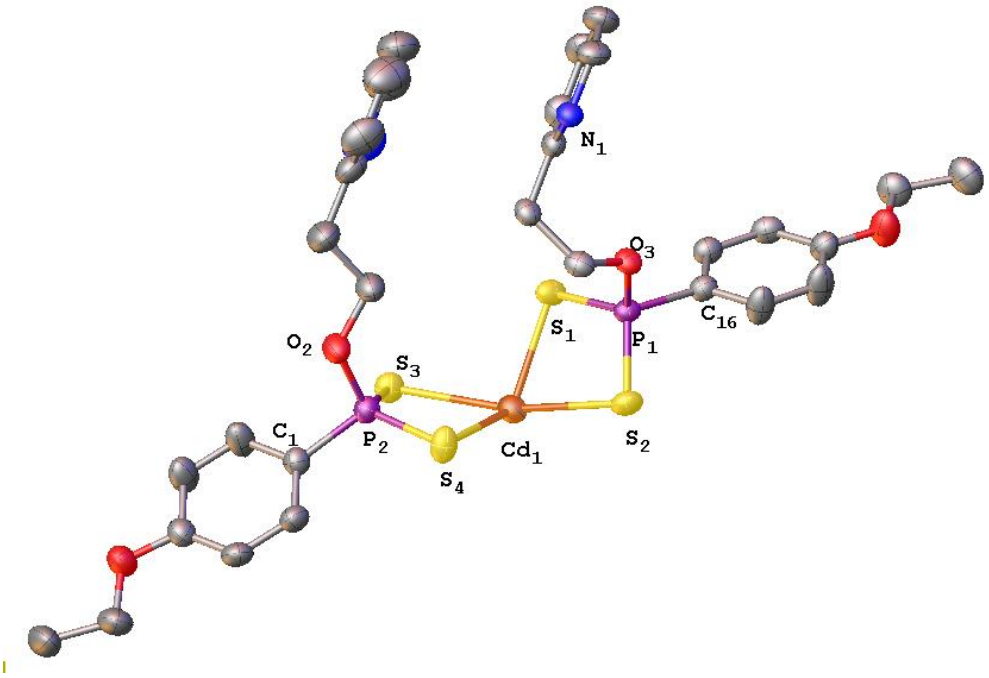

Figure 5.21. Molecular representation of the asymmetric unit present in **21**.

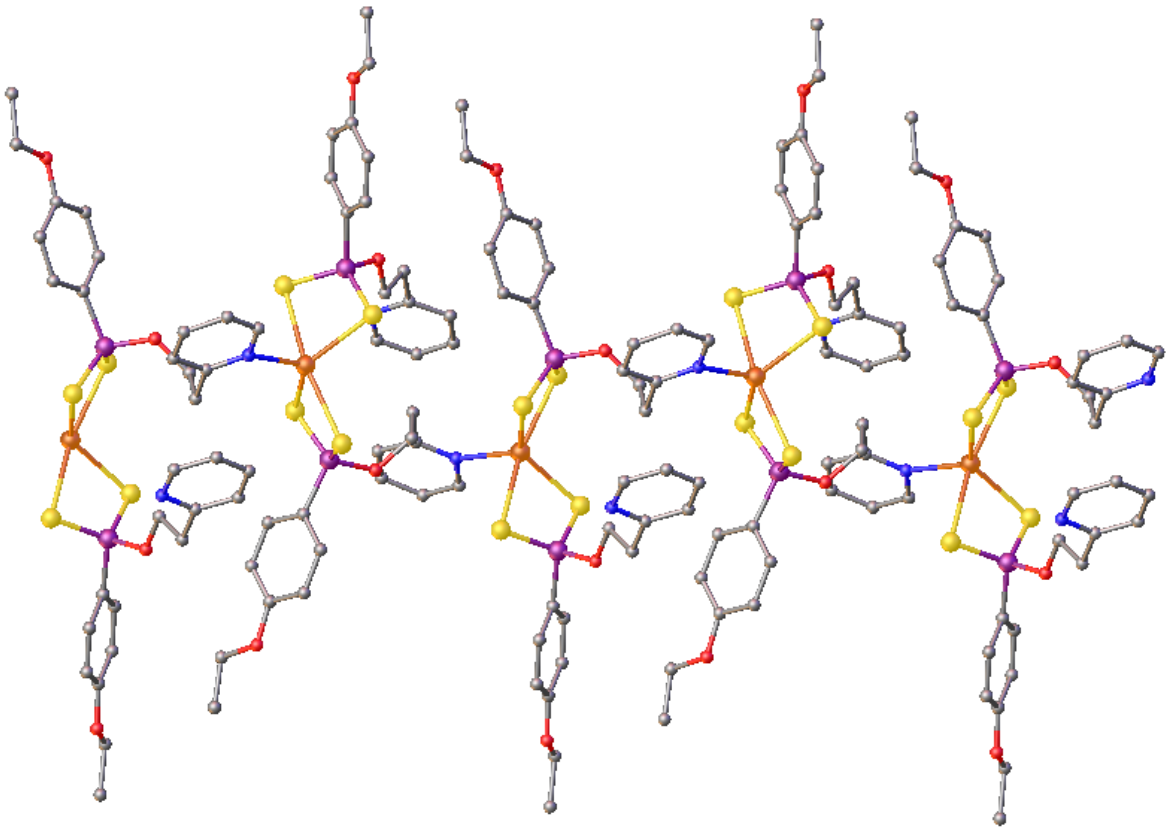

Figure 5.22. Ball and stick representation of polymer network in **21**.

Table 5.7. Selected bond lengths [Å] and angles [°] for **21**.

P(1)-S(1)	1.9980(11)	Cd(1)-S(1)	2.7002(9)
P(1)-S(2)	1.9954(11)	Cd(1)-S(2)	2.5601(9)
P(1)-S(3)	1.9897(12)	S(1)-P(1)-S(2)	111.30(5)
P(1)-S(4)	2.0048(12)	S(3)-P(2)-S(4)	111.73(5)
P(1)-O(3)	1.601(2)	S(2)-Cd(1)-S(3)	165.30(3)
P(1)-O(2)	1.592(2)	S(1)-Cd(1)-S(4)	128.04(3)
Cd(1)-N(1)^{1}	2.261(3)	N(1)^{1}-Cd(1)-S(1)	121.75(6)
Cd(1)-S(1)	2.5861(9)	N(1)^{1}-Cd(1)-S(4)	109.48(7)
Cd(1)-S(2)	2.6493(10)		

Table 5.8. Data collection and refinement data for **L11z**, **16**, **17a, 17b** and **18**-**21.**

Compound	**L 11z**	**16**	**17a**	**17b**
Empirical formula	$C_{30}H_{36}N_2O_4P_2S_4$	$C_{30}H_{34.5}CoN_2O_4P_2S_4$	$C_{30}H_{34}N_2NiO_4P_2S_4$	$C_{22.5}H_{25.5}N_{1.5}Ni_{0.8}O_3P_{1.5}S_3$
Mw	678.79	736.21	735.52	551.64
Temperature[K]	100(2)	100(2)	100(2)	100(2)
Size [mm]	0.28 x 0.45x0.37	0.15 x 0.13 x 0.06	0.16 x 0.089 x 0.046	0.27 x 0.16 x 0.09
Crystal System	Monoclinic	Monoclinic	Triclinic	Triclinic
Space Group	C2/c	$P2_1/c$	P-1	P-1
a[Å]	33.544(5)	20.082(3)	9.8107(5)	10.2354(3)
b[Å]	14.694(2)	13.4338(15)	9.8419(5)	12.6531(3)
c[Å]	14.0422(16)	24.540(3)	10.3495(5)	19.3580(5)
α[°]	90	90.00	104.559(3)	94.9320(10)
β[°]	110.795(6)	94.787(4)	102.528(3)	94.5150(10)
γ[°]	90	90.00	112.895(2)	90.9260(10)
V[Å^3]	6470.5(16)	6597.3(14)	833.67(7)	2489.35(11)
Z	8	8	1	4
Absorption coefficient [mm^{-1}]	0.431	0.909	0.966	0.970
***Θ*range [°]**	1.30 to 25.45	3.34 to 49.62	4.34 to 57	2.12 to 50.76
Data/restraints/parameters	5268/0/389	11115/0/779	3693/0/197	9093/0/585
Goodness of fit F^2	0.968	1.124	1.039	1.085
Final *R* indices [$I > 2\sigma(I)$]	$R_1 = 0.0640$, $wR_2 = 0.0997$	$R_1 = 0.0795$, $wR_2 = 0.1734$	$R_1 = 0.0402$, $wR_2 = 0.1004$	$R_1 = 0.0331$, $wR_2 = 0.0742$
***R* indices (all data)**	$R_1 = 0.0997$, $wR_2 = 0.2007$	$R_1 = 0.1240$, $wR_2 = 0.1975$	$R_1 = 0.0516$, $wR_2 = 0.1075$	$R_1 = 0.0477$, $wR_2 = 0.0861$
Largest diff peak/hole [e/Å^3]	0.663/-0.738	1.59/-1.21	0.96/-0.55	1.24/-0.50

Compound	**18**	**19**	**20**	**21**
Empirical formula	$C_{26}H_{30}N_4NiO_4P_2S_4$	$C_{30}H_{34}NO_4P_2PdS_4$	$C_{30}H_{34}Au_2N_2O_4P_2S_4$	$C_{30}H_{34}CdN_2O_4P_2S_4$
Mw	711.46	783.24	1070.70	846.87
Temperature[K]	296(2)	100(2)	173(2)	296(2)
Size [mm]	0.17 x 0.28 x 0.13	0.28 x 0.42 x 0.26	0.43 x 0.40 x 0.37	0.24 x 0.47 x 0.36
Crystal System	Triclinic	Triclinic	Monoclinic	Monoclinic
Space Group	P-1	P-1	P 21/c	$P2_1/n$
a[Å]	9.3410(4)	7.4195(3)	12.265(3)	15.5307(8)
b[Å]	9.7808(4)	10.7431(4)	9.831(2)	13.3610(7)
c[Å]	9.8175(4)	11.5025(4)	14.517(3)	17.3779(8)
α[°]	74.023(1)	103.570(2)	90	90.00
β[°]	68.841(1)	105.051(2)	101.128(2)	100.344(2)
γ[°]	83.310(1)	103.468(2)	90	90.00
V[Å^3]	804.02(6)	817.43(6)	1717.4(6)	3547.4(3)
Z	1	1	2	4
Absorption coefficient [mm^{-1}]	1.000	0.960	8.907	1.492
***Θ*range [°]**	4.34 to 57.28	3.86 to 55.28	2.52 to 25.34	3.24 to 56.84
Data/restraints/parameters	4050/0/187	3677/0/197	3123/0/200	8867/0/390
Goodness of fit F^2	1.051	1.050	1.036	1.029
Final *R* indices [$I > 2\sigma(I)$]	R_1 = 0.0310, wR_2 = 0.0859	R_1 = 0.0354, wR_2 = 0.0882	R_1 = 0.0181, wR_2 = 0.0435	R_1 = 0.0382, wR_2 = 0.1135
***R* indices (all data)**	R_1 = 0.0360, wR_2 = 0.0909	R_1 = 0.0430, wR_2 = 0.0933	R1 = 0.0214, wR2 = 0.0448	R_1 = 0.0621, wR_2 = 0.1368
Largest diff peak/hole [e/ Å^3]	0.37/-0.70	0.78/-0.45	0.852/-0.458	0.49/-0.70

In summary, this chapter dealt with the combination of two different donor atoms onto one ligand which is readily available to engage in metal coordination. Of note is that it afforded the first example of a Co(II) dithiophosphonate complex which can be synthesized in water and is not susceptible to oxidation. The robust ligand system afforded seven new crystal structures. This unique approach has been shown to be an effective method for the synthesis of coordination polymers in the case of **16** and **21**. Ni(II) complexes showed interesting solution characteristics, which were further investigated in the solid state, with two different coordination geometries and magnetic properties. The flexibility of the ligand system is in line with the overall principles outlined for the donor-acceptor methodology to the preparation of molecular frameworks and offers an alternative to the homoleptic system described earlier in the study.

5.3 Experimental

Phenetole, phosphorus-pentasulfide and 2-pyridineethanol, were obtained from Sigma Aldrich. Ammonia gas was purchased from Afrox (South Africa). Metal perchlorates, cadmium(II) chloride and palladium(II) chloride were all obtained from SAARCHEM. Gold solution was donated by Rand Refineries. ^{1}H and $^{31}P\{^{1}H\}$ spectra were recorded on a Bruker Advance 400 MHz spectrometer at 298 K. NMR data are expressed in parts per million (ppm). ^{1}H spectra are referenced internally to residual proton impurity in the deuterated solvents ($CDCl_3$ in all cases). ^{31}P NMR spectra chemical shifts were referenced relative to an 85% H_3PO_4 in D_2O external standard solution. Data are reported as resonance position (δ_H), multiplicity, assignment, and relative integral intensity. Melting points were determined with an Electrothermal 9100 melting point apparatus.

5.3.1 Synthesis of [NH_4 {$S_2P(4\text{-}C_6H_4OMe)(OCHCH_2\text{-}2\text{-}C_5H_5N)$}], (**L11**).

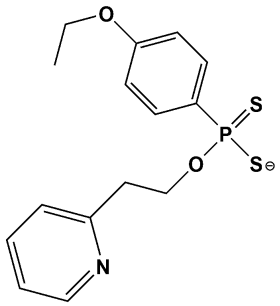

L 11

A Schlenk flask was charged with $(4\text{-}C_6H_4OEtP(S)S)_2$ (1.5g, 3.48mmol) and placed under vacuum for 30 minutes. The solid was heated to 70 °C, 2-$(2\text{-}C_5H_5N)OCHCH_2$ (810mg, 7.42 mmol) and toluene (2 mL) was added. The temperature was maintained at 70 °C for 3 hours, until dissolution of all the solids had been observed. The residue was cooled to room temperature, before being placed in an ice bath for 10 minutes. Anhydrous NH_3 gas was bubbled through the residue with vigorous agitation. The pale brown solid was dissolved in THF (20mL) and subsequent addition of diethyl ether (40mL) resulted in precipitation of a white powder. The mother liquor is removed by cannula and the precipitate washed with portions of cold diethyl ether. Yield 1.832 g (70%) ^{1}H NMR (400 MHz, CD_3OD): δ (ppm), *J*(Hz) 1.37(t, CH_3, 3H, $J_{H\text{-}H}$ = 7.00), 3.00(t, CH_2, 2H, $J_{H\text{-}H}$ = 6.56), 4.06(q, OCH_2, 2H, $J_{H\text{-}H}$ = 6.98), 4.62(m, OCH_2, 2H), 6.83(dd, ArCH, 2H, $J_{H\text{-}H}$ = 8.78, $J_{P\text{-}H}$ 2.58), 7.36(dd, ArCH (py), 1H, $J_{H\text{-}H}$ = 7.80), 7.41(dd, ArCH (py), 1H, $J_{H\text{-}H}$ = 7.84), 7.89(dd, ArCH, 2H,$J_{H\text{-}H}$ = 8.68, $J_{P\text{-}H}$ = 13.4), 7.76(m,ArCH (py), 1H), 8.40(bs, ArCH (py), 1H). ^{31}P NMR(CD_3OD) ppm: 107.22. Anal. calc. for $C_{15}H_{21}N_2O_2PS_2$: C, 50.54; H, 5.94; N, 7.86 %. Found: C 51.22, H 6.04, N 8.22 %.

5.3.2 Synthesis of [$Co\{S_2P(4\text{-}C_6H_4OEt)(OCHCH_2\text{-}2\text{-}C_5H_5N)\}]_2$, (**16**).

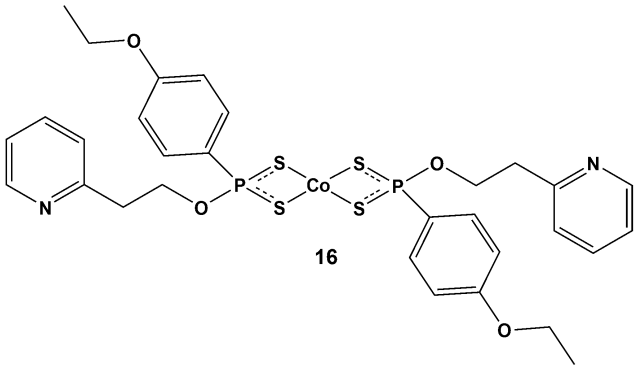

16

A beaker was charged with **L11** (400 mg, 1.12 mmol) and dissolved in EtOH (40 mL). To the clear solution, a solution of $Co(ClO_4)_2{\cdot}6H_2O$ (205 mg, 0.56 mmol) in water was added dropwise and stirred for 30 min, resulting in the formation of a turbid blue-green solution. The reaction mixture was extracted with DCM (2 x 20 mL) and the combined extracts washed with water. The extract was dried over $MgSO_4$, filtered and allowed to slowly evaporate to yield blue-green crystals of **16**. Yield 316 mg (77 %). Melting Point 121.3-121.6 °C. Single crystals suitable

for X-ray diffraction studies were selected. ESI-MS (m/z) (cal.) 736.0305 (736.0287) for ([Co{$S_2P(4\text{-}C_6H_4OEt)(\ OCHCH_2\text{-}2\text{-}C_5H_5N)$}] + H^+)

5.3.3 Synthesis of [Ni{$S_2P(4\text{-}C_6H_4OEt)(\ OCHCH_2\text{-}2\text{-}C_5H_5N)$}]$_2$, (**17**)

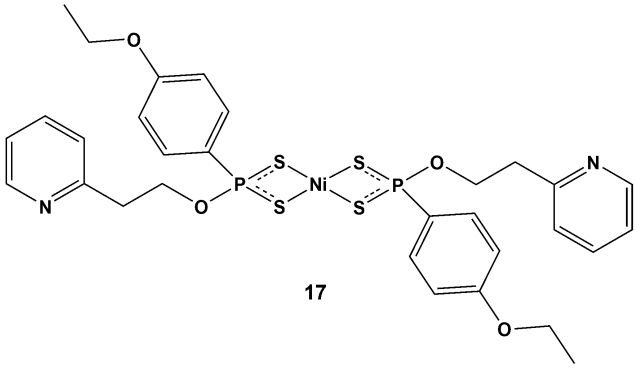

17

A beaker was charged with **L11** (300 mg, 0.820 mmol) and dissolved in EtOH (40 mL). To the clear solution, a solution of $Ni(ClO_4)_2{\cdot}6H_2O$ (95 mg, 0.416 mmol) in water was added dropwise and stirred for 30 min, resulting in the formation of a turbid orange-brown suspension. The reaction mixture is then extracted with DCM and washed with water. The purple extract was dried over $MgSO_4$, filtered and allowed to slowly evaporate to yield purple (**17a**) and orange crystals (**17b**). Single crystals suitable for X-ray diffraction studies were selected. Yield 239 mg (78 %). Melting point 119.5-119.7 °C ^{1}H NMR (400 MHz, CD_3OD): δ (ppm), *J*(Hz) 1.43 (t, CH_3, 6H, $J_{H\text{-}H}$ = 6.96), 3.29 (t,CH_2, 4H, $J_{H\text{-}H}$ = 6.56), 4.09 (q, OCH_2, 4H, $J_{H\text{-}H}$ = 6.96), 4.75(m,OCH_2, 4H), 6.94(d, ArCH, 4H, $J_{H\text{-}H}$ = 7.96), 7.20 (dd, ArCH(py), 2H, $J_{H\text{-}H}$ = 6.04, 6.04), 7.29(d, ArCH(py), 2H, $J_{H\text{-}H}$ =7.60), 7.64(dd, ArCH(py), 2H, $J_{H\text{-}H}$ = 7.20, 7.20), 7.88 (dd, ArCH, 4H, $J_{H\text{-}H}$ = 6.04, $J_{P\text{-}H}$ = 13.53), 8.66(bs, ArCH(py), 2H) ^{31}P NMR (CDCl3) ppm: 100.42. ESI-MS (m/z) (cal.) 756.9084 (757.013) for ([Ni{$S_2P(4\text{-}C_6H_4OEt)(\ OCHCH_2\text{-}2\text{-}C_5H_5N)$}] + Na^+)

5.3.4 Synthesis of [Pd{$S_2P(4\text{-}C_6H_4OEt)(\ OCHCH_2\text{-}2\text{-}C_5H_5N)\}]_2$, (**19**).

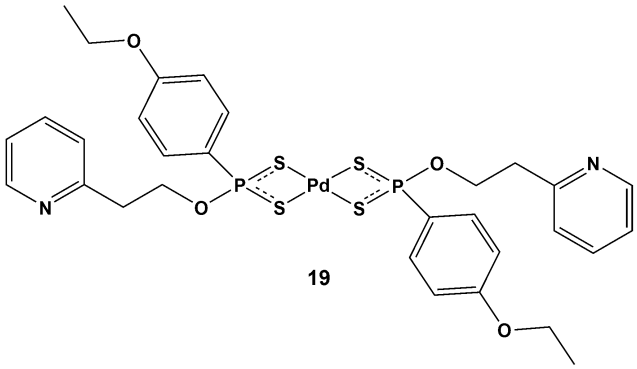

A schlenk tube was charged with **L11** (80mg, 0.224mmol) and dissolved in EtOH (40 mL). To the clear solution, $PdCl_2$ (20 mg, 0.112 mmol) was added and stirred for 30 min, resulting in the formation of a turbid red solution. The solvent is removed in *vacuo* and the residue extracted with DCM and filtered through celite. The filtrate is allowed to slowly evaporate on standing and yielded red crystals of **19**. Single crystals suitable for X-ray diffraction studies were selected. Yield 64 mg (72 %). Melting point 115.4 – 116.2 °C. ^{1}H NMR for *trans* and *cis*-isomer(400 MHz, CD_3OD): δ (ppm), *J*(Hz) 1.43 (m, CH_3, 6H), 3.28 (m,CH_2, 4H), 4.07 (m, OCH_2, 4H), 4.66(m,OCH_2, 4H), 6.91(m, ArCH, 4H), 7.16(m, ArCH(py), 2H), 7.25(m, ArCH(py), 2H), 7.62(m, ArCH(py), 2H), 7.83 (m, ArCH, 4H), 8.56(m, ArCH(py), 2H) ^{31}P NMR (CDCl3) ppm: 114.3750, 114.4517. ESI-MS (m/z) (cal.) 804.9774 (804.9809) for ([Pd{$S_2P(4\text{-}C_6H_4OEt)(OCHCH_2\text{-}2\text{-}C_5H_5N)\}] + Na^+)

5.3.5 Synthesis of [Au{$S_2P(4\text{-}C_6H_4OMe)(\ OCHCH_2\text{-}2\text{-}C_5H_5N)\}]_2$, (**20**).

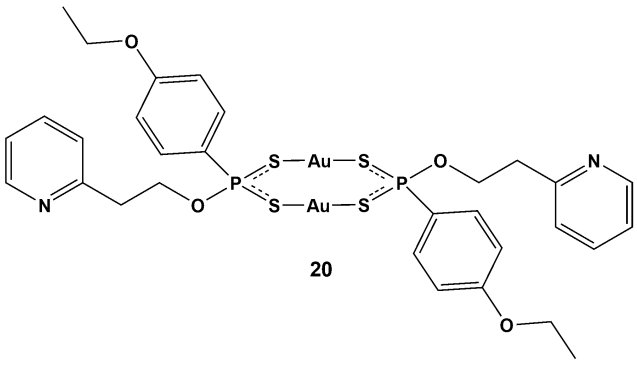

A Schlenk flask was charged with **L11** (112 mg, 0. 314 mmol) and dry tetrahydrofuran (40 mL). To the clear solution [Au(tht)]Cl (100 mg, 0.312 mmol) was added and the reaction stirred for 30 min, resulting in the formation of a turbid yellow solution. The solvent was removed in *vacuo,* followed by extraction with 50 mL of dichloromethane. The extract was filtered through a composite of Celite/anhydrous $MgSO_4$. The volume of the filtrate was reduced in *vacuo*. A yellow powder was consolidated and washed with diethyl ether (2 x 5 mL). Single crystals suitable

for X-ray diffraction studies were grown by slow diffusion of hexane layered onto a concentrated DCM solution of **20**. Yield 252 mg (75 %). Melting point 171.4-171.8 °C. ^{1}H NMR (400 MHz, $CDCl_3$): δ (ppm), *J*(Hz) 1.43(t, CH_3, 6H, J_{H-H} = 7.00), 3.12(t, CH_2, 4H, J_{H-H} = 6.56), 4.06(q, OCH_2, 4H, J_{H-H} = 6.98), 4.72(m, OCH_2, 4H), 6.93(dd, ArCH, 4H, J_{H-H} = 8.78, J_{P-H} 2.58), 7.18(m, ArCH (py), 2H), 7.41(m, ArCH (py), 2H), 7.89(m, ArCH, 4H), 7.76(m, ArCH (py), 2H), 8.40(bs, ArCH (py), 2H). ^{31}P NMR($CDCl_3$) ppm: 101.25, 103.44. Anal. calc. for $C_{30}H_{34}Au_2N_2O_4P_2S_4$: C, 33.65; H, 3.20; N, 2.62 %. Found: C, 34.24; H, 3.65; N, 2.56 %.

5.3.6 Synthesis of $[CdS_2P(4\text{-}C_6H_4OMe)(OCHCH_2\text{-}2\text{-}C_5H_5N)]_2$, (**21**).

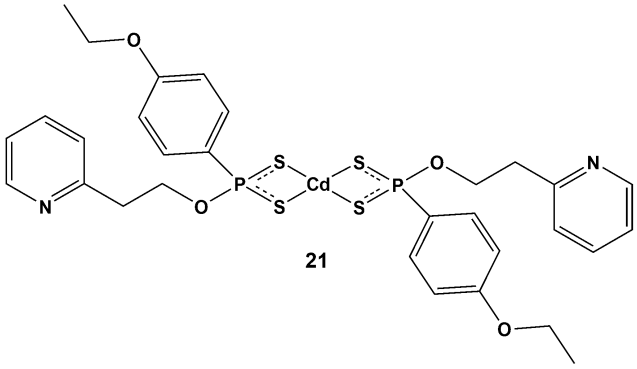

21

A beaker was charged with **L11** (356 mg, 1.00 mmol) and dissolved in EtOH (50 mL). A solution of $CdCl_2{\cdot}H_2O$ (114 mg, 0.56 mmol) in water was added dropwise to the ligand solution and stirred for 30 min, resulting in the formation of a white precipitate. The precipitate is collected by vacuum filtration and dissolved in DCM. The DCM solution was dried over anhydrous $MgSO_4$, filtered and solvent removed in *vacuo* to yield a pale yellow powder. Single crystals suitable for X-ray diffraction studies were grown by slow diffusion of hexane layered onto a concentrated DCM solution of **21**. Yield 390 mg (88 %). Melting point 120.6-121.4 °C. ^{1}H NMR (400 MHz, CD_3OD): δ (ppm), *J*(Hz) 1.43 (t, CH_3, 6H, J_{H-H} = 6.96), 3.292 (t,CH_2, 4H, J_{H-H} = 6.56), 4.09 (q, OCH_2, 4H, J_{H-H} = 6.96), 4.75(m,OCH_2, 4H), 6.94(d, ArCH, 4H, J_{H-H} = 8.76, J_{P-H} = 3.2018), 7.20 (dd, ArCH(py), 2H, J_{H-H} = 6.04, 6.04), 7.29(d, ArCH(py), 2H, J_{H-H} =7.60), 7.64(dd, ArCH(py), 2H, J_{H-H} = 7.20, 7.20), 8.00 (dd, ArCH, 4H, J_{H-H} = 8.70, J_{P-H} = 14.54), 8.66(bs, ArCH(py), 2H) ^{31}P NMR (CDCl3) ppm: 105.358. ESI-MS (m/z) (cal.) 812.9839 (812.9808) for ([Cd{$S_2P(4\text{-}C_6H_4OEt)(OCHCH_2\text{-}2\text{-}C_5H_5N)$}] + Na^+)

5.4 References

1. D. Sun and R.-B. Huang, *Acta Cryst.*, 2011, **C67**, m315-m317.
2. M. C. Aragoni, M. Arca, N. R. Champness, M. De Pasquale, F. A. Devillanova, F. Isaia, V. Lippolis, N. S. Oxtoby and C. Wilson, *CrystEngComm*, 2005, **7**, 363-369.
3. M. C. Aragoni, M. Arca, N. R. Champness, A. V. Chernikov, F. A. Devillanova, F. Isaia, V. Lippolis, N. S. Oxtoby, G. Verani, S. Z. Vatsadze and C. Wilson, *Eur. J. Inorg. Chem.*, 2004, 2008-2012.
4. M. C. Aragoni, M. Arca, F. Demartin, F. A. Devillanova, C. Graiff, F. Isaia, V. Lippolis, A. Tiripicchio and G. Verani, *J. Chem. Soc., Dalton Trans.*, 2001, 2671-2677.
5. W. E. van Zyl and J. P. Fackler, *Phosphorus, Sulfur, Silicon Rel. Elem.*, 2000, **167**, 117-132.
6. B.-L. Song, R.-G. Xiong, X.-Z. You and X.-Y. Huang, *Acta Cryst.*, 1995, **C51**, 2258-2259.
7. W. E. van Zyl, R. J. Staples and J. J. P. Fackler, *Inorg. Chem. Comm.*, 1998, **1**, 51-54.
8. W. E. van Zyl, J. M. Lopez-de-Luzuriaga, A. A. Mohamed, R. J. Staples and J. P. Fackler, Jr., *Inorg. Chem.*, 2002, **41**, 4579-4589.

Chapter 6
Conclusions

This thesis has demonstrated that the incorporation of multiple coordination moieties into a common ligand backbone is an effective tool in the pursuit of multinuclear metal topologies. An initial investigation into the ligand synthesis, yielded the first examples of structurally characterized *intra*molecular S-S coupling of dithiophosphonates reported. Variation of the alcohol chain length led to the formation of two ring sizes and multiple ferrocene moieties. Importantly the redox activity of the ferrocenyl groups are significantly different from ferrocene, and a loss of reversibility for ferrocene/ferrocenium redox couple was apparent.

The first design approach incorporated two identical coordination moieties onto a common flexible organic linker. Variability in the ligand conformation was found to be a key factor in accommodating a wide variety of metal centres and the bis(anionic) ligand successfully stabilised Cu(I), Ag(I), Au(I), Au(III) and Ni(II). This resulted in several novel topologies which have not been previously reported in literature. The Cu(I) cluster is the first tetranuclear cluster to have a Cu_4L_2 configuration, and represents only the second dithiophosphonate tetranuclear cluster reported to date. Its Ag(I) counterpart is the first dithiophosphonate stabilised Ag(I) cluster and contains a total of six argentophilic interactions. The hexanuclear Au(I) metallatriangle is the largest Au(I) metallatriangle reported to date and the oxidation product is the first Au(III) complex, produced by the addition of bromide across a S-P-S framework. Furthermore the cofacial dinuclear nickel complex afforded the elusive *cis* configuration.

The apparent lack of tetranuclear Cu(I) dithiophosphonate clusters in literature was addressed and an alternative synthetic methodology afforded several clusters in aqueous conditions was reported. The luminescent characteristics were determined and electronic calculations confirmed that the luminescence arose from an interaction between the metal core and the primary coordination sphere, with no significant contributions from the ligand substituents to the emission profile.

An alternative approach to the incorporation of two coordination moieties led to the formation of a novel ligand system. The combination of an N-donor ligand with the dithiophosphonate motif, proved to be highly successful. The coordination capabilities of the ligand were evaluated with a variety of metals and afforded seven new crystal structures. This unique approach has been shown to be an effective method for the synthesis of coordination polymers in the case of **16** and **21**. Notably it afforded the first Co(II) dithiophosphonate complex. The ethyl bridge was proven to be the ideal linker between the two moieties and facilitated the formation of the polymers. The Ni(II) derivative displayed interesting configurational isomerisation and two coordination modes of the ligand were determined in the solid state. The flexibility of the ligand system is in line with the overall principles outlined for the donor-acceptor methodology to the preparation of molecular frameworks and offers an alternative to the homoleptic system.

Due to the novelty of the ligand systems presented in this study, a relatively new aspect in dithiophosphonate chemistry has been created. Thus there exists significant potential in future investigations into coordination chemistry. Furthermore, the complexes reported here can warrant an investigation into their catalytic activity, especially due to the relatively large nuclearity observed for certain complexes.

In particular the coordinative ability of the bis(dithiophosphonate) ligand is undeniable and application to other metal atoms is plausible. Furthermore, the ability of the ligand to stabilise relatively large metal topographies, can provide access to different coordination frameworks in the future. The synthetic protocol outlined for the synthesis of Cu(I) clusters, should increase its availability for the application to systems requiring luminescent materials. The pyridyl dithiophosphonate ligands, affords the opportunity to prepare mixed metal complexes *via* differential coordination between the two groups (not exploited in this study).

Appendix

The accompanying compact disc, contains supporting information not included in this dissertation.